UILU-ENG-96-2009

CIVIL ENGINEERING STUDIES
Hydraulic Engineering Series No. 51

ISSN: 0442-1744

MEAN FLOW AND TURBULENCE IN A LABORATORY CHANNEL WITH SIMULATED VEGETATION

By

Chad Dunn[1]

Fabián López[1]

and

Marcelo García[2]

[1] **Research Assistant**

[2] **Associate Professor**

Sponsored by:

**U.S. Army Corps of Engineers
Waterways Experiment Station
(Contract DACW39-94-K-0010)**

**HYDROSYSTEMS LABORATORY
DEPARTMENT OF CIVIL ENGINEERING
UNIVERSITY OF ILLINOIS AT URBANA-CHAMPAIGN
URBANA, ILLINOIS**

October 1996

ABSTRACT

Much is unknown about the flow structure and turbulence characteristics in open-channels with vegetative canopies. All models of open-channel flow through and above vegetative canopies require a quantitative measure of the ability of the plants to absorb momentum by form drag. This ability is commonly characterized by a drag coefficient. The present work experimentally investigates the flow structure and determines drag coefficients in a channel with simulated vegetation under uniform flow conditions. Vegetation is simulated by rigid and flexible cylinders placed in a laboratory flume. An acoustic Doppler velocimeter is employed to measure velocity and turbulence characteristics in and above the cylinder canopy and a new procedure is developed and used in the computation of drag coefficients. This procedure allows for the first measurements of the vertical profile of the vegetation-induced drag coefficient in an open-channel flow. Results for flow through rigid cylinders show that the drag coefficient is not constant in the vertical, as many models have assumed, but instead, reaches a maximum at about one-third of the canopy height. For flow through flexible cylinders, the shape of the drag coefficient profile is dependent on the amount of cylinder deformation in the channel and may take on one of two shapes: either a shape similar to that for flow through rigid cylinders when these are slightly deflected, or a shape which decreases with distance from the bed when the cylinders are highly deflected. Bulk drag coefficients and a shape factor are defined and computed and the effects of channel and flow parameters on the magnitude of these values are investigated. Measured drag coefficients are in good agreement with previously estimated values. In an open channel lined with rigid cylinders, the bulk drag coefficient is 1.13 ± 0.2 and is not dependent on any of the flow parameters. In the presence of flexible cylinders, the bulk drag coefficient is significantly reduced when the cylinders become highly deflected.

ACKNOWLEDGMENTS

The funding provided by the U.S. Army Corps of Engineers, Waterways Experiment Station under contract DACW39-94-K-0010 with Mr. Brad Hall as Project Officer and the tuiton assistance provided to the first author by the United States Geological Survey, Urbana office, are gratefully acknowledged.

This report is based on the thesis submitted by Chad Dunn in partial fulfillment of the requirements for the degree of Master of Science in Civil Engineering

TABLE OF CONTENTS

LIST OF TABLES

LIST OF FIGURES

LIST OF SYMBOLS

A - obstructed frontal area

a - plant density in units of per meter

C_D - drag coefficient for a single cylinder

C_D' - horizontally averaged drag coefficient in a multi-cylinder arrangement

C_D'' - mean drag coefficient as defined by den Hartog and Shaw (1975)

$\overline{C_D}$ - bulk or mean drag coefficient

$\overline{\overline{C_{DA}}}$ - integrated average bulk drag coefficient within canopy

$\overline{\overline{C_{DB}}}$ - bulk drag coefficient integrated to top of canopy

$\overline{\overline{C_{DH}}}$ - bulk drag coefficient integrated to free surface

$\overline{\overline{C_{DM}}}$ - bulk drag coefficient estimated with Manning's equation

D - cylinder or plant diameter

EI - stem flexural rigidity

F_D - drag force

f_D - drag force per unit volume

Fr - Froude number

G - total shear stress per unit density in a two-dimensional flow

GR - slope gauge reading

g - gravitational acceleration

$\vec{g}$ - gravitational acceleration vector

g_x - component of gravitational acceleration in the x-direction

g_y - component of gravitational acceleration in the y-direction

g_z - component of gravitational acceleration in the z-direction

H - flow depth

h - average undeflected canopy height

h_p - average deflected canopy height

$\bar{i}_c$ - mean dimensionless turbulence intensity within canopy

k - turbulence kinetic energy

M - relative density of plants

N - blade density in a unit area

n - Manning's coefficient

p - pressure

p_h - horizontally averaged pressure

Q - channel discharge

R - hydraulic radius

Re - flow Reynolds number

Re_D - cylinder Reynolds number

S - local bed slope

S_f - friction slope

SC1 - secondary current term due to vertical velocity

SC2 - secondary current term due to spanwise velocity

SUW - secondary term due to Reynolds stress $\overline{u'w'}$

T - water temperature

t - dimensional averaging interval

t* - dimensionless averaging interval

U - mean channel velocity

U_c - mean canopy velocity

u - instantaneous velocity in mainstream direction

u_∞ - uniform flow velocity upstream of obstruction

$\overline{u}$ - local time-averaged mainstream velocity

u_h - mainstream velocity averaged in horizontal plane

$\overline{u}_h$ - horizontally averaged and time-averaged mainstream velocity

u_{ref} - mainstream velocity at top of canopy

$\overline{u}_{10}$ - time-averaged velocity at 10 minutes of averaging

u' - local fluctuation from mean velocity in mainstream direction

$\sqrt{\overline{u'^2}}$, u_{rms} - turbulence intensity of u component of velocity

$\sqrt{\overline{u'^2}}_h$ - horizontally averaged turbulence intensity of u component of velocity

u_c - mainstream velocity in nearly constant portion of canopy

u_* - shear velocity

u_{rms10} - turbulence intensity of u component of velocity at 10 minutes of averaging

$\overline{u'v'}_{10}$ - value of $\overline{u'v'}$ at 10 minutes of averaging

V - volume

V - mean velocity in y-direction

v - mean velocity in a stratum

v - instantaneous velocity in bed-normal direction

v_h - horizontally averaged bed-normal velocity

$\overline{v}$ - time-averaged vertical velocity

v' - fluctuation from mean velocity in vertical direction

$\sqrt{\overline{v'^2}}$, v_{rms} - turbulence intensity of v component of velocity

W - mean velocity in z-direction

w - instantaneous velocity in spanwise direction

$\overline{w}$ - time-averaged spanwise velocity

w' - fluctuation from mean velocity in spanwise direction

$\sqrt{\overline{w'^2}}$, w_{rms} - turbulence intensity of w component of velocity

X - local resistance coefficient

x - downstream direction

y - bed-normal direction, or height above the bed

z - spanwise direction

α - dimensionless parameter characterizing plant flexibility

β - Boussinesq or momentum coefficient

Δ - characteristic roughness spacing

Δ_x - distance between obstructions in x-direction

Δ_z - distance between obstructions in z-direction

Δx - mainstream dimension of control volume

Δz - spanwise dimension of control volume

ε - turbulence dissipation rate

ϕ - angle between the roughness element and the horizontal plane

γ - specific weight of water

η - bed elevation from datum

φ - deflection angle of cylinder from vertical

μ - absolute dynamic viscosity of fluid

θ - channel bed angle from horizontal

ρ - fluid density

$-\rho\overline{u'v'}$ - dominant Reynolds stress

$-\rho\overline{u'v'}_h$ - horizontally averaged Reynolds stress

τ - total shear stress

τ_b - total bed shear stress

τ_h - horizontally averaged total shear stress

τ_{vis} - viscous shear stress

τ_{turb} - turbulent shear stress

ξ - water surface elevation from datum

1. INTRODUCTION

1.1 Motivation

Vegetation growth in open-channel waterways has been classically seen as a nuisance primarily because of the resulting reduction in discharge capacity. Maintenance work has been typically carried out to remove bank and channel vegetation for this reason. However, attitudes toward river and wetland management have been swiftly changing. The costly and ecologically harmful procedures of removing channel vegetation and destroying wetlands have been replaced by new approaches which recognize the considerable environmental benefits that vegetation brings to an aquatic ecosystem. Vegetation cover is known to increase bank stability, reduce erosion and water turbidity, provide aquatic and terrestrial wildlife, attenuate floods, provide aesthetic properties, and filter pollutants carried by runoff. The favorable effects of vegetative linings have made them a widely used and effective alternative (sometimes referred to as biotechnical stabilization) in river restoration projects.

With this new attitude towards waterway and wetland management comes an increased need for an understanding of open-channel flow through and above vegetation. Vegetative linings influence not only the flow resistance of rivers and the habitat quality, but also affect transport processes by reducing both transport capacity and entrainment capabilities of sediment into suspension. Therefore, more conclusive knowledge of the hydraulic properties of channels with vegetation is essential for their effective engineering design and for accurately assessing their influence on the total quality and effectiveness of a stream.

Historically, vegetation in waterways has been dealt with by increasing the Manning's coefficient to account for the increased roughness and decreased flow conveyance of the channel (Ree and Palmer, 1949). The Manning's n value was determined empirically and provided little insight into the fluid mechanics of this flow phenomenon. Later, more sophisticated models describing various aspects of vegetated open-channel flows were proposed (Li and Shen, 1973; Reid and Whitaker, 1976; Kao and Barfield, 1978; Hino, 1981; Burke and Stolzenbach, 1983; Christensen, 1985; Saowapon and Kouwen, 1989) and experimental observations on the turbulence structure were performed (Tsujimoto et al., 1991: Tsujimoto et al., 1992; Tsuji-

moto and Nagasaki, 1992). Although these investigations delved deeper into the flow mechanics of this process, there is still much that is unknown about the flow structure and turbulence characteristics of flow through a vegetative canopy. In addition, all of the existing models require some quantitative estimation of the ability of plants to absorb momentum by form and viscous drag, the former being typically characterized by a drag coefficient. The k-ε model proposed by Burke and Stolzenbach (1983) is significant in that it allows the drag coefficient to be specified locally within the plant canopy, although no measurements of the vertical variation of the drag coefficient exist.

Most research has not established any standards for values of drag coefficients to be used in models of vegetated channels. Thus, there is a clear need to complete research that will contribute some of the much needed hydrodynamic knowledge and further the state of knowledge of open-channel flow through vegetation.

1.2 Objectives

It is the intent of the following investigation to measure the flow and turbulence structure in and above simulated plant canopies in a laboratory flume under uniform flow conditions, thus allowing for the characterization of local and bulk drag coefficients. Recently available technology, an acoustic Doppler velocimeter, will be used for these measurements. More specifically, the research herein has the following detailed objectives:

1. To introduce a backwater model for open-channel flow through emergent vegetation to provide both a motivation for examining drag and Boussinesq coefficients and a practical application for the new knowledge resulting from the study.

2. To measure velocity and Reynolds stress profiles in and above a simulated plant canopy to learn more about the flow structure.

3. To introduce and test a new technique requiring only time-series measurements of point velocities to determine vertical profiles of the horizontally-averaged local as well as bulk values of the drag coefficient.

4. To determine the effect of flow and channel vegetation characteristics on the flow structure and the bulk drag coefficient.

In Chapter 2, a literature review is presented in which various attempts to study, model, and measure flow characteristics in vegetated channels are described. In Chapter 3, a model for open-channel flow through vegetation for non-uniform flow conditions is presented

as well as a method of computing drag coefficients under uniform flow conditions. Chapter 4 presents the experimental setup and procedure used to measure flow characteristics in a simulated vegetated channel. In Chapter 5, the results of the experimental study are presented and analyzed. Conclusions and recommendations for future research are made in Chapter 6.

2. LITERATURE REVIEW

2.1 Introduction

The flow of water and air through vegetation has received considerable attention by researchers in the past 50 years. Diverse practical interests motivated most of the early work resulting in research that was mainly empirical and observational. The flow of air through vegetation has been given the most consideration by past researchers. For the flow of water, no general and successful theory has unified this research and still much is unknown about the flow properties and turbulent characteristics induced by vegetation in an open channel. Only recently has the research emphasis shifted from primarily experimental work aimed at determining empirical methods of design towards work oriented at providing a physical explanation of the flow phenomenon.

As will be discussed in this chapter, the inclusion of vegetation in an open channel primarily affects its conveyance by increasing the flow resistance. This is accomplished by the addition of form and viscous drag from the plant stems and leaves. At high Reynolds numbers, the form drag provides the dominant resistance in the channel. A major obstacle in the study of vegetated open-channel flows has been the parameterization of this form drag through a drag coefficient. Past research into the description of the drag imposed by vegetation is the focus of the third section of this chapter. The final section is dedicated to reviewing previous methods for modeling vegetation in open-channels in the laboratory.

2.2 Flow Through and Above Vegetation

There are many aspects of flow through vegetation that have interested researchers. This section reviews the research efforts into selected aspects of this flow phenomenon. The early attempts at determining the flow capacity of a vegetated channel are discussed as well as many follow-up efforts. Other attempts at modeling flow in a vegetated channel are covered and some previous turbulence measurements in a simulated vegetated open-channel are reviewed.

Because of its importance in aerodynamics and atmospheric sciences, much of the assembled body of knowledge of flow around and through plant-like obstructions pertains to air flows. Although the two flow situations are in many ways similar, the review that follows is aimed at the study of open-channel flow through vegetation and primarily considers these endeavors.

2.2.1 Discharge Determination in a Vegetated Channel

Pioneering work into flow through vegetated channels was performed by Ree and Palmer (1949). The aim of these researchers was to determine the discharge capacity of a vegetated channel. They created a series of curves showing Manning's n values versus the product of the mean velocity, U, and the hydraulic radius, R, known as n-UR curves. Using these curves they concluded that the n-UR relationship depends on the physical properties of the grass and is independent of channel geometry and flow conditions. As did many early attempts at characterizing flow through vegetation, Ree and Palmer's method employed the often used Manning's equation and attempted to provide the necessary empirical constants. Although no theoretical justification for this approach is given and it provides little insight into the mechanics of the flow process, it does provide a useful method of estimating vegetated channel discharge and constitutes one of the earliest attempts at examining open-channel flow in a vegetated waterway.

Nicholas Kouwen with various other researchers at the University of Waterloo in Canada have attempted to reproduce the empirical n-UR curves by a mathematical model based on boundary layer theory, dimensional analysis, and parameter values from laboratory tests. In a series of laboratory experiments of flow over a cover of flexible plastic strips used to simulate grass, Kouwen and Unny (1973) determined that three possible flow regimes may exist: erect, waving, and prone. They found that the Manning's n value for the erect and waving regimes is primarily a function of the relative roughness; whereas for the prone condition, the n value is a function of the product of U and R as suggested by Ree and Palmer. They also introduced a stiffness parameter, MEI, where M is the relative density of the plants and EI is the stem flexural rigidity.

Other researchers have attempted to use Manning's equation to characterize vegetated flows. Their work is therefore steered towards determining the elusive Manning's coefficient. Petryk and Bosmajian (1975) developed a quantitative procedure for predicting the Manning's

n value as a function of flow depth and vegetation characteristics. Their method considered flow depths that were less than or equal to the maximum height of the vegetation and its most useful application is in predicting the variation of the Manning's n value with depth in a vegetated channel.

Kouwen and Li (1980) postulated that if the flow retardance value is primarily dependent on the relative roughness, then the problem of determining the Manning's n value reduces to finding the biomechanical properties of various vegetation types (i.e., the value of MEI). By using artificial flexible roughness in a manner analogous to the use of sand roughness to represent the roughness of naturally rough surfaces, they determined their stiffness parameter for various vegetation types. Kouwen (1988) later introduced two field methods for estimating the biomechanical properties of a vegetative channel lining: a "board drop test" method and a vegetation height method.

For flows through emergent vegetated wetlands, Kadlec (1990) indicated that open-channel equations, such as Manning's, should not be used because they apply to situations of fully turbulent flow where bed resistance controls the flow. In vegetated wetlands, vegetation drag is the main control mechanism and the flow is often in the transition region between turbulent and laminar flow conditions. Kadlec maintains that the appropriate choice of equations to describe the flow is the drag expression for isolated submerged objects (equation 2.1) where fluid friction is computed from drag on a single object, not channel or packed bed equations since stem spacing is large (roughly 10 stem diameters for wetland vegetation).

$$S_f = C_D a \frac{v^2}{2g} = X \frac{v^2}{2g} \tag{2.1}$$

where S_f is the friction slope, C_D is the drag coefficient, a is the frontal area per unit volume, v is the actual mean velocity in the stratum (where a stratum is a section of constant a), g is gravitational acceleration, and X is a local resistance coefficient. Kadlec introduces a computational procedure to determine discharge through a wetland using equation 2.1 and requiring knowledge of a depth-distribution function, a frontal area versus depth function, and a drag coefficient correlation.

2.2.2 Relevant Models of Vegetated Open-channel Flow

The previously described investigations were all attempts to determine the discharge capacity of a vegetated waterway, but researchers have studied other aspects of this flow phe-

nomenon. Li and Shen (1973) investigated the effect of tall emergent vegetation on flow and sediment transport by modeling the vegetation with cylinders. They employed a wake superposition method to predict the drag on each cylinder and the velocity profile across the channel when the following data were given: the size and distribution of cylinders; the discharge; the bottom slope and the width of the channel; the local coefficient of drag of the cylinders in the channel; and the flow depth. They continued their analysis by using the model to predict and compare the relative effect on sediment yields by various combinations of tall vegetation, although they only considered bedload.

Reid and Whitaker (1976) developed a numerical model to simulate steady-state water surface profiles for flat-bottomed wind driven flows through and above obstructions. They divided the water depth into two layers, one within the canopy, and one above it and averaged the equations of motion in each layer. They assumed the canopy to be composed of rigid uniform structures oriented normal to the flow and evenly distributed over the bottom. The dimensions of the vegetation and a drag coefficient were used to characterize the vegetation. Three cases were modeled to emulate possible flow conditions. In Case I, the wind was directed from the model marsh toward the open water, while the opposite was assumed for Case II. The wind was assumed to be parallel to the marsh-open water boundary for Case III. The main drawback of their method is the need to specify the value of the interfacial stress at the top of the canopy. It is also necessary to specify a drag coefficient of the roughness elements , the vegetation density, and a turbulence closure assumption for the shear stress.

Burke and Stolzenbach (1983) employed a turbulence model for flow through obstructions in which the characteristic velocity and length scales of the turbulence were computed and did not have to be specified by the user. They took a low Reynolds number k-ε model developed for non-obstructed open-channel flows and extended its capabilities to include obstructed flow processes. The two equation k-ε technique parameterized the turbulent stress using a scheme, in which the turbulence length and velocity scales were determined from differential transport equations for the turbulent kinetic energy and the turbulent dissipation rate. The model was able to accurately reproduce the vertical variation of mean horizontal velocity (velocity profile), as well as more general turbulent properties such as turbulent kinetic energy and dissipation. While their model predictions were in good agreement, they recognized the lack of knowledge about the dependence of the drag coefficient on obstruction geometry,

flexibility, and density and recommended that detailed studies be performed with this specific intent.

Additional models describing velocity profiles in and above vegetation have also received fair attention from a number of researchers. Due to the flexible nature of vegetation, velocity profiles in vegetated channel are much more complicated than those in non-vegetated channels. Researchers have found that the classic logarithmic velocity profile is adequate to describe flow over the canopy, but flow within the canopy can not be well represented by a logarithmic velocity distribution (Kouwen and Unny, 1973). Using the mixing length approach to compute eddy viscosities, Christensen (1985) developed an explicit formula for the velocity profile over a flexible roughness layer to be used in heavily vegetated rivers and channels. Using this velocity profile, he derived a Manning-type power formula for the discharge through vegetated waterways. The main value of the modified velocity profile derived by Christensen is that it provides realistic values of the velocity inside the canopy. It does however require knowledge of two roughness characteristics, the apparent roughness and the apparent thickness of the vegetative bottom layer, which must be obtained from measurements of the velocity profile.

Recently, Saowapon and Kouwen (1989) have offered a physically based model to determine the resistance parameters and velocity profiles for open channels lined with artificial flexible roughness. The model uses a force equilibrium approach to formulate the velocity distribution inside the canopy. The parameters of the model are: grass length and stiffness, coefficient of drag, and eddy viscosity. Laboratory results of flow over plastic strips show that the model accurately predicts velocity profile measurements for erect and waving roughness, but not for prone roughness. While both the Christensen model and the Saowapon and Kouwen model look rather encouraging when compared against laboratory observations, it is clear that the algebraic scheme used to compute eddy viscosities (i.e., mixing length approach) provides only limited information on the effect of roughness elements on the diffusion of momentum and sediment.

2.2.3 Turbulence Measurements in a Simulated Vegetative Canopy

Tsujimoto with other researchers at Kanazawa University in Japan have performed a number of experiments on flow over rigid and flexible vegetation. Tsujimoto, Okada, and Kitamura (1991) simulated flow over flexible vegetation by affixing strips of transparent films of equal height to the channel bottom at equal spacing. The authors noted that most natural vegetation are not inflexible, but will deform, vibrate, and sometimes sway coherently in the flow of water. Such behaviors are expected to change the turbulence characteristics of flow over a vegetated bed. They found that the induced shear flow velocity in the vegetated layer is higher in the case of flexible vegetation than in the case of rigid vegetation.

Tsujimoto et al. (1992) have measured turbulence characteristics of a steady uniform flow in laboratory flumes with cylinders of the same height, diameter, and spacing to simulate flow over rigid vegetation. Based on the experimental data, they modified the classical mixing-length model to describe the velocity profile. They found that the turbulence characteristics in the free-surface region above the canopy are little affected by the vegetation layer, while the flow in the vegetation layer is strongly affected by faster surface flows.

In an attempt to further study the flow of water over flexible vegetation, Tsujimoto and Nagasaki (1992) investigated flow over a swaying bed. They allowed the vegetation to sway in the horizontal and vertical planes only. Their measurements suggest that the velocity distribution follows the logarithmic law if the theoretical wall (i.e. zero velocity) is postulated inside the vegetation layer. The theoretical wall falls with increasing flow velocity. The drawback of shifting the origin of the logarithmic law into the vegetation layer is that it yields unrealistic negative values near the bed.

2.3 Drag in Simulated Vegetation

The common assumption of most laboratory models is that vegetation can be simulated in a laboratory flume with cylindrical objects and that the Reynolds number of the flow is sufficiently high enough that form drag dominates and therefore viscous drag can be neglected. The form drag force exerted by a single infinite cylinder in a uniform flow of velocity u_∞ is typically parameterized through a drag coefficient as follows:

$$F_D = \frac{\rho A C_D u_\infty^{\,2}}{2} \tag{2.2}$$

where F_D is drag force, ρ is fluid density, A is obstructed area of the cylinder, and C_D is a drag coefficient. Usually, researchers determine the pressure on an object, and then integrate the pressure over the surface area of the object to find the drag force. The water velocity is measured with an instrument such as a hot-wire anemometer and equation 2.2 is then solved for C_D. What follows is a review of the attempts and current theories on the characterization of the drag coefficient, C_D.

2.3.1 Drag on a Single Cylinder

Drag on a single semi-infinite cylinder in uniform flow has been researched extensively and is commonly discussed in general fluid mechanics text books (Schlichting, 1979; Vennard and Street, 1982; Granger, 1985). Early work was performed by Tritton (1959) on flow past a circular cylinder at low Reynolds numbers and by Roshko (1960) on flows at high Reynolds numbers. As is common, these researchers placed a rigid cylindrical object in a wind tunnel. There are number of ways of measuring the drag. Tritton calculated the drag by measuring the deflection of a cylindrical fiber and using simple bending moment theory. Roshko employed a more direct method by locating pressure orifices in the cylinders and connecting pressure transducers.

Researchers have found that the drag coefficient on a single cylinder is highly dependent on the cylinder Reynolds number, Re_D. White (1991) has offered a fairly simple curve-fit formula

$$C_D \approx 1 + \frac{10}{\mathrm{Re}_D^{2/3}} \tag{2.3}$$

which fits fairly well up to $Re_D \approx 10^3$. From $Re_D \approx 10^4$ to $Re_D \approx 10^5$, $C_D \approx 1.2$. Figure 2.1 has been extracted from Schlichting (1979) and shows the standard drag coefficient curve for cylinders.

Graf and Ko (1971) have postulated that the turbulence intensity of the flow affects the drag coefficient. They claim that at low turbulence intensities, less than 7%, the drag coefficient will be below the standard C_D versus Re_D curve. And likewise at higher turbulence intensities, greater than 10%, the drag coefficient will be above the standard C_D versus Re_D curve. Furthermore, an increase in turbulence intensity will cause an increase in the drag coefficient. They conclude that while the turbulence intensity exerts a noticeable influence upon the drag coefficient, the effect of the cylinder Reynolds number is less pronounced. Little work has been done to support this theory.

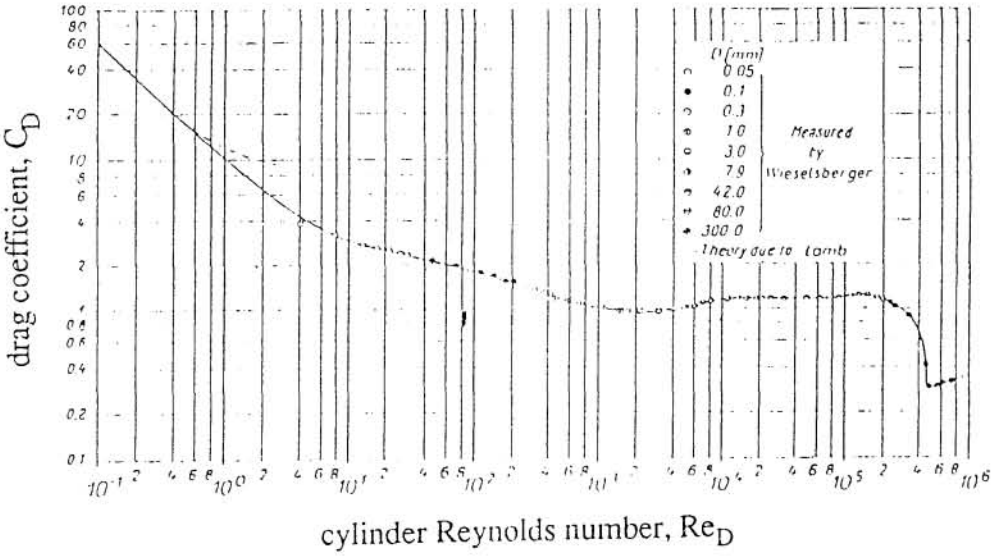

Figure 2.1 Standard cylinder drag curve
(extracted from Schlichting, 1979)

2.3.2 Drag on Two Cylinders

When one begins to study flow through, and the subsequent drag on two or more cylinders, the problem becomes complicated very quickly. The flow interference between the cylinders will vary depending on the cylinder pattern, spacing, and flow characteristics. A review of the available literature reveals a disordered and fragmented body of research performed with the primary interest of solving immediate and practical problems in various branches of engineering and science.

A general review on the flow interference between two circular cylinders was performed by Zdravkovich (1977). Zdravkovich and Pridden (1977) also completed experimental work using a wind tunnel and pressure tappings equally spaced around the periphery of the cylinder. The review of this research has provided insight into how the drag coefficient varies when two cylinders are placed at various positions with respect to each other, however the flow situation through a vegetative canopy is much more complex because of the mutual interference of neighboring obstructions. Also, vegetation in open-channels are generally spaced many diameters apart, may be of various shapes and geometries, and may be flexible as well a rigid, consequently further complicating the problem.

2.3.3 Drag in Vegetated Channels

Characterizing the drag in models of open-channels with vegetative linings is a much more complicated task than that tackled by the investigators mentioned above. The previously mentioned studies considered ideal flow conditions where the velocity profile was uniform along the axis of the cylinder. Drag in vegetated open-channels is complicated by free surface effects, turbulence, and non-uniform velocity profiles. The effects of each of these is discussed by Petryk (1969). Also many adjacent obstructions may alter the drag of a single cylinder. These complications make the utility of equation 2.2 very limited for vegetated open-channels. To overcome these difficulties, researchers have defined bulk, or mean, drag coefficients such as

$$F_D = \rho \frac{A\overline{C_D}U^2}{2} \tag{2.4}$$

where $\overline{C_D}$ is a bulk drag coefficient and U is the average channel velocity. $\overline{C_D}$ characterizes the average drag force imposed by the cylinder canopy and is therefore constant everywhere in

the canopy. Generally, A is computed by multiplying the cylinder diameter by either the cylinder height or the water depth, whichever is smaller. Some researchers have set up laboratory arrangements to measure the value of $\overline{C_D}$. Others have actually taken field measurements in streams, marshes, floodplains, fields, forests, and wetlands. Much of this work is described in Section 2.1 and although most of this work was not specifically performed to determine the drag coefficient, an estimate of the drag coefficient was needed in the models. This section is devoted to examining previous attempts at measuring drag coefficients in vegetated boundary layer flows, and reviews the estimates of the drag coefficients used in various vegetation models. A summary of these investigations is presented in Table 2.1.

As mentioned above, Li and Shen (1973) used a wake superposition model and the experimental results of Petryk (1969) to predict a bulk drag coefficient in a channel with emerging cylinders where free surface effects were small (i.e. low Froude numbers). They defined the bulk drag coefficient by equation 2.4 using the mean channel velocity and the flow depth. In their model, they chose a constant local drag coefficient (the drag coefficient on a single cylinder) of 1.2 as reported in standard texts for the cylinder Reynolds number range of 8×10^3 to 2×10^5 since there was "no strong evidence to prove otherwise". These researchers studied numerically the effects of cylinder spacing and pattern on the bulk drag coefficient. They found that the mean drag coefficient within the vegetative canopy reached some asymptotic value as the point of interest progressed downstream, usually about 200 diameters downstream of the first cylinder. This asymptotic value was between 1.1 and 1.2 for staggered cylinders and a cylinder Reynolds number of 9×10^3. The bulk drag coefficient slightly decreased with increased spacing, but at greater than eight diameter spacing, the drag coefficient remained relatively constant at approximately 1.13.

Table 2.1 Summary of Bulk Drag Coefficient Measurements in Turbulent Shear Flows

Researcher	Obstruction material	Obstruction shape	Fluid	Computational method	Investigation type	$\overline{C_D}$ value
Li and Shen (1973)	rigid	cylinders	water	wake superposition model	computational	1.13
Klaassen and Van Der Zwaard (1974)	fairly rigid shrubs	fruit trees	water	Chezy formula	laboratory	~ 1.5
den Hartog and Shaw (1975)	flexible corn canopy	corn stalks	air	momentum balance	field	~ 0.3
Reid and Whitaker (1976)	rigid wire screen	cylinders	water	Manning's equation	laboratory	1.77
Seginer et al. (1976)	rigid aluminum	cylinders	air	momentum balance	laboratory	~ 0.4
Burke and Stolzenbach (1983)	flexible stems	cylinders	water	k-ε model	computational	2.5
Saowapon and Kouwen (1989)	flexible plastic	cylinders	water	$\overline{C_D} = 2.0 \cdot \sin^3 \phi$	laboratory	varies from 0 to 2.0

Klaassen (1974) has criticized the magnitude of the values determined by Li and Shen. In a model study of the effect of fruit trees on the roughness of floodplains, Klaassen and Van Der Zwaard (1974) obtained significantly higher values than 1.2 for bulk drag coefficients. They computed their drag coefficients with the help of the Chezy formula. Klaassen states that the higher values of the mean drag coefficient may have been caused by a higher turbulent intensity in the fruit tree experiments. Li and Shen (1974) comment that inaccurate projected-area values may have been used in Klaassen's work which would result in higher mean drag coefficients than 1.2 to compensate for the effect of tree branches, etc.

Consistent with Li and Shen's conclusions, however, is Klaassen and Van Der Zwaard's finding of a slight tendency for a decrease of the bulk drag coefficient with an increase of the mean distance between the trees normal to the flow direction. This is at odds with the finding of Seginer et al. (1976) who noted in a review of data from compact heat exchangers that the bulk drag coefficient of circular cylinders decreased with increasing density. Seginer's data came from studying compact heat exchangers at $Re_D \approx 10^3$. The cylinder density varied up to 50 per meter, which is an order of magnitude higher than that found in natural vegetative canopies. Such a large difference in the obstruction density brings into question the applicability of these data for vegetated channels.

From experiments in a wind tunnel, Seginer et al. (1976) also estimated local drag coefficients within the canopy by two different methods. The first method was from a balance of horizontal momentum in a uniform canopy flow and required measurements of flow velocity and shear stress within the canopy. The second method was from pressure tappings around one the rods in their experiments. These researchers found that increasing the cylinder density increased the turbulence intensity inside the canopy and they believed that this caused the decrease in the drag coefficient described above. This conclusion is in direct contrast to the conclusion of Graf and Ko as discussed earlier, although Graf and Ko's results were for a single obstruction. Seginer et. al also measured the vertical variation of the local drag coefficient within the canopy by the two methods and found that there was a slight tendency for the local drag coefficient to increase with distance from the bed. It is worth noting that the author has found that investigations of air flow vegetation have consistently found drag coefficient values that are significantly smaller than values found for the flow of water through vegetative canopies.

In a series of laboratory experiments aimed at developing a method to determine the flow depth in a vegetated channel, Kao and Barfield (1978) evaluated the drag coefficient. They assumed that since flow through vegetation is usually quite slow, viscous shear, rather than turbulent shear dominates near the channel bed. They then used conservation of momentum and their knowledge of the velocity distribution and shear stress within the viscous flow region near the boundary to derive an equation for the drag coefficient. They grouped $\overline{C_D}$ with the number of vegetation obstructions in a unit area, N, the specific weight of water, γ, and the channel slope, S, to form a parameter, $(N \cdot \overline{C_D} / \gamma \cdot S)$. They found distinctive relationships between their resistance parameter and the cylinder Reynolds number. However, since the drag coefficient varies significantly less than the other parameters in their resistance coefficient, there remains considerable doubt that the drag coefficient has any actual effect on their resistance parameter. A more critical characteristic of their resistance parameter is that it is not dimensionless. In fact, the dimensions of the results reported by Kao and Barfield are not even reported making it impossible to effectively use their results.

Other researchers have used various values and equations for the drag coefficient without performing tests to specifically determine its value. Reid and Whitaker (1976) estimated the bulk drag coefficient to be 1.77 by analyzing measurements of Manning's n as a function of roughness spacing for different mean depths, and used this value in all applications of their numerical model. Their model considered submerged rigid cylindrical obstructions and they defined the bulk drag coefficient with equation 2.4 using the mean velocity in the plant canopy and the vegetation height. Although their model allowed for C_D to vary in the vertical direction, Burke and Stolzenbach (1983) determined that a constant value of $C_D = 2.5$ would work for their entire velocity range for stems in a *Spartina* marsh. They did however explicitly recognize the lack of knowledge of the precise value of the drag coefficient and its variance with flow, channel, and vegetation parameters. They recommended research be conducted at this specific aim. Saowapon and Kouwen (1989) related the bulk drag coefficient to the angle between the roughness element and the horizontal plane, ϕ, as given by Hoerner (1958):

$$\overline{C_D} = 2.0 \cdot \sin^3 \phi \qquad (2.5)$$

They defined the bulk drag coefficient for submerged vegetation with the mean channel velocity and the frontal area of the plants. Kadlec (1990) recommends using the standard drag coefficient curve to determine C_D in his model where he allows C_D to vary in the vertical.

A field study was performed by den Hartog and Shaw (1975) of atmospheric exchange processes within a corn canopy. In this study, they determined values of a mean drag coefficient, C_D'' . Their mean drag coefficient was defined so that it represented the total effect of the vegetation layer on the flow at any given point such that:

$$\tau(y) = \rho \cdot C_D''(y) \cdot u(y)^2 \tag{2.6}$$

This drag coefficient therefore varied from point to point within the boundary layer and had non-zero values above the canopy top. They found mean drag coefficients between 0.2 and 0.043 which varied with the depth above the bed. They attempted to describe the vertical profile of their mean drag coefficient within the canopy and found that the mean drag coefficient increased with depth into the canopy and approximated the profile with the following exponential relationship:

$$C_D''(y) = C_D''(h_p)\exp\left[2.34\left(1 - y/h_p\right)\right] \tag{2.7}$$

where h_p is the average canopy height and y is the height above the bed. They also found that the mean drag coefficient was not dependent on the velocity at the measuring height.

2.4 Modeling Vegetation in the Laboratory

The majority of the detailed studies of flow with vegetation have been performed in the laboratory. The mechanics of vegetated open-channel flow is extremely complex. Factors such as vegetation height, density, stiffness, and size are crucial. Channel characteristics such as slope, bed roughness, and channel dimensions are also critical parameters. The characteristics of the flow itself, for example the flow velocity and depth, can also play an important part in the flow mechanics. The large number of meaningful parameters makes the laboratory environment an ideal place to study this flow process. In the following, the attempts by previous researchers at modeling vegetation in the laboratory are reviewed.

Many researchers have used simulated vegetation in laboratory flumes to model actual vegetation in open channels. Both rigid and flexible materials have been used by past researchers. Although the least realistic, rigid vegetation is the easiest to simulate in the laboratory. The common assumption is that the vegetation in open channels can be modeled by cylindrical objects spaced many diameters apart. The materials used to simulate rigid vegetation vary and seem to be limited only by the imagination of the researcher. Petryk (1969) em-

ployed metal and Plexiglas cylinders. Tollner (1974) mounted nails in a plywood base in an attempt to analyze sediment filtration in vegetated channels. Although the material is not specified, Tsujimoto et. al. (1992) used cylinders of equal height and diameter placed at equal spacing in a square pattern on smooth flume beds to model rigid vegetation.

Modeling vegetation with rigid cylinders has its advantages, primarily because it simplifies set-up and flow modeling. Allowing for deformation in the cylinder introduces parameters which are difficult to determine and many times results in the vegetation vibrating or even swaying coherently, thus further complicating the equations of flow and drag. It is imperative to understand the relevant flow processes through rigid cylinders before the more difficult task of examining those same flow processes through simulated flexible vegetation. Of course the major disadvantage of studying simulated rigid vegetation is that it is relevant to few natural channels. Other than very slow flow through vegetation or flow through rigid trees, natural vegetation will bend when subjected to the force of flowing water.

Realizing the limited applicability of studying rigid vegetation, many researchers have attempted to model flexible vegetation in the laboratory. The difference between flow over a flexible lining and a lining composed of rigid material lies in the tendency of flexible material to deform under an imposed shear. Generally, investigators have used some sort of plastic to model flexible plants. Kao and Barfield (1978), Kouwen and Li (1980), and Tsujimoto and others (1991) have all used plastics strips of various flexibilities in their laboratory models. Again, researchers believe that flexible plastic more closely imitates the behavior of actual vegetation when subjected to fluid flow. Some arguments supporting this conclusion has been presented quite clearly by Kouwen and Li (1980). They claim that both flexible plastic roughness and actual vegetation have the three basic flow regimes discussed earlier. Also laboratory measurements with artificial roughness results in n-UR curves and velocity profiles that agree closely to those of natural flexible roughness.

3. THEORETICAL ANALYSIS

3.1 Introduction

As cited in Chapter 2, many models have been developed for flow through vegetative linings under uniform flow conditions. The following discussion rigidly formulates a model for non-uniform flow conditions. Boundary layer theory is applied to open-channel flow through emergent vegetation resulting in a backwater flow model. As it is common in models of vegetated channels, the resistance to the flow caused by the vegetation is characterized by a drag coefficient in this model. The largest obstacle to the characterization of the frictional resistance to flow induced by vegetation is in the determination of such drag coefficient. The need for this coefficient in the backwater model, as well as in the models discussed previously, provides sufficient motivation for experimentally investigating vegetation-induced drag. This chapter reviews the concept of Reynolds stress and describes a new experimental technique which allows for the computation of local drag coefficients from measurements of the vertical profiles of Reynolds stress and velocity under uniform flow conditions. The final section of this chapter introduces various definitions of the bulk drag coefficient which will be useful in this study.

3.2 Boundary Layer Theory Applied to Open-channel Flow Through Vegetation

The following theory was first proposed by García (1994) and formulates a backwater equation for open-channel flow through emerging vegetation, such as in a wetland. The need for information about assumptions made and coefficients required in this formulation warrants the laboratory investigation described in Chapters 4 and 5.

Consider open-channel flow through emergent vegetation modeled as cylinders as illustrated in Figure 3.1. For the remainder, the following nomenclature is maintained: x, y, and z = downstream, bed-normal, and spanwise directions, respectively; and u, v, and w = instantaneous velocities in downstream, bed-normal, and spanwise directions, respectively. θ, η, and ξ are defined in Figure 3.1. The bed-normal direction will often be referred to as vertical because the

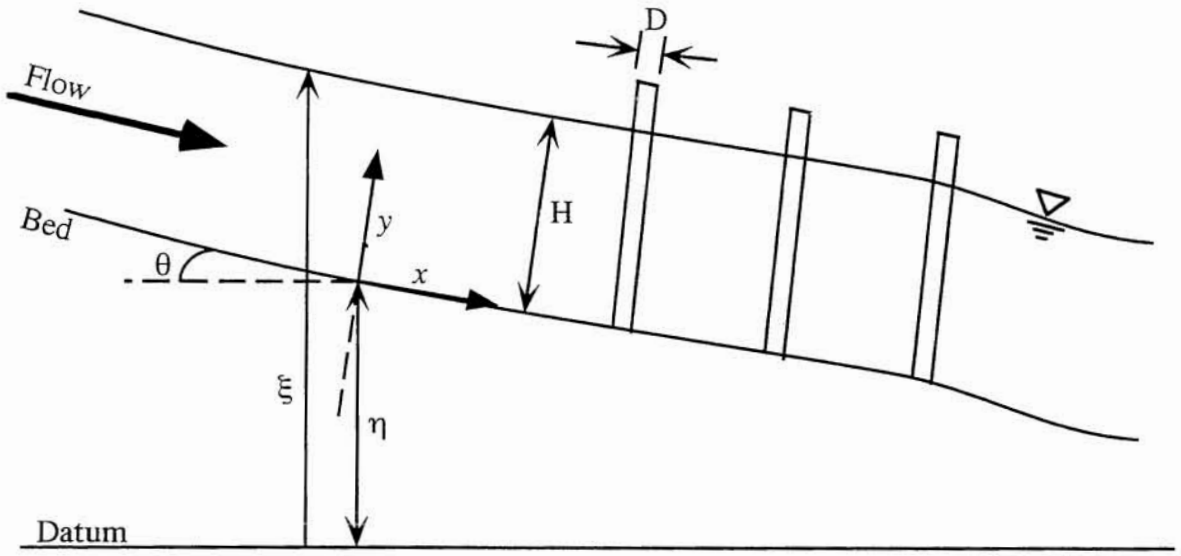

Figure 3.1 Open-channel flow through emergent vegetation

bed slopes of most natural channel are extremely small, and therefore so are values of θ as defined in Figure 3.1. This approximation will not introduce any significant errors.

Assume two-dimensional, steady, non-uniform flow with no lateral inflows and that the boundary layer approximation is valid so that $u >> v$ and $\frac{\partial}{\partial y} >> \frac{\partial}{\partial x}$ everywhere. The local bed slope, S, is

$$S = -\frac{\partial \eta}{\partial x} \tag{3.1}$$

The system x-y is a local boundary layer coordinate system, then the gravitational acceleration vector, $\vec{g}$, is defined as

$$\vec{g} = \left(g \cdot \sin\theta, -g \cdot \cos\theta\right) \tag{3.2}$$

where g is the gravitational acceleration. For wetlands and most natural open-channels, the angle θ is very small, therefore

$$\cos\theta \equiv 1 \quad \text{and} \quad \sin\theta \equiv \tan\theta \tag{3.3a,b}$$

and

$$\vec{g} = \left(g \cdot \tan\theta, -g\right) = \left(+g\frac{\partial \eta}{\partial x}, -g\right) \tag{3.4}$$

The drag force per unit volume, f_D, can be represented by the following relation

$$f_D = \tfrac{1}{2} a \rho C_D' u_h^2 \tag{3.5}$$

where u_h is the mainstream velocity averaged in the horizontal plane, C_D' is a local drag coefficient that is also averaged in the horizontal plane, ρ is the density of the water, and a is the vegetation density or the frontal area of a plant per unit volume having units of L^{-1}. If the plants are assumed to be cylindrical and equally spaced throughout the channel, a can be computed by

$$a = \frac{A}{V} = \frac{D \cdot H}{(\Delta_x \cdot \Delta_z)H} = \frac{D}{\Delta^2} \tag{3.6}$$

where A is frontal area of the cylinder, V is volume influenced by a single cylinder, D is cylinder diameter, H is the flow depth, and Δ_x and Δ_z are the distance between plants in the x and z directions, respectively.

Raupach and Shaw (1982) presented a procedure for multiconnected flow regions, in particular for atmospheric flows through vegetation, to transform the three-dimensional governing equations into a more tractable one-dimensional frame of work. Following this approach, the drag-related (and other additional dispersive) terms naturally appear in the equations as a consequence of the averaging procedure and the non-commuation of spatial average and spatial derivation for some variables, in particular for horizontal pressure fluctuations. More recently, Lopez and Garcia (1996) applied this procedure to obtain the one-dimensional conservation laws for uniform open-channel flow in the presence of vegetation. Following this approach, it can be shown that the resulting momentum equation contains horizontally averaged values of mainstream and bed-normal velocity, u_h and v_h respectively, total shear stress (defined as viscous plus turbulent shear stress), τ_h, and pressure, p_h, and includes a term characterizing the drag force with the horizontally averaged drag coefficient C_D'

$$\frac{\partial u_h}{\partial t} + u_h \frac{\partial u_h}{\partial x} + v_h \frac{\partial u_h}{\partial y} = -\frac{1}{\rho}\frac{\partial p_h}{\partial x} + \frac{1}{\rho}\frac{\partial \tau_h}{\partial y} + gS - \tfrac{1}{2} C_D' a u_h^2 \tag{3.7}$$

(Herein the temporal and spatial fluctuations due to the turbulence and the vegetation, respectively, are assumed to have smaller scales than the horizontal variations due to any backwater effect) The momentum equation in the vertical, y, direction can be reduced to approximately

$$0 = -\frac{1}{\rho}\frac{\partial p_h}{\partial y} + g \tag{3.8}$$

Integrating 3.8 once with respect to y yields

$$p_h = -\rho g y + \text{constant} \tag{3.9}$$

Using as a boundary condition that the pressure at the free surface is equal to zero, then

$$p_h\Big|_{y=H} = -\rho g H + \text{constant} = 0 \tag{3.10}$$

so

$$p_h = \rho g (H - y) \tag{3.11}$$

where H is a function of x. Rearranging and taking the partial derivative in the x direction leads to

$$\frac{1}{\rho}\frac{\partial p_h}{\partial x} = g\frac{\partial H}{\partial x} \tag{3.12}$$

which can be substituted into equation 3.7 to produce

$$\frac{\partial u_h}{\partial t} + u_h \frac{\partial u_h}{\partial x} + v_h \frac{\partial u_h}{\partial y} = -g\frac{\partial H}{\partial x} + \frac{1}{\rho}\frac{\partial \tau_h}{\partial y} + gS - \tfrac{1}{2} C_D' a u_h^2 \tag{3.13}$$

With the help of the two-dimensional horizontally averaged fluid mass conservation law

$$\frac{\partial u_h}{\partial x} + \frac{\partial v_h}{\partial y} = 0 \tag{3.14}$$

the momentum equation 3.13 can be rewritten as

$$\frac{\partial u_h}{\partial t} + \frac{\partial u_h^2}{\partial x} + \frac{\partial u_h v_h}{\partial y} = -g\left(\frac{\partial H}{\partial x} - S\right) + \frac{1}{\rho}\frac{\partial \tau_h}{\partial y} - \frac{1}{2} C_D' a u_h^2 \tag{3.15}$$

In order to integrate both conservation equations in the vertical we will make use of Leibnitz' rule, which states:

$$\int_{\alpha_1}^{\alpha_2} \frac{\partial F}{\partial x}\, dy = F_{(y=\alpha_1)} \frac{\partial \alpha_1}{\partial x} - F_{(y=\alpha_2)} \frac{\partial \alpha_2}{\partial x} + \frac{\partial}{\partial x} \int_{\alpha_1}^{\alpha_2} F\, dy \tag{3.16}$$

Let us start the vertical intergation ($\alpha_1 = 0 \quad , \alpha_2 = H$) with the continuity equation 3.14. Using Leibnitz rule the first term on the left can be written as:

$$\int_0^H \frac{\partial u_h}{\partial x} dy = \frac{\partial}{\partial x} \int_0^H u_h\, dy - u_{h(y=H)} \frac{\partial H}{\partial x} \tag{3.17}$$

whereas the second term yields:

$$\int_0^H \frac{\partial v_h}{\partial y} dy = v_{h(y=H)} - v_{h(y=0)} = v_{h(y=H)} \tag{3.18}$$

So that the integrated continuity equation becomes:

$$\frac{\partial}{\partial x} \int_0^H u_h\, dy - u_{h(y=H)} \frac{\partial H}{\partial x} + v_{h(y=H)} = 0 \tag{3.19}$$

which by using the kinematic boundary condition at the free surface:

$$\frac{\partial H}{\partial t} + u_{h(y=H)} \frac{\partial H}{\partial x} = v_{h(y=H)} \tag{3.20}$$

finally becomes:

$$\frac{\partial H}{\partial t} + \frac{\partial}{\partial x} \int_0^H u_h\, dy = 0 \tag{3.21}$$

Let us integrate now the momentum equation term by term, starting with the first term on the left of equation 3.15:

$$\int_0^H \frac{\partial u_h}{\partial t} dy = \frac{\partial}{\partial t} \int_0^H u_h \, dy - u_{h(y=H)} \frac{\partial H}{\partial t} \tag{3.22}$$

Integration of the second and third terms yield:

$$\int_0^H \frac{\partial u_h^{\,2}}{\partial x} dy + \int_0^H \frac{\partial u_h v_h}{\partial y} dy = \frac{\partial}{\partial x} \int_0^H u_h^{\,2} \, dy - u_h^{\,2}{}_{(y=H)} \frac{\partial H}{\partial x} + u_{h(y=H)} v_{h(y=H)} - u_{h(y=0)} v_{h(y=0)} \tag{3.23}$$

So that the integrated left hand side of equation 3.15 yields:

$$\int_0^H \frac{\partial u_h}{\partial t} dy + \int_0^H \frac{\partial u_h^{\,2}}{\partial x} dy + \int_0^H \frac{\partial u_h v_h}{\partial y} dy =$$

$$\frac{\partial}{\partial t} \int_0^H u_h \, dy - u_{h(y=H)} \frac{\partial H}{\partial t} + \frac{\partial}{\partial x} \int_0^H u_h^{\,2} \, dy - u_h^{\,2}{}_{(y=H)} \frac{\partial H}{\partial x} + u_{h(y=H)} v_{h(y=H)} - u_{h(y=0)} v_{h(y=0)} \tag{3.24}$$

Considering the kinematic boundary condition at the free surface, and the fact that $u_{h(y=0)} v_{h(y=0)} = 0$, equation 3.24 simplifies to:

$$\int_0^H \frac{\partial u_h}{\partial t} dy + \int_0^H \frac{\partial u_h^{\,2}}{\partial x} dy + \int_0^H \frac{\partial u_h v_h}{\partial y} dy = \frac{\partial}{\partial t} \int_0^H u_h \, dy + \frac{\partial}{\partial x} \int_0^H u_h^{\,2} \, dy \tag{3.25}$$

And finally the integrated x-momentum equation yields:

$$\frac{\partial}{\partial t} \int_0^H u_h \, dy + \frac{\partial}{\partial x} \int_0^H u_h^{\,2} dy = -g \left(\frac{\partial H}{\partial x} - S \right) \int_0^H dy + \left(\tau_h \big|_H - \tau_h \big|_0 \right) \frac{1}{\rho} - \tfrac{1}{2} a \int_0^H C_D' \, u_h^{\,2} dy \tag{3.26}$$

In what follows we will assume negligible shear stress at the free surface (i.e. $\tau_h \big|_H = 0$). If we further define a mean or bulk drag coefficient, $\overline{C_D}$, then

$$\overline{C_D} \int_0^H u_h^{\,2} dy = \int_0^H C_D' \, u_h^{\,2} dy \tag{3.27}$$

Furthermore, if we assume similarity for u_h so that

$$u_h = U \cdot f(\eta_*) \quad \text{where} \quad \eta_* = \frac{y}{H} \tag{3.28a,b}$$

and U is the space-averaged downstream flow velocity, we can define a shape factor, β, such that

$$\int_0^1 f(\eta_*)^2 \, d\eta_* = \beta \tag{3.29}$$

β is commonly known as the momentum or Boussinesq coefficient (Chow, 1959; Henderson, 1966; Chow et al., 1988). Equation 3.27 leads to the following expression

$$\int_0^H u_h^{\,2} dy = U^2 H \int_0^1 f(\eta_*)^2 d\eta_* = U^2 H \beta \tag{3.30}$$

The value of the Boussinesq coefficient, β, can easily be determined in a laboratory investigation by measuring velocity profiles in vegetated channels. β is always slightly larger than the limiting value of unity at which the velocity distribution is strictly uniform. Chow (1959) reports that for a fairly straight prismatic open-channel, β averages around 1.05. For a velocity distribution with the 1/6 power law, β is 1.02. For river valleys with floodplains, β can range up to 1.33 (Chow et al., 1988). Notice that β is not a function of x because of the similarity assumption.

Finally, after performing the integrals in equation 3.26 and substituting equations 3.27, and 3.30 the steady-state momentum equation can be written as

$$\frac{dU^2 H\beta}{dx} = -gH\frac{dH}{dx} + gHS - \frac{\tau_b}{\rho} - \tfrac{1}{2}\overline{C_D} a U^2 H\beta \tag{3.31}$$

The left hand side of equation 3.31 can be rewritten as

$$\frac{dU^2 H\beta}{dx} = \underbrace{U\beta\frac{dUH}{dx}}_{=0} + UH\beta\frac{dU}{dx} \tag{3.32}$$

The first term of right hand side of equation 3.32 can be eliminated because the specific discharge q = UH is constant under steady conditions, so

$$UH\beta\frac{dU}{dx} = U^2\beta\frac{dH}{dx} + H\beta\frac{dU^2}{dx} \tag{3.33}$$

and

$$UH\beta\frac{dU}{dx} = U^2\beta\frac{dH}{dx} + 2\cdot UH\beta\frac{dU}{dx} \tag{3.34}$$

and therefore

$$UH\beta\frac{dU}{dx} = -U^2\beta\frac{dH}{dx} = \frac{dU^2 H\beta}{dx} \tag{3.35}$$

Substituting equation 3.35 into 3.31 and dividing through by gH yields

$$\left(1 - \frac{U^2\beta}{gH}\right)\frac{dH}{dx} = S - \frac{\tau_b}{\rho gH} - \frac{1}{2g}\overline{C_D} a U^2\beta \tag{3.36}$$

Introducing the friction slope, S_f, and the Froude number, Fr, as defined below

$$S_f = \frac{\tau_b}{\rho g H} \tag{3.37}$$

and

$$Fr = \sqrt{\frac{U^2}{gH}} \tag{3.38}$$

equation 3.36 can be reduced to

$$\boxed{\frac{dH}{dx} = \frac{S - S_f - \frac{1}{2}\overline{C_D} aH \cdot Fr^2 \beta}{\left(1 - Fr^2 \beta\right)}} \tag{3.39}$$

which is simply a backwater curve for open-channel flow through emerging vegetation. Under uniform flow conditions, when no backwater effects are present, equation 3.39 reduces to

$$S - S_f - \tfrac{1}{2}\overline{C_D} aH \cdot Fr^2 \beta = 0 \tag{3.40}$$

The coefficients $\overline{C_D}$ and β must be determined by experimentation. This is part of the motivation for the experimental study described in Chapters 4 and 5. Values of $\overline{C_D}$ and β are determined under uniform flow conditions in a simulated vegetative canopy, and are therefore applicable to equation 3.40. It is expected that the values of $\overline{C_D}$ and β obtained for uniform flow conditions are approximately equal to the values needed for the backwater equation 3.39. A new technique for obtaining drag coefficients from laboratory measurements is introduced below.

3.3 Reynolds Stresses

With the intent of devising a method to experimentally determine drag coefficients, the following theory is reviewed. For incompressible turbulent flow the Navier-Stokes and continuity equations are as follows:

x-momentum

$$\rho \frac{\partial u}{\partial t} + \rho \frac{\partial \left(u^2\right)}{\partial x} + \rho \frac{\partial (uv)}{\partial y} + \rho \frac{\partial (uw)}{\partial z} = -\frac{\partial p}{\partial x} + \mu \nabla^2 u + \rho g_x \tag{3.41}$$

y-momentum

$$\rho \frac{\partial v}{\partial t} + \rho \frac{\partial (uv)}{\partial x} + \rho \frac{\partial \left(v^2\right)}{\partial y} + \rho \frac{\partial (vw)}{\partial z} = -\frac{\partial p}{\partial y} + \mu \nabla^2 v + \rho g_y \tag{3.42}$$

z-momentum

$$\rho\frac{\partial w}{\partial t}+\rho\frac{\partial(uw)}{\partial x}+\rho\frac{\partial(wu)}{\partial y}+\rho\frac{\partial(w^2)}{\partial z}=-\frac{\partial p}{\partial z}+\mu\nabla^2 w+\rho g_z \tag{3.43}$$

and

$$\frac{\partial u}{\partial x}+\frac{\partial v}{\partial y}+\frac{\partial w}{\partial z}=0 \tag{3.44}$$

where μ is the absolute dynamic viscosity of the fluid and g_x, g_y, and g_z are the components of the gravitational acceleration projected in the x, y, and z directions, respectively.

If Reynolds averaging is used to obtain the time-averaged continuity relation, the resulting equation will take the same form as the instantaneous continuity relation 3.44. However, if equations 3.41 through 3.43 are also time averaged, the resulting equations will contain mean values of velocity and pressure plus three mean products of fluctuating velocities. The fluctuations about the mean velocity in the mainstream, vertical, and spanwise directions are denoted as u', v', and w', respectively. In a uniform, steady, incompressible flow, only the time-averaged momentum equation in the mainstream, or x, direction is of any consequence (the other momentum equations reduce to the law of hydrostatic pressure with the help of the boundary layer approximation). When the mean pressure does not vary with x, it takes the form

$$0=\rho g_x+\frac{\partial}{\partial x}\left(\mu\frac{\partial\overline{u}}{\partial x}-\rho\overline{u'^2}\right)+\frac{\partial}{\partial y}\left(\mu\frac{\partial\overline{u}}{\partial y}-\rho\overline{u'v'}\right)+\frac{\partial}{\partial z}\left(\mu\frac{\partial\overline{u}}{\partial z}-\rho\overline{u'w'}\right) \tag{3.45}$$

The three terms $-\rho\overline{u'^2}$, $-\rho\overline{u'v'}$, and $-\rho\overline{u'w'}$ are known as apparent, turbulent, or Reynolds stresses because they represent momentum transfer due to turbulence and are paired alongside the viscous stress terms $\mu(\partial\overline{u}/\partial x)$, etc. The stress $-\rho\overline{u'v'}$ associated with x-y plane normal to the bed is dominant in fully turbulent uniform flow, and we can approximate equation 3.45 with good accuracy with a simpler streamwise momentum equation

$$0\cong\rho g_x+\frac{\partial\tau}{\partial y} \tag{3.46}$$

where

$$\tau=\mu\frac{\partial\overline{u}}{\partial y}-\rho\overline{u'v'}=\tau_{vis}+\tau_{turb} \tag{3.47}$$

For fully turbulent uniform flow in a wide rectangular open-channel with a viscous sublayer, the partition of the total shear stress between the laminar shear stress and turbulent

Reynolds stress is illustrated in Figure 3.2. The mean total shear stress varies linearly and follows the equation

$$\tau = \tau_b \left(1 - \frac{y}{H}\right) \tag{3.48}$$

where

$$\tau_b = \rho g H S \tag{3.49}$$

Equations 3.48 and 3.49 can be derived by integrating equation 3.46 from the bed to the free surface, and with the conditions of vanishing mean shear and normal stress at the water surface. In many practical cases of turbulent flow, the apparent, or Reynolds stress far outweighs its viscous counterpart outside the viscous sublayer, with the result that the viscous stress can be neglectedwith very little loss of accuracy. The viscous stress is important only very near the bed in the viscous sublayer. In all other cases the turbulent stress dominates so

$$\tau = -\rho \overline{u'v'} \tag{3.50}$$

The relation described by equation 3.50 is commonly termed the Reynolds stress in the remainder of this work although it is understood that it is just one of nine stress terms in the Reynolds stress tensor.

3.4 Experimental Determination of the Drag Coefficient

The above review of the computational formation of Reynolds stress is useful in describing the shear stress in a flow and leads to an experimental method to estimate drag coefficients. In uniform open-channel flow with no sidewall effects, we can substitute equation 3.50 into equation 3.46 and simplify to formulate an equation for the rate of change of the total shear stress in the vertical direction, y, outside the viscous sublayer

$$\frac{d\tau}{dy} = \frac{d\left(-\rho \overline{u'v'}\right)}{dy} = -\rho g S \tag{3.51}$$

Equation 3.51 is consistent with figure 3.2 in that the slope of the total shear stress curve should be constant and negative.

The addition of cylindrical obstructions in the channel is expected to suppress the turbulent Reynolds stress within the cylinder canopy as discussed in Chapter 2. Figure 3.3 illustrates the anticipated effect of the cylinder canopy on the total and turbulent shear stress as suggested by experimental measurements performed by Tsujimoto et al. (1991), where H is flow depth, and

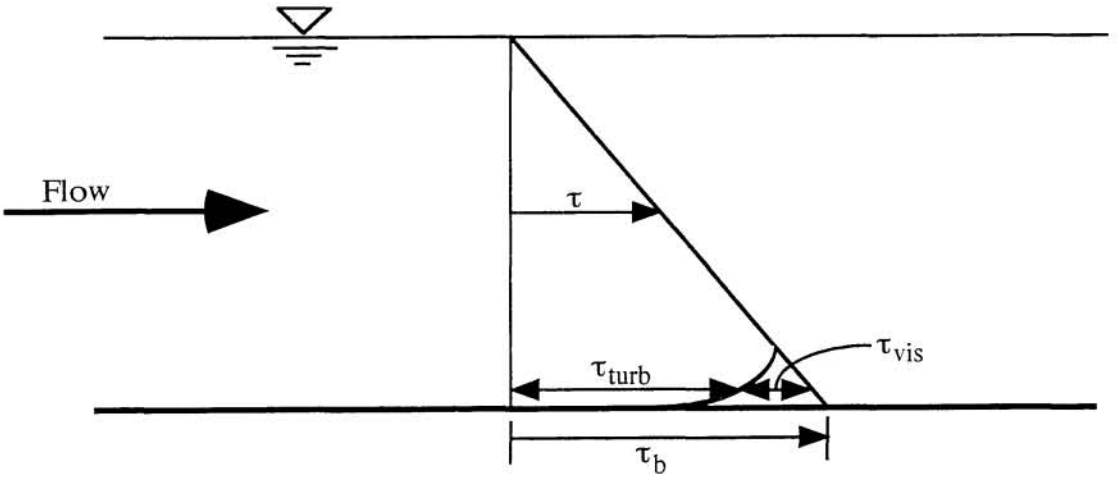

τ_{turb}: Reynolds stress
τ_{vis}: Viscous stress
τ: Total shear stress
τ_b: Total bed shear stress

Figure 3.2 Stress partition for fully turbulent flow with a viscous sublayer in a wide rectangular channel

h_p is mean canopy height. Within the canopy, the difference between the total stress and Reynolds stress is due to the stresses imposed by the form drag of the cylinders themselves. Therefore for flow through a cylinder canopy, equation 3.43 must be modified to include the stress partitioned to the cylinder drag. This is accomplished by horizontally averaging the Navier-Stokes equations as described by Raupach and Shaw (1982) and discussed in Section 3.2. The averaging procedure essentially results in horizontally averaged values of Reynolds stress, $-\rho\overline{u'v'}_h$, and total shear stress, τ_h, in equation 3.41 above, and an additional term for the drag force per unit volume

$$\frac{d\tau_h}{dy} = \frac{d\left(-\rho\overline{u'v'}_h\right)}{dy} - f_D = -\rho g S \tag{3.52}$$

where f_D is defined by equation 3.5. By eliminating density, which is common to all of the terms of equation 3.52 equation 3.53 results

$$\frac{d\left(\overline{u'v'}_h\right)}{dy} = gS - \tfrac{1}{2}aC_D{}'\overline{u}_h^2 \tag{3.53}$$

Solving equation 3.45 for the drag coefficient, C_D', yields

$$\boxed{C_D{}' = \frac{gS - \frac{d}{dy}(\overline{u'v'}_h)}{\frac{a}{2}\overline{u}_h^2}} \tag{3.54}$$

Equation 3.54 defines the one-dimensional local drag coefficient. C_D' is spatially averaged in the mainstream and spanwise directions but may vary in the vertical direction. This equation will be used in this study to determine the drag coefficient after measuring all other terms in the equation. Again, equation 3.54 is applicable for fully developed uniform shear flow through cylindrical obstructions where there are no sidewall and secondary currents effects and viscous effects can be neglected.

3.5 Various Bulk Drag Coefficients

Equation 3.54 is very useful in that it defines a local one-dimensional drag coefficient which may only vary in the vertical direction. However, many models require a bulk drag coefficient which is assumed to be constant anywhere in the plant canopy, such as the one required for the theory introduced in Section 2. There are many ways to calculate the bulk drag coefficient. A few of these methods are discussed below.

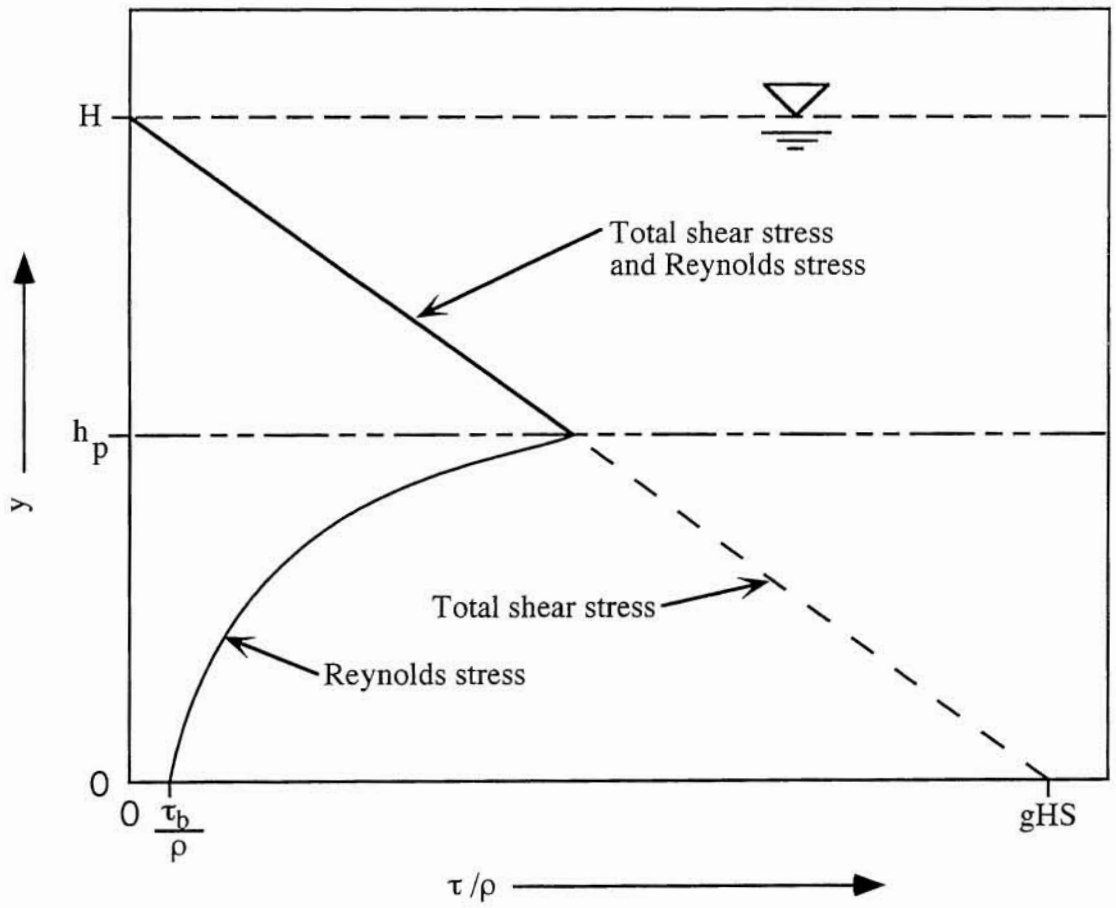

Figure 3.3 Expected effect of canopy on total stress and turbulent shear stress (from measurements by Tsujimoto et al., 1991)

The backwater model derived in Section 2 requires the following bulk drag coefficient

$$\overline{C_{DH}} = \frac{\int_0^H C_D' u_h^2 dy}{\int_0^H u_h^2 dy} \tag{3.55}$$

where C_D' and u_h are local-horizontally averaged values. Equation 3.55 is valid for emergent vegetation since the integration is performed from the bed to the water surface.

A similar definition of the bulk drag coefficient which is more appropriate for submerged vegetation is

$$\overline{C_{DB}} = \frac{\int_0^{h_p} C_D' u_h^2 dy}{\int_0^{h_p} u_h^2 dy} \tag{3.56}$$

Equation 3.56 is integrated to the top of the deflected vegetative canopy, h_p.

An intuitively simple definition of the bulk drag coefficient for submerged vegetation is the common integral average of the local drag coefficient up to the plant height

$$\overline{C_{DA}} = \frac{1}{h_p}\int_0^{h_p} C_D' dy \tag{3.57}$$

Although not explicitly illustrated here, equation 3.57 also holds for emergent vegetation when integrated up to the water depth, H.

A fourth method of calculating a bulk drag coefficient in a uniform flow can be derived with equation 3.32 formulated in Section 2 and Manning's equation. Solving equation 3.32 for $\overline{C_D}$ yields

$$\overline{C_{DM}} = \frac{2(S - S_f)}{aH \cdot Fr^2 \beta} \tag{3.58}$$

where the friction slope S_f can be solved for by Manning's equation

$$S_f = \left(\frac{nU}{R^{2/3}}\right)^2 \tag{3.59}$$

where U is average channel velocity, n is Manning's coefficient, and R is hydraulic radius. Equation 3.59 can be used to determine the bulk drag coefficient for an individual obstruction for strictly emergent vegetation.

If the four bulk drag coefficients defined above are computed for submerged cylinders, it is expected that the values of $\overline{C_{DB}}$ and $\overline{C_{DA}}$ will be very similar. Also, the values of $\overline{C_{DH}}$ and $\overline{C_{DM}}$

are expected to be about equal. The similarities in the drag coefficients are expected since the bulk drag coefficients $\overline{C_{DB}}$ and $\overline{C_{DA}}$ are computed by an integration process from the bed to the top of the cylinders. They characterize the drag force imposed on the layer of flow passing through the cylinder canopy only, and thus the drag on a single cylinder in a multi-cylinder arrangement. $\overline{C_{DH}}$ and $\overline{C_{DM}}$ represent different ways of determining the same bulk drag coefficient and characterize the drag force imposed by the cylinder layer on the total flow column. Thus, the effect of the canopy is averaged over the entire flow column, thereby reducing the drag coefficient.

4. EXPERIMENTAL STUDY

4.1 Introduction

Motivated by the need for data about the drag and Boussinesq coefficients in the backwater model described by equation 3.29, an experimental study was performed. The experiments consisted of passing a steady, uniform flow through a laboratory flume which contained simulated vegetation. Point velocity measurements along vertical profiles were taken with an acoustic Doppler velocimeter which measures velocities in three dimensions. These measurements allowed for the computation of the Boussinesq coefficient, Reynolds stresses, and ultimately for drag coefficients. Although the drag and Boussinesq coefficients that were determined by the experiments described herein were for uniform flow conditions, it is hoped that these values will provide reasonable approximations for gradually varying flows.

After describing the relevant dimensionless variables in the experiments, this chapter discusses the experimental setup, including the laboratory facilities and measuring devices. Then the measuring procedure is described in detail.

4.2 Dimensional Analysis

In an attempt to determine the relevant parameters in this complex flow situation, a similar analysis to the one developed by Parker and Anderson (1977) for rivers will be presented. The following variables are considered to play a role in the resistance of vegetation in an open-channel,

$$q_w, U, H, S, \tau_b, g, D, a, h_p, \mu, \rho, C_D, \alpha, p_i$$

where α is a nondimensional parameter characterizing the plant flexibility, p_i is a vector containing all other relevant parameters characterizing plant size distribution, shape, orientation, etc. and all other variables are as defined in Chapter 3. Next, dimensional analysis is used to reduce the list of variables. By selecting g, ρ, and H as fundamental variables, the following functional relationship is obtained:

$$\phi\left(\frac{q_w}{H\sqrt{gH}},\frac{U}{\sqrt{gH}},\frac{\rho H\sqrt{gH}}{\mu},S,\frac{\tau_b}{\rho gH},\frac{D}{H},Ha,\frac{H}{h_p},C_D,\alpha,p_i\right)=0 \tag{4.1}$$

Note that a combination of the second (Froude number) and third parameters yields the flow Reynolds number $\frac{\rho UH}{\mu}$. Equation 4.1 reveals no new physical information, it only helps in determining the minimum amount of dimensionless parameters that characterize a free-surface flow through vegetation. Now, we should note that two universal constraints allow for further reduction, namely the conservation equations of mass and momentum (Parker and Anderson, 1977). Conservation of water imposes that $q_w = UH$, and momentum conservation yields $\tau_b = \rho gHS$, thus two parameters can be eliminated from 4.1; which are arbitrarily chosen to be $\frac{q_w}{H\sqrt{gH}}$ and $\frac{\tau_b}{\rho gH}$. With these considerations in mind, we may now rewrite equation 4.1 as:

$$C_D = \hat{\phi}\left(\frac{U}{\sqrt{gH}},\frac{\rho HU}{\mu},S,\frac{D}{H},Ha,\frac{H}{h_p},\alpha,p_i\right)=0 \tag{4.2}$$

Finally, equation 4.2 allows us to determine the dimensionless quantities that play a role in the determination of the drag coefficient, and that therefore have to be carefully considered in the planification of the experimental work. Except from p_i, all other dimensionless parameters were varied in the experimental investigation described herein.

4.3 Experimental Setup

The experimental study was conducted in the Hydrosystems Laboratory of the Civil Engineering Department at the University of Illinois. The experimental facilities and the velocity measuring device employed in the study are described below.

4.3.1 Experimental Facilities

The experiments were conducted in a 19.5 meter long, 0.91 meter wide, and 0.61 meter deep tilting flume. A schematic of the laboratory setup is included as Figure 4.1. To maintain a constant discharge throughout an experiment, water was supplied to the channel from a constant head tank. Upon entering the channel, the flow passed through a series of honeycomb grids to straighten the flow so that it was uniform across the width of the channel. A hydraulically operated tail-gate weir allowed for water depth adjustments in the channel. The flume was equipped with a mechanism which allowed it to be tilted to adjust the bed slope. Channel slopes could be set from 0 to 10 percent. Flow leaving the flume entered a large sump under the laboratory floor, where it was recirculated to the constant head tank with a set of pumps.

The available head from the constant head tank permitted for a maximum discharge through the flume of approximately 180 L/s. However, preliminary measurements indicated that the honeycomb grids did not perform satisfactorily near discharges of about 120 L/s. For this reason, discharges around this value were not used in the experimental study. To be safe, the maximum discharge of 180 L/s was used for high discharge experiments and discharges below 100 L/s were used for low discharge experiments. An elbow meter was calibrated with a set of weighing tanks to measure discharge. The calibration curve is included as Figure 4.2a.

To assist in the quick determination of the channel slope, a gauge was constructed at the side of the flume which measured the flume's vertical position. The gauge was then calibrated after measuring various bed slopes with a point gauge. The calibration curve for the slope meas-uring gauge is also included as Figure 4.2b. Channel slopes for the current research ranged from 0.0036 to 0.0161.

Both rigid and flexible cylinders were used to simulate vegetation. Rigid plants were simulated with ¼ inch wooden dowels. The dowels were cut to approximately 6 inches in length. Flexible plants were simulated with ¼ inch diameter by 7-¾ inch long plastic commercial drinking straws (Carnival brand). The drinking straws were made with a flexible bend at one end. In order to place the straws and dowels in the channel, a false bottom was con

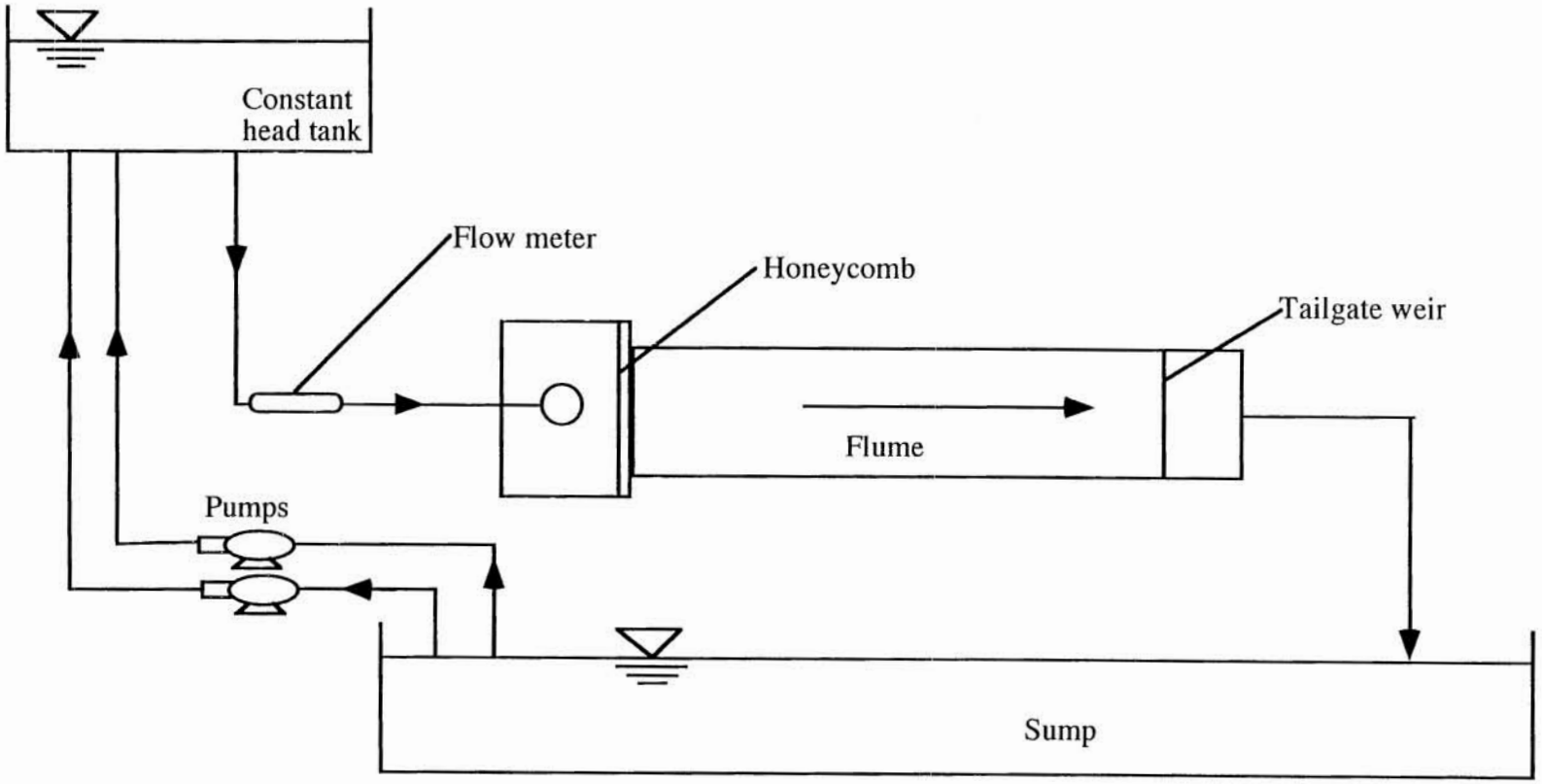

Figure 4.1 Schematic of laboratory setup

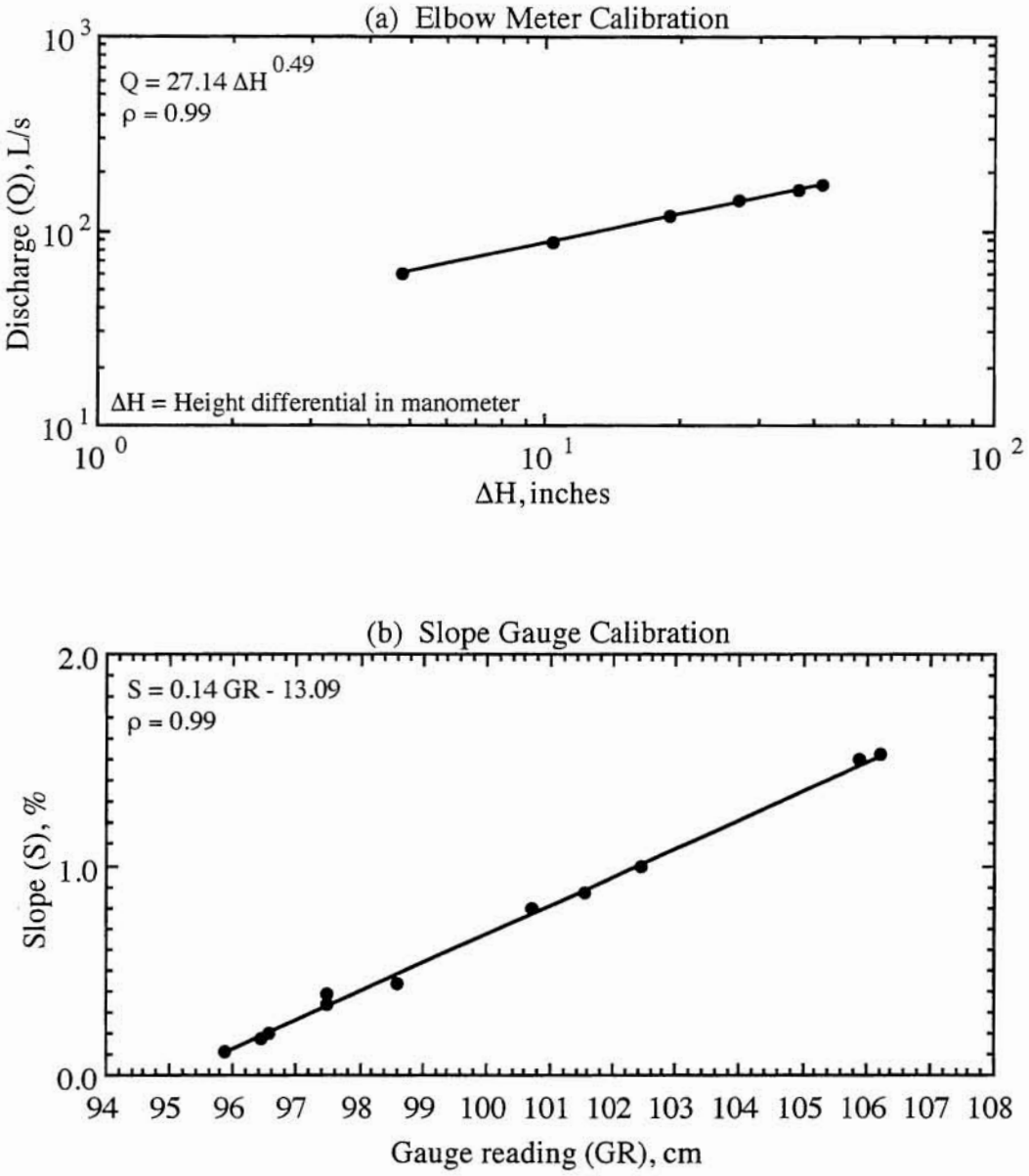

Figure 4.2 Calibration curves for measuring discharge (a) and channel slope (b)

structed with 8 foot long sheets of ¼ inch pegboard. The pegboard consisted of ¼ inch diameter holes spaced at 1 inch on centers. The straws were place in the pegboard with the flexible end down so that the straws would bend at or near the channel bed. To prolong the life of the pegboard, the sheets were coated with a water repellent. The false bottom was anchored with concrete blocks beneath it, leaving anywhere from 0 to 2 inches of space beneath the pegboard channel bottom. To limit the flow under the false bottom boards were fixed underneath the bottom which ran across the channel and effectively prevented significant underflow from occurring. The concrete blocks under the false bottom also aided in limiting underflow. The variation of space beneath the pegboard resulted in variable dowel heights extending into the channel. For the rigid cylinder experiments, the dowels did not deflect and their average height within the flow of water, h_p, was measured to be 11.8 ± 1.67 centimeters. For the flexible cylinder experiments, the average undeformed straw height, h, was 16.9 ± 1.61 centimeters. Of course the flexible nature of the straws allowed them to deform to a new average height when placed in the water flow. Mean straw heights within the flow, h_p, are reported with the experimental results in Table 5.5. For all of the experiments, the cylinders were arranged in a staggered pattern and spaced at 2, 3, 4, and 6 inches on centers. Two basic staggered patterns were used and are illustrated in Figure 4.3.

Figures 4.4 and 4.5 are photographs of the flume with flexible cylinders before and during an experimental run, respectively. These photographs were taken while the channel was filled with drinking straws placed at the highest density (experiment 17 and 18, respectively).

To accurately obtain uniform flow conditions, a piezometer-type setup was installed. Plastic tubes were inserted from underneath the pegboard into empty holes at the upstream and downstream ends of the channel. These tubes were run underneath the pegboard bottom to the downstream end of the channel where they were fixed side by side to the channel wall. This made it possible to measure the elevation change of the water surface from one end of the channel to the other. By measuring the distance between the entrances of the two tubes, it was possible to determine the slope of the water surface. Uniform flow conditions could then be confirmed by comparing the water surface slope to the known bed slope.

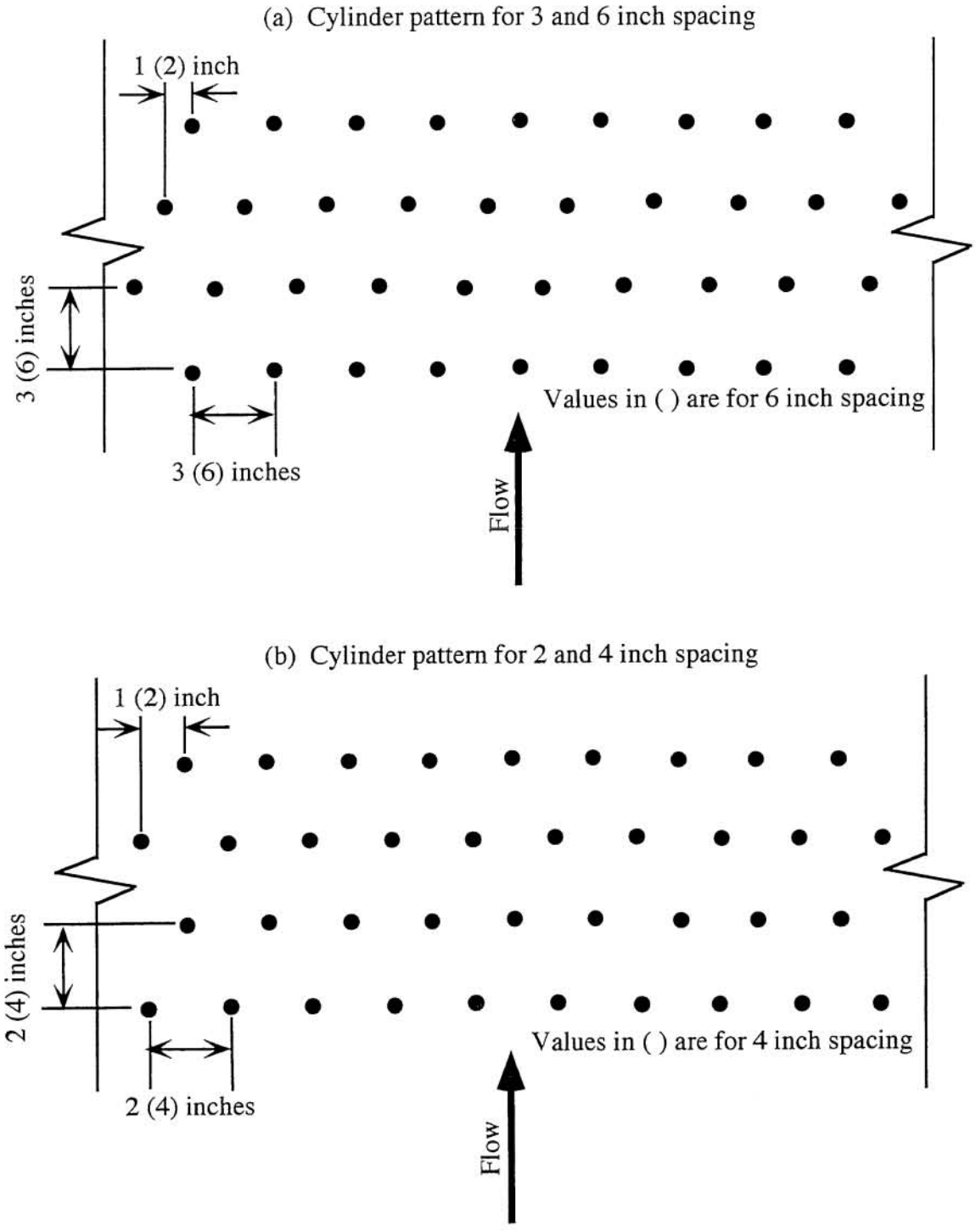

Figure 4.3 Staggered cylinder patterns

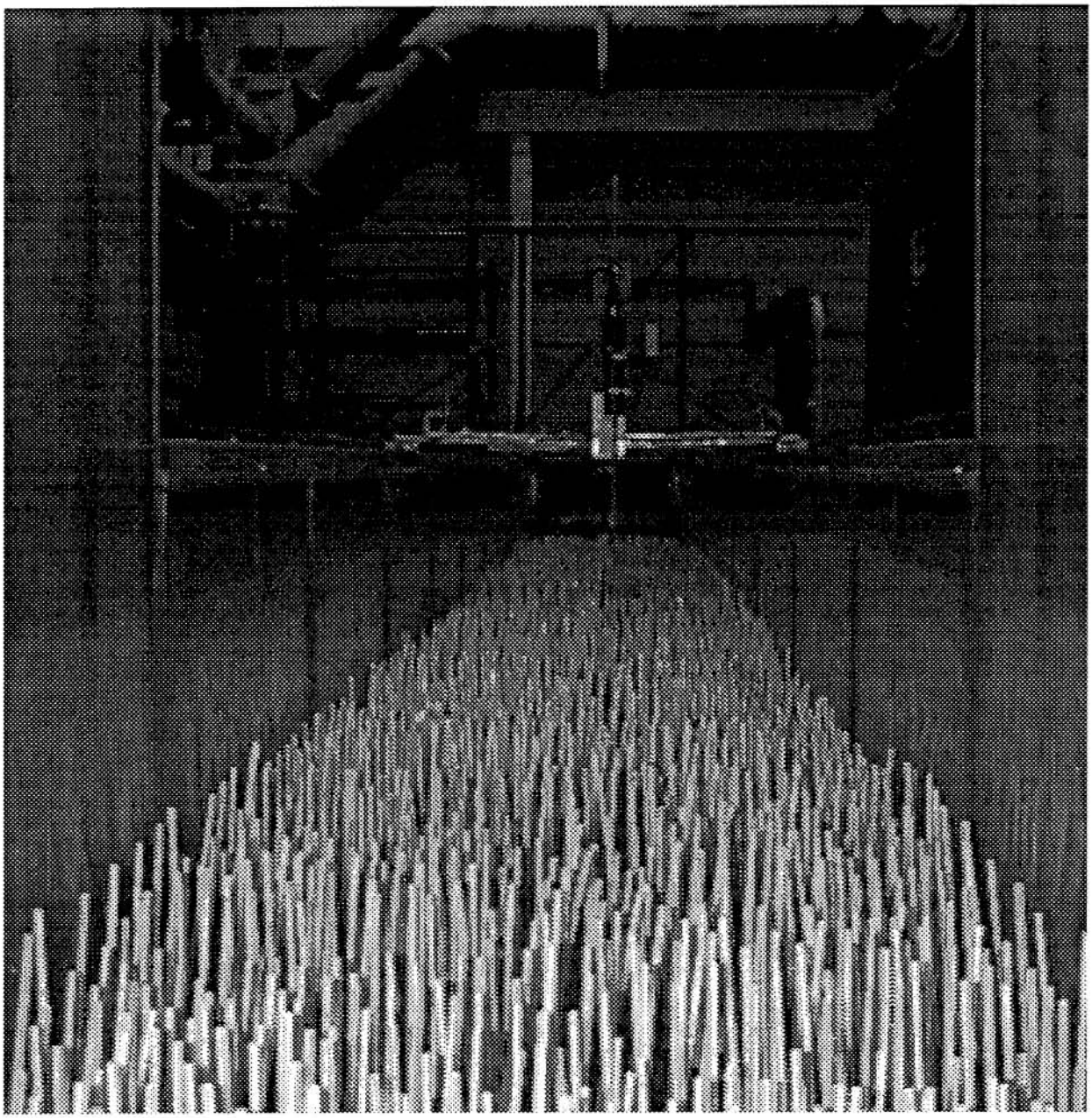

View is looking downstream. ADV is also shown

Figure 4.4 Experimental flume filled with flexible cylinders at highest density (Experiment 17)

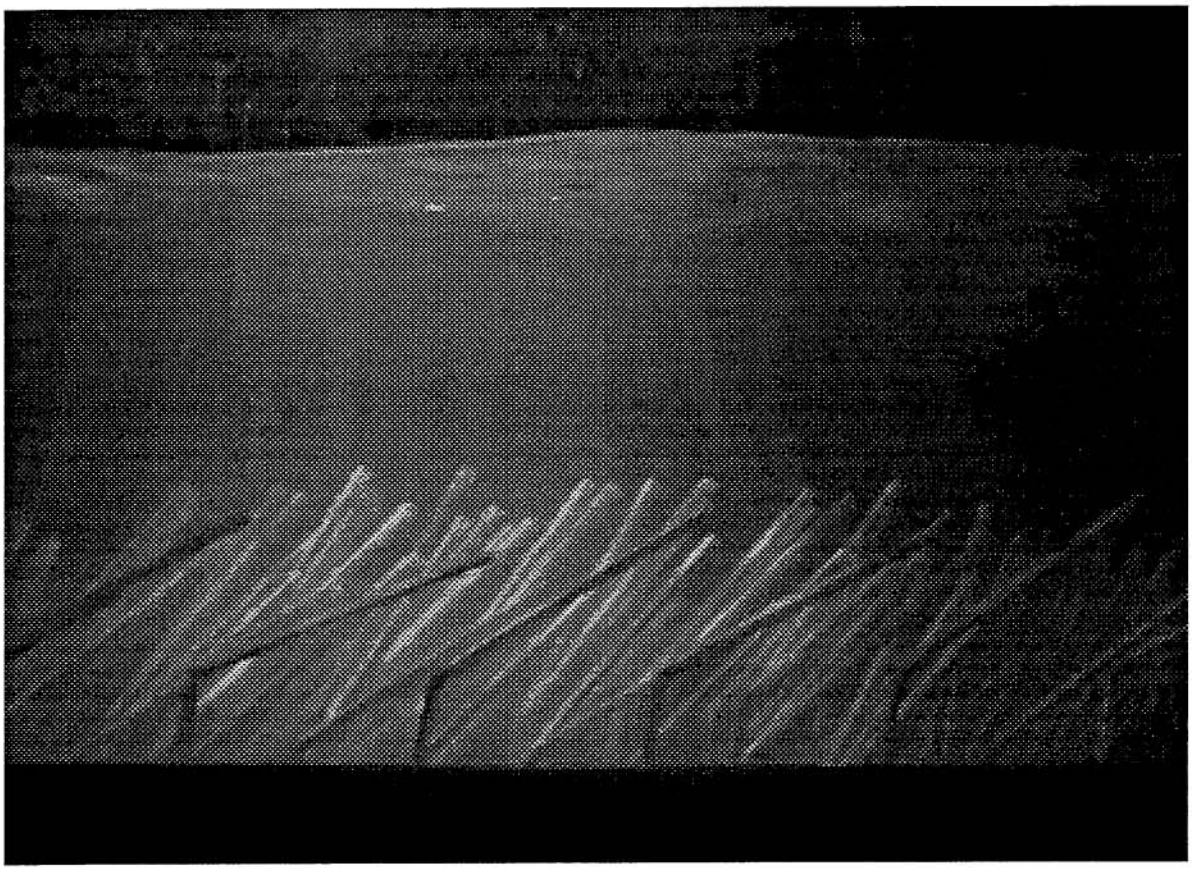

Figure 4.5 Side view of flexible cylinders during experimental run at highest density (Experiment 18)

4.3.2 Velocity Measuring Device

The three components of velocity were measured with a new technology, a three-dimensional acoustic Doppler velocimeter (ADV). The ADV is developed and manufactured by Son-Tek. It is a point-type current meter based on the acoustic Doppler shift velocity measurement principle. Acoustic pulses are sent out from the ADV and are reflected off small particles suspended in the flow. The reflected signals are then captured by the receivers and processed by computer software. It is therefore implicitly assumed that the tiny suspended particles in the flow move with the flow. The water in the lab was naturally seeded well enough so that the ADV could be utilized without any complications. The ADV samples an eliptically-shaped volume of less than 1 cm^3, measuring 9 millimeters along the vertical axis and 4 millimeters along its minor axis, which is parallel to the bed. The sampling volume is approximately 5 centimeters away from the bottom of the instrument sender. A time-series measurement of velocity is taken at a sampling rate of 25 Hz and is recorded in a 486 personal computer. Figure 4.6 illustrates a schematic of the ADV setup. For further information regarding the operational and technical aspects of the ADV, readers are referred to the paper by Kraus, Lohrmann, and Cabrera (1994) .

The primary advantage of the ADV was that it allowed for an undisturbed measurement of the three flow velocity components; consequently allowing for the measurement of Reynolds stress. However, Lohrmann, Gelfenbaum, and Haines (1995) report that ADV measurements of Reynolds stress at low flows (<10 cm/s) result in values that have a slight positive bias. This positive offset is caused by variation in the sensitivity of the three ADV receivers that lead to differences in magnitude of the noise terms. At higher flows, the noise terms become negligible and the positive offset of the Reynolds stress should not occur. Preliminary measurements for this study indicated that the Doppler noise was equally balanced in all three channels. It was therefore believed that for the flow velocity ranges considered in these experiments (which were well above 10 cm/s), the Reynolds stress estimates were unbiased and positive offset errors did not occur.

The primary disadvantage of using the ADV for this experimental study was the inherent loss of the measurable depth of the water column. Five centimeters of depth was always lost to the distance from the probe to the measuring volume and another 1 to 8 centimeters was lost to the required submergence depth (See Figure 4.6), which was dependent on the water

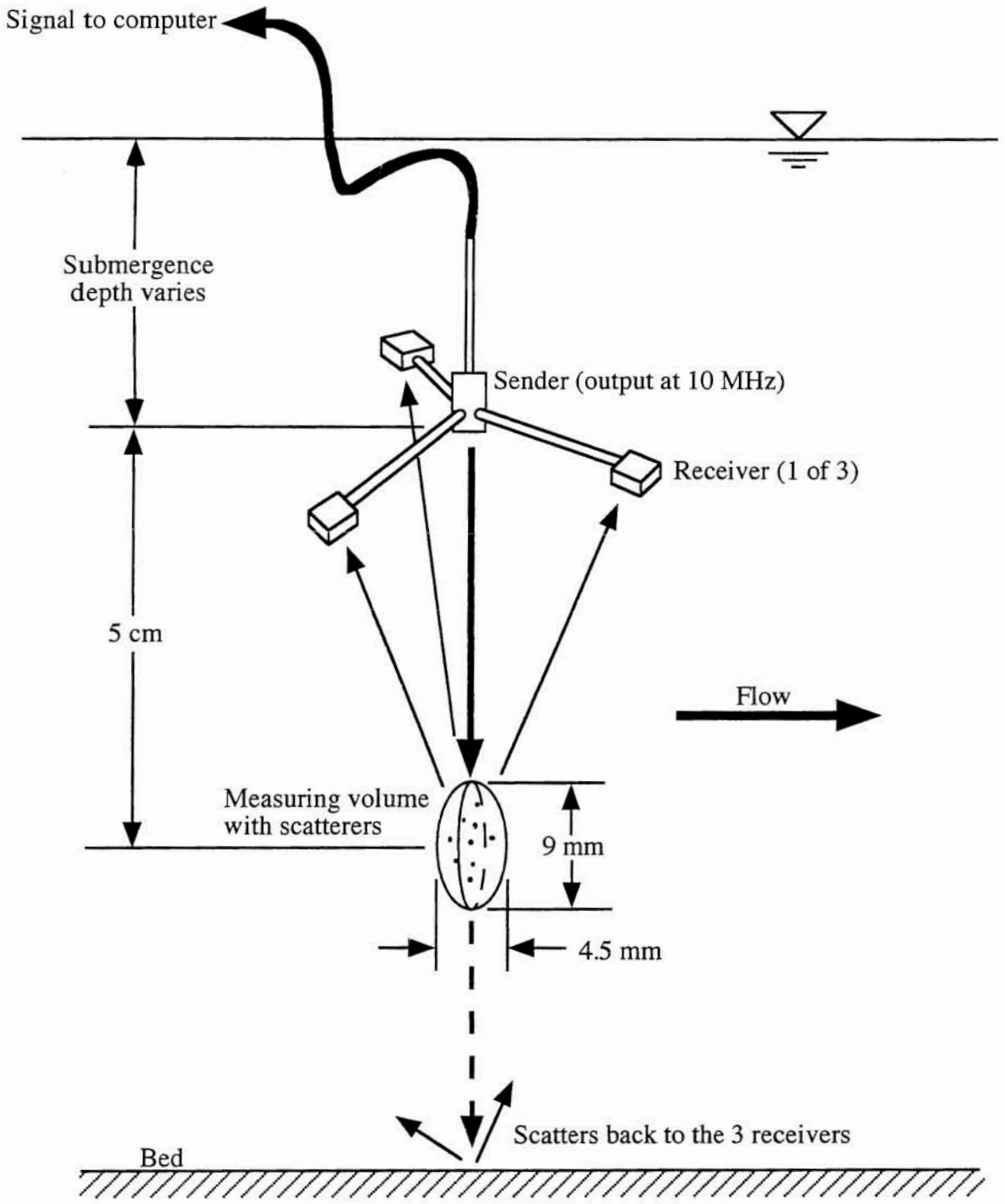

Figure 4.6 Schematic of acoustic Doppler velocimeter (ADV)

velocity near the water surface. The resulting loss of measurable water column was up to 13 centimeters, which was a substantial amount for this laboratory investigation. However the ability to effectively measure velocities and Reynolds stresses more than justified the use of the device in the experiments.

4.4 Experimental Procedure

18 Experiments were performed (12 with rigid cylinder and 6 with flexible cylinders) to investigate the profiles of velocity, Reynolds stress, turbulence intensity, and drag in a simulated vegetated channel. The controllable variables in the laboratory where flow discharge, channel bed slope, cylinder spacing, and cylinder flexibility. By controlling these four variables, all of the relevant variables discussed in Section 2 could be changed. Table 4.1 shows the combinations of the four variables used for each experiment. What follows is a detailed description of the common procedural routine performed for each experiment.

To begin each experiment, the channel slope, cylinder spacing, and discharge were adjusted to their predetermined values. To obtain uniform flow, the tailgate was adjusted. The presence of normal depth throughout the channel was insured by measuring water depths along the channel with a common yardstick and then fine-tuning with the piezometer tubes described in Section 4.3.1.

Table 4.1 Experimental Conditions				
Experiment Number	Discharge, Q (L/s)	Bed Slope, S (%)	Cylinder Spacing, Δ (cm)	Cylinder Flexibility
1	179	0.36	7.62	rigid
2	88	0.36	7.62	rigid
3	46	0.36	7.62	rigid
4	178	0.76	7.62	rigid
5	98	0.76	7.62	rigid
6	178	0.36	15.24	rigid
7	95	0.36	15.24	rigid
8	180	0.36	5.08	rigid
9	58	0.36	5.08	rigid
10	180	1.61	5.08	rigid
11	177	0.36	10.16	rigid
12	181	1.08	10.16	rigid
13	179	0.36	7.62	flexible
14	180	1.01	7.62	flexible
15	93	0.36	7.62	flexible
16	179	0.36	15.24	flexible
17	78	0.36	5.08	flexible
18	179	1.01	5.08	flexible

The goal of these experiments was to obtain one-dimensional statistics where the variation in the mainstream, x, and spanwise, z, directions were averaged out. To determine the desired horizontally averaged profiles, four sets of profiles were measured at various locations within the cylinders. The locations of these measurements were random but obeyed the following criteria.

1. All profiles were at least 4.88 feet downstream of the first row of cylinders. Li and Shen (1973) suggest that the drag coefficient becomes constant after about 200 cylinder diameters downstream of the first row of cylinders. 4.88 feet is therefore believed to be highly conservative. In addition, all profiles were taken within 4.57 feet of the most upstream measurement:

2. All profiles were taken within the center 16 centimeters of the channel. Preliminary measurements showed that within this center portion of the channel, the mean velocity and Reynolds stress profiles were nearly constant along the z-axis. In this portion of the channel, the effect of the sidewalls had entirely dissipated.

3. Two profiles were taken on each side of the centerline, and no two profiles were taken at the same location on the z-axis.

4. Profiles were not taken directly behind a cylinder but at least one profile was taken inside of the wake of a cylinder. Profiles taken directly behind a cylinder were significantly altered when compared to profiles measured anywhere else in the channel. Therefore, profiles taken behind a cylinder would unfairly influence the average profiles if they were included, since only 4 profiles were being averaged. However, to obtain the most representative horizontal average of the flow, profiles were taken within cylinder wakes. Seginer et al. (1976) have found that profiles measured within cylinder wakes are not significantly different than those measured outside cylinder wakes. The profiles measured in this investigation support this observation.

Ten points were taken in each profile and each profile was made up of measurements taken at the same depths. These points were approximately evenly spaced in the vertical, however in some instances points were taken closer together within and at the top of the canopy since these were the areas of primary concern. Also, because of problems with signal reflections, the probe was unable to accurately measure velocity fluctuations when positioned so that the measuring volume was near 2.5 centimeters from the bed. Therefore, no points were taken between 3.5 and 1.75 centimeters from the bed.

In order to obtain accurate measurements of Reynolds stress, a sampling interval of 3 minutes was selected for each experiment. Preliminary measurements showed that the time-averaged values of mainstream velocity, $\bar{u}$, Reynolds stress, $-\rho\overline{u'v'}$, and turbulence intensity, u_{rms}, were highly dependent on the total averaging time of the ADV record, but that as the averaging time was extended, the values of the above parameters became relatively constant. Figure 4.7 shows the variation of the velocity, turbulence intensity, and Reynolds stress with the dimensionless total averaging time, t*. These statistics have been normalized with their values after 10 minutes of averaging. The averaging time has been made dimensionless so that $t^* = t\,\bar{u}_{10} / h_p$. Since the sizes of the eddies within the canopy is determined by the characteristic length of the cylinders, the canopy height, h_p, was chosen to normalize the time scale. The convection velocity of the eddies is dependent on the measured velocity at that point in the channel and therefore the value of $\bar{u}_{10}$ was also used to make the averaging time dimensionless. These measurements were taken within the canopy under extreme flow conditions where

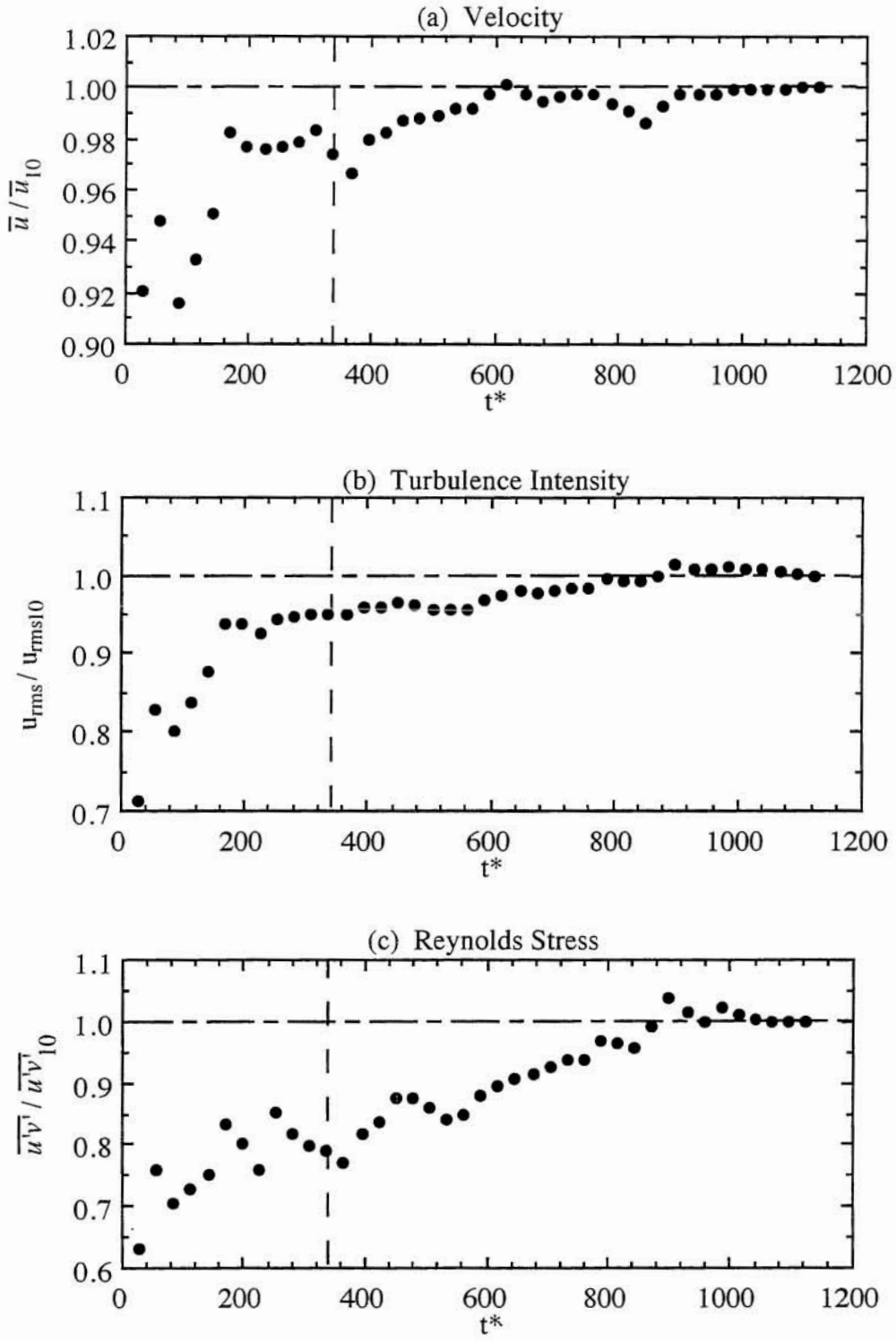

Figure 4.7 Variation of mean statistics with dimensionless averaging time. Statistics have been normalized with their mean values after 10 minutes of averaging.

the canopy velocity was low (because of a high cylinder density). Therefore, the convection velocity of the eddies within the flow was relatively small and we would consequently need to average over a longer period of time than if the velocity in the channel was greater. A compromise had to be reached between the need to extend the record length so as to increase the measurement accuracy and the need to shorten the record length so that 40 measurement points could be measured in a reasonable amount of time. The dimensionless time of 340 was chosen as an appropriate length of time to average. For the flow conditions corresponding to Figure 4.7, the dimensionless time of 340 corresponds to a 3 minute averaging interval. Choosing this averaging interval does introduce some error into the computations of the statistics, especially for the computation of the Reynolds stress. Figure 4.7 shows that when averaging the Reynolds stress, even over an extremely long interval of time such as 10 minutes, the relative uncertainty in the measurements will be no better than 5%. For the highest cylinder density, it was found that using a 3 minute averaging interval yielded about a 15% error in the measurement of the Reynolds stress. For lower cylinder densities, the convection velocity of the eddies is greater and the chosen averaging interval will result in smaller errors in the measurement of the Reynolds stress. It was found that at the lowest tested cylinder density, the error in the measurement of the Reynolds stress was below the minimum uncertainty. However, the slight errors in the Reynolds stress measurements are not believed to cause equal errors in the computation of the drag coefficient. In the computation of the drag coefficient, we are only interested in the gradient of the Reynolds stress profiles and not on their actual magnitude. Therefore, it is recognized that up to a 15 percent error may exist in the measurements of the Reynolds stress, but that this error should not significantly affect the computations of the drag coefficient.

Once each profile was completed (resulting in 40 measuring points of 3 minutes each), the position of each profile with respect to adjacent cylinders was recorded. The cylinder height of each adjacent cylinder was also measured and recorded. In the case of the flexible cylinders, a video camera was used to record the deflection of the cylinders. Then, imaging software allowed for accurate measurements of the deflection angle of the cylinders. An estimate of the deflected cylinder height was also obtained by randomly measuring a sample of cylinders and averaging this group.

The data from each experiment was processed and further analyzed by a computer program. The specifics of the program and results of the data analysis is described in detail in Chapter 5.

5. EXPERIMENTAL RESULTS AND DISCUSSION

5.1 Introduction

The results of the experimental study described in Chapter 4 are presented below. Each of the detailed objectives described in Chapter 1 are addressed. First, the methodology and assumptions required for the processing of the experimental data are explained. Then, the results of the experiments are summarized, including values of the drag and Boussinesq coefficients needed in the backwater curve derivation performed in Chapter 3. The profiles of velocity, Reynolds stress, turbulence intensity, and drag coefficient are analyzed, and the merits of the techniques used in their measurement are discussed. Then, the significance of each of the parameters obtained in the dimensional analysis of Chapter 4 on the magnitude of the bulk drag coefficient is examined. Finally, the results of the experimental study are compared to findings of other investigators who have studied similar flows.

5.2 Data Processing

The data from each experiment was processed by a FORTRAN computer program given in Appendix A. The program computed various statistics including mean velocities, Reynolds stresses, turbulent intensities, and drag coefficients and shape factors. A few operations and assumptions within the program are worth discussing and are therefore commented upon below.

As explained by Lohrman et al. (1995), small tilt angles of the ADV may cause significant errors in the estimation of Reynolds stresses. It was therefore necessary to correct for ADV tilt and rotation in the computer program. Since every effort was made to eliminate tilt when the probe was set up in the laboratory, tilt and rotation corrections were very small. The approach used for tilt corrections was to simply rotate the coordinate system of the uppermost point of each profile around the z and y axes until the velocity in the mainstream direction, $\overline{u}$, was maximized. The presence of uniform flow required this condition to be true above the

plant canopy. Then it was assumed that tilt and rotation errors were consistent throughout the profile and the resulting correction was applied to each velocity measurement in that profile.

With the corrected velocities, time-averaged values of the velocities: $\overline{u}$, $\overline{v}$, and $\overline{w}$; the Reynolds stresses per unit density: $-\overline{u'v'}$, $-\overline{u'w'}$, and $-\overline{v'w'}$; and the root-mean-squared velocities fluctuations (turbulent intensities): $\sqrt{\overline{u'^2}}$, $\sqrt{\overline{v'^2}}$, and $\sqrt{\overline{w'^2}}$ were computed. Then, the values of $\overline{u}$ and $-\overline{u'v'}$ for all the verticals were averaged at each distance from the bed. For instance, if all of the measured profiles contained a point that was 1 centimeter from the bed, then the velocities and Reynolds stresses were averaged at this point. The results of this averaging process, when performed over the entire flow column, were one-dimensional profiles of these two quantities. These profiles were assumed to vary only in the vertical because all spanwise and flow-directional variations were averaged out.

In order to evaluate equation 3.44 for the drag coefficient, C_D', the derivative of the horizontally averaged Reynolds stress curve with respect to y must be calculated at various depths within the plant canopy. With this aim, a third order polynomial was fit through the averaged Reynolds stress points below the top of the cylinders. The derivative of this polynomial was then computed and its value at each of the measured depths was calculated. The value of the derivative, along with the mean velocity averaged in the horizontal plane were used in equation 3.44 to compute the local drag coefficient at each depth. The result was a horizontally averaged vertical profile of the drag coefficient. The program then computed the four bulk drag coefficients described in Section 3.5.

The Boussinesq coefficient, β, described by equation 3.19 was also computed for the horizontally averaged velocity profiles. This integration was only an estimate however, since the velocity profiles were not complete (much of the water column was lost to the submergence depth of the ADV). The top and bottom points of each velocity profile were estimated by the simplest assumption possible: a linear extension of the measured profile. This assumption allowed for the estimation of the average mainstream velocity, U, in the channel, and subsequently the channel discharge, Q, with satisfactory results. In general, the estimated channel discharge was within 10 percent of the discharge measured by the elbow flow meter.

5.3 Summary of Results

The data gathered from the experimental study consisted of elevations of the measuring volume and raw values of the three components of mean velocity. For each profile, these data are listed in Appendix B along with the adjusted values of the three components of mean velocity, root-mean-squared velocity fluctuations, and Reynolds stress. The horizontally averaged profile data is listed in Appendix C and will be discussed in detail in the following section. The profile data in these appendices was manipulated as described in Section 5.2 and bulk drag coefficients, Boussinesq coefficients, and Manning's n values were computed. Tables 5.1 and 5.2 report these values for the rigid and flexible cylinder experiments, respectively. The bulk drag coefficients are defined in Section 3.5 and the coefficient, β, is defined by equation 3.19. Preliminary measurements in the channel when no cylinders were present indicated a Manning's n value of 0.011 for the smooth flume bed, which was used in the computation of $\overline{C_{DM}}$. Tables 5.3 and 5.4 report the values of the relevant dimensionless parameters for each experiment for the rigid and flexible cylinders, respectively.

Table 5.1 Results for Rigid Cylinders

Experiment	$\overline{C_{DB}}$	$\overline{C_{DA}}$	$\overline{C_{DH}}$	$\overline{C_{DM}}$	β	Manning's n ($m^{1/6}$)
1	1.01	1.05	0.13	0.15	1.10	0.034
2	0.95	1.04	0.20	0.30	1.07	0.041
3	0.86	1.03	0.25	0.60	1.09	0.048
4	1.29	1.32	0.25	0.34	1.08	0.038
5	1.18	1.21	0.35	0.42	1.12	0.045
6	1.46	1.42	0.40	0.52	1.05	0.025
7	1.39	1.38	0.61	0.64	1.05	0.027
8	0.94	1.02	0.06	0.07	1.15	0.042
9	1.13	1.20	0.14	0.31	1.15	0.056
10	1.19	1.28	0.19	0.26	1.14	0.052
11	1.06	1.11	0.20	0.25	1.06	0.031
12	1.14	1.25	0.33	0.36	1.12	0.036

Table 5.2 Results for Flexible Cylinders						
Experiment	$\overline{C_{DB}}$	$\overline{C_{DA}}$	$\overline{C_{DH}}$	$\overline{C_{DM}}$	β	Manning's n ($m^{1/6}$)
13	1.13	1.19	0.16	0.19	1.13	0.039
14	0.33	0.41	0.13	0.17	1.09	0.034
15	1.45	1.44	0.27	0.41	1.13	0.045
16	0.55	0.57	0.18	0.25	1.02	0.020
17	1.19	1.23	0.17	0.26	1.27	0.061
18	0.59	0.64	0.09	0.12	1.16	0.046

Table 5.3 Dimensionless Parameters for Rigid Cylinders						
Experiment	Re	Fr	S	D/H	Ha	h_p/H
1	2.24×10^5	0.33	0.0036	0.0190	0.365	0.351
2	1.13×10^5	0.29	0.0036	0.0277	0.250	0.518
3	0.57×10^5	0.24	0.0036	0.0387	0.179	0.714
4	1.91×10^5	0.36	0.0076	0.0230	0.301	0.426
5	1.25×10^5	0.37	0.0076	0.0313	0.221	0.578
6	1.96×10^5	0.39	0.0036	0.0238	0.073	0.441
7	1.20×10^5	0.42	0.0036	0.0347	0.050	0.641
8	2.58×10^5	0.29	0.0036	0.0162	0.962	0.300
9	0.70×10^5	0.19	0.0036	0.0297	0.526	0.549
10	2.03×10^5	0.40	0.0161	0.0240	0.652	0.442
11	2.22×10^5	0.35	0.0036	0.0204	0.191	0.377
12	2.38×10^5	0.58	0.0110	0.0273	0.143	0.505

Table 5.4 Dimensionless Parameters for Flexible Cylinders						
Experiment	Re	Fr	S	D/H	Ha	h_p/H
13	2.28×10^5	0.28	0.0036	0.0173	0.401	0.413
14	2.57×10^5	0.62	0.0101	0.0274	0.253	0.495
15	1.12×10^5	0.23	0.0036	0.0247	0.280	0.513
16	2.27×10^5	0.56	0.0036	0.0276	0.063	0.422
17	0.95×10^5	0.18	0.0036	0.0228	0.686	0.578
18	2.50×10^5	0.45	0.0101	0.0224	0.699	0.426

As is reported in Tables 5.1 and 5.2, the values $\overline{C_{DB}}$ and $\overline{C_{DA}}$ were very similar (generally within 10%), and the values of $\overline{C_{DH}}$ and $\overline{C_{DM}}$ were also similar (although they varied somewhat more). This is illustrated in Figure 5.1. These similarities were expected as discussed in Chapter 3. The differences between $\overline{C_{DH}}$ and $\overline{C_{DM}}$ were probably due to sidewall effects, since $\overline{C_{DM}}$ included the effects of these sidewalls (in the computation of Manning's n) and $\overline{C_{DH}}$ did not. There close agreement indicated that sidewall effects were minimal however.

In the present study, the bulk drag coefficient $\overline{C_{DB}}$ was of primary interest because of its application to the backwater model derived in Chapter 3 and because the experimental study was performed for submerging flow conditions. From the experimental study, values of $\overline{C_{DB}}$ between 0.33 and 1.46 were obtained where the relevant dimensionless parameters varied in the ranges defined below.

$$0.57 \times 10^5 < \mathrm{Re} < 2.58 \times 10^5$$

$$0.18 < \mathrm{Fr} < 0.62$$

$$0.0036 < \mathrm{S} < 0.0161$$

$$0.0173 < \mathrm{D/H} < 0.0387$$

$$0.073 < Ha < 0.699$$

$$0.300 < h_p/\mathrm{H} < 0.714$$

The effects of the above parameters on the bulk drag coefficients will be discussed in Section 5.8.

5.4 Boussinesq Coefficient

One of the primary objectives of this study was to determine values of the Boussinesq coefficient, β, which was described in equation 3.19 and is repeated here for clarity as equation 5.1.

$$\beta = \int_0^1 \left(\frac{\bar{u}_h}{U}\right)^2 d\left(\frac{y}{H}\right) \tag{5.1}$$

The results listed above indicated that β was slightly greater than 1.0 and was dependent on the density of the cylinders in the channel. When the cylinder density was less sparse, velocity profiles more closely resembled that of a regular open-channel and Boussinesq coefficients ap-

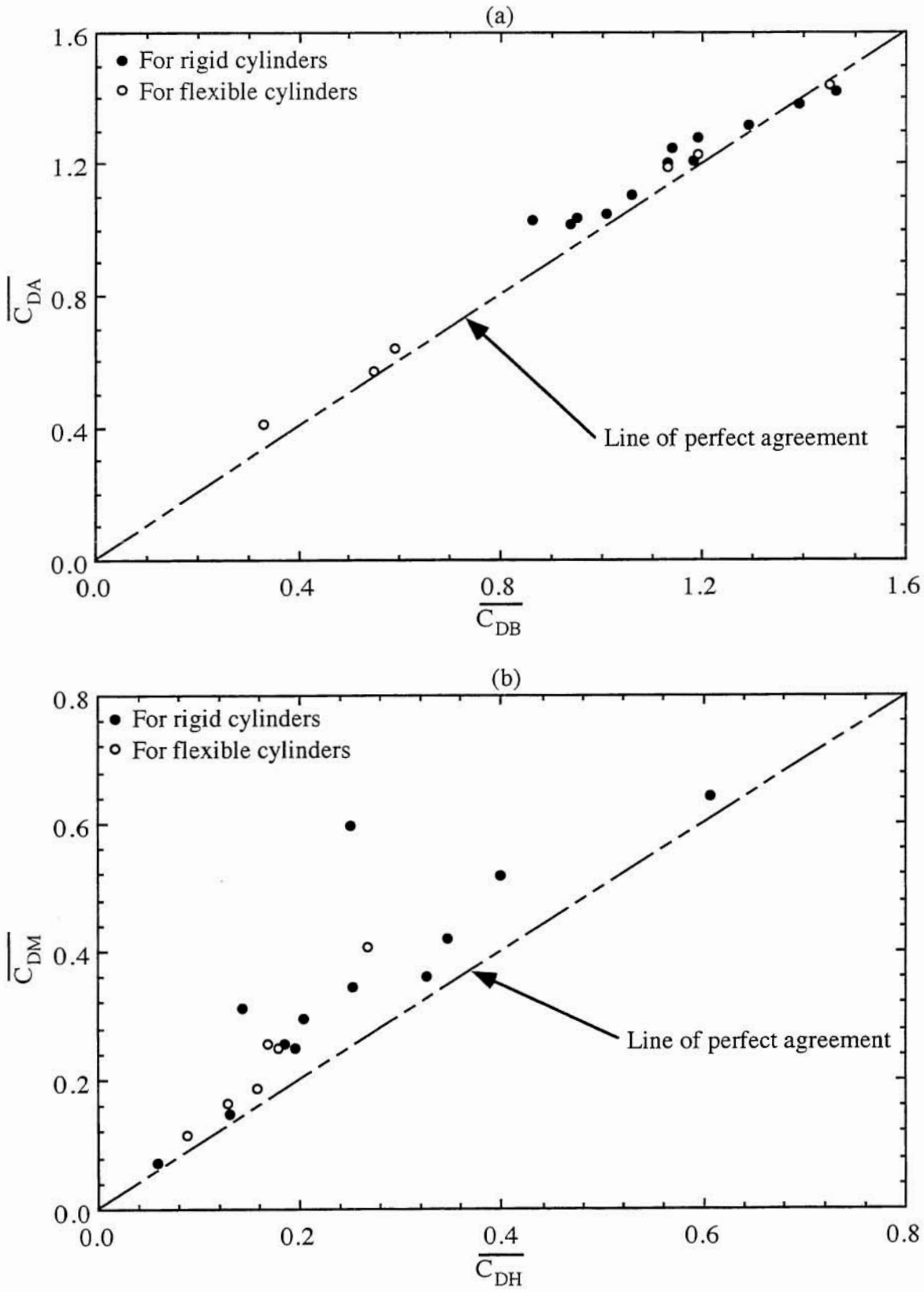

Figure 5.1 Comparison of computed bulk drag coefficients

proached the value of 1.02. As the cylinder density became sparser, the velocity profiles diverged from that of a standard open-channel and Boussinesq coefficients moved further away from 1.02. For rigid cylinders at a given density, the Boussinesq coefficient was essentially constant and as the cylinder density increased, so did values of the Boussinesq coefficient. The lowest density resulted in a Boussinesq coefficient of 1.05, whereas the greatest density yielded a value of 1.15.

For the flexible cylinders, the same trends were evident; however, Boussinesq coefficients varied by greater amounts. At the lowest density, β was 1.02, while at the maximum density β increased up 1.27. Unlike the Boussinesq coefficients for flow through rigid cylinders, those for flow through flexible cylinders were not constant at a given cylinder density. There was an obvious trend for the Boussinesq coefficient to decrease as the magnitude of the flow velocity increased for a given cylinder density. This occurred because the cylinders would deflect more under higher velocities and would offer less resistance to the flow. The resulting velocity profile was more similar to that of a non-vegetated open-channel flow yielding a Boussinesq coefficient that was closer to 1.02. Although a limited number of experiments through flexible cylinders was performed, the Boussinesq coefficient varied by as much as 9 percent for a given cylinder density.

5.5 Deflection Angle

Some simple laboratory observations may be helpful in understanding flow through simulated vegetation and in explaining some of the results that will follow. As expected, the flexible cylinders deflected under the shear stress of the fluid flow (see Figure 4.5) resulting in a deflection angle ,φ, from the vertical. How much a cylinder deflected depended largely on the velocity of the water within the cylinder canopy and on the cylinder flexibility. Since the flexibility of the cylinders was equal in all the trials, the deflection angle increased with increasing mean canopy velocity, U_c, where U_c has been defined as

$$U_c = \frac{1}{h_p}\int_0^{h_p} \bar{u}_h dy \qquad (5.2)$$

The deflection of the cylinders resulted in an altered average cylinder height. The values of the mean canopy velocity, deflection angle, and deflected cylinder height are reported in table 5.5 below along with the bulk drag coefficient $\overline{C_{DB}}$. Plots of the mean deflection angle versus U_c

and $\overline{C_{DB}}$ are shown as Figure 5.2 (a) and (b), respectively. The straws seemed to become more flexible as they were exposed to repeated trials, thus explaining why the cylinder in experiments 13 and 15 deflected almost the same amounts even though the cylinders in the earlier Experiment 13 were placed in a smaller canopy velocity.

Table 5.5 Statistics for Deflected Cylinders

Experiment	U_C, (cm/s)	φ, (degrees)	h_p, (cm)	$\overline{C_{DB}}$
13	32.8	35	15.2	1.13
14	72.2	51	11.5	0.33
15	25.6	34	13.2	1.45
16	73.4	65	9.7	0.55
17	18.0	12	16.1	1.19
18	44.4	45	12.1	0.59

It is apparent from Table 5.5 and Figure 5.2 that the angle of deflection, and thus the flow velocity in the canopy, played an important role in the magnitude of the bulk drag coefficient. It is clear that at some deflection angle between 35 and 45 degrees the bulk drag coefficient significantly dropped. This drop seemed to be quite sudden. As discussed earlier in Chapter 2, Kouwen and Unny (1973) described two separate flow regimes for vegetated channels: (1) rigid or swaying, and (2) prone. The drop in the bulk drag coefficient probably indicated the transition of the simulated vegetative lining from the swaying condition to the prone condition.

The flexible cylinders not only deflected under the flow of water, but also vibrated and swayed in both the vertical and transverse directions. How violently the straws swayed was not easy to predict however. At low flows, and especially when flow depths were slightly greater than the average cylinder height, the straws swayed rather violently in the transverse direction. As the discharge increased, the cylinders swayed less in the transverse direction but began to sway more in the vertical direction. These swaying motions had a definite effect on the measured profiles of velocity and Reynolds stress, and ultimately on the drag coefficient. This will be discussed in further detail in the next section.

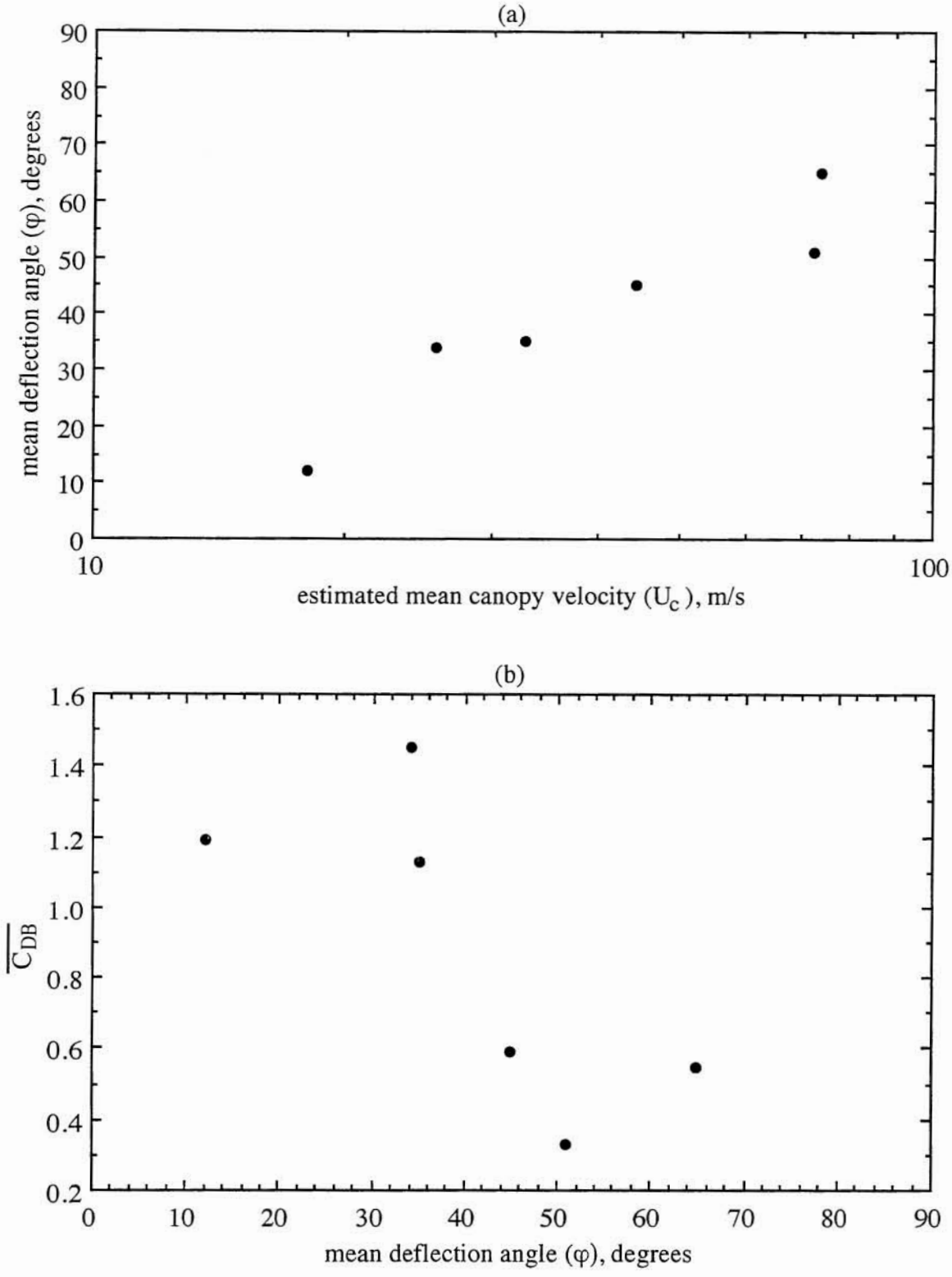

Figure 5.2 Variation of mean deflection angle of the flexible cylinders with (a) mean canopy velocity and (b) bulk drag coefficient $\overline{C_{DB}}$

5.6 Profile Data

For each experimental run, four vertical profiles of 10 points each were measured with the ADV as described in Chapter 4. The data sets of point velocity were analyzed with a computer program (Appendix A) and profiles of velocity, root-mean-squared velocity fluctuations, and Reynolds stress were computed (Appendix B). Since the velocity measurements were taken at the same depths in the flow column, the measurements at equal depths were averaged in the horizontal plane resulting in one-dimensional profiles as discussed previously. These profiles are reported in Appendix C. With the help of equation 3.44, the horizontally averaged profiles of $\overline{u}_h$ and $-\overline{u'v'}_h$ were used to determine values of the local drag coefficient C_D'. This section analyzes the shapes of the profiles described above and discusses the effects of various flow and channel parameters on the profiles

5.6.1 Velocity Profiles

The horizontally averaged velocity profiles through rigid cylinders had a characteristic shape that was dependent on the cylinder density. This explains the constant Boussinesq coefficient for each cylinder density as presented in Section 5.3. Figure 5.3 shows the shapes of the velocity profiles with $\overline{u}_h$ made dimensionless with respect to the velocity at the top of the cylinder canopy, u_{ref}, and the distance from the bed, y, made dimensionless with the average cylinder height, h_p. Four different cylinder densities were tested resulting in four different dimensionless profiles. Figure 5.3 illustrates that the dimensionless velocity profiles collapsed extremely well. The profiles through the more dense simulated vegetation had lower dimensionless velocities within the canopy, therefore a higher percentage of the flow existed in the layer above the cylinder canopy. The shapes of these velocity profiles are less like that of a non-vegetated open-channel and the Boussinesq coefficients are further away from the value of 1.02.

The results of the experiments with flexible cylinders are markedly different as illustrated in Figure 5.4. Three different cylinder densities were tested. The shapes of these dimensionless profiles indicated that the cylinder density indeed still played a major role. However, since the profiles did not collapse well at all, there was substantial evidence that the cylinder density was not the only parameter that had a significant effect on the shapes of the velocity profiles. The absence of this collapse in the velocity profiles explains why the Boussinesq coefficients reported in Section 5.3 were not constant for a given cylinder density.

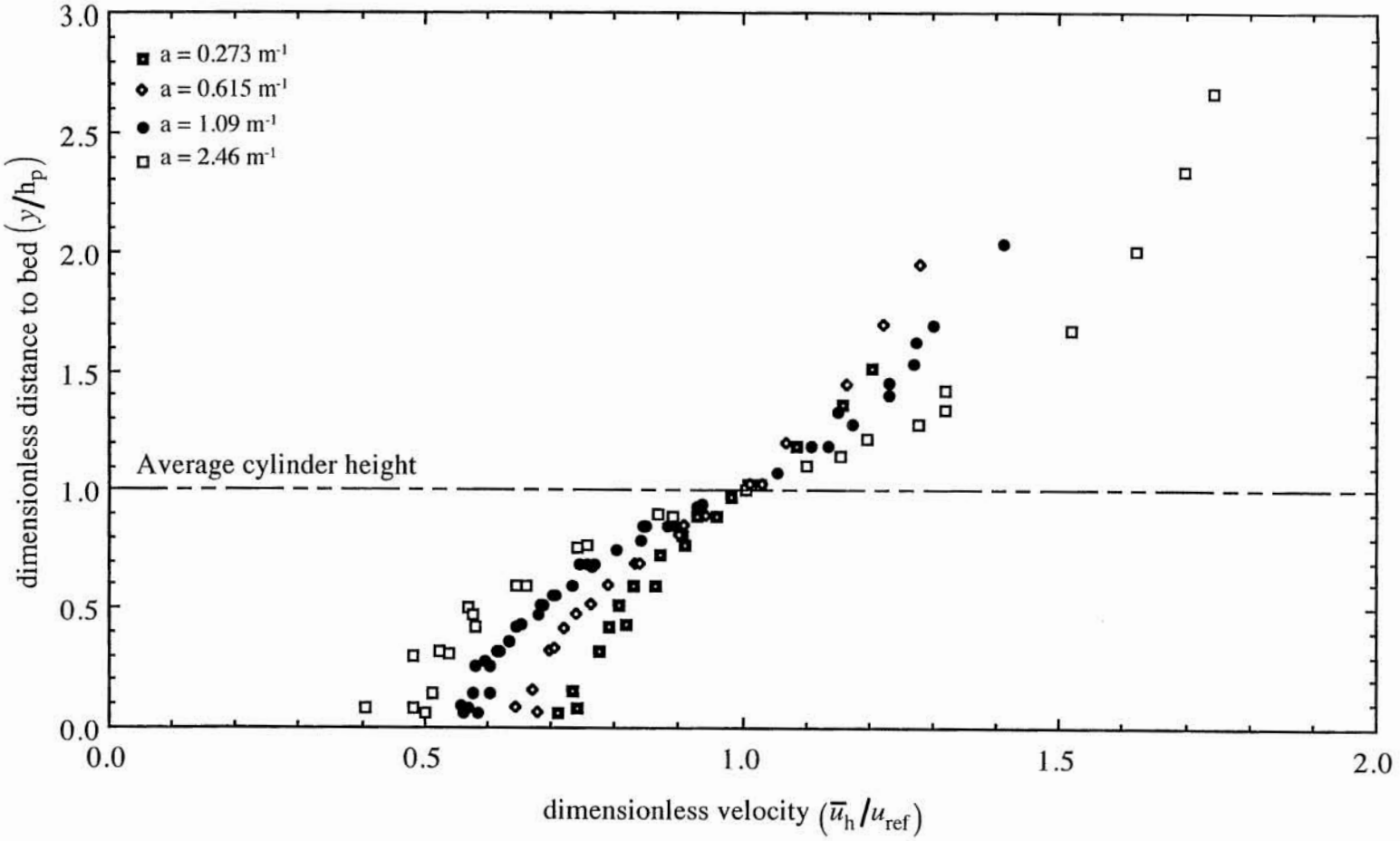

Figure 5.3 Dimensionless velocity profiles for flow through rigid cylinders

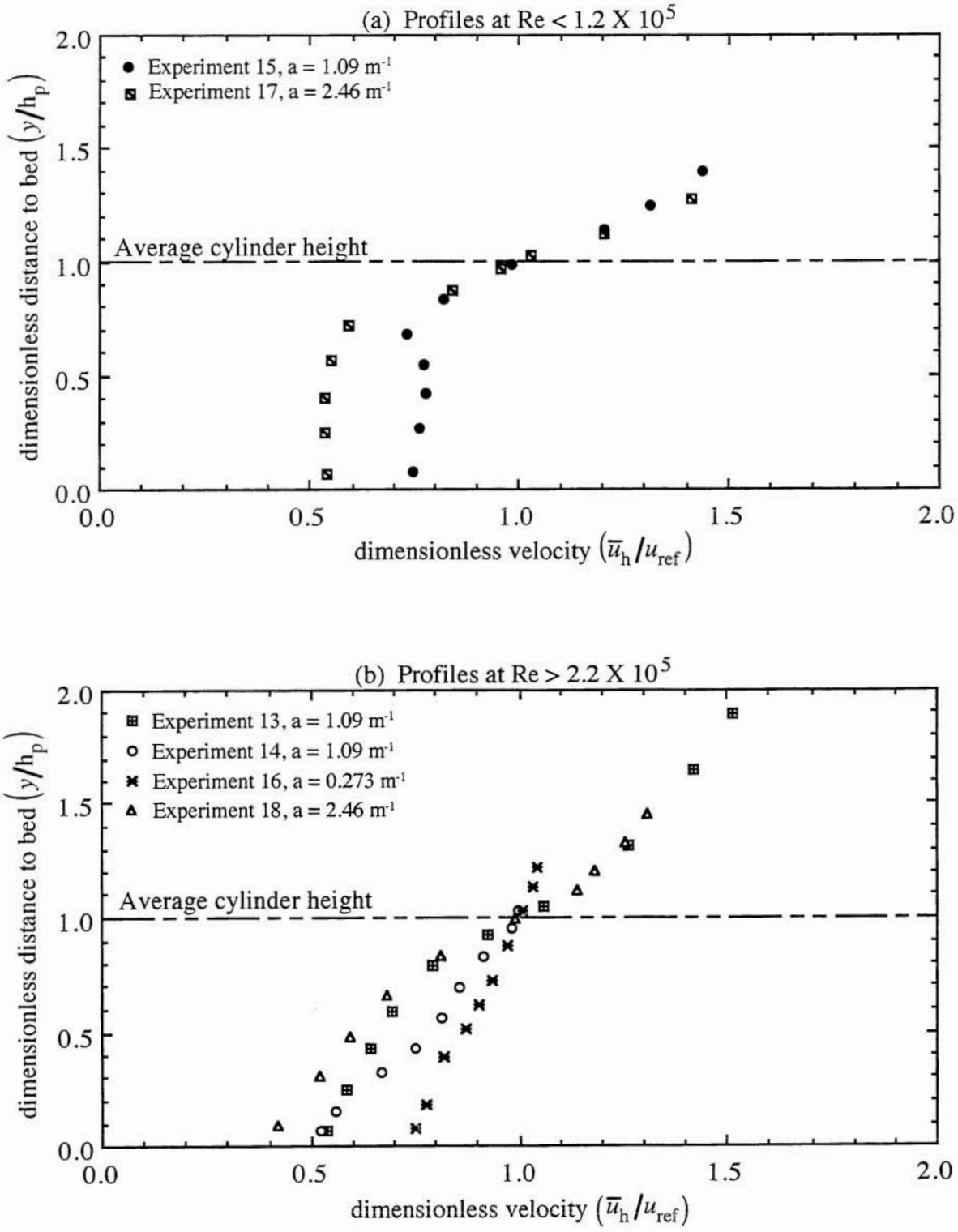

Figure 5.4 Dimensionless velocity profiles for flow through flexible cylinders

The velocity profiles varied significantly in general shape and magnitude even for the limited experimental conditions tested for flexible cylinders. For instance, the profile for Experiment 17 resulted in nearly constant velocities within the canopy, whereas the profile for Experiment 18 resulted in a profile that varied much more within the canopy even though these profiles were measured at the same cylinder density. The shapes of these profiles can best be explained by the experimental observations made in Section 5.5. When the deflection angle was relatively low, as was the case in Experiment 17, the profile exhibited a nearly constant velocity within the canopy. This is believed to be the consequence of the lateral swaying of the flexible cylinders at low deflection angles. However, high angles of deflection yielded velocity profiles that more closely resembled that of a standard open-channel. The deflected cylinders apparently offered less resistance to the flow. The most noticeable difference between the profiles through rigid cylinders and profiles through the slightly deflected flexible cylinders was that the slightly deflected cylinders offered greater resistance to the flow near the top of the canopy than did the rigid cylinders. This was the result of the violent swaying motion of the flexible cylinders at low flows. The violent swaying of the cylinders in the z-y plane offered much more drag than the fixed rigid cylinders.

For flexible vegetation, it is apparent that many factors affected the shape of the velocity profiles. The cylinder density was important, but so were the cylinder flexibility and the canopy velocity since they determined the deflection and swaying of the cylinders. The two profiles with $Re < 1.2 \times 10^5$ were of significantly different shape than the three with $Re > 2.2 \times 10^5$ as illustrated in Figure 5.4. The profiles with the lower Re values exhibited nearly constant velocities in the cylinder canopies.

5.6.2 Turbulence Intensity Profiles

Although not a major focus of this study, profiles of turbulence intensity were measured. Appendix B reports the values of the three components of root-mean-squared velocity fluctuations. These profiles were not horizontally averaged like the velocity measurements. To illustrate the typical shape of the three turbulent intensity profiles, Figure 5.5 is presented. This figure is for Experiment 13, profile number 1 through flexible cylinders and was chosen because its shape was typical of the measured profiles. The profiles of the root-mean-squared velocity fluctuations showed no obvious differences between flow through rigid or flexible cylinders; in both cases, the turbulence intensities were suppressed inside the canopy.

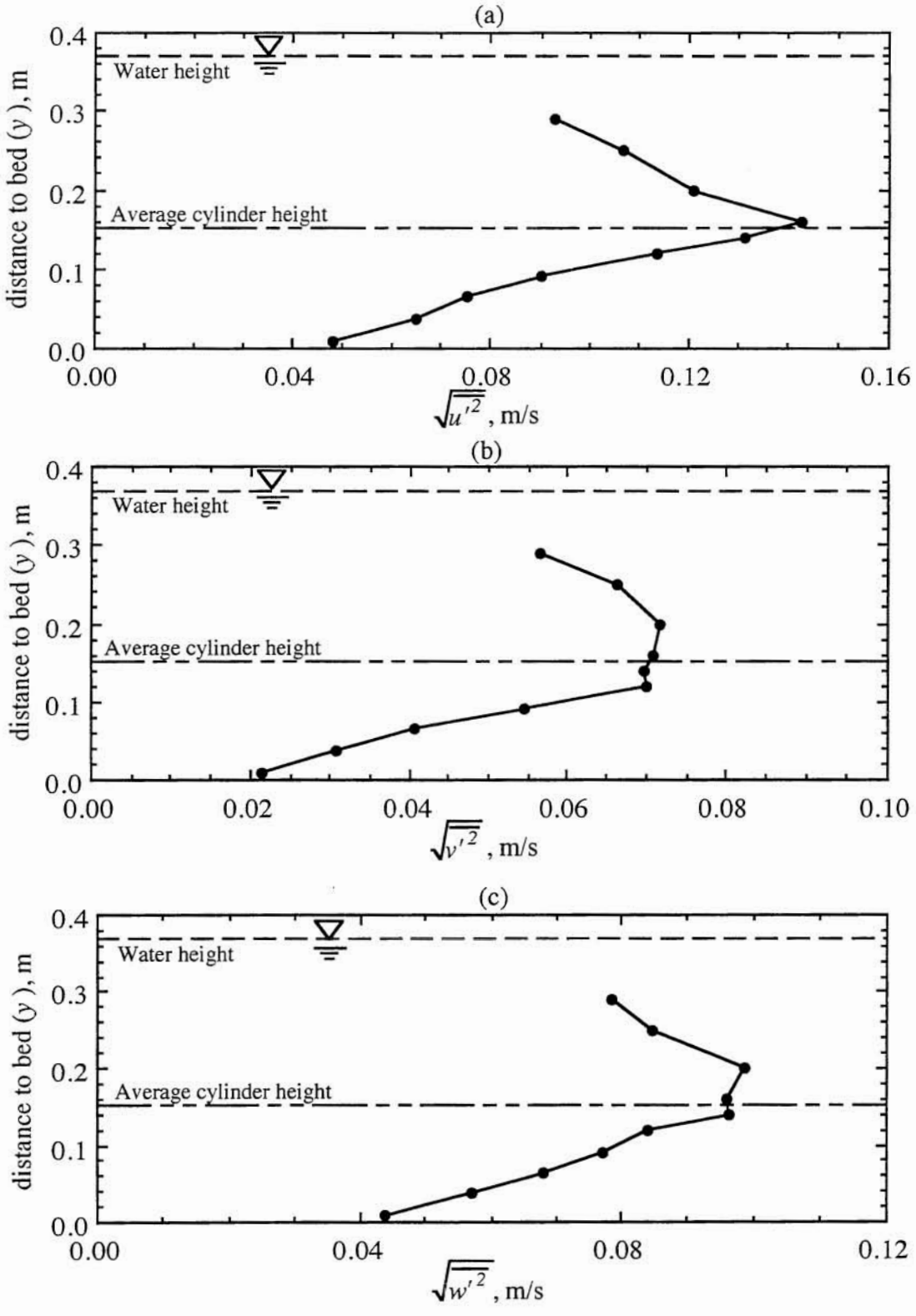

Figure 5.5 Turbulence intensity profiles for Experiment 13, profile number 1

An interesting tendency that was discovered in the course of the analysis was that the mean turbulence intensity, $\bar{i}_c$, (defined by equation 5.3) within the canopy was strongly related to the dimensionless variable H*a* (the product of flow depth and cylinder density). This is illustrated in Figure 5.6.

$$\bar{i}_c = \frac{1}{h_p} \int_0^{h_p} \frac{\sqrt{\overline{u'^2}}_h}{u_h} dy \tag{5.3}$$

This correlation was not totally unexpected however, since an increase in cylinder density, *a*, was expected to increase the level of turbulence in the canopy as discussed by Seginer et al. (1976) and mentioned in Chapter 2. However, the dimensionless variable H*a* was found to be more strongly correlated to $\bar{i}_c$ than to the cylinder density, *a*, alone.

5.6.3 Reynolds Stress Profiles

The Reynolds stress profiles had characteristic shapes that were much like the anticipated shapes discussed in Chapter 3 and illustrated in Figure 3.3. The dimensionless horizontally averaged profiles for rigid cylinders are shown in Figure 5.7. The profiles have been made dimensionless by dividing the Reynolds stress by the maximum Reynolds stress for that profile. Typically the maximum Reynolds stresses occurred at the top of the cylinder canopy. The y-axis was made dimensionless by dividing the distance to the bed, *y*, by the average cylinder height, h_p, in the region within the canopy, and dividing the quantity (y-h_p) by (H-h_p) above the canopy. These profiles collapsed for equal plant densities, although quite a bit of scatter existed. It is evident though, that trials with lower cylinder densities produced profiles with higher dimensionless Reynolds stresses, which was especially evident closer to the bed. This trend can be explained as follows. For densely vegetated open-channels, most of the resistive force is supplied by the vegetation and not by the bottom friction. Therefore, the turbulent stress near the bed is lower in a more densely vegetated canopy. As the vegetation density decreases, the measured Reynolds stress near the bed approaches the theoretical value for open-channels shown in Figure 3.2. This explanation is consistent with the measured profiles in Figure 5.7.

The profiles of dimensionless Reynolds stress for flow through flexible cylinders shown in Figure 5.8 had the same general trend as those through rigid cylinders in that the Reynolds stress was damped inside of the vegetative canopy, but the degree to which the Reynolds stress

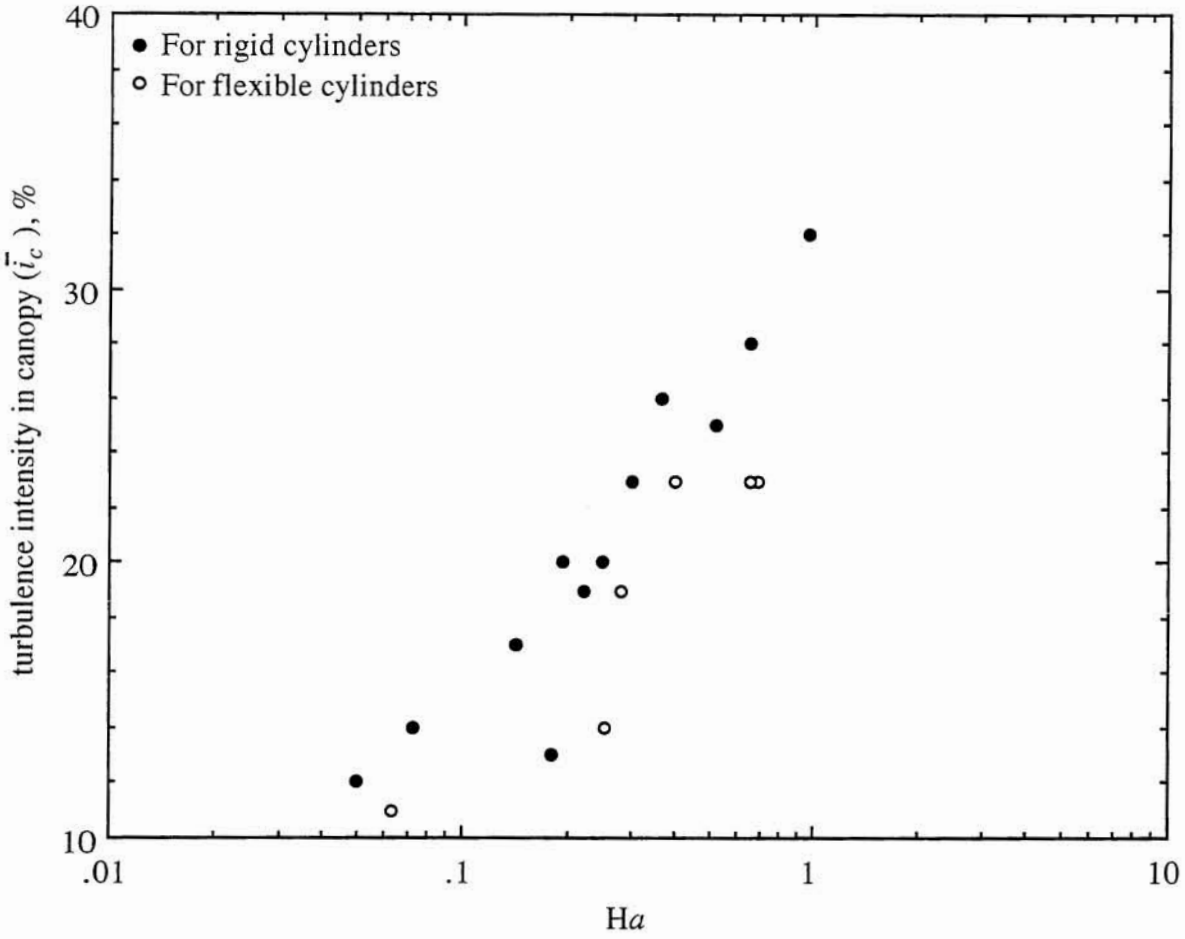

Figure 5.6 Correlation between the turbulence intensity in the canopy and the dimensionless parameter H*a*

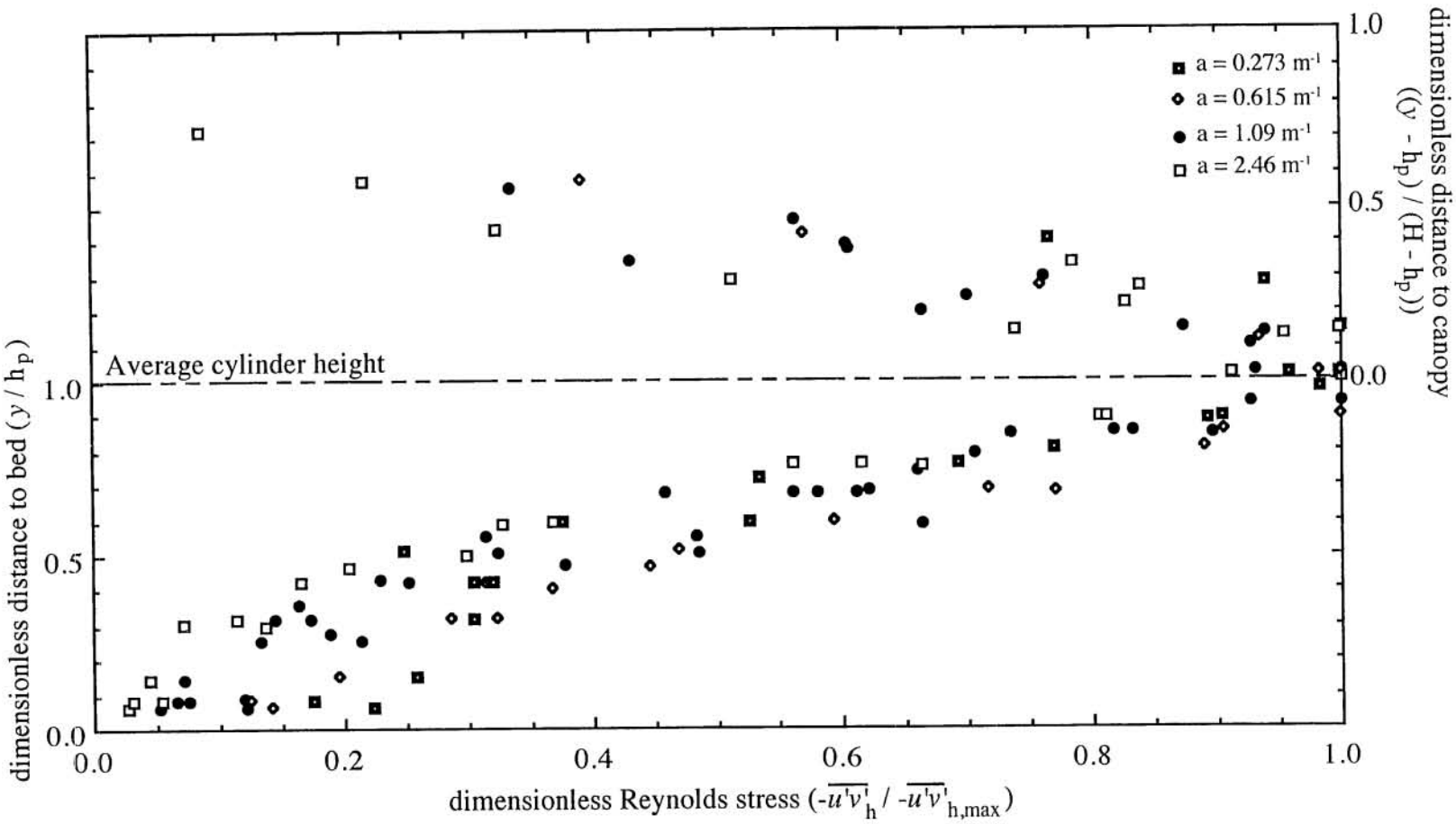

Figure 5.7 Dimensionless Reynolds stress profiles for flow through rigid cylinders

was suppressed was quite different. Again, the plant density appeared to be a major factor in the shape and magnitude of the profiles. When the cylinder density was low, and the Reynolds number and deflection angles were high, the drag imposed by the cylinders was reduced and the profiles within the canopy moved towards the theoretical profile for open-channel flow without vegetation. The profiles for experiments 14 and 16 shown in Figure 5.8(b) are good examples of this phenomenon. Unlike all of the other measured profiles, these two profiles appear to be concave up. In addition, the velocity profiles of these two experiments shown in Figure 5.4(b) were the least affected by the vegetation, thus possibly explaining the different shapes of these two Reynolds stress profiles. The limited experimental data and its relatively high scatter, along with the relative complexity of this flow condition made it difficult to determine what variables were relevant in determining the shapes of the Reynolds stress profiles for flexible vegetation. Although it is clear that the cylinder density and flexibility played a major role in the Reynolds stress profiles, factors such as Reynolds number and Froude number may have also played an important part. Further experimentation is required to determine this conclusively.

An interesting observation comes from the measured profiles for experiments 15 and 17. Notice from Figure 5.4(a) that these profiles had nearly constant values of $\overline{u}_h$ within the canopy. Figure 5.8(a) illustrates that these two profiles also had nearly constant values of Reynolds stress below the dimensionless height of 0.5. The data in Appendix C shows that the Reynolds stresses were approximately equal to zero. This means that very little turbulent vertical transport of momentum occurred in these profiles below 0.5 units and the velocity was almost constant, thereby approximating flow conditions in which drag coefficients for cylinders have been readily measured.

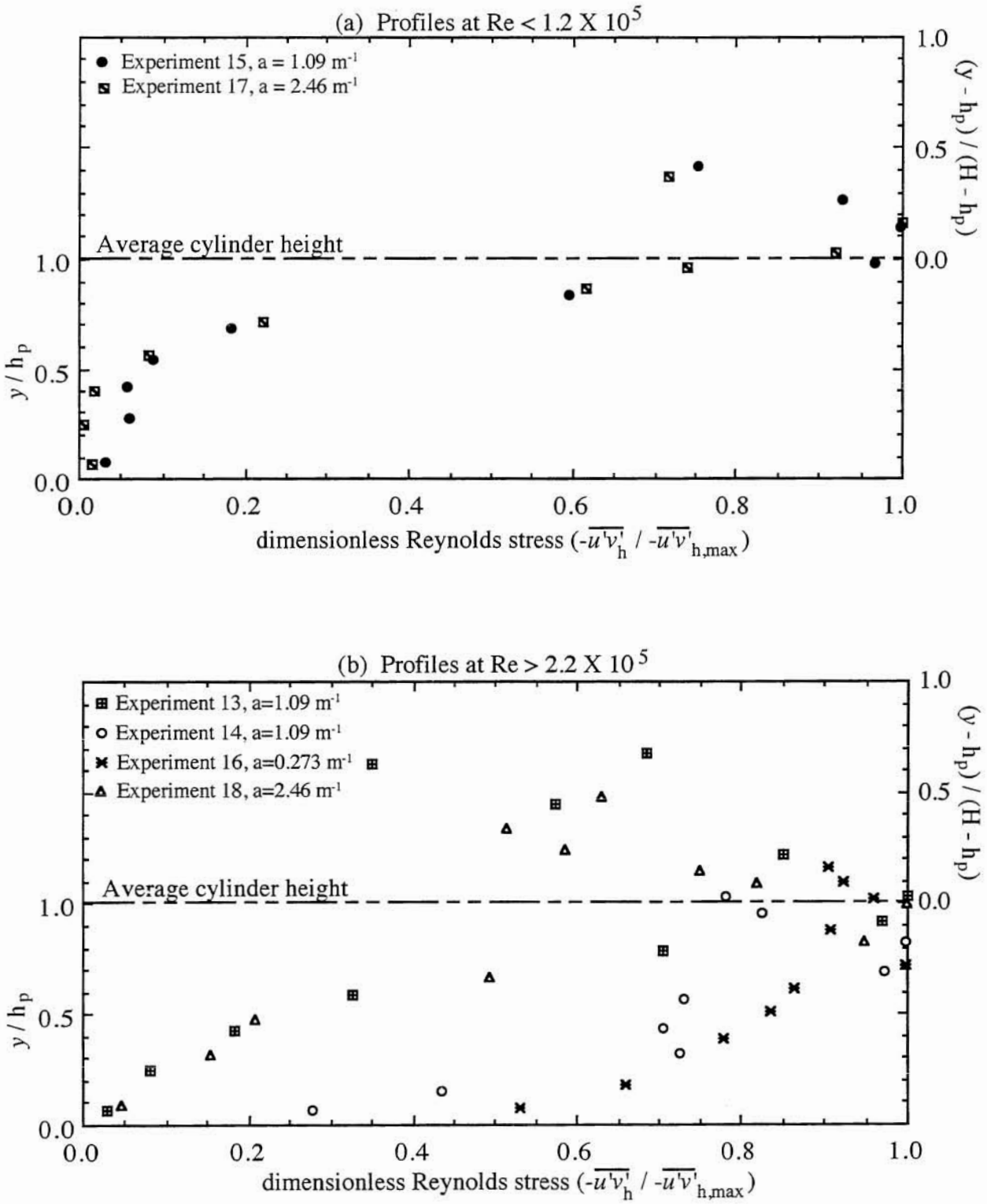

Figure 5.8 Dimensionless Reynolds stress profiles for flow through flexible cylinders

5.6.4 Drag Coefficient Profiles

Equation 3.44, along with the horizontally averaged velocity and Reynolds stress profiles described above, were used to compute local horizontally averaged drag coefficients. The values of the computed drag coefficient profiles are included in Appendix C. Figure 5.9 shows two of the computed profiles of C_D' for flow through rigid cylinders. The computed drag coefficient profiles were not constant throughout the canopy as many researchers have assumed, but instead typically reached a maximum within the canopy and diminished towards a minimum at the top of canopy. At the top of the canopy, there is a discontinuity in the value of the drag coefficient. This discontinuity occurs because of the discontinuity in the profiles of the horizontally averaged Reynolds stress. Since the gradients of the measured Reynolds stress profiles above the canopy were approximately linear and nearly equal to the theoretical gradient of the total shear stress (gS), the values of C_D' above the canopy computed from equation 3.44 were nearly equal to zero. This phenomenon can be seen in Figure 5.10 where four drag coefficient profiles have computed extending above the canopy top (using the value of a within the canopy. These four profiles were selected because they contained an adequate number of points above the canopy. Notice the discontinuity in the values of C_D' at the canopy top and that the value of C_D' are effectively equal to zero above the canopy. The greater value of C_D' at $y = h_p$ was computed in one of two ways. When the largest value of $-\overline{u'v'}_h$ was measured below the top of the canopy, $C_D'(h_p)$ was estimated by extrapolating a straight line from the points measured directly below h_p. When the largest value of $-\overline{u'v'}_h$ was measured slightly above the top of the canopy, C_D' at this point was calculated with the value of a inside the plant canopy, and $C_D'(h_p)$ was estimated by interpolating between the values of C_D' directly below and above the top of the plant canopy. The profiles selected for Figure 5.9 typify the tendency of the profiles to reach a maximum within the canopy. C_D' generally reached a maximum around the dimensionless height of 0.38, but this value ranged from 0.25 to 0.50. Eleven of the twelve C_D' profiles measured for rigid cylinders displayed this trend. All of these values of C_D' are shown in Figure 5.11, where y has been made dimensionless with the canopy height and C_D' has been made dimensionless with the integrated average bulk drag coefficient, $\overline{C_{DA}}$. A third degree polynomial has been fit through the points with a correlation coefficient of 0.77 and is given below:

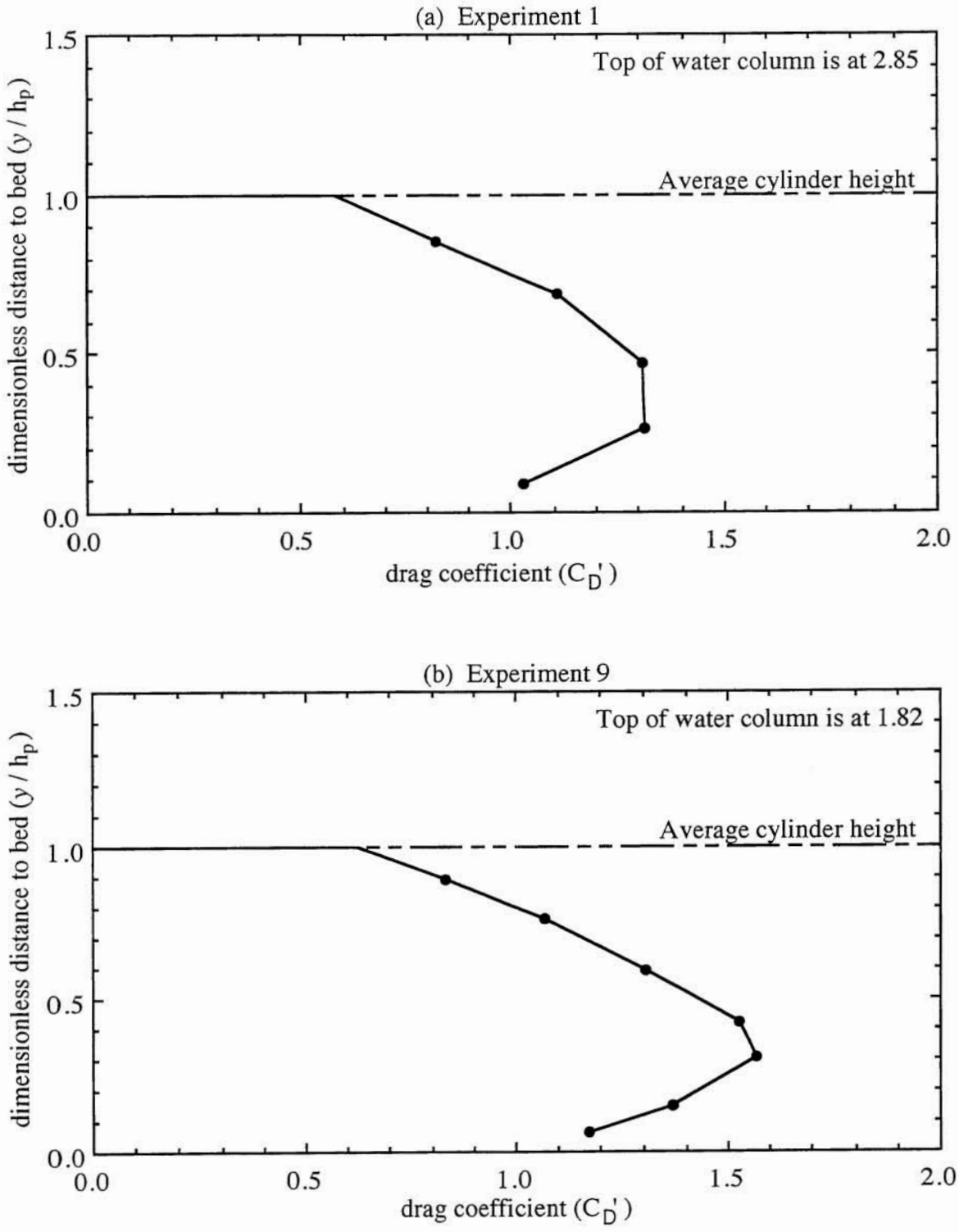

Figure 5.9 Profiles of the horizontally averaged drag coefficient for two experimental runs through rigid cylinders

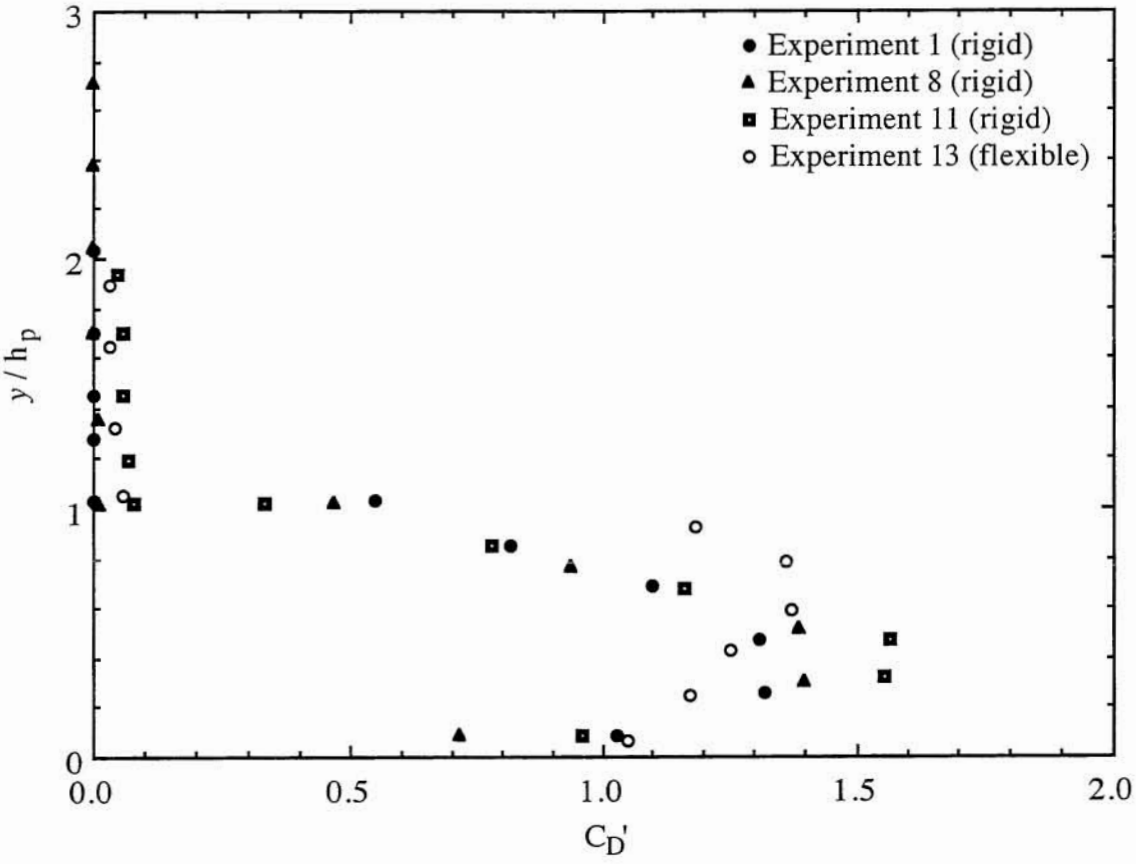

Figure 5.10 Profiles of the drag coefficient with values computed above the canopy for four experiments

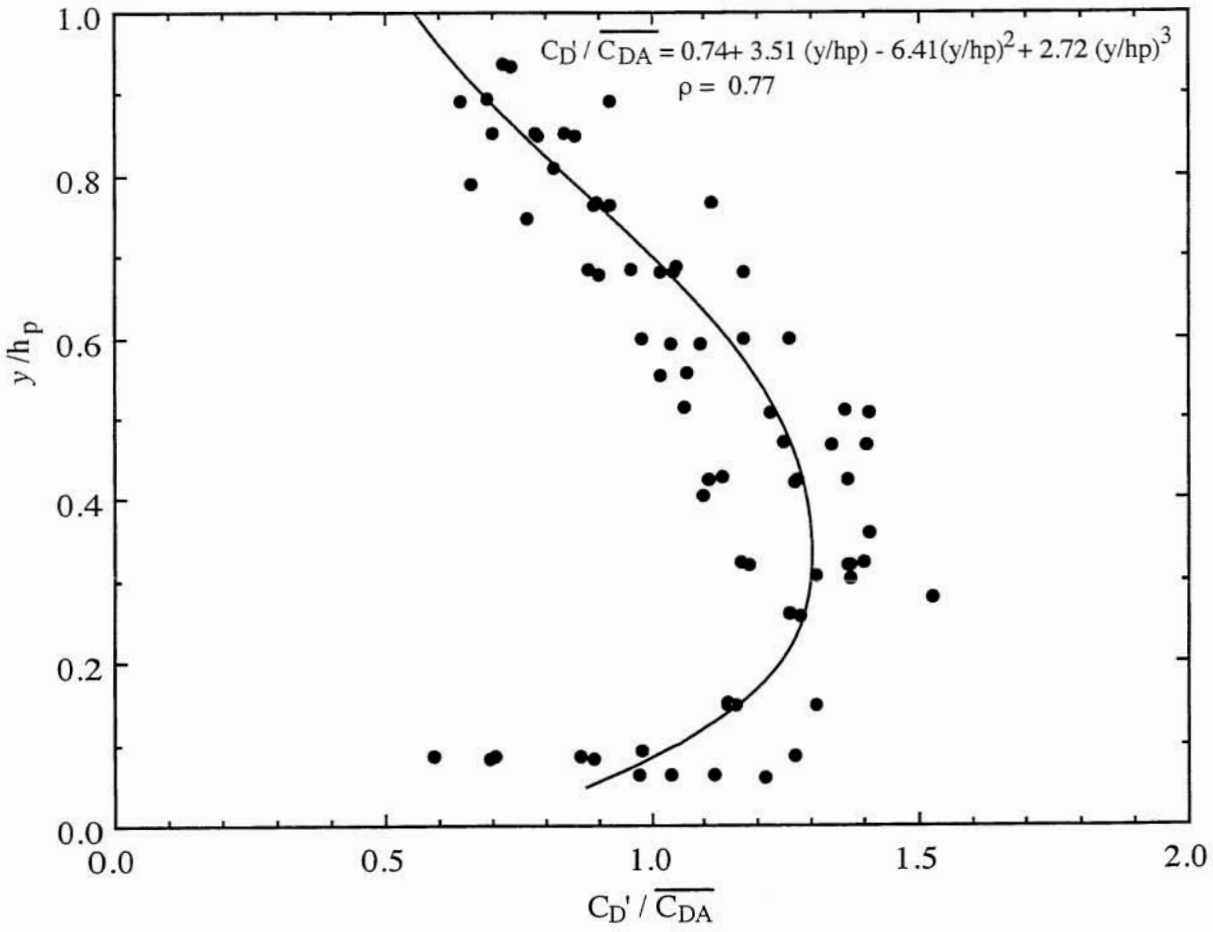

Figure 5.11 Vertical variation of the drag coefficient inside the canopy for rigid cylinders

$$\frac{C_D'}{C_{DA}} = 0.74 + 3.51\left(\frac{y}{h_p}\right) - 6.41\left(\frac{y}{h_p}\right)^2 + 2.72\left(\frac{y}{h_p}\right)^3 \qquad (5.4)$$

The bulk drag coefficient characterizes the C_D' profile and the parameters influencing the bulk drag coefficient will be examined exhaustively in Section 5.8.

The profiles of C_D' for flexible vegetation revealed two general profile shapes. Two measured profiles are shown in Figure 5.12 and exhibit the shapes that were commonly found. The profile of Experiment 13, Figure 5.12(a), reached a maximum within the canopy, much like those for rigid cylinders, although the maximum was higher in the profile than that typically found for rigid cylinders. This was common for the profiles of this shape in flexible cylinders. The cylinders in the experimental runs resulting in this characteristic drag coefficient profile swayed (sometimes violently in the transverse direction) but never deflected more than 45 degrees. The similarity between these profiles and the profiles for rigid vegetation may be linked to the similarities as described by Kouwen and Unny (1973) between the rigid and swaying vegetation flow regimes.

The second general shape of the C_D' profiles is illustrated by Experiment 16 in Figure 5.12(b). In this case, C_D' was maximum near the bottom and decreased as the distance from the bed increased. The profiles with this shape resulted from experiments where the cylinder deflected by at least 50 degrees. Again, the differences between the prone and rigid/swaying regimes may account for this entirely different shape of the C_D' profile.

5.7 Effectiveness of Measuring Techniques and Computational Methods

The results discussed in this chapter allow for some remarks about the general effectiveness of the velocity measuring device, flexible vegetation modeling technique, and drag coefficient computation method. Each of these will be discussed below.

5.7.1 Acoustic Doppler Velocimeter

The ADV was an effective method of measuring point velocity, Reynolds stress, and turbulence intensity. It was exceptionally easy to setup and use. The data gathered by the ADV appeared to be accurate with the following exception. Near 2.75 centimeters from the bottom of the channel, a problem with reflections from the bed caused inaccurate measurements of velocity fluctuations, although the mean values were unaffected. In some cases, a measuring point was taken too close to this location and the resulting turbulence intensity was

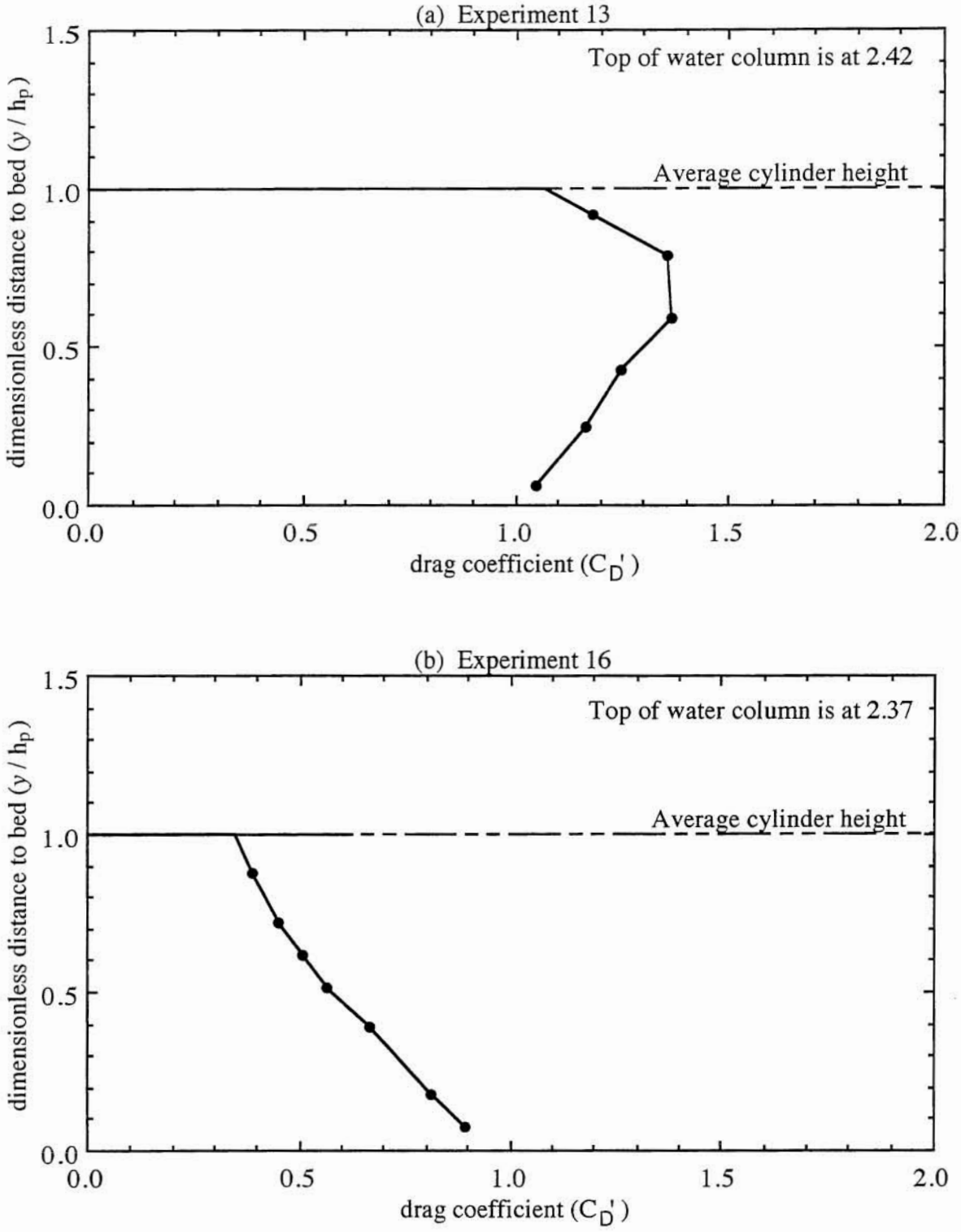

Figure 5.12 Profiles of the horizontally averaged drag coefficient for two experimental runs through flexible cylinders

excessive. These points were easy to detect from simple observations of the turbulence intensity profiles. Reynolds stress values appeared to be only slightly affected by this problem.

The largest problem in using the ADV was in the loss of the measurable water column when measuring a vertical profile. This resulted in the need for the upper portion of the profiles to be estimated, and therefore shape factors which were based on estimated values near the top of the water column. The loss of the measurable water column also prohibited the consideration of emergent cylinders, since much of the water column within the canopy would have been impossible to measure.

A second problem was encountered while measuring profiles in the flexible cylinders. As the cylinders progressively deflected, it became increasingly difficult to place the ADV into the canopy. Care had to be taken to insure that the placement of the ADV was such that, as it was lowered into the canopy, one of its three receivers did not contact a cylinder. This problem imposed a minimum cylinder spacing of 5.08 centimeters for the experiments.

5.7.2 Simulated Flexible Vegetation

The drinking straws used to simulate flexible vegetation were an effective method of introducing the flexibility parameter into the system. The results presented above show that the flexibility of the cylinders significantly affected the various profiles and the values of the bulk drag coefficients. This indicates that care should be taken when extending the results of rigid obstruction flow experiments to cases of flexible vegetation.

The flexible cylinders deflected and swayed in the water flow. This phenomenon is consistent with the observations of Tsujimoto et al. (1991) and Kouwen and Li (1980) for natural vegetation in open-channels. In addition, the straws in these experiments swayed more violently for smaller submerging discharges. Whether this is a characteristic common to natural vegetation is unknown.

5.7.3 Method of Computing Horizontally Averaged Drag Coefficients

The accuracy of the method of computing the horizontally averaged drag coefficient, C_D', introduced in Chapter 3 was dependent upon the validity of the assumptions that were needed for its conception and on the accuracy of the measurements that went into it. As discussed in Section 5.7.1, the accuracy of the ADV measurements of $\overline{u}_h$ and $\overline{u'v'}_h$ were believed to be of very good quality. The other variables in equation 3.44 are a and S. The plant density,

a, was constant throughout the channel for each experiment and easy to accurately calculate as shown in equation 3.6. Errors in the measurement of the slope, S, introduced some error into the computation of C_D', since extremely small slopes were considered. However, care was taken to accurately measure the slope of the channel and water surface, so these errors were believed to be minimized.

The validity of equation 3.44 was dependent on the assumption that two-dimensional flow existed above the canopy and that the total shear stress above the canopy was totally due to the turbulent stress $-\rho\overline{u'v'}$. The other Reynolds stresses were assumed to be unimportant. It was possible to check these assumptions by plotting the dimensionless depth in the water column, y/H, versus the Reynolds stress per unit density made dimensionless with the shear velocity squared, gHS, and then comparing the points above the canopy to the theoretical average shear stress for two-dimensional flows, where the theoretical total shear stress per unit density was computed by

$$G = gS(H - y) \quad \text{for } y \geq h_p \tag{5.5}$$

The value of H was used in the definition of the shear velocity and not R, because in the center of the channel, where the measurements were taken, the effects of the wall were negligible. This was done for each experiment. The results were consistent and a typical plot is shown in Figure 5.13, which is for Experiment 8. Figure 5.13 clearly illustrates that the measured Reynolds stress above the simulated canopy was consistently smaller than the theoretical one for two-dimensional open-channel flows, G. However, this phenomenon is typical for free-surface flows (Nezu and Nakagawa, 1993). The deviation being explained by the action of secondary currents as well as other components of the Reynolds stress tensor and the magnitude of these effects being a function of the width-to-depth ratio (aspect ratio). The primary flow, U, and secondary currents V and W are described by (Nezu and Nakagawa, 1993)

$$V\frac{\partial U}{\partial y} + W\frac{\partial U}{\partial z} = gS + \frac{\partial\left(-\overline{u'v'}\right)}{\partial y} + \frac{\partial\left(-\overline{u'w'}\right)}{\partial z} \tag{5.6}$$

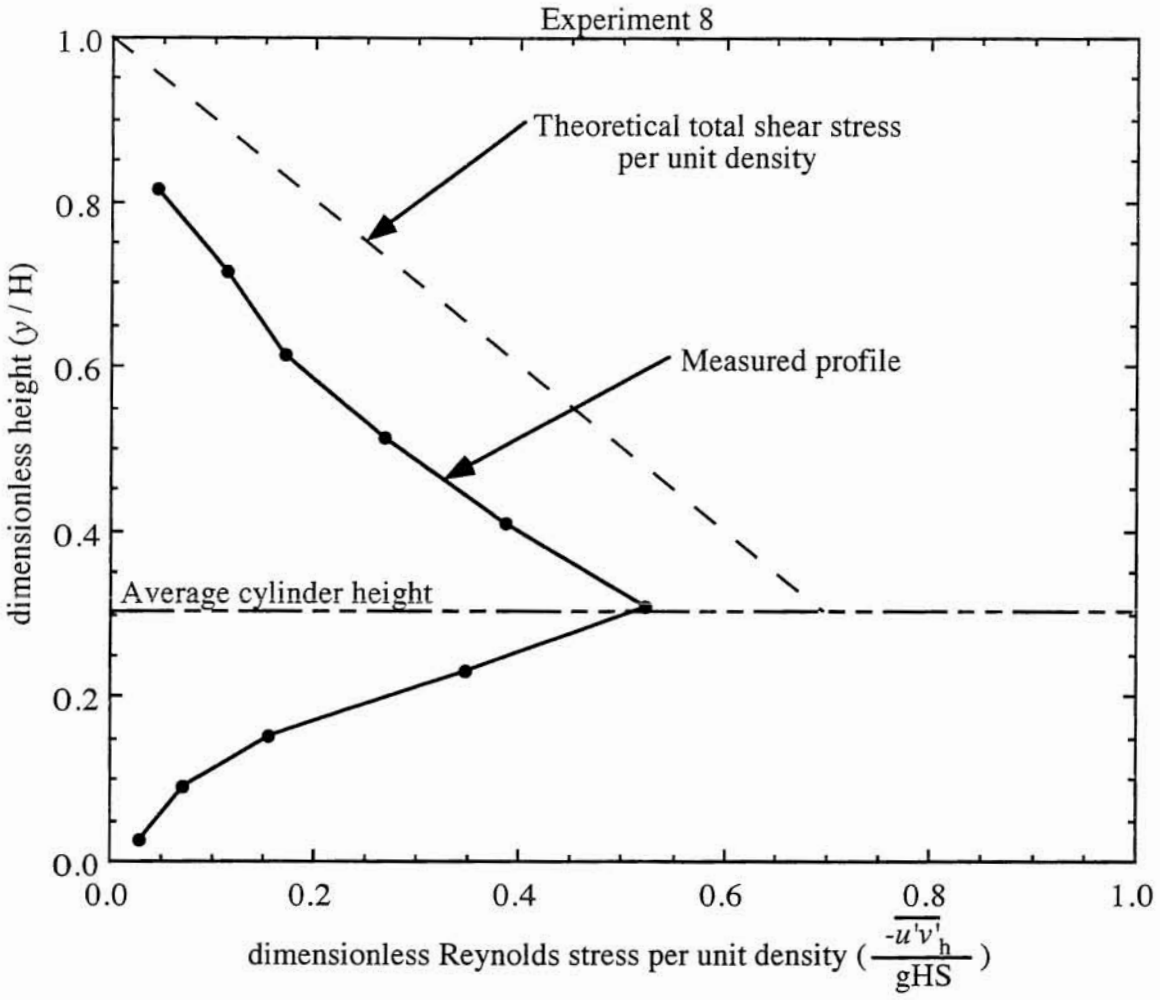

Figure 5.13 The dimensionless height versus the horizontally averaged dimensionless Reynolds stress per unit density. This figure shows the difference between the measured values of $-\overline{u'v'}_h$ and the theoretical total shear stress for Experiment 8, but is typical of all experiments.

when there are no pressure deviations in the x-direction. Integration of this equation in both the vertical and spanwise directions for high Reynolds numbers yields

$$\frac{\tau}{\rho} = \underbrace{gS(H-y)}_{G} + \underbrace{\int_H^y V\frac{\partial U}{\partial y}dy}_{SC1} + \underbrace{\int_H^y W\frac{\partial U}{\partial z}dy}_{SC2} + \underbrace{\int_H^y \frac{\partial}{\partial z}\left(\overline{u'w'}\right)dy}_{SUW} \tag{5.7}$$

where the quantities SC1, SC2 and SUW are as defined above. All of the measurements in the present investigation were taken very near the center of the channel, hence with W = 0, thereby reducing equation 5.7 to

$$-\overline{u'v'} = \underbrace{gS(H-y)}_{G} - \underbrace{\int_y^H V\frac{\partial U}{\partial y}dy}_{SC1} - \underbrace{\int_y^H \frac{\partial \overline{u'w'}}{\partial z}dy}_{SUW} \tag{5.8}$$

Now consider the last two terms on the right hand side of equation 5.8 (SC1 and SUW, respectively). In the upflow region dU/dy and V are both positive, hence VdU/dy > 0. Our results for flow above the canopy yielded positive transverse gradients of $\overline{u'w'}$ in the centerline region as shown in Figure 5.14. Thus, we expect these two terms to decrease the measured value of the primary Reynolds stress compared to the ideal two-dimensional flow conditions. This result is confirmed by observations of other researchers as illustrated in Figure 5.15, extracted from Nezu and Nakagawa (1993), which clearly shows the negative contribution of the two aforementioned terms as well as SC2 being nearly equal to zero.

Moreover, our observations show that the vertical gradient of the primary Reynolds stress is very close to the value of gS in the bulk of the flow (see Figure 5.13), thus indicating that all other terms in equation 5.6 also have to be in balance. We expect this balance to be altered only very close to the free surface, with $-\overline{u'v'}$ becoming positive. Experimental results of the present investigation confirm these expectations as shown in Figure 5.15, where SC1 is of the same order as SUW and the measured primary Reynolds stress profile is parallel to the G term distribution. We may therefore conclude that the measured bed and free-surface slope is very close to the one that provides the balance in the x-momentum equation (Yen, 1973 and 1992), and is thus the value that has been used throughout the present computations.

Finally, regarding the flow structure within the simulated vegetation, our observations indicate a negligible transverse gradient of $\overline{u'w'}$ as illustrated in Figure 5.16. Since the effects of

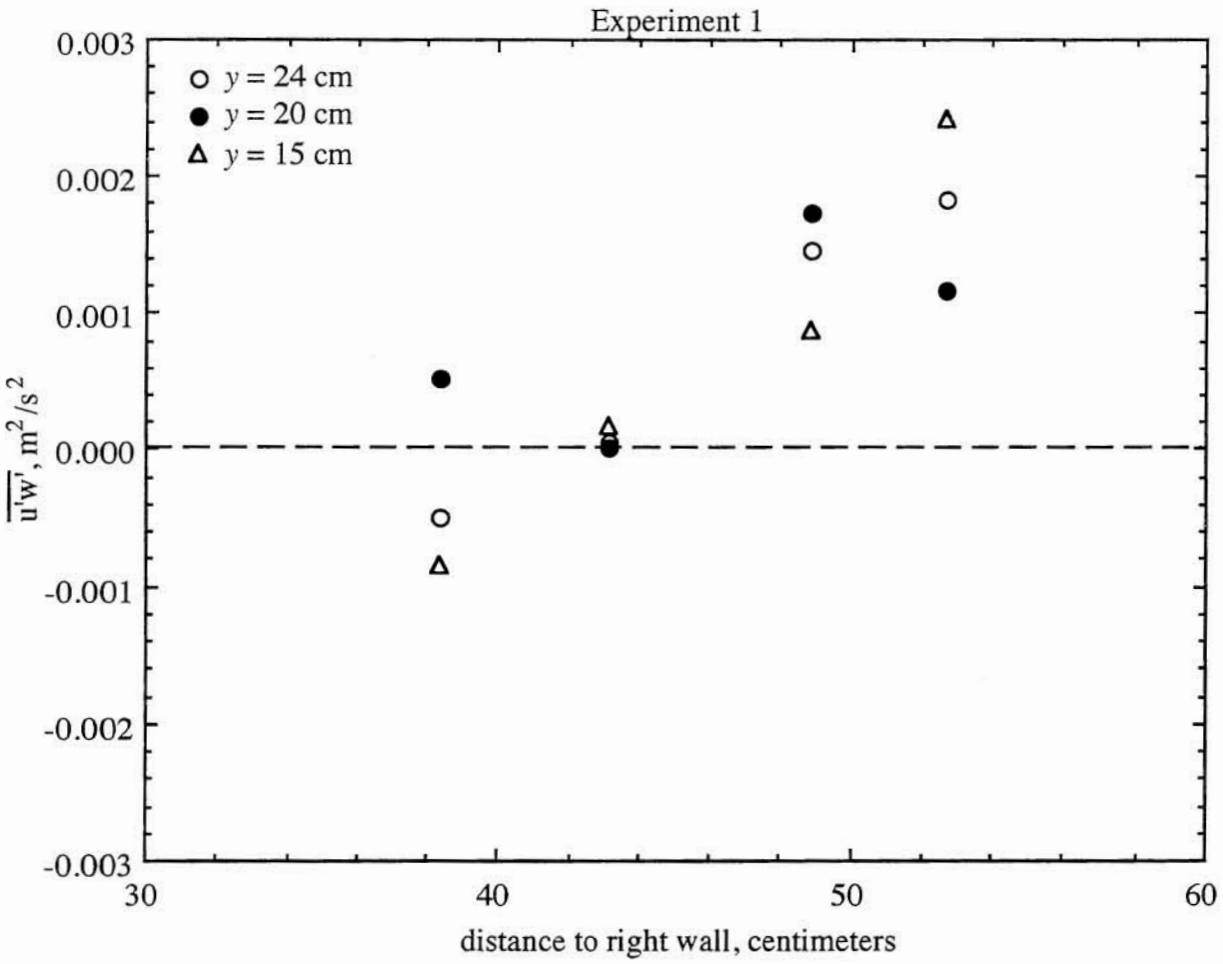

Figure 5.14 Cross-sectional distribution of $\overline{u'w'}$ above the canopy

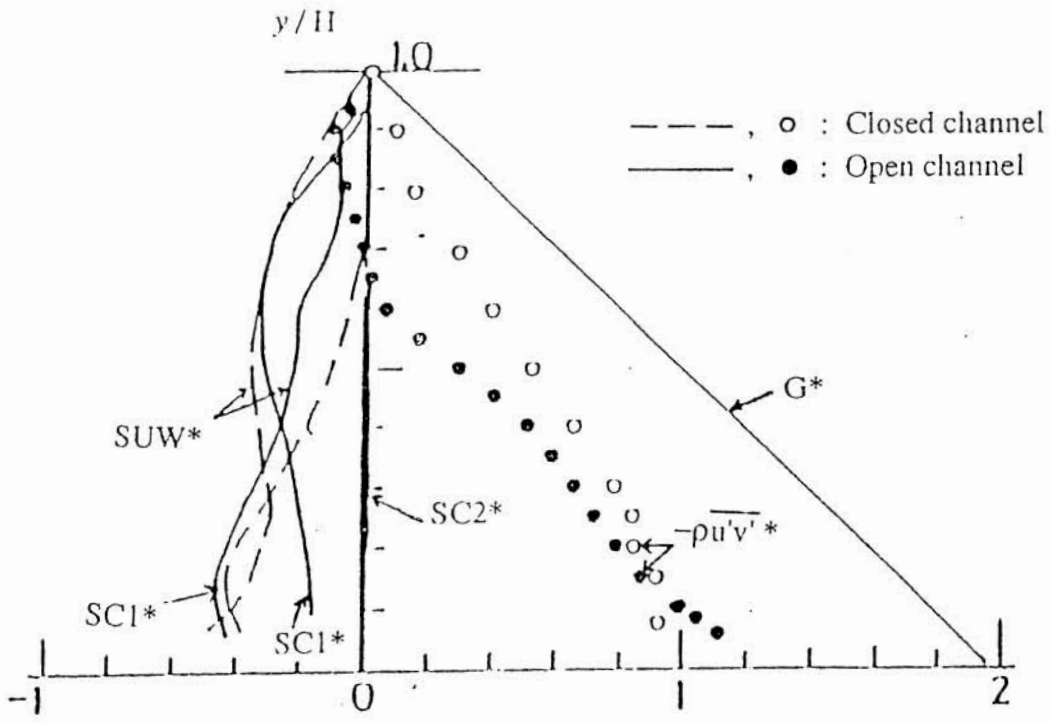

* indicates that the value has been made dimensionless with τ_b

Figure 5.15 Contributions of secondary currents to the shear stress (extracted from Nezu and Nakagawa, 1993)

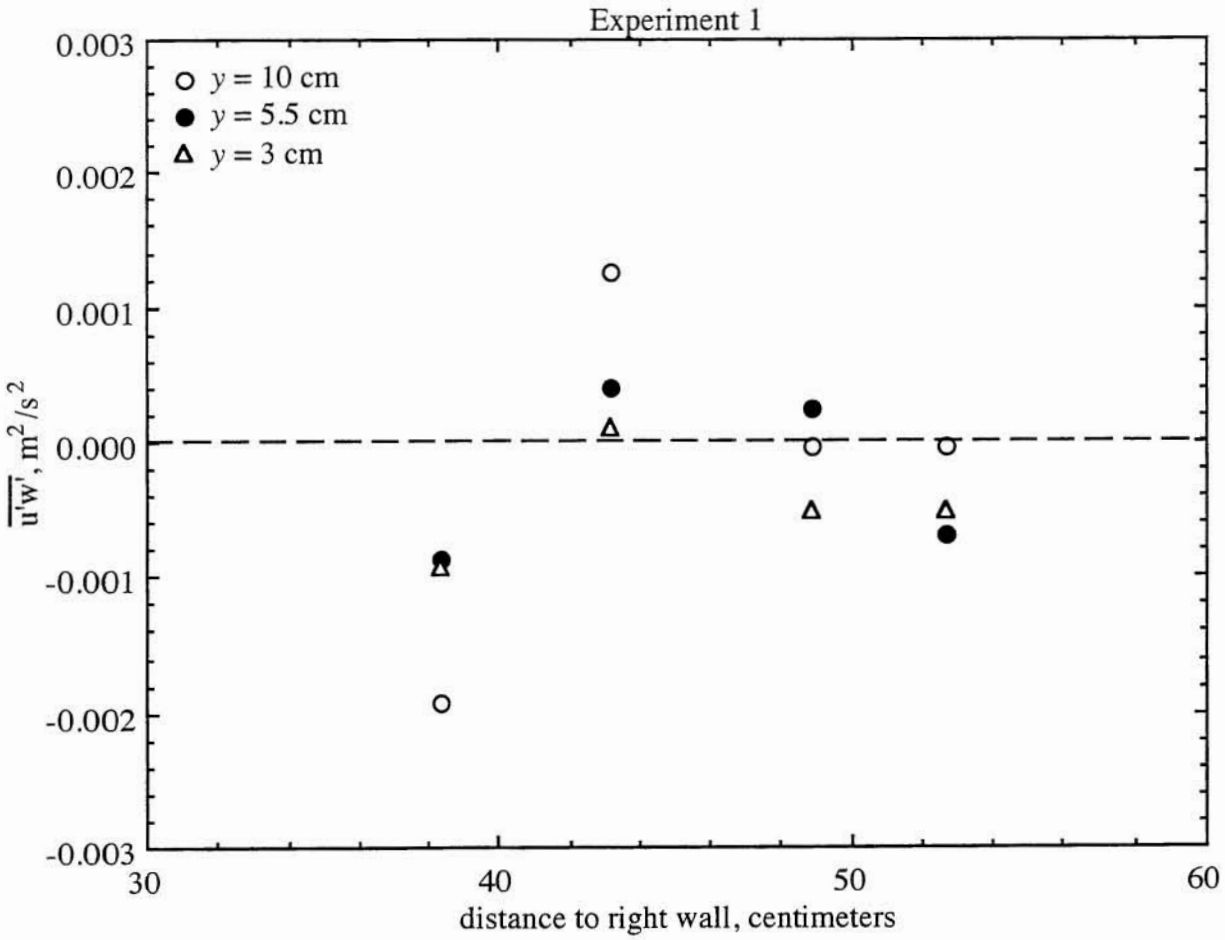

Figure 5.16 Cross-sectional distribution of $\overline{u'w'}$ within the canopy

secondary currents are also believed to be negligible inside the canopy as well as the viscous term, equation 5.6 reduces to equation 3.43, hence validating our computational procedure.

An observation of the profiles of velocity and Reynolds stress for Experiments 15 and 17 allowed for an easy check of the method described by equation 3.44 for computing drag coefficients. As discussed in Section 5.6.3, the profiles for experiment 15 and 17 displayed nearly constant values of velocity, u_c, and Reynolds stress inside the plant canopy below $y/h_p = 0.5$. Since the velocity profiles in this region were nearly uniform and the turbulent stresses were approximately negligible, the flow condition approached that of ideal uniform flow although with some level of turbulence intensity ($\sqrt{\overline{u'^2}}/\overline{u}_h \cong 3\%$, $\sqrt{\overline{v'^2}}/\overline{v}_h \cong 1$ to 3%,, and $\sqrt{\overline{w'^2}}/\overline{w}_h \cong$ 2.5 to 3.5%). Therefore, the estimate of the drag coefficient from equation 3.44 in this region of the flow should be very near to the value from the standard cylinder drag curve (see Figure 1.1). Equation 3.44 was used to compute the drag coefficient in the regions of constant velocity in these two experiments. Table 5.6 reports the estimates of C_D from equation 3.44 and those from the standard drag coefficient curve.

Table 5.6 Drag Coefficients for Approximately Ideal Flow Conditions

Experiment number	Velocity, u_c (m/s)	Cylinder Reynolds number	C_D from equation 3.44	C_D from standard drag curve
Experiment 15	0.248	1,868	1.05	0.97
Experiment 17	0.155	1,143	1.20	1.0

Table 5.6 shows that the values computed with equation 3.44 are in good agreement with values of C_D obtained from the standard drag curve (within 10%). This simple test corroborated the validity of this new method of computing drag coefficients.

The largest source of error introduced into the computation of C_D' was believed to be in the curve fitting procedure of $\overline{u'v'}_h$ within the plant canopy. As discussed in section 5.2, a third order polynomial was fit through the measured values of $\overline{u'v'}_h$ so that its rate of change with respect to y could be computed. In some cases only 4 or 5 points were measured within the canopy and the resulting curve fit had a low correlation. The computed value of C_D' depended heavily on the value of the derivative, $\frac{d}{dy}\left(\overline{u'v'}\right)_h$, and therefore depended quite heavily on the regression procedure. To increase the accuracy of the drag coefficient measurements,

it is recommended that as many points as possible be taken within the plant canopy and that a more accurate regression on these points be performed.

5.8 Effects of Channel and Flow Parameters on Bulk Drag Coefficients

The measured profiles discussed earlier in this chapter allowed for the computation of the various bulk drag coefficients ($\overline{C_{DB}}$, $\overline{C_{DH}}$, $\overline{C_{DA}}$, and $\overline{C_{DM}}$) defined in Chapter 3. Most of the developed vegetated open-channel models, including the backwater model introduced in the present study, employ a bulk drag coefficient to characterize the form drag created by the vegetation. The computed values of these coefficients for each experiment were reported in Tables 5.1 and 5.2. A primary objective of the present study was to determine the effects of various flow and channel parameters on the bulk drag coefficients. This section is dedicated to revealing the trends found in the analysis of the influences of the dimensionless parameters discussed in Chapter 4 on the various bulk drag coefficients.

Of primary interest in this study were the bulk drag coefficients $\overline{C_{DB}}$ and $\overline{C_{DH}}$ because of their direct application in equation 3.30. The values of these coefficients were plotted against each of the dimensionless parameters discussed in Chapter 4 (except α) to determine the influences of the individual parameters on their values. These plots have been included as Figure 5.17. The results for the rigid and flexible cylinders have been plotted together. To help identify the significance of the prone vegetation condition on the results, deformation angles have been included in the plots beside their respective points for flexible cylinders. General trends in the data plots revealed the possible significance of the dimensionless variables for the ranges given in Section 5.3. Since the values of $\overline{C_{DA}}$ closely agree with those of $\overline{C_{DB}}$, the trends plotted for $\overline{C_{DA}}$ closely resembled those for $\overline{C_{DB}}$. Likewise, the plots of $\overline{C_{DM}}$ versus the dimensionless parameters were much like those for $\overline{C_{DH}}$, because of the agreement between these drag coefficients.

Analysis of these plots revealed a possible influence of the Froude number on the value of $\overline{C_{DB}}$ for flow through flexible cylinders (see Figure 5.17(c)). There was a significant tendency for the value of $\overline{C_{DB}}$ to increase as Fr decreased in the flexible cylinder flow experiments. This trend was not evident for flow through rigid cylinders.

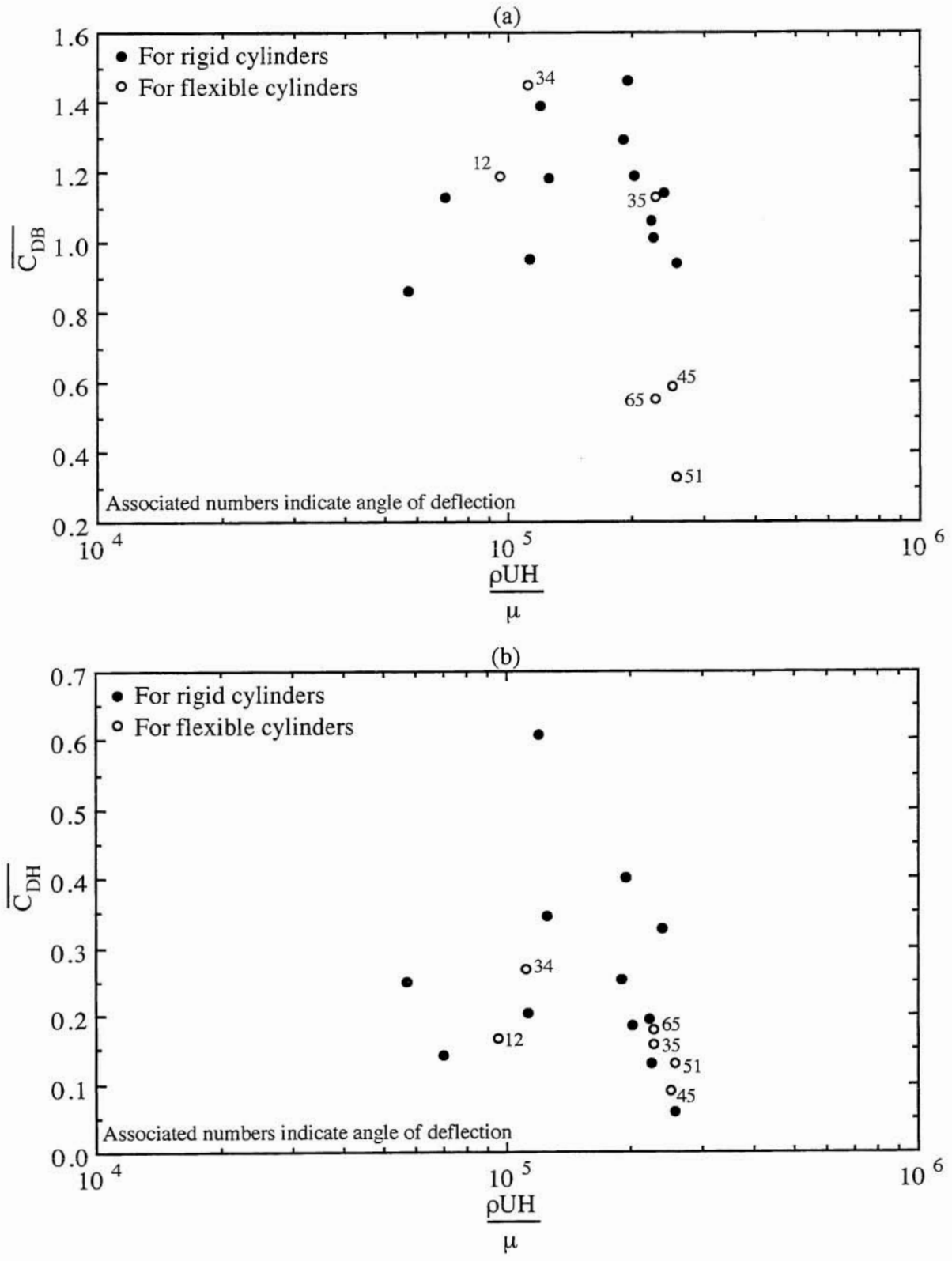

Figure 5.17 (a) and (b) Plots of the dimensionless parameters against the bulk drag coefficients $\overline{C_{DB}}$ and $\overline{C_{DH}}$ for rigid and flexible cylinders

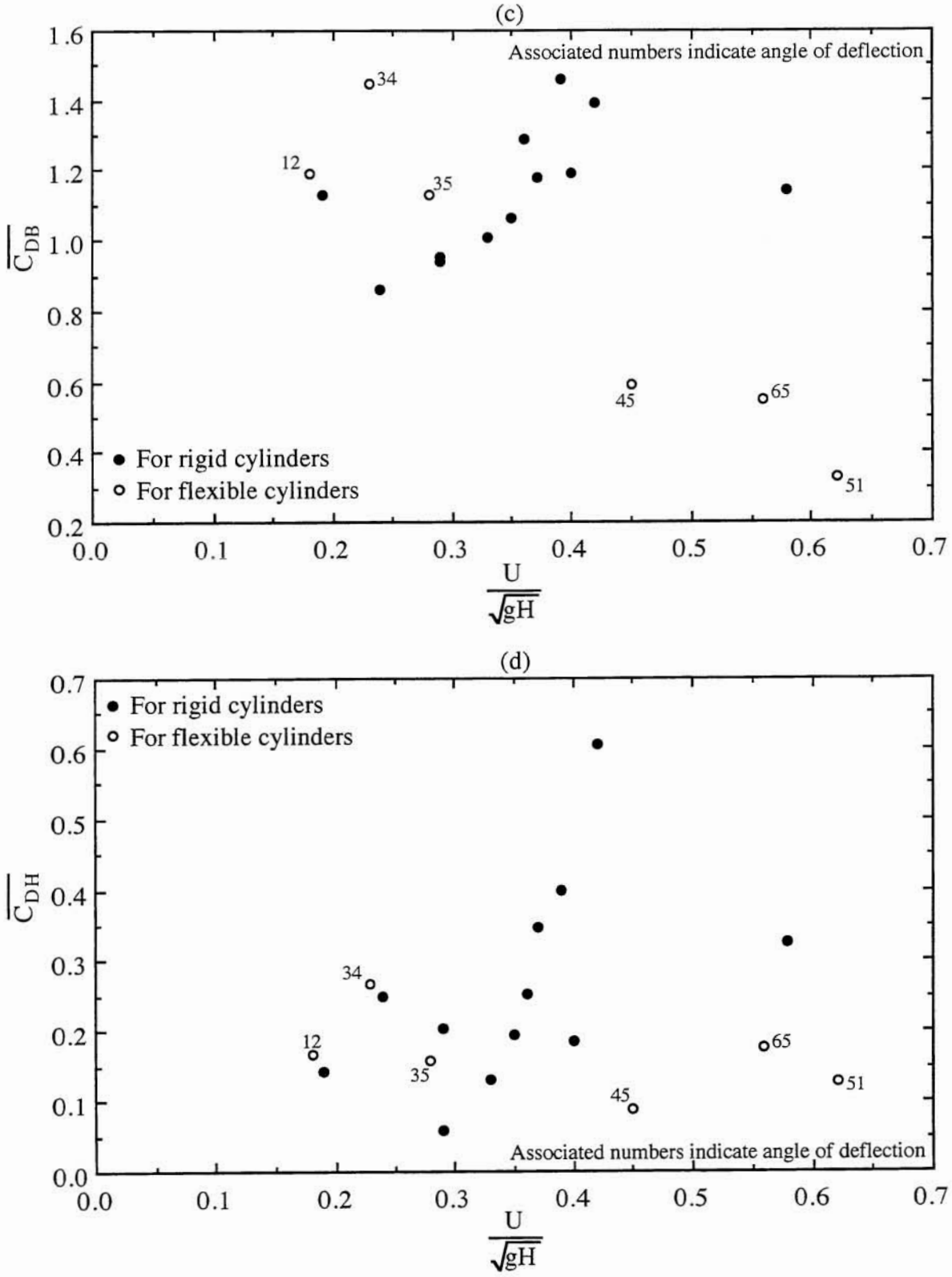

Figure 5.17 (c) and (d)

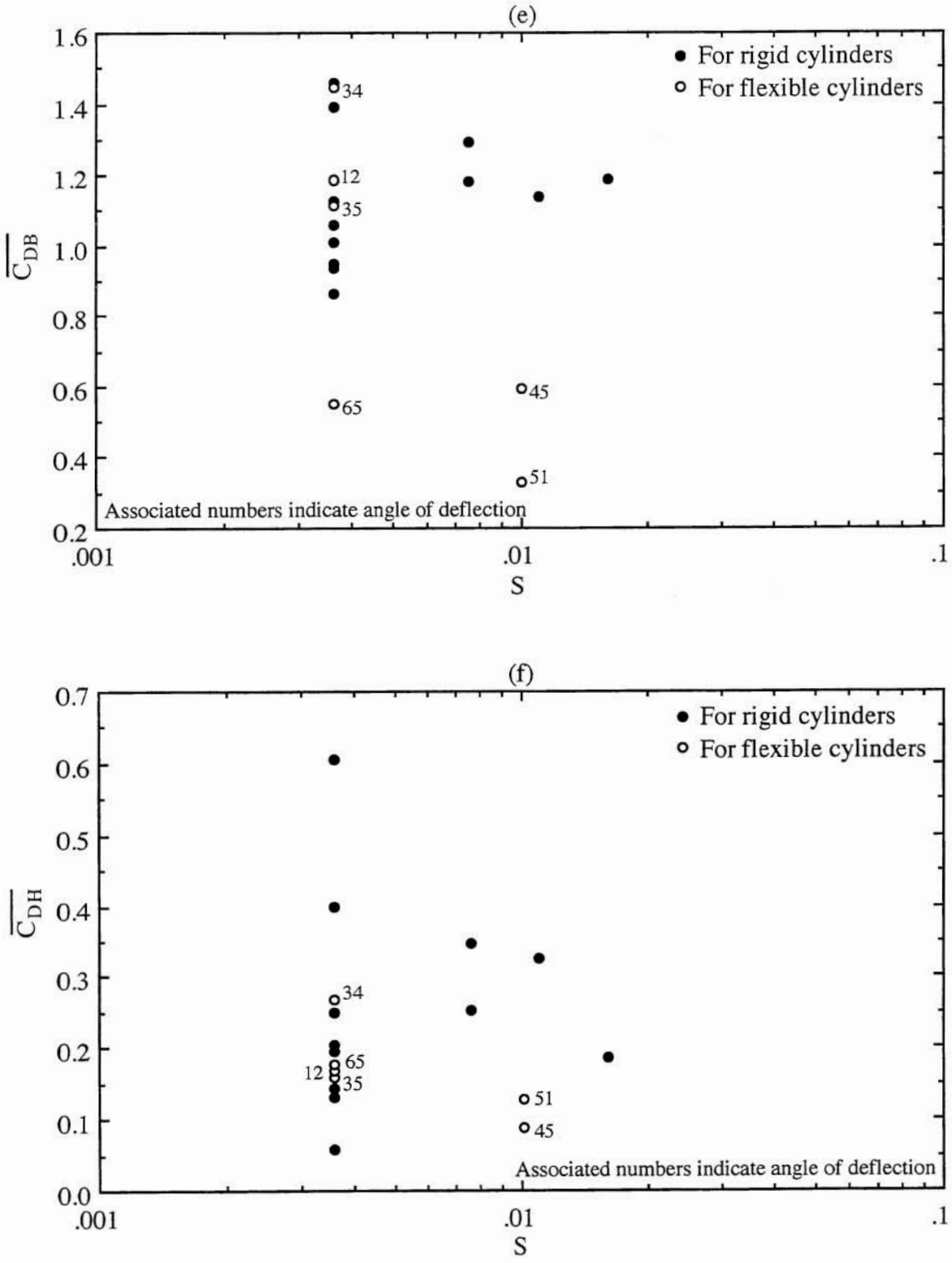

Figure 5.17 (e) and (f)

The most significant trend demonstrated in Figure 5.17 was the tendency of $\overline{C_{DH}}$ to decrease with increasing values of the dimensionless parameter H*a* (see Figure 5.17(j)). Both the rigid and flexible cylinder results fit into this trend. The points that tended to lie outside of this trend where for experiments with high deflection angles, possible indicating the presence of the prone vegetation condition. This was another indication that flow through prone vegetation should be analyzed separately than flow through the rigid and swaying vegetation regimes. Since the mean dimensionless turbulence intensity, $\bar{i}_c$, was strongly dependent on the H*a*, as previously discussed, $\overline{C_{DH}}$ was strongly correlated to $\bar{i}_c$. The effect of the cylinder density, *a*, on $\overline{C_{DB}}$ was not clear; however, in all but one case, as the cylinder Reynolds number (defined as $\rho U_c D/\mu$) for a given cylinder density increased, so did the value of $\overline{C_{DB}}$ for the rigid cylinders (see Figure 5.18). For the flexible cylinder experiments, this trend was reversed and as the cylinder Reynolds number decreased, $\overline{C_{DB}}$ increased. Analysis of the influences of *a* on $\overline{C_{DH}}$ revealed no similar trends.

The analysis of each of the dimensionless parameters performed in Figure 5.17 and discussed above indicated that no dimensionless parameter particularly influenced the value of $\overline{C_{DB}}$ for flow through rigid cylinders. For flexible cylinders only the Froude number appeared to significantly affect $\overline{C_{DB}}$. The bulk drag coefficient $\overline{C_{DH}}$ was noticeably influenced by the value of H*a* only. It is unclear whether most of the dimensionless parameters explicated in Chapter 4 were not found to influence the values of the bulk drag coefficients because only a limited range of their values were tested or because they were in fact not relevant. Experimental and computational errors may account for the variance in the values of the bulk drag coefficients alone. Further experimentation over larger ranges of the dimensionless parameters is recommended for more conclusive results.

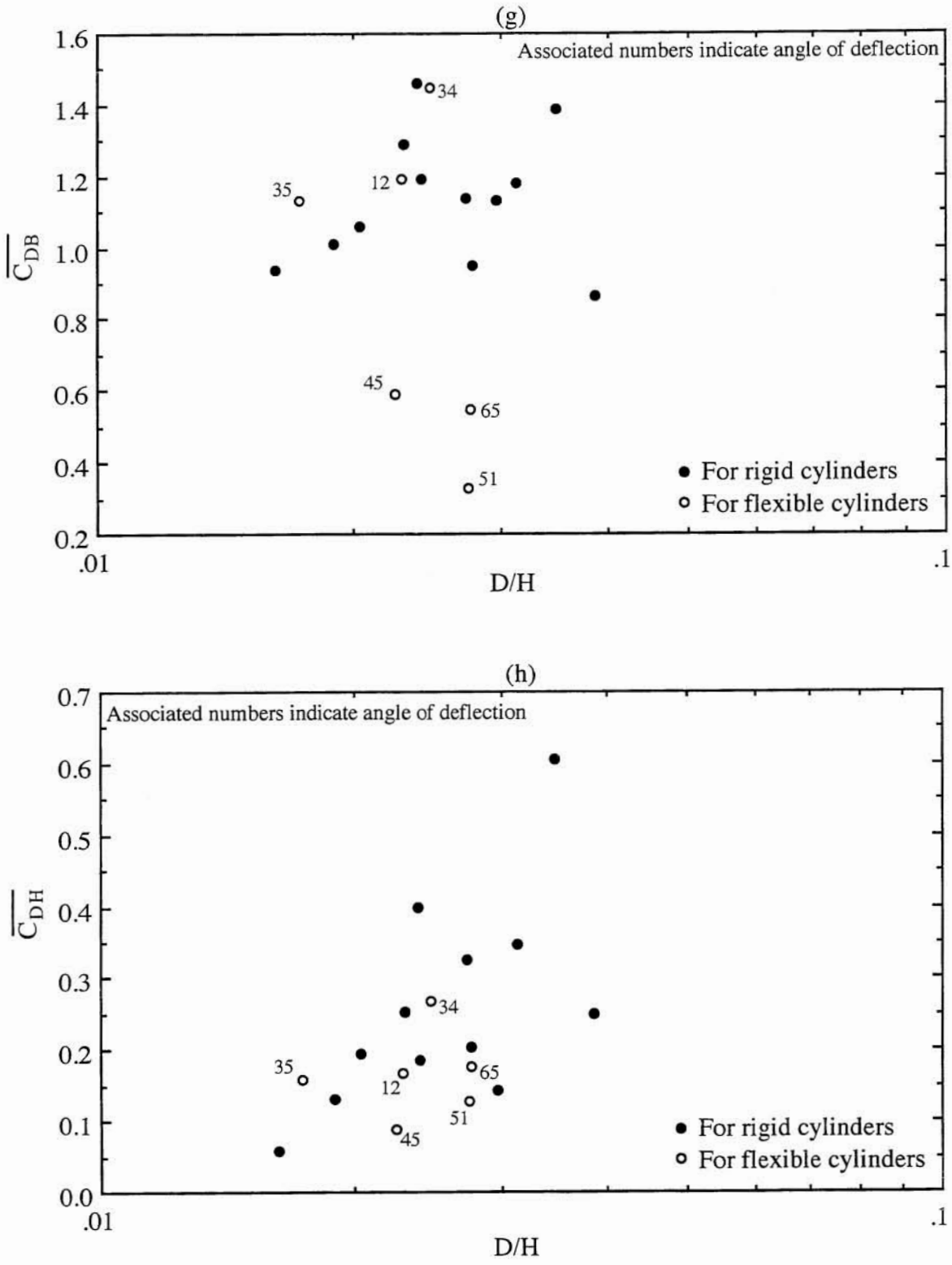

Figure 5.17 (g) and (h)

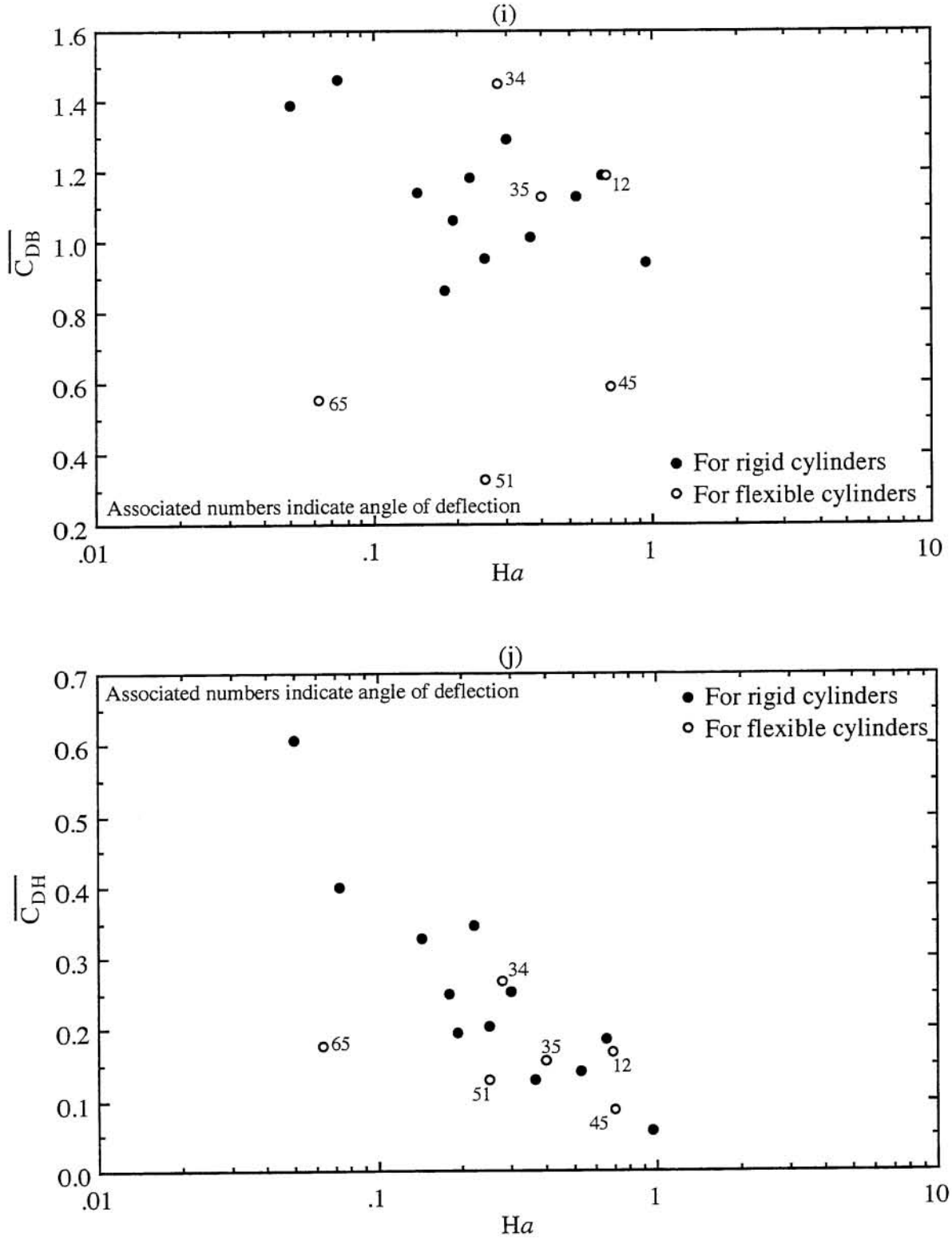

Figure 5.17 (i) and (j)

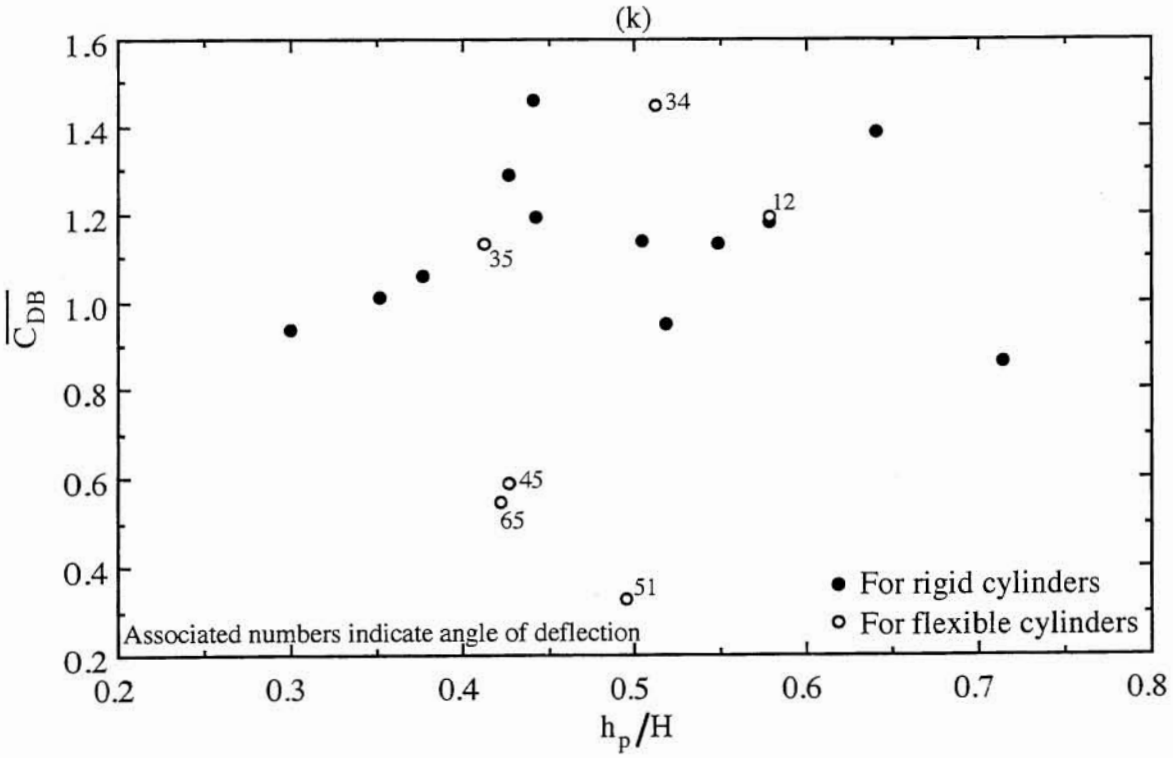

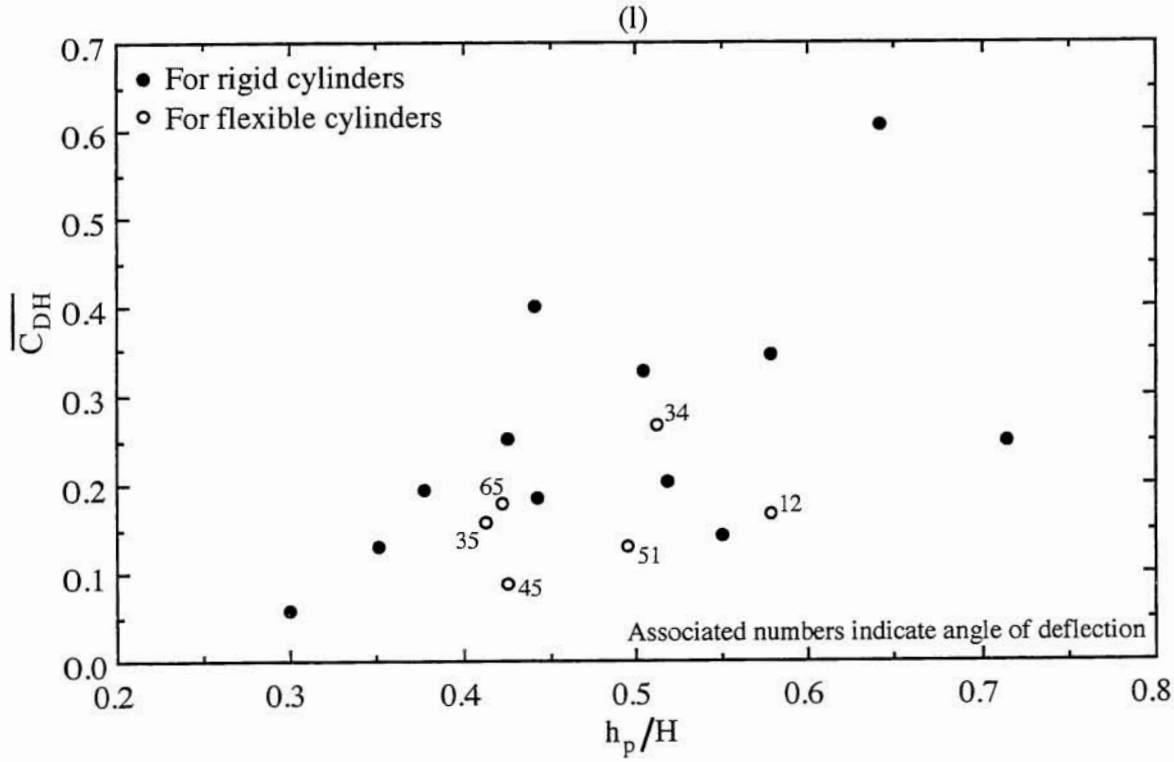

Figure 5.17 (k) and (l)

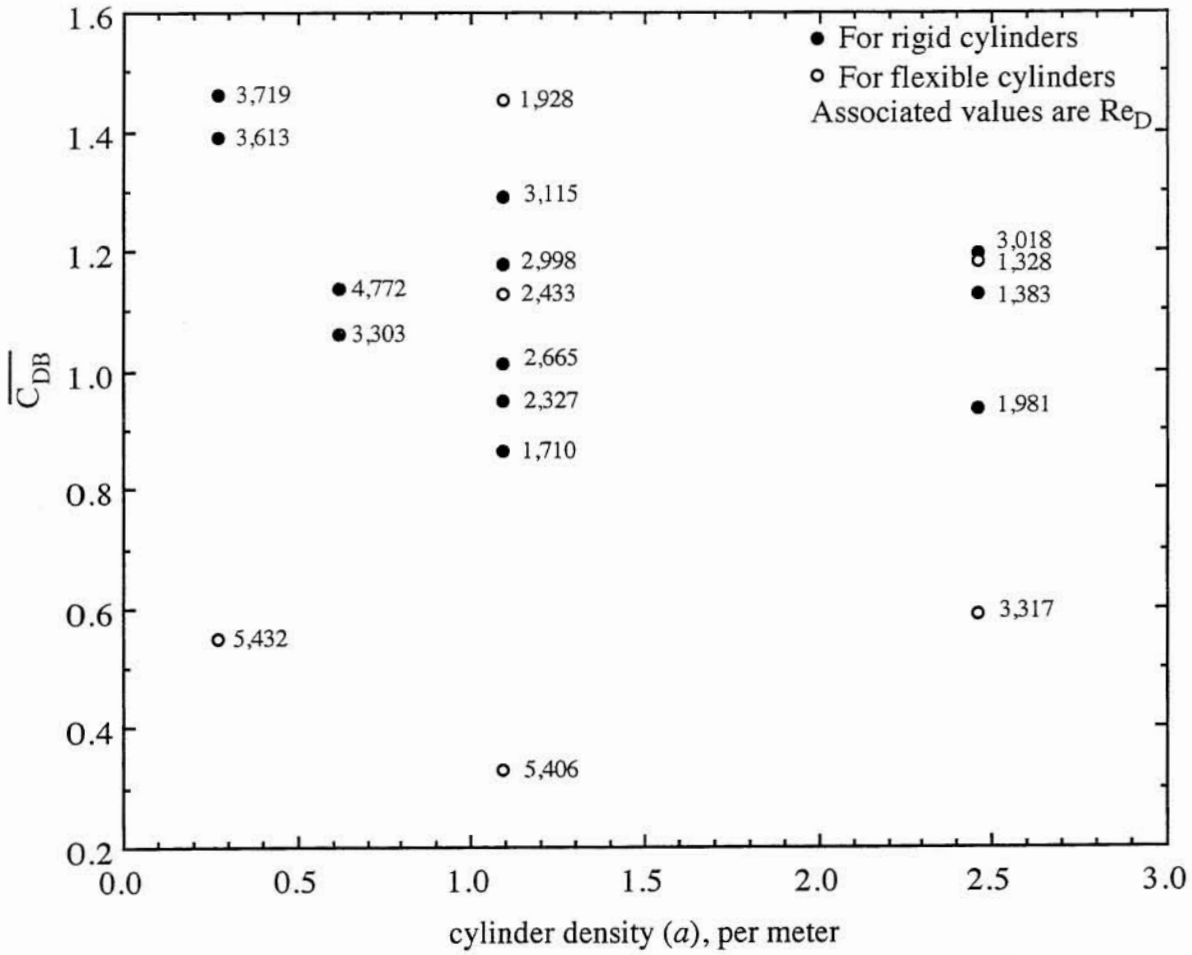

Figure 5.18 Variation of the bulk drag coefficient $\overline{C_{DB}}$ with cylinder density and cylinder Reynolds number

5.9 Comparison of Experimental Results with the Work by Others

The attempts of other researchers to measure drag coefficients and the various vertical profiles were discussed in Chapter 2. Although the aforementioned body of work was performed with a wide array of objectives and has produced varied results, it is helpful to compare the results of this work to those of the present investigation to better understand the significance of the present study. It is also helpful to identify some of the previous findings and theories that are corroborated by findings of the present work.

Kouwen and Unny (1973) described two separate hydraulic flow regimes: an erect or waving regime, and a prone regime. They found that the roughness imposed by these two regimes varied from one another. The results of this experimental study seemed to support the findings of Kouwen and Unny. This was indicated by many of the similarities found in the present study between the profiles and drag coefficients between the rigid and flexible swaying cylinders which contrasted to the results for highly deformed flexible cylinders. For instance the Reynolds stress profiles for the rigid and slightly deformed cylinders were similar, as shown in Figures 5.7 and 5.8. Whereas, the Reynolds stress profiles for the highly deformed cylinders were altered. A more telling example however, is in the values of the bulk drag coefficient $\overline{C_{DB}}$. Figure 5.17 clearly illustrates that this bulk drag coefficient was considerably smaller when the deflection angle was high. In addition, the points that fell outside the trend between $\overline{C_{DH}}$ and H*a* corresponded to highly deformed canopies, which indicated that the flow regime may have considerably influenced the trends plotted in Figure 5.17. It is difficult to determine exactly when the swaying flow regime becomes prone, but it is clear from the findings of this report and those of Kouwen and Unny that these two separate hydraulic regimes do exist and affect the flow in different ways.

Kouwen and Unny also tested the accuracy of the n-UR method of estimating the value of Manning's n as described by Ree and Palmer (1949). They found that the value of Manning's n was not dependent on the product of U and R for the rigid/swaying flow regime. For this flow regime, they found that n was dependent on the value of the relative roughness h_p/H. For a constant value of h_p/H, Manning's n was constant. The n value decreased as the value of h_p/H decreased. A similar analysis was performed with the data collected from the present experimental investigation. Figure 5.19 shows plots of the Manning's n versus the product of U and R for each cylinder density tested. Consistent with the finding of Kouwen and Unny is

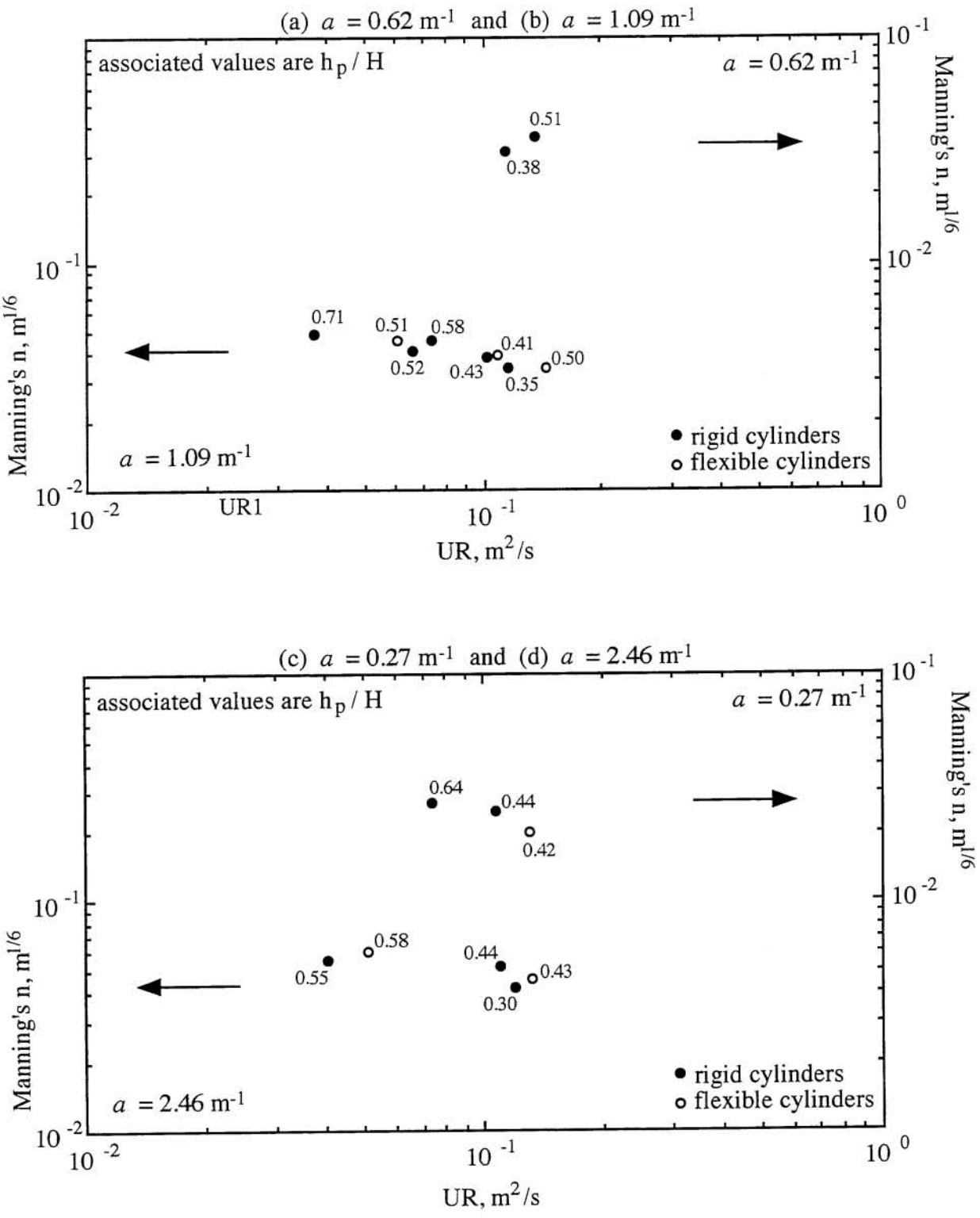

Figure 5.19 n-UR plots for each cylinder density

the trend for Manning's n to decrease with decreasing values of h_p/H. However, the value of Manning's n varied with the cylinder density. Thus, this study has found that the value of Manning's n for rigid and swaying vegetation is not only dependent on the relative roughness, h_p/H, but is also dependent on the cylinder density. Not enough measurements were performed in the prone vegetation regime to make any conclusions.

Measurements of velocity, Reynolds stress, and turbulence intensity have been measured at Kanazawa University in Japan (Tsujimoto et al., 1991; Tsujimoto et al., 1992; Tsujimoto and Nagasaki, 1992) in and above simulated vegetation. The profiles measured in the present study agreed qualitatively with their profiles. Because of the varying channel and flow conditions, a quantitative comparison was not possible, but the shapes of these profiles were in good agreement. In particular, all of the investigations found that as the canopy became more sparse, the velocity profiles became more like the typical profile for regular open-channels. Profiles in more dense cylinder arrangements deviated from the standard open-channel shape and became concave down within the canopy with an inflection point near the top of the canopy. Seginer et al. (1976) reported a similar finding in a wind tunnel and den Hartog and Shaw (1975) measured similar profiles in an atmospheric field study. None of the previous studies have determined the Boussinesq coefficient, β, from their profiles.

In addition, the measurements of Reynolds stress performed at Kanazawa University agreed with those of the present study in that the stress within the canopy was significantly suppressed. The Reynolds stress profile reached a maximum at the top of the canopy and was not noticeably affected above the top of the cylinders in both studies. The data of Seginer et al. was in agreement. All of these studies indicated that the Reynolds stress curve was concave down within the canopy.

The measurements of turbulence intensity were similar to those of Reynolds stress, in that a maximum was reached near the top of the canopy. The measurements performed at Kanazawa University and those performed by Seginer et al. were in good qualitative agreement with those of the present study.

As discussed in Chapter 2, many researchers have attempted to measure or empirically fit values of the bulk drag coefficient. These studies have generally used equation 2.4 to define the bulk drag coefficient where the characteristic height was taken to be h_p or H, whichever was smaller. Since the experimental study considered submerging flows where h_p was smaller than

H, the most appropriate value to compare to the findings of other researchers was $\overline{C_{DB}}$. Tables 5.1 and 5.2 reports $\overline{C_{DB}}$ values ranging from 0.9 to 1.5 for rigid or slightly deflected cylinders with a mean of 1.16.

Li and Shen (1973) numerically determined values of $\overline{C_D}$ between 1.1 and 1.2 for emergent rigid cylinders at a cylinder Reynolds number of 9×10^3. These values were based on a local drag coefficient (for an idealized two-dimensional flow) of 1.2. Since the flow investigated in the present study was for slightly lower cylinder Reynolds numbers (between 1×10^3 and 5×10^3), the local drag coefficient read from the standard cylinder drag curve will be slightly smaller, reducing the expected value of $\overline{C_D}$. The values of $\overline{C_{DB}}$ reported in tables 5.1 and 5.2 are in good agreement with those of Li and Shen. In fact, the mean of all of the values of $\overline{C_{DB}}$ for rigid cylinders was 1.13, the same value reported by Li and Shen.

As previously discussed, Klaassen (1974) criticized Li and Shen's values of $\overline{C_D}$ as being too low. He reports values of $\overline{C_D}$ between 0.8 and 3.0 for a range of Re_D between 1×10^3 and 9×10^3. The mean of his $\overline{C_D}$ measurements was well above 1.2 (probably near 1.5). Although the range of $\overline{C_D}$ measured by Klaassen was quite wide, the values seem to be in fair agreement with those found in the present study. The findings of this report indicate that Klaassen's values were often too high. Klaassen concluded that his higher $\overline{C_D}$ values may have resulted from higher turbulence intensities inside the canopy, although no turbulence measurements were taken to support this conclusion. The findings of the present study and the study by Seginer et al. (1976) contradict Klaassen's conclusion. Both the present investigation and Seginer et al.'s have found that increasing the turbulence intensity within the canopy resulted in decreasing bulk drag coefficients.

Li and Shen's and Klaassen's results did agree that the value of $\overline{C_D}$ increased as the obstruction density increased. However, Seginer et al. reported the opposite trend: as density increased, the bulk drag coefficient decreased. The results of the present study were unclear, but seemed to indicate that the bulk drag coefficient increased as the cylinder density decreased.

Reid and Whitaker (1976) found values of $\overline{C_D}$ between 1.40 and 2.05 with a mean of 1.77 from experimental data. From best fits of their model to various laboratory and field data,

Burke and Stolzenbach (1983) determined a $\overline{C_D}$ value of 2.5. Their model did have the capability to consider varying vertical profiles of the drag coefficient; however, there were no measurements of drag coefficient profiles for them to utilize at the time their model was developed. The values of $\overline{C_D}$ used in these studies by Reid and Whitaker and by Burke and Stolzenbach were significantly higher than any of the values found in the present investigation.

Saowapon and Kouwen (1989) used equation 2.5 to predict bulk drag coefficients for their model. This equation allowed the bulk drag coefficient to change as the plant deflected. Table 5.7 is presented that compares the results of equation 2.5 to the values of $\overline{C_{DB}}$ determined in the present study for the measured deflection angles. Table 5.7 reports that the same general trend for both values of bulk drag coefficient. As the deflection angle increased, the value of $\overline{C_D}$ decreased. However, the values computed by equation 2.5 do not compare very well to those of the experimental study. It is apparent that the drag coefficient cannot be predicted from an equation considering only the deflection angle, and that other parameters must play an important role. This is especially evident when looking at the results of experiments with zero deflection angle.

Table 5.7 Values of $\overline{C_D}$ from Experimental Study and from Equation 2.5

Deflection angle (degrees)	$\overline{C_{DB}}$ from experimental study	$\overline{C_D}$ from equation 2.5
0	from 0.86 to 1.46	2.0
12	1.19	1.87
34	1.45	1.14
35	1.13	1.10
45	0.59	0.71
51	0.33	0.50
65	0.55	0.15

As discussed in Chapter 2, Kao and Barfield (1978) developed a resistance parameter ($N \cdot \overline{C_D} / \gamma \cdot S$). This parameter was criticized in Chapter 2 primarily because it was not dimensionless. A more useful dimensionless resistance parameter is derived below.

Consider a control volume of water flowing through a vegetated channel as shown in Figure 5.20. The driving force projected on the x-axis on a volume of fluid can be written as

$$\gamma \cdot \Delta x \cdot \Delta z \cdot H \cdot S \tag{5.9}$$

where Δx and Δz are the downstream and spanwise dimensions of the control volume as defined in Figure 5.20. The resisting force due to the vegetation can be written as

$$N \cdot \frac{\overline{C_D}}{2} \cdot D \cdot h_p \cdot U^2 \cdot \rho \tag{5.10}$$

where N is the number of vegetation blades per unit area. Therefore, the ratio of the resisting force to the driving force is

$$\frac{N \cdot \frac{\overline{C_D}}{2} \cdot D \cdot h_p \cdot U^2 \cdot \rho}{\Delta x \cdot \Delta z \cdot H \cdot S \cdot \rho \cdot g} \tag{5.11}$$

and since

$$a = \frac{N \cdot D}{\Delta x \cdot \Delta z} \tag{5.12}$$

the ratio reduces to the following dimensionless grouping

$$\frac{\overline{C_D}}{2} \cdot \frac{1}{S} \cdot h_p a \cdot Fr^2 \tag{5.13}$$

This dimensionless resistance parameter has been plotted against the cylinder Reynolds number in Figure 5.21 using the value of $\overline{C_{DB}}$ as the bulk drag coefficient. The trend displayed in Figure 5.21 is consistent with the trend found between Kao and Barfield's resistance parameter and Re_D in that the resistance parameter decreases with increasing values of Re_D. We feel that the resistance parameter described by equation 5.13 is an improvement on the model described by Kao and Barfield.

Seginer et al. (1976) reported that the drag coefficient slightly increased with height in the canopy. Their results were from a wind tunnel study through simulated vegetation were highly scattered. They did not find that drag coefficient profiles reached a maximum within the canopy as the present investigation has.

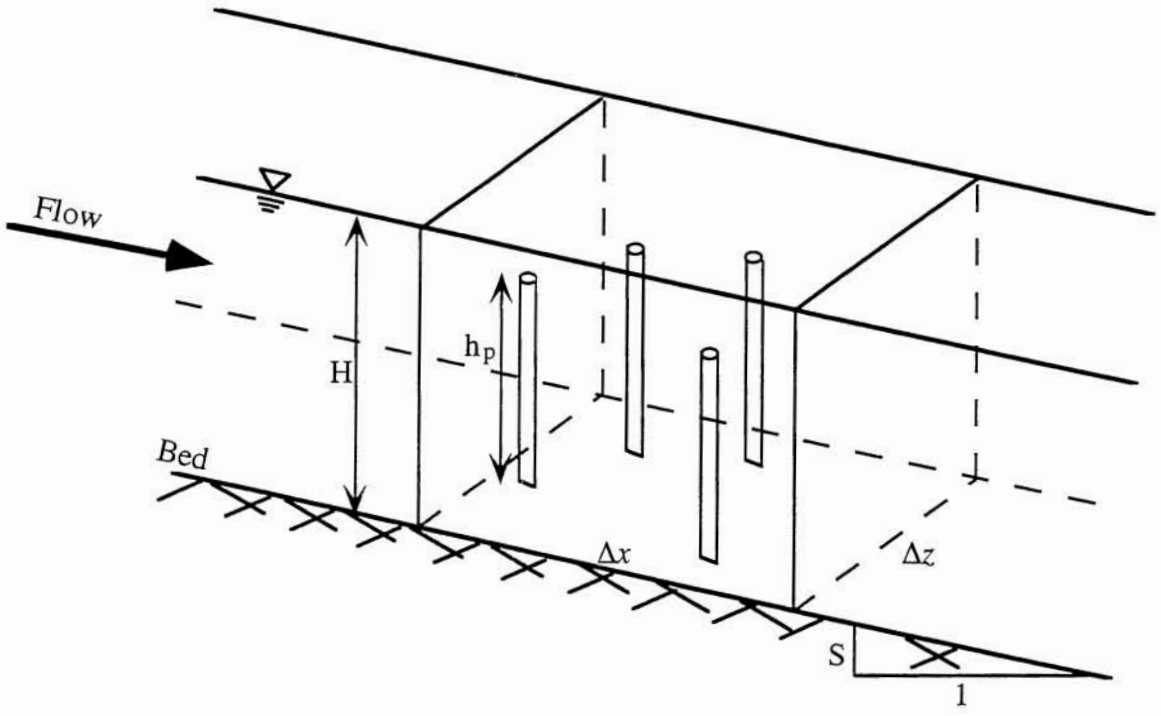

Figure 5.20 Control volume of a vegetated open-channel

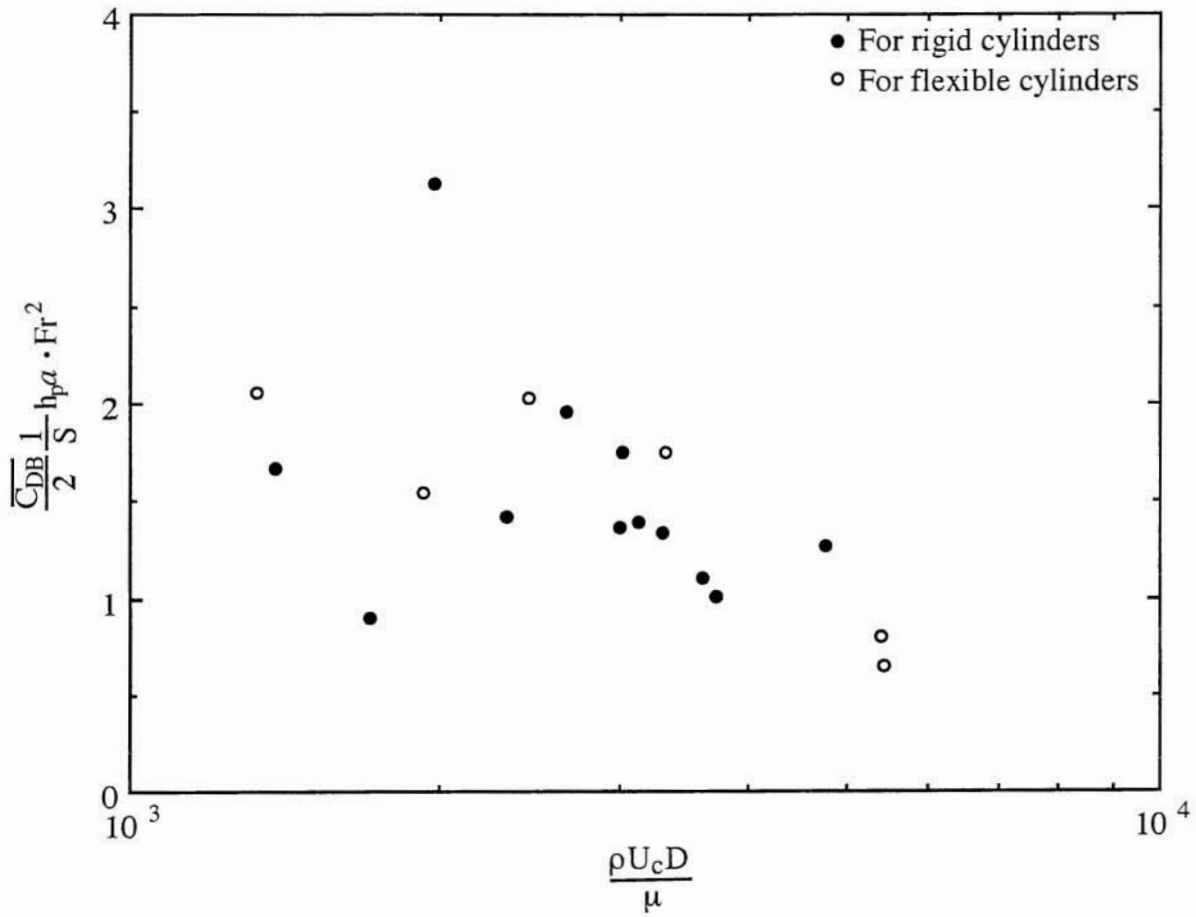

Figure 5.21 Resistance parameter versus cylinder Reynolds number

6. SUMMARY AND CONCLUSIONS

6.1 Summary

The aim of this research has been to investigate the horizontally-averaged vertical profiles of velocity, Reynolds stress, and local drag coefficient in uniform open-channel flow with a simulated vegetative lining. To accomplish this, an experimental study was performed at the Hydrosystems Laboratory of the University of Illinois in a laboratory flume filled with rigid and flexible simulated vegetation. Time-series measurements of point velocity by an Acoustic Doppler velocimeter allowed for the computation of the Reynolds stresses and drag coefficients. In addition, a backwater model for flow through emergent vegetation was introduced which requires a bulk drag coefficient and a shape factor (i.e. Boussinesq coefficient). Bulk drag coefficients were defined and the effects of the relevant dimensionless parameters on the bulk drag coefficients were examined.

As discussed in Chapter 2, the previous models of flow through vegetative canopies have all required a means of quantifying the ability of plants to absorb momentum by form drag, usually characterized by a drag coefficient. Although many studies have defined drag coefficients for semi-infinite domains with non-turbulent uniform approaching flows around semi-infinitely long obstructions, only a few studies (Petryk, 1969; Li and Shen, 1793; Klaassen, 1974) have been performed specifically to evaluate this coefficient in non-idealized open-channel flows. All of these studies have been interested in a bulk drag coefficient that characterizes the mean ability of a plant to absorb momentum by form drag. One of the objectives of this study has been to compute bulk drag coefficients and compare these values to those of previous investigations. In addition, profiles of the local drag coefficient have been measured in the present study, which has not been accomplished in any of the aforementioned investigations. The measured drag coefficient profiles from the experiments are directly applicable to the k-ε model for obstructed low-Reynolds number flows introduced by Burke and Stolzenbach (1983) and the k-ε model for high-Reynolds number flows proposed by López and García (1995).

To compute local drag coefficients for uniform flows, a new method was developed by a momentum balance within the canopy. This method requires only measurements of bed slope and obstruction density, along with horizontally averaged measurements of velocity and Reynolds stress. The experimental study described in Chapter 4 was set up to measure these variables.

This investigation has provided some valuable insight into flow and turbulence characteristics of open-channel flow through a simulated vegetative lining. The knowledge it has provided on the behavior of the drag coefficient profile within the canopy will be useful for more complex models of this flow process. In addition, its implications for sediment deposition and resuspension will be useful into pioneering investigations into these mechanisms in vegetated open-channels (e.g. López and García, 1995).

6.2 Conclusions on Velocity Profiles and Shape Factors

The analysis of the experimental study in Chapter 5 shows that the horizontally averaged velocity profiles through the rigid cylinders had a characteristic shape that was dependent of the cylinder density. For each cylinder density, a constant Boussinesq coefficient was observed. This characteristic shape was absent for flow through flexible cylinders and consequently, the computed values of the Boussinesq coefficient varied for a given cylinder density. The profiles were similar in shape to those measured by previous researchers (den Hartog and Shaw, 1975; Seginer et al., 1976; Tsujimoto et al., 1991; Tsujimoto et al., 1992; Tsujimoto and Nagasaki, 1992). These results suggest that the plant density is of primary importance to the shape of the velocity profile in a vegetated channel. In a channel with a flexible lining, other parameters play a crucial role, particularly the flexibility of the plants that make up the lining and the cylinder Reynolds number.

6.3 Conclusions on Reynolds Stress Profiles and Turbulence Intensity Profiles

The measured profiles of Reynolds stress and turbulence intensity show that these values reach a maximum near the top of the canopy and are significantly suppressed inside the canopy. These tendencies are supported by measurement by Seginer et al., 1976; Tsujimoto et al., 1991; Tsujimoto et al., 1992; and Tsujimoto and Nagasaki, 1992. A significant tendency was observed for the average turbulence intensity inside the canopy to increase as the dimensionless parameter Ha increased.

6.4 Conclusions on Drag Coefficient Profiles

The analysis of the measured profiles of the local horizontally averaged drag coefficient shows that for rigid cylinders, the drag coefficient was not constant throughout the canopy as many researchers have assumed, but instead reached a maximum at about one-third of the canopy height and diminished towards a minimum at the top of the canopy. At the top of the canopy, their was a discontinuity in the value of the drag coefficient and above the canopy, the drag coefficient found to be effectively equal to zero. For flow through flexible cylinders, two separate shapes of the drag coefficient profiles were observed. One profile shape was observed for the swaying cylinder regime that resembled the profiles for the rigid cylinders, except that the maximum was typically reached higher in the canopy. The second general profile shape was exhibited when the cylinders were highly deflected, possibly indicating the existence of the prone vegetation condition. The second profile shape decreased with depth into the canopy and did not reach a maximum. The existence of two distinctly different drag coefficient profiles suggests the existence of two distinct hydraulic regimes in a vegetated channel. This conclusion is supported by Kouwen and Unny (1973) who found distinctly different roughness conditions for (1) erect, including waving roughness, and (2) prone roughness.

The maximum value of the drag coefficient reached in each of the profiles for flow through rigid cylinders ranged from 1.32 to 1.86. The maximum value was not found to be dependent on any of the flow parameters. The mean maximum value of the drag coefficient was found to be 1.55 ± 0.18. All of the maximum values were within 20% of the mean maximum value.

Computations of the drag coefficient under nearly ideal flow conditions (where the velocity profile was uniform along the axis of the cylinder and the Reynolds stress was negligible) resulted in values that were very nearly equal to those read from the standard cylinder drag curve for a single cylinder in idealized flow. This observation supports the validity of the new method of computing drag coefficients introduced in this report. In addition, within the canopy, transverse gradients of the secondary Reynolds stress were found to be negligible and secondary currents were believed to be unimportant. These findings validate our computational procedure. The computational method requires nearly two-dimensional flow conditions and accurate measurements of the local bed slope and obstruction density.

6.5 Conclusions on Bulk Drag Coefficients

As do the previous models of flow through vegetation, the backwater curve model derived in this study requires a bulk drag coefficient that characterizes the mean effect of a plant on the flow. Various definitions of the bulk drag coefficient were discussed in this study, the two most useful being $\overline{C_{DB}}$ and $\overline{C_{DH}}$. $\overline{C_{DB}}$ was defined with the plant height and $\overline{C_{DH}}$ was defined with the flow depth. Values of $\overline{C_{DB}}$ for flexible cylinders indicate that when the cylinders become highly deflected, $\overline{C_{DB}}$ is significantly decreased. This observation further corroborates the existence of two distinct regimes.

Another of the major objectives of this study was to determine the influence of the relevant flow and channel parameters on the values of these bulk drag coefficients. This analysis revealed highly scattered results from which it was difficult to make any definite inferences. However, it was apparent that the Froude number had some influence on the value of the bulk drag coefficient $\overline{C_{DB}}$ for flexible cylinders; $\overline{C_{DB}}$ markedly decreased with increasing Froude number. For both rigid and flexible cylinders, $\overline{C_{DH}}$ decreased with increasing values of the dimensionless parameter Ha (the product of the flow depth and cylinder density). The mean dimensionless turbulence intensity inside the cylinder canopy was found to be highly dependent on the parameter Ha, and therefore, there was a strong tendency for $\overline{C_{DH}}$ to decrease as the mean dimensionless turbulence intensity inside the canopy increased. This finding is supported by the conclusions of Seginer et al. (1976) who also found that the bulk drag coefficient decreased as the turbulence intensity increased.

For rigid cylinders, no parameter was found to have a significant effect on the value of $\overline{C_{DB}}$. The scatter in the results is believed to be the result of experimental and computational errors. The mean value of $\overline{C_{DB}}$ for flow though rigid cylinders was found to be 1.13 ± 0.18. All of the values of $\overline{C_{DB}}$ were within 30% of the computed mean. This amount of scatter is not excessive however, especially in comparison to other experimental attempts at measuring the bulk drag coefficient. Klaassen and Van Der Zwaard's (1974) measurements of the bulk drag coefficient varied by as much as 100% and Reid and Whitaker's (1976) estimates varied by 20% from the mean even though they only computed three values of the bulk drag coefficient. The mean computed $\overline{C_{DB}}$ value of 1.13 in this study is the same value of $\overline{C_D}$ computationally es-

timated by Li and Shen (1973). This fact corroborates the validity of the values measured in the present study.

6.6 Limitations of Simulated Vegetation

Vegetation in the laboratory investigation was simulated with rigid and flexible cylinders. The use of simulated vegetation, rather than actual vegetation, imposes some limitations on the use of the results of this study. Simulated rigid vegetation is directly applicable to very few natural channels. The flexible cylinders more closely resemble most natural vegetation; however, whether the vibrating tendencies of the simulated vegetation actually occurs for real vegetation has not been shown. In particular, it is unclear whether the tendency of the flexible cylinders to vibrate in the mainstream and transverse direction with a characteristic frequency is also a property of natural vegetation. All of the profiles measured in the experimental study are expected to be significantly altered if the canopy contains vegetation that is leafy and is not uniformly dense in the vertical. Profiles in natural channels with unequally spaced vegetation may also have different shapes than those found in this study. However, this study does effectively describe the general shape of the vertical profiles of flow velocity, Reynolds stress, turbulence intensity, and the drag coefficient for a vegetated channel. In addition, the ranges of the shape factor and bulk drag coefficients found in this study provides some insight into the values that one should expected in naturally vegetated channels for these coefficients.

This research has shown that the velocity and Reynolds stress profiles through flexible simulated vegetation are often dissimilar to the profiles through rigid simulated vegetation, resulting in drag coefficient values and profiles that can be extremely different. Care must be taken when extending the results of studies through rigid or even mildly swaying obstructions to flow through actual vegetated channels.

6.7 Recommendations

The computational method for local drag coefficients introduced in this study can be optimized by measuring as many points as possible within the plant canopy for each profile. Measuring as many profiles as possible and averaging these profiles yields the most suitable profiles for the analysis. In the present investigation, a third degree polynomial was regressed through the Reynolds stress points below the top of the canopy; however, the computation of the local drag coefficient could be further improved by fitting a more complex regression equa-

tion through these points, but only if enough points are measured within the canopy to make this appropriate.

Because of the limitations of the experimental facilities and equipment used in this study, limited ranges of the relevant dimensionless parameters were investigated. The resulting analysis of the effects of the dimensionless parameters on the bulk drag coefficients revealed some possible trends but was far from conclusive. Further investigation over a wider range of dimensionless variables is recommended to confirm the trends found in this study. Additional experiments are especially recommended for flexible linings because of the limited number of experiments performed in this investigation through this type of lining. The next step would be to research turbulent open-channel flows through natural vegetation. The possibility of using a flume inside of a greenhouse would seem the most appropriate way to study more realistic flows, yet under controlled laboratory conditions.

REFERENCES

Burke, R.W. and Stolzenbach, K.D. (1983). "Free Surface Flow Through Salt Marsh Grass". *MIT-Sea Grant Report MITSG 83-16*. Cambridge, Mass., 252p.

Christensen, B.A. (1985). "Open Channel and Sheet Flow Over Flexible Roughness". *International Association for Hydraulic Research, 21st Congress*. Melbourne, pp. 463-467.

Chow, V.T. (1959). *Open-channel Hydraulics*. McGraw-Hill, New York, 680p.

Chow, V.T., Maidment, D.R., and Mays, L.W. (1988). *Applied Hydrology*. McGraw-Hill, New York, 680p.

den Hartog, G. and Shaw, R.H. (1975). "A Field Study of Atmospheric Exchange Processes Within a Vegetative Canopy". In D.A. deVries and N.H. Afgan, eds., *Heat and Mass Transfer in the Biosphere*. John Wiley and Sons.

García, M.H. (1994). Class Notes for "Environmental Hydrodynamics". University of Illinois at Urbana-Champaign.

Graf, W.H. and Ko, S.C. (1971). "Tests on Cylinders in Turbulent Flow". *Journal of the Hydraulics Division*, ASCE. Vol. 97, No. 8, pp. 1265-1267.

Granger, R.A. (1985). *Fluid Mechanics*. Holt, Rinehart, and Winston, New York, 884p.

Henderson, F.M. (1966). *Open Channel Flow*. Macmillan Publishing Company, 522p.

Hino, M. (1981). "Ecohydrodynamics". *Advances in Hydroscience*. Vol. 12, pp. 143-193.

Hoerner, S.F. (1958). *Fluid-Dynamic Drag*. Published by the author, Midland Park, New Jersey.

Kadlec, R.H. (1990). "Overland Flow in Wetlands: Vegetation Resistance". *Journal of Hydraulic Engineering*, ASCE. Vol. 116, No. 5, pp. 691-706.

Kao, D.T.Y. and Barfield, B.J. (1978). "Prediction of Flow Hydraulics for Vegetated Channels". *Transactions of the ASAE*. Paper No. 76-2057, pp. 489-495.

Klaassen, G.J. (1974). Discussion of "Effect of Tall Vegetations on Flow and Sediment" by R.M. Li and H.W. Shen, 1973. *Journal of the Hydraulics Division*, ASCE. Vol. 100, No. 3, pp. 495-497.

Klaassen, G.J. and Van Der Zwaard, J.J. (1974). "Roughness Coefficients of Vegetated Flood Plains". *Journal of Hydraulic Research*. Vol. 12, No. 1, pp. 43-63.

Kouwen, N. and Unny, T.E. (1974). "Flexible Roughness in Open Channels". *Journal of the Hydraulics Division*, ASCE. Vol. 99, No. 5, pp. 723-728.

Kouwen, N. and Li, R.M. (1980). "Biomechanics of Vegetative Channel Linings". *Journal of the Hydraulics Division*, ASCE. Vol. 106, No. 6, pp. 1085-1103.

Kouwen, N. (1988). "Field Estimation of the Biomechanical Properties of Grass". *Journal of Hydraulic Research*. Vol. 26, No. 5, pp. 559-568.

Kraus, N.C., Lohrmann, A., and Cabrera, R. (1994). "New Acoustic Meter for Measuring 3D Laboratory Flows". *Journal of Hydraulic Engineering*, ASCE. Vol. 120, No. 3, pp. 406-412.

Li, R.M. and Shen, H.W. (1973). "Effect of Tall Vegetations on Flow and Sediment". *Journal of the Hydraulics Division*, ASCE. Vol. 99, No. 5, pp. 793-813.

Li, R.M. and Shen, H.W. (1974) "Effect of Tall Vegetations on Flow and Sediment", reply to the discussion by Klaassen, 1974. *Journal of the Hydraulics Division*, ASCE. Vol. 100, No. 10, pp. 1484.

Lohrmann, A., Cabrera, R., Gelfenbaum, G., and Haines, J. (1995). "Direct Measurements of Reynolds Stress with an Acoustic Doppler Velocimeter". *IEEE*. pp. 205-210.

López, F. and García, M. (1995). "Simulation of Suspended Sediment Transport in Vegetated Open Channel Flows with a k-ε Turbulence Model". *Water Resources Engineering*. Vol. 1, pp. 104-108.

López, F. and García, M. (1996). "Open-channel flow through simulated vegetation: turbulence modeling and sediment transport". Contr. Rep. DACW39-94-K-0010. U.S. Army Corps of Engineers. Washington, D.C.

Nezu, I. and Nakagawa, H. (1993). *Turbulence in Open-channel Flows*. IAHR Monograph series. A.A. Balkema, Rotterdam, Netherlands, 281p.

Petryk S. (1969). "Drag on Cylinders in Open Channel Flow". Phd. Thesis, Colorado State University.

Petryk, S. and Bosmajian, G. (1975). "Analysis of Flow Through Vegetation". *Journal of Hydraulic Engineering*, ASCE. Vol. 101, No. 7, pp. 871-884.

Raupach, M.R. and Shaw, R.H. (1982). "Averaging Procedures for Flow within Vegetation Canopies". *Boundary-Layer Meteorology*. Vol. 22, pp 79-90.

Ree, W.O. and Palmer, V.J. (1949). "Flow of Water in Channels Protected by Vegetative Linings". *U.S. Soil Conservation Bulletin No. 967*, Feb., 115p.

Reid, R.O. and Whitaker, R.E. (1976). "Wind-driven Flow of Water Influenced by a Canopy". *Journal of the Waterways, Harbors, and Coastal Engineering Division*, ASCE. Vol. 102, No. 1, pp. 61-77.

Roshko, A. (1960). "Experiments on the Flow Past a Circular Cylinder at Very High Reynolds Numbers". *Journal of Fluid Mechanics*. Vol. 10, pp. 345-357.

Saowapon, C. and Kouwen, N. (1989). "A Physically Based Model for Determining Flow Resistance and Velocity Profiles in Vegetated Channels". *Symposium on Manning's Equation*. B.C. Yen, Ed., Virginia, pp. 559-568.

Schlichting, H. (1979). *Boundary-Layer Theory*. 7th ed., New York, McGraw-Hill, 817p.

Seginer, I., Mulhearn, P.J., Bradley, E.F., and Finnigan, J.J. (1976). "Turbulent Flow in a Model Plant Canopy". *Boundary-Layer Meteorology*. No. 10, pp. 423-453.

Tollner, E.W. (1974). "Modeling the Sediment Filtration Capacity of Simulated, Rigid Vegetation". M.S. Thesis, University of Kentucky.

Tritton, D.J. (1959). "Experiments on the Flow Past a Circular Cylinder at Low Reynolds Numbers". *Journal of Fluid Mechanics*. Vol. 6, pp. 547-568.

Tsujimoto, T., Okada, T., and Kitamura, T. (1991). "Turbulent Flow Over Flexible Vegetation-covered Bed in Open Channels". *KHL-Progressive Report*. Kanazawa University, No. 2, pp. 31-40.

Tsujimoto, T., Shimizu, Y., Kitamura, T., and Okada, T. (1992). "Turbulent Open-channel Flow Over Bed Covered by Rigid Vegetation". *Journal of Hydroscience and Hydraulic Engineering*, JSCE. Vol. 10, No. 2, pp. 13-26.

Tsujimoto, T. and Nagasaki, T. (1992). "Turbulent Characteristics of Flow Over Vegetation Swaying on a Bed". *KHL-Progressive Report*. Kanazawa University, No. 12, pp. 9-19.

Vennard, J.K. and Street, R.L. (1982). *Elementary Fluid Mechanics*, 6th ed. New York, John Wiley and Sons, 689p.

White, F.M. (1991). *Viscous Fluid Flow*. 2nd ed., New York, McGraw-Hill, 614p.

Yen, B.C. (1973). "Open-Channel Flow Equations Revisited". *Journal of the Engineering Mechanics Division*, ASCE. Vol. 99, No. 10, pp. 979-1009.

Yen, B.C. (1992). "Hydraulic Resistance in Open Channels" in *Channel Flow Resistance: Centennial of Manning's Formula*. B.C. Yen editor, Water Resources Publications, Littleton Colorado, pp1-135

Zdravkovich, M.M. (1977). "Review of Flow Interference Between Two Circular Cylinders in Various Arrangements". *Journal of Fluids Engineering*, ASME. December, pp. 618-633.

Zdravkovich, M.M. and Pridden, D.L. (1977). "Interference Between Two Circular Cylinders; Series of Unexpected Discontinuities". *Journal of Industrial Aerodynamics*. Vol. 2, pp. 255-270.

APPENDIX A: Computer Program

This appendix contains the FORTRAN computer program which was used to analyze the experimental data. The program computes mean values of velocity, Reynolds stress, and turbulence intensity; horizontally averaged profiles of velocity, Reynolds stress, and local drag coefficient; shape factors; and bulk drag coefficients.

```
* Date 9/08/95
* Program:  vegetcd.ftn
************************************************************
*       This program computes a variety of statistics for
*       the experiments conducted on 8/30/95 - experiment 18.
*       The main goal of this experiment is to find velocity
*       distributions, drag coefficients, and shape factors for
*       for flow through simulated vegetation.
************************************************************
c
c       Variables to Change
c
c       np = number of data points per VEL input file
c       npr = number of profiles taken
c       nv = number of points in each profile
c       nm = total number of measurements taken
c       nif = number of input files - should be 2 x nm
c       nbasis = the degree of the polynomial in the regression of
c                       the reynolds stress curve
c       ndata = the number of data points below the vegetation line -
c                       this is the number of points that are regressed
c       h = water depth in meters
c       S = water surface slope in meters/meter (bed slope)
c       pdens = the vegetation density in per meter
c       veght = the vegetation height in meters
c       xx = distance of measurement from right wall in centimeters
c       rn = Manning's n for smooth open-channel
c
ccccccccccccccccccccccccccccccccccccccccccccccccccccccccccccccccccccc
        integer nbasis, ndata, ict, il
        parameter (np=4500, npr=4, nv=10, nm=40, nif=80, nbasis=3
      &, ndata=6)
        real u(np), v(np), w(np), um, vm, wm, h, umd(nv), angle
        real re(npr), error(npr), alpha(npr,nv), beta(npr,nv)
        real ump(npr,nv), z(npr,nv), max, max1, min1, uq2(npr),xx(npr)
        real delta2(npr,nv), umeas(npr), g, S, zpos(nv), uvd(nv)
        real feta(npr,nv), eta(npr,nv), tfeta(npr), bfeta(npr), uq1(npr)
        real urmsp(npr,nv), vrmsp(npr,nv), wrmsp(npr,nv), uvp(npr,nv)
        real a(nbasis+1), f, fdata(ndata), sse, weight(ndata)
        real aeta(nv), afeta(nv)
        real xdata(ndata), deriv(nv), cd(nv), pdens, uwp(npr,nv)
        external f, fnlsq

*****************************************************
*       Read data from data files
*****************************************************
        open (unit =1, file='0830-1.VEL',status='old')
        open (unit =2, file='0830-1.CTL',status='old')
        UP TO 78 ADDITIONAL READ FILES HERE
        open (unit =nif+1, file='0830.data')
        open (unit =nif+2, file='0830.misc')
c       open (unit =nif+3, file='0830.fix')
        open (unit =nif+4, file='avgvel.prof')
        open (unit =nif+5, file='cd.prof')
        open (unit =nif+6, file='z1.prof')
```

```
      open (unit =nif+7, file='z2.prof')
      open (unit =nif+8, file='z3.prof')
      open (unit =nif+9, file='z4.prof')
      open (unit =nif+10, file='z5.prof')
      open (unit =nif+11, file='z6.prof')
      open (unit =nif+12, file='z7.prof')
      open (unit =nif+13, file='z8.prof')
      open (unit =nif+14, file='z9.prof')
      open (unit =nif+15, file='z10.prof')
      open (unit =nif+16, file='x1.prof')
      open (unit =nif+17, file='x2.prof')
      open (unit =nif+18, file='x3.prof')
      open (unit =nif+19, file='x4.prof')
      open (unit =nif+20, file='uv1.prof')
      open (unit =nif+21, file='uv2.prof')
      open (unit =nif+22, file='uv3.prof')
      open (unit =nif+23, file='uv4.prof')
      open (unit =nif+24, file='uvavg.prof')

      do jkl = 1 , nm
      um = 0.
      vm = 0.
      wm = 0.
      h = .284
      S = .0101
      g = 9.81
      Rh = (.9144*h)/(.9144+2.*h)
      ustar = sqrt(g*h*S)
      pdens = 2.46
      veght = .121
      rn = 0.020

      xx(1) = 46.2
      xx(2) = 51.8
      xx(3) = 39.1
      xx(4) = 45.6

      ivel = jkl*2-1
      ictl = jkl*2
      write(nif+1,17)
17    format(////,'Profile Data','----------',/)
      write(nif+1,*) ' jkl = ', jkl, 'ivel = ', ivel, ' ictl = '
     &, ictl

************************************************************
*       Set up individual profile measurements
************************************************************

c
c     Set up vertical layers

      ik = int((jkl-1)/nv)
      k = jkl-nv*ik
      l = int((jkl-1)/nv)+1
c
```

```
**************************************************
*       Find probe angle from downstream, alpha
**************************************************
      pi = 4.*atan(1.)
c
c     Read data & compute uncorrected mean
      do j = 1 , np
c           write(nif+2,*) ivel
            read(ivel,*) time, x, y, u(j), w(j), v(j)
c           write(nif+2,*) j, time,x,y,u(j),w(j),v(j)

                  u(j) = u(j)/100.
                  v(j) = v(j)/100.
                  w(j) = w(j)/100.
                  um = u(j)/real(np)+um
                  vm = v(j)/real(np)+vm
                  wm = w(j)/real(np)+wm
      enddo

      read(ictl,77) ydist
      write(nif+1,*) 'Distance to bottom =', ydist
77    format(/////////////////////,35x,f5.2)
      write(nif+1,99)
99    format(/,'MEAN VALUES','----------',/)
      write(nif+1,*) 'Um = ', um
      write(nif+1,*) 'Vm = ', vm
      write(nif+1,*) 'Wm = ', wm

c     Find probe oriontation for top point only

            max = 0.
            if (k.eq.1) then
                  alpha(l,k) = 0.
25                max1 = um*cos(alpha(l,k)) + wm*sin(alpha(l,k))
                  if (max1.gt.max) then
                        alpha(l,k) = alpha(l,k) + .5/180.*pi
                        max = max1
                        go to 25
                  endif
                  alpha(l,k) = alpha(l,k) - .5/180.*pi
                  max = 0
27                max1 = um*cos(alpha(l,k)) + wm*sin(alpha(l,k))
                  if (max1.gt.max) then
                        alpha(l,k) = alpha(l,k) - .5/180.*pi
                        max = max1
                        go to 27
            endif
                  alpha(l,k) = alpha(l,k) + .5/180.*pi
                  do k=2,nv
                        alpha(l,k) = alpha(l,1)
                  enddo
                  k=1
            endif
            write(nif+1,*) 'Alpha = ', alpha(l,k)
**************************************************
```

```
*       Find probe angle in the vertical, beta
*****************************************************
c
c       Find probe oriontation in the vertical

                bmax = 0.
                beta(l,k) = 0.
35              bmax1 = um*cos(beta(l,k)) + vm*sin(beta(l,k))
                if (bmax1.gt.bmax) then
                        beta(l,k) = beta(l,k) + .25/180.*pi
                        bmax = bmax1
                        go to 35
                endif
                beta(l,k) = beta(l,k) - .25/180.*pi
                bmax = 0
37              bmax1 = um*cos(beta(l,k)) + vm*sin(beta(l,k))
                if (bmax1.gt.bmax) then
                        beta(l,k) = beta(l,k) - .25/180.*pi
                        bmax = bmax1
                        go to 37
                endif
                beta(l,k) = beta(l,k) + .25/180.*pi
                write(nif+1,*) 'Beta = ', beta(l,k)
*
*****************************************************
*       Correct data for oriontation and re-compute means
*****************************************************
c       Correct u and w with the value of alpha
c
                um = 0.
                vm = 0.
                wm = 0.
                do j = 1, np
                        up = u(j)
                        vp = v(j)
                        wp = w(j)
                        u(j) = up*cos(alpha(l,k))+wp*sin(alpha(l,k))
                        u(j) = u(j)*cos(beta(l,k))+vp*sin(beta(l,k))
                        w(j) = -up*sin(alpha(l,k))+wp*cos(alpha(l,k))
                        v(j) = -up*sin(beta(l,k))+vp*cos(beta(l,k))
c                       write (nif+3,*) u(j), v(j), w(j)
c
c
c       Compute corrected mean values
c
                        um = u(j)/real(np)+um
                        vm = v(j)/real(np)+vm
                        wm = w(j)/real(np)+wm
                enddo
                        write(nif+1,98)
98                      format(/,'corrected MEAN VALUES','----------',/)
                        write(nif+1,*) 'Um = ', um
                        write(nif+1,*) 'Vm = ', vm
                        write(nif+1,*) 'Wm = ', wm
*****************************************************
*       Compute reynolds stresses and turbulent intensities
```

```
**********************************************************
c
c       Compute turbulent intensities
c
        ums = 0.
        vms = 0.
        vms = 0.
        do i = 1 , np
                ums = (u(i) - um)**2/real(np)+ums
                vms = (v(i) - vm)**2/real(np)+vms
                wms = (w(i) - wm)**2/real(np)+wms
        enddo
        urms = sqrt(ums)
        vrms = sqrt(vms)
        wrms = sqrt(wms)
        urmsum = urms/um
        vrmsvm = vrms/vm
        wrmswm = wrms/wm

        write(nif+1,23)
23      format(/,' Turbulent Intensities',/)
        write(nif+1,*) 'Urms = ', urms
        write(nif+1,*) 'Urms/Um = ', urmsum
        write(nif+1,*) 'Vrms = ', vrms
        write(nif+1,*) 'Vrms/Vm = ', vrmsvm
        write(nif+1,*) 'Wrms = ', wrms
        write(nif+1,*) 'Wrms/Wm = ', wrmswm
c
c
c       Compute Reynolds stresses
c
        uv = 0.
        uw = 0.
        vw = 0.
        do i = 1 , np
                uv = (u(i) - um)*(v(i)-vm)/real(np)+uv
                uw = (u(i) - um)*(w(i)-wm)/real(np)+uw
                vw = (v(i) - vm)*(w(i)-wm)/real(np)+vw
        enddo
        write(nif+1,30)
30      format(/,'Reynolds Stresses',/)
        write(nif+1,*)'uv = ', uv
        write(nif+1,*)'uw = ', uw
        write(nif+1,*)'vw = ', vw
        write(nif+2,62) ydist, um , urms , vrms, wrms, uv
62      format(6(2x,f10.6))
**************************************************
*       Create graph of -u'v'/u*^2 versus z/H
**************************************************
                z(l,k) = ydist/100.
                yaxis = z(l,k)/h
                xaxis = -uv/ustar**2
                ib = 0.
                do ia=1,npr
                        ib=ib+1
```

```
                        if (ia.eq.l) write(nif+5+nv+npr+ib,*) l,k,xaxis,yaxis
                    enddo

c       Compute error of measurement from theoretical value
c
                    delta2(l,k) = (1 - yaxis - xaxis)**2

************************************************************
*       Print misc. data for each profile and vertical position
************************************************************
c
c       Compute individual profile data and print to files
c
        ump(l,k)=um
        urmsp(l,k)=urms
        vrmsp(l,k)=vrms
        wrmsp(l,k)=wrms
        uvp(l,k)=uv
        uwp(l,k)=uw

c       ***End Main Loop***
        enddo

c
        do l=1,npr
                ic = 0
                do k=1,nv
                        ic = ic+1
                        write(nif+5+ic,*) l, z(l,k), ump(l,k), urmsp(l,k),
   &vrmsp(l,k), wrmsp(l,k), -uvp(l,k), uwp(l,k), xx(l)
                enddo
        enddo
c
c
        do k=1,nv
                id = 0
                do l=1,npr
                        id = id+1
                        write(nif+5+nv+id,*) l, z(l,k), ump(l,k), urmsp(l,k),
   &vrmsp(l,k), wrmsp(l,k), -uvp(l,k), uwp(l,k)
                enddo
        enddo

************************************************************
*       Average profiles and compute velocity statistics
************************************************************
c
        do k = 1, nv
        zpos(k)=0.
        umd(k)=0.
        uvd(k)=0.
c
                do l = 1, npr
c
c        Compute Average Depth and the Velocity at Each Depth
```

```
c
                        zpos(k) = z(l,k)/real(npr)+zpos(k)
                        umd(k) = ump(l,k)/real(npr)+umd(k)
                        uvd(k) = -uvp(l,k)/real(npr)+uvd(k)
                enddo
                write(nif+2,*) 'zpos(',k,') = ',zpos(k),'  umd(',k,') = '
   &,umd(k),'  uvd(',k,') = ',uvd(k)
                write(nif+4,*) zpos(k), umd(k), uvd(k)
c
c       Create graph of -u'v'/u*^2 versus z/H
c
        y2axis = zpos(k)/h
        x2axis = uvd(k)/ustar**2
        write(nif+5+nv+2*npr+1,*) k,x2axis,y2axis

        enddo
c
c       Create points for the computation of d(-u'v')/dz
c
        do k=1,ndata
                xdata(k) = zpos(nv-ndata+k)
                fdata(k) = uvd(nv-ndata+k)
                write(nif+2,*) xdata(k), fdata(k)
        enddo
c
c
        ic = 0
        do l = 1, npr
c
c     Estimate Top Point by a Linear Extrapolation for Each Profile
c
            st = (z(l,1)-z(l,2))/(ump(l,1)-ump(l,2))
            ut = (h-z(l,1))/st+ump(l,1)
c
c     Estimate Bottom Point by Two Methods for Each Profile
c
                        sb = (z(l,nv-1)-z(l,nv))/(ump(l,nv-1)-ump(l,nv))
                        ub1 = ump(l,nv)-z(l,nv)/sb
                        ub2 = 0.
                        ic = ic+1
                        write(nif+5+ic+nv,*) ic, .33, ut
                        write(nif+5+ic+nv,*) ic, 0, ub1
c
                        write(nif+2,*) ut, ub1, ub2
c
c       Integrate velocity profiles to get average velocities
c
                        umptot = 0.
                        do k = nv,2,-1
                umptot = umptot + (ump(l,k)+ump(l,k-1))*(z(l,k-1)-z(l,k))
                enddo
                write (nif+2,*) umptot
        uq1(l) =1./2./h*((ub1+ump(l,nv))*(z(l,nv))+umptot+(ump(l,1)+ut)
   &*(h-z(l,1)))
        uq2(l) =1./2./h*((ub2+ump(l,nv))*(z(l,nv))
```

```
     &+umptot+(ump(l,1)+ut)*(h-z(l,1)))
           umeas(l) = 1./2./(z(l,1)-z(l,nv))*umptot
           write (nif+2,*) 'uq1(',l,')= ',uq1(l), '  uq2(',l,')= ',uq2(l),
     &'  umeas(',l,')= ',umeas(l)
           write (nif+2,*) 'ut(',l,')= ',ut, '  ub1(',l,')= ',
     &ub1, '  ub2=', ub2
c          write(nif+2,*) l, umeas(l)

*********************************************************
*          Find Shape Factors for Each Profile
*********************************************************
c
c       Compute a Dimensionless Height and Velocity
c
                   do k = 1, nv
                            eta(l,k)=z(l,k)/h
                            feta(l,k)=ump(l,k)/uq1(l)
                            write (nif+2,*) 'feta(',l,',',k,')=  ',feta(l,k),
     &'  eta(',l,',',k,')= ',eta(l,k)
                   enddo
c
                   bfeta(l)=feta(l,nv)-eta(l,nv)/((eta(l,nv-1)-eta(l,nv))/
     &(feta(l,nv-1)-feta(l,nv)))
                   tfeta(l)=(1-eta(l,1))/((eta(l,1)-eta(l,2))/(feta(l,1)
     &-feta(l,2)))+feta(l,1)
c
                   write (nif+2,*) 'bfeta(',l,')= ',bfeta(l), '  tfeta(',l,')
     &= ',tfeta(l)
c
c      Compute Shape Factor
c
                   sftot = 0.
                   do k = nv,2,-1
                            sftot = sftot+(feta(l,k)**2+feta(l,k-1)**2)*(eta(l,k-1)
     &-eta(l,k))
                   enddo
                   sf = 1./2.*((bfeta(l)**2+feta(l,nv)**2)*(eta(l,nv))+sftot+
     &(feta(l,1)**2+tfeta(l)**2)*(1-eta(l,1)))
                   write(nif+2,*) 'Shape Factor(',l,')=  ',sf
                   write(nif+1,31)
31                 format(/,'Shape Factor',/)
                   write(nif+1,*)'shape factor (',l,') = ',sf
c
          enddo
c
*********************************************************
*          Perform regression of on average reynolds stress points
*********************************************************
c         Compute Least Squares Fit with An Intercept
          intcep = 1
          iwt = 0
c
          call fnlsq(f,intcep, nbasis, ndata, xdata, fdata, iwt, weight,
     &a, sse)
c
```

```
      write (nif+1,96)
      write (nif+1,91) sse, a(1), (a(i),i=2,nbasis+1)
96    format (//,' Coefficients are: ',/,'  sse      intercept'
     &,'      coefficients ',/)
91    format (1x, f8.5, 5x, f9.5, 5x, 4f9.5, //)
*************************************************************
*     Find the drag coefficient as a function of depth
*************************************************************
c
c     Find the derivitive d(uv)/dz and the drag coeff. at z
c
      do k=nv,nv-ndata+1,-1
            deriv(k)=a(2)+2*a(3)*zpos(k)+3*a(4)*zpos(k)**2
            write (nif+2,*) 'deriv (',k,') = ', deriv(k)
            cd(k) = (g*S+deriv(k))/(pdens/2*umd(k)**2)
            write (nif+1,*) 'cd (',k,') = ', cd(k)
            write (nif+5,*) zpos(k), cd(k)
      enddo
c
*****************************************************************
*     Find the average drag coefficient by simple integration
*****************************************************************
      cdb = 0.
      scd = (cd(nv-ndata+1)-cd(nv-ndata+2))/(zpos(nv-ndata+1)-
     &zpos(nv-ndata+2))
      cdt = scd*(veght-zpos(nv-ndata+1))+cd(nv-ndata+1)
      cdtot = 0.
      do k = nv,nv-ndata+2,-1
            cdtot = cdtot + (cd(k)+cd(k-1))*(zpos(k-1)-zpos(k))
      enddo
      cdavg = 1./2./veght*((cdb+cd(nv))*(zpos(nv))+cdtot+
     &(cd(nv-ndata+1)+cdt)*(veght-zpos(nv-ndata+1)))
      write(nif+1,*) 'Average Drag Coefficient = ', cdavg
*****************************************************************
*     Find the bulk drag coefficients integrated to hp and H, resp.
*****************************************************************
c Compute top of both integral equations
      cdbar = 0.
      do k=nv,nv-ndata+2,-1
            cdbar = cdbar + ((cd(k)*umd(k)**2)+(cd(k-1)*umd(k-1)**2))*
     &(zpos(k-1)-zpos(k))
      enddo
c Assume that the product of cd * U**2 is 0 at bed and top of plants
      prodt = 0.
      prodb = 0.
      rinttop= 1./2.*((prodb+(cd(nv)*umd(nv)**2))*(zpos(nv))+cdbar
     &+((cd(nv-ndata+1)*umd(nv-ndata+1)**2)+prodt)*(veght-zpos(nv-
     & ndata+1)))
      write(nif+2,*) 'rinttop = ', rinttop
c
c Integrate bottom of integral equation up to hp
      cdsu = (umd(nv-ndata+1)**2-umd(nv-ndata+2)**2)/(zpos
     &(nv-ndata+1)-zpos(nv-ndata+2))
      cduhp = cdsu*(veght-zpos(nv-ndata+1))+umd(nv-ndata+1)**2
      cdsb = (umd(nv)**2-umd(nv-1)**2)/(zpos(nv)-zpos(nv-1))
```

```
      cdub = -cdsb*(zpos(nv))+umd(nv)**2
      cduplant = 0
      do k = nv,nv-ndata+2,-1
            cduplant = cduplant + (umd(k)**2+umd(k-1)**2)*(zpos(k-1)
     &-zpos(k))
      enddo
      rbot = 1./2.*((cdub+umd(nv)**2)*(zpos(nv))+cduplant+
     &(umd(nv-ndata+1)**2+cduhp)*(veght-zpos(nv-ndata+1)))
      cdhpbulk = rinttop/rbot
      write(nif+1,*) 'Bulk Drag Coefficient up to hp = ', cdhpbulk
c
c Integrate bottom of integral equation up to H
      cddenom = 0.
      do k=nv,2,-1
            cddenom = cddenom+((umd(k)**2)+(umd(k-1)**2))*(zpos(k-1)
     &-zpos(k))
      enddo
      rintbot= 1./2.*((ub1*(umd(nv)**2))*zpos(nv) + cddenom + ((umd
     &(1)**2)+ut)*(h-zpos(1)))
      write(nif+2,*) 'rintbot = ', rintbot
      cdbulk = rinttop/rintbot
      write(nif+1,*) 'Bulk Drag Coefficient up to H = ', cdbulk
c
*******************************************************
*     Estimate Channel Discharge
*******************************************************
c      Compute the Average Velocity in the Channel
      uchan1 = 0.
      uchan2 = 0.
      do l=1,npr
            uchan1 = uq1(l)/real(npr) + uchan1
            uchan2 = uq2(l)/real(npr) + uchan2
      enddo
c
c      Compute Discharge
      q1 = uchan1*.9144*h
      q2 = uchan2*.9144*h
      write(nif+2,*) 'chan vel1= ',uchan1,'  chan vel2= ',uchan2
      write(nif+2,*) 'discharge1 = ',q1, 'discharge2 = ',q2
      write(nif+1,*) 'average channel velocity = ',uchan1
      write(nif+1,*) 'approximate channel discharge = ',q1
c
*************************************************************
*     Find Bulk Drag Coeff. from Estimate of Manning's n
*************************************************************
c
      slopef = (rn*uchan1/Rh**(2./3.))**2
      fr = uchan1/((g*h)**0.5)
      cdman = 2.0*( S-slopef )/(pdens*h*fr**2.0)
      write(nif+1,*) 'Bulk Drag Coeff. from Man. n = ', cdman
c     write(nif+1,*) 'friction slope = ', slopef
c
*******************************************************
*     Find average shape factor
*******************************************************
```

```
c       Compute Dimensionless Parameters for Average Profile
                do k = 1, nv
                        aeta(k)=zpos(k)/h
                        afeta(k)=umd(k)/uchan1
                enddo
c
                abfeta=afeta(nv)-aeta(nv)/((aeta(nv-1)-aeta(nv))/
     &(afeta(nv-1)-afeta(nv)))
                atfeta=(1-aeta(1))/((aeta(1)-aeta(2))/(afeta(1)
     &-afeta(2)))+afeta(1)
c
c       Compute Average Shape Factor
                asftot = 0.
                do k = nv,2,-1
                        asftot = asftot+(afeta(k)**2+afeta(k-1)**2)*(aeta(k-1)
     &-aeta(k))
                enddo
                asf = 1./2.*((abfeta**2+afeta(nv)**2)*(aeta(nv))+asftot+
     &(afeta(1)**2+atfeta**2)*(1-aeta(1)))
                write(nif+1,*) 'Average Shape Factor =  ',asf

        stop
        end

c       This subroutine tells program how to perform regression
        real function f(ki, x)
        integer ki
        real x
c
        f = x**ki
        return
        end
```

APPENDIX B: Experimental Data

This appendix contains the data from the experimental study. The values of the distance to the bed, raw velocities, corrected velocities, root-mean-squared velocity fluctuations, and Reynolds stresses are reported for each experiment.

Experiment 1 Laboratory Measurements

H = 0.335 m S = 0.0036 Q = 179 L/s a = 1.09 m^{-1} T = 24.8 °C h_p = 0.1175 m

Profile 1

	Raw Velocities			Corrected Velocities			RMS Velocity Fluctuations			Reynolds Stresses		
y (m)	$\bar{u}$ (m/s)	$\bar{v}$ (m/s)	$\bar{w}$ (m/s)	$\bar{u}$ (m/s)	$\bar{v}$ (m/s)	$\bar{w}$ (m/s)	u_{rms} (m/s)	v_{rms} (m/s)	w_{rms} (m/s)	$\overline{u'v'}$ (m^2/s^2)	$\overline{u'w'}$ (m^2/s^2)	$\overline{v'w'}$ (m^2/s^2)
0.2386	0.7480	-6.99e-3	4.19e-2	0.7492	-4.63e-4	2.72e-3	0.1048	6.63e-2	8.18e-2	-1.62e-3	5.33e-5	-6.11e-5
0.2011	0.6852	-5.95e-3	4.17e-2	0.6864	3.32e-5	5.74e-3	0.1250	7.32e-2	8.83e-2	-3.31e-3	9.30e-6	9.15e-6
0.1709	0.6460	-1.08e-2	4.51e-2	0.6476	4.48e-4	1.13e-2	0.1274	7.53e-2	9.21e-2	-4.03e-3	-1.54e-4	2.64e-4
0.1511	0.6206	-1.33e-2	4.12e-2	0.6220	1.93e-4	8.67e-3	0.1393	7.78e-2	9.48e-2	-5.18e-3	1.65e-4	2.74e-4
0.1209	0.5352	-1.08e-2	4.00e-2	0.5367	9.22e-4	1.19e-2	0.1444	7.45e-2	9.07e-2	-5.66e-3	1.21e-3	2.81e-4
0.0999	0.4559	-2.98e-2	3.05e-2	0.4578	7.24e-5	6.64e-3	0.1442	6.82e-2	9.98e-2	-5.54e-3	1.26e-3	3.28e-4
0.0810	0.3406	-1.68e-2	2.68e-2	0.3420	-4.53e-4	8.94e-3	0.1169	7.67e-2	0.1066	-3.80e-3	4.85e-4	2.86e-4
0.0551	0.3077	2.93e-3	2.69e-2	0.3087	2.40e-4	1.07e-2	8.99e-2	5.82e-2	9.55e-2	-1.30e-3	4.04e-4	-5.22e-5
0.0310	0.2613	5.41e-3	2.63e-2	0.2623	-2.87e-4	1.26e-2	7.40e-2	4.24e-2	7.90e-2	-9.62e-4	9.99e-5	-9.16e-5
0.0105	0.2493	1.34e-2	2.74e-2	0.2508	3.81e-4	1.44e-2	6.97e-2	3.55e-2	7.63e-2	-6.16e-4	2.69e-4	2.23e-5

Profile 2

	Raw Velocities			Corrected Velocities			RMS Velocity Fluctuations			Reynolds Stresses		
y (m)	$\bar{u}$ (m/s)	$\bar{v}$ (m/s)	$\bar{w}$ (m/s)	$\bar{u}$ (m/s)	$\bar{v}$ (m/s)	$\bar{w}$ (m/s)	u_{rms} (m/s)	v_{rms} (m/s)	w_{rms} (m/s)	$\overline{u'v'}$ (m^2/s^2)	$\overline{u'w'}$ (m^2/s^2)	$\overline{v'w'}$ (m^2/s^2)
0.2399	0.7295	6.26e-3	3.90e-2	0.7305	-1.10e-4	7.86e-4	0.1168	6.88e-2	8.25e-2	-2.21e-3	1.46e-3	1.40e-4
0.2000	0.6727	9.81e-3	3.93e-2	0.6739	1.00e-3	4.03e-3	0.1290	7.82e-2	8.91e-2	-3.83e-3	1.73e-3	-2.32e-4
0.1703	0.6228	9.36e-3	4.50e-2	0.6244	1.20e-3	1.23e-2	0.1354	7.75e-2	9.33e-2	-4.85e-3	1.97e-3	-6.51e-5
0.1494	0.6138	1.34e-3	4.44e-2	0.6153	1.34e-3	1.22e-2	0.1466	7.86e-2	9.40e-2	-5.35e-3	8.64e-4	-1.72e-4
0.1208	0.5166	1.16e-2	4.29e-2	0.5183	3.28e-4	1.58e-2	0.1430	7.77e-2	8.92e-2	-6.10e-3	9.68e-4	-1.51e-4
0.1002	0.4585	9.97e-3	4.68e-2	0.4604	-3.00e-5	2.28e-2	0.1252	7.51e-2	8.80e-2	-5.05e-3	-3.82e-5	1.12e-4
0.0802	0.4108	1.06e-2	4.66e-2	0.4128	-1.87e-4	2.50e-2	0.1065	6.84e-2	8.16e-2	-3.31e-3	1.27e-3	-1.91e-4
0.0557	0.3671	8.48e-3	3.45e-2	0.3685	4.69e-4	1.52e-2	9.41e-2	5.22e-2	7.21e-2	-2.18e-3	2.32e-4	2.89e-4
0.0299	0.3290	-2.70e-3	2.90e-2	0.3301	1.75e-4	1.17e-2	8.00e-2	3.90e-2	6.53e-2	-1.03e-3	-5.23e-4	4.74e-4
0.0108	0.3054	2.45e-3	2.90e-2	0.3065	-2.11e-4	1.30e-2	6.31e-2	2.90e-2	5.62e-2	-6.29e-4	-2.35e-4	3.02e-4

Profile 3

	Raw Velocities			Corrected Velocities			RMS Velocity Fluctuations			Reynolds Stresses		
y (m)	$\bar{u}$ (m/s)	$\bar{v}$ (m/s)	$\bar{w}$ (m/s)	$\bar{u}$ (m/s)	$\bar{v}$ (m/s)	$\bar{w}$ (m/s)	u_{rms} (m/s)	v_{rms} (m/s)	w_{rms} (m/s)	$\overline{u'v'}$ (m^2/s^2)	$\overline{u'w'}$ (m^2/s^2)	$\overline{v'w'}$ (m^2/s^2)
0.2403	0.7476	3.14e-3	2.60e-2	0.7481	-1.23e-4	-9.28e-5	0.1181	6.75e-2	8.20e-2	-2.21e-3	1.83e-3	-2.52e-4
0.2004	0.6706	8.13e-3	3.00e-2	0.6713	-6.47e-4	6.53e-3	0.1291	7.90e-2	9.24e-2	-4.22e-3	1.16e-3	-5.09e-5
0.1695	0.6449	3.17e-3	3.59e-2	0.6457	3.57e-4	1.34e-2	0.1419	7.59e-2	9.16e-2	-4.92e-3	1.30e-3	-1.49e-4
0.1507	0.5878	8.15e-3	3.15e-2	0.5886	4.52e-4	1.09e-2	0.1488	7.90e-2	9.01e-2	-6.21e-3	2.42e-3	-1.52e-4
0.1209	0.5401	1.11e-3	3.01e-2	0.5409	1.11e-3	1.13e-2	0.1522	7.73e-2	9.13e-2	-6.63e-3	1.76e-3	-2.02e-4
0.1009	0.4184	1.08e-2	2.28e-2	0.4190	-1.86e-4	8.22e-3	0.1363	7.49e-2	8.22e-2	-6.45e-3	-3.97e-5	-4.33e-4
0.0803	0.3787	3.95e-3	2.46e-2	0.3793	6.50e-4	1.14e-2	0.1191	7.26e-2	8.57e-2	-4.24e-3	-1.08e-3	-5.26e-4
0.0549	0.3466	-2.63e-3	2.12e-2	0.3471	3.92e-4	9.13e-3	9.34e-2	5.33e-2	6.75e-2	-2.29e-3	-6.93e-4	5.19e-5
0.0310	0.3190	-8.86e-3	1.74e-2	0.3195	-5.02e-4	6.25e-3	8.26e-2	4.23e-2	6.40e-2	-1.35e-3	-5.16e-4	9.81e-5
0.0109	0.2990	-6.82e-4	1.13e-2	0.2993	6.22e-4	8.59e-4	7.06e-2	3.17e-2	5.86e-2	-7.06e-4	-1.73e-4	-1.98e-5

Profile 4

	Raw Velocities			Corrected Velocities			RMS Velocity Fluctuations			Reynolds Stresses		
y (m)	$\bar{u}$ (m/s)	$\bar{v}$ (m/s)	$\bar{w}$ (m/s)	$\bar{u}$ (m/s)	$\bar{v}$ (m/s)	$\bar{w}$ (m/s)	u_{rms} (m/s)	v_{rms} (m/s)	w_{rms} (m/s)	$\overline{u'v'}$ (m^2/s^2)	$\overline{u'w'}$ (m^2/s^2)	$\overline{v'w'}$ (m^2/s^2)
0.2373	0.7291	2.68e-3	3.55e-2	0.7299	-5.02e-4	-2.69e-3	0.1202	6.89e-2	8.30e-2	-2.43e-3	-4.98e-4	9.40e-5
0.1995	0.6897	4.37e-3	3.31e-2	0.6905	1.36e-3	-3.09e-3	0.1266	7.63e-2	8.69--2	-3.87e-3	-5.25e-4	3.10e-4
0.1707	0.6649	1.69e-3	3.58e-2	0.6659	-1.21e-3	9.15e-4	0.1301	7.67e-2	9.14e-2	-3.79e-3	-8.67e-4	3.42e-4
0.1502	0.6312	5.74e-3	2.81e-2	0.6318	2.27e-4	-4.96e-3	0.1429	7.89e-2	8.96e-2	-5.24e-3	-8.44e-4	3.05e-4
0.1201	0.5461	1.88e-3	-3.97e-4	0.5453	-5.01e-4	-2.90e-2	0.1544	8.25e-2	8.98e-2	-6.78e-3	-4.23e-4	2.25e-4
0.9950	0.5163	4.07e-3	-3.48e-3	0.5154	-4.38e-4	-3.05e-2	0.1579	6.80e-2	9.03e-2	-3.91e-3	-1.92e-3	7.71e-4
0.0811	0.4791	-1.16e-2	-1.06e-3	0.4786	9.34e-4	-2.61e-2	0.1417	6.75e-2	8.14e-2	-4.27e-3	-9.55e-4	6.39e-5
0.0553	0.4001	-7.98e-3	-5.66e-3	0.3993	7.49e-4	-2.66e-2	0.1165	6.15e-2	7.75e-2	-3.74e-3	-8.75e-4	5.80e-5
0.0304	0.3517	-1.66e-2	-2.01e-3	0.3515	3.10e-4	-2.04e-2	9.87e-2	5.02e-2	6.69e-2	-2.05e-3	-9.34e-4	-1.91e-5
0.0105	0.3167	-1.16e-2	-6.57e-3	0.3161	-5.45e-4	-2.31e-2	8.37e-2	3.78e-2	6.64e-2	-1.05e-3	-9.82e-4	-1.67e-5

Experiment 2 Laboratory Measurements

H = 0.229 m S = 0.0036 Q = 88 L/s a = 1.09 m^{-1} T = 25.5 °C h_p = 0.1175 m

Profile 1

	Raw Velocities			Corrected Velocities			RMS Velocity Fluctuations			Reynolds Stresses		
y (m)	$\bar{u}$ (m/s)	$\bar{v}$ (m/s)	$\bar{w}$ (m/s)	$\bar{u}$ (m/s)	$\bar{v}$ (m/s)	$\bar{w}$ (m/s)	u_{rms} (m/s)	v_{rms} (m/s)	w_{rms} (m/s)	$\overline{u'v'}$ (m^2/s^2)	$\overline{u'w'}$ (m^2/s^2)	$\overline{v'w'}$ (m^2/s^2)
0.1594	0.5147	-1.11e-2	7.90e-3	0.5149	1.36e-4	-1.09e-3	8.11e-2	4.62e-2	5.85e-2	-1.23e-3	9.78e-4	2.66e-4
0.1402	0.4845	1.51e-2	-2.62e-2	0.4848	-1.65e-4	6.62e-3	8.81e-2	4.71e-2	6.03e-2	-1.86e-3	2.28e-4	5.24e-4
0.1206	0.4184	-1.69e-2	9.94e-3	0.4189	-5.08e-4	2.64e-3	9.50e-2	5.04e-2	6.05e-2	-2.57e-3	1.01e-3	3.07e-4
0.1098	0.3851	-1.08e-2	4.93e-3	0.3853	-7.63e-4	-1.79e-3	8.91e-2	5.48e-2	6.07e-2	-2.47e-3	6.39e-4	4.02e-4
0.1007	0.3621	-5.50e-3	4.02e-3	0.3622	-7.63e-4	-2.31e-3	8.25e-2	5.56e-2	5.97e-2	-2.06e-3	3.37e-4	7.16e-4
0.0797	0.3396	-4.96e-3	1.50e-2	0.3399	-5.13e-4	9.10e-3	7.35e-2	4.11e-2	5.80e-2	-1.12e-3	5.32e-4	7.98e-5
0.0649	0.3292	-7.99e-3	1.88e-2	0.3296	6.27e-4	1.31e-2	7.04e-2	4.03e-2	5.21e-2	-1.20e-3	6.45e-4	-1.14e-5
0.0498	0.3021	-5.73e-3	1.79e-2	0.3024	-4.59e-4	1.26e-2	6.01e-2	3.53e-2	4.59e-2	-8.33e-4	1.88e-4	5.99e-5
0.0300	0.2688	-8.69e-3	2.06e-2	0.2693	-4.77e-4	1.59e-2	5.40e-2	2.80e-2	5.07e-2	-3.29e-4	8.08e-5	2.23e-6
0.0108	0.2600	-2.82e-3	2.10e-2	0.2603	-5.48e-4	1.65e-2	3.89e-2	2.05e-2	3.42e-2	-1.23e-4	1.55e-4	2.78e-5

Profile 2

	Raw Velocities			Corrected Velocities			RMS Velocity Fluctuations			Reynolds Stresses		
y (m)	$\bar{u}$ (m/s)	$\bar{v}$ (m/s)	$\bar{w}$ (m/s)	$\bar{u}$ (m/s)	$\bar{v}$ (m/s)	$\bar{w}$ (m/s)	u_{rms} (m/s)	v_{rms} (m/s)	w_{rms} (m/s)	$\overline{u'v'}$ (m^2/s^2)	$\overline{u'w'}$ (m^2/s^2)	$\overline{v'w'}$ (m^2/s^2)
0.1578	0.5340	-9.20e-3	1.99e-2	0.5344	1.19e-4	1.26e-3	8.06e-2	4.42e-2	6.02e-2	-1.17e-3	8.10e-4	1.83e-4
0.1394	0.5137	-1.62e-2	2.72e-2	0.5146	-4.78e-4	9.27e-3	8.83e-2	4.68e-2	6.29e-2	-1.61e-3	5.78e-4	1.39e-4
0.0120	0.4769	-3.01e-2	2.96e-2	0.4786	-9.62e-4	1.29e-2	9.10e-2	4.84e-2	6.96e-2	-2.21e-3	2.95e-4	4.38e-4
0.1101	0.4177	-4.22e-2	3.53e-2	0.4208	-1.23e-4	2.07e-2	0.1232	5.70e-2	8.34e-2	-3.35e-3	2.20e-3	1.07e-3
0.0996	0.3325	-1.86e-2	3.00e-2	0.3338	2.89e-4	1.84e-2	0.1168	6.59e-2	0.1020	-2.00e-3	3.47e-3	1.30e-3
0.0807	0.2907	1.06e-2	3.14e-2	0.2918	4.55e-4	2.12e-2	8.91e-2	5.03e-2	8.77e-2	-1.08e-3	2.12e-3	-1.67e-4
0.0648	0.2820	9.62e-3	3.42e-2	0.2832	-2.27e-4	2.43e-2	7.25e-2	4.29e-2	7.42e-2	-8.42e-4	1.75e-3	-3.26e-4
0.0507	0.2716	6.16e-3	3.10e-2	0.2726	2.29e-4	2.15e-2	6.33e-2	3.76e-2	6.52e-2	-7.37e-4	1.39e-3	-7.19e-5
0.0303	0.2472	2.29e-3	3.19e-2	0.2481	1.34e-4	2.32e-2	6.10e-2	3.03e-2	6.62e-2	-4.34e-4	6.53e-4	-6.59e-6
0.0101	0.2376	7.03e-3	3.40e-2	0.2388	-2.30e-4	2.57e-2	4.79e-2	2.48e-2	5.00e-2	-3.11e-4	8.06e-4	-2.10e-4

Profile 3

	Raw Velocities			Corrected Velocities			RMS Velocity Fluctuations			Reynolds Stresses		
y (m)	$\bar{u}$ (m/s)	$\bar{v}$ (m/s)	$\bar{w}$ (m/s)	$\bar{u}$ (m/s)	$\bar{v}$ (m/s)	$\bar{w}$ (m/s)	u_{rms} (m/s)	v_{rms} (m/s)	w_{rms} (m/s)	$\overline{u'v'}$ (m^2/s^2)	$\overline{u'w'}$ (m^2/s^2)	$\overline{v'w'}$ (m^2/s^2)
0.1581	0.5255	-9.36e-3	2.54e-2	0.5262	-1.87e-4	-2.09e-3	7.66e-2	4.49e-2	5.99e-2	-1.18e-3	-5.51e-4	-9.65e-5
0.1399	0.5222	-1.86e-2	2.10e-2	0.5229	-3.35e-4	-6.33e-3	8.90e-2	4.60e-2	5.83e-2	-1.85e-3	-2.84e-4	-1.72e-4
0.1203	0.4768	-9.07e-3	2.21e-2	0.4774	-7.45e-4	-2.90e-3	9.94e-2	5.14e-2	5.83e-2	-2.92e-3	-4.40e-4	-4.25e-4
0.1102	0.4517	-3.95e-3	1.58e-2	0.4519	-1.26e-5	-7.85e-3	9.79e-2	5.06e-2	6.28e-2	-2.78e-3	-6.90e-4	-4.30e-4
0.0996	0.4208	8.66e-3	-8.73e-3	0.4207	-7.98e-4	-1.34e-2	8.64e-2	4.96e-2	6.19e-2	-2.25e-3	-8.86e-4	-2.58e-4
0.0804	0.3778	-4.84e-3	1.06e-2	0.3779	1.04e-4	-9.17e-3	7.26e-2	4.26e-2	5.91e-2	-1.40e-3	-7.09e-4	-1.24e-4
0.0653	0.3533	-4.17e-3	4.87e-3	0.3531	4.51e-4	-1.36e-2	6.56e-2	4.02e-2	5.36e-2	-1.17e-3	-5.65e-4	-1.48e-4
0.0494	0.3263	-2.48e-3	5.59e-3	0.3262	3.71e-4	-1.15e-2	5.80e-2	3.43e-2	4.64e-2	-8.15e-4	-1.06e-4	-2.92e-4
0.0307	0.2937	-6.17e-3	8.18e-3	0.2938	2.43e-4	-7.20e-3	5.82e-2	2.70e-2	5.29e-2	-4.79e-4	-3.31e-4	-1.31e-4
0.0104	0.2739	-1.38e-3	7.80e-3	0.2740	-1.88e-4	-6.55e-3	3.99e-2	1.95e-2	3.79e-2	-2.48e-4	-1.01e-4	-5.68e-5

Profile 4

	Raw Velocities			Corrected Velocities			RMS Velocity Fluctuations			Reynolds Stresses		
y (m)	$\bar{u}$ (m/s)	$\bar{v}$ (m/s)	$\bar{w}$ (m/s)	$\bar{u}$ (m/s)	$\bar{v}$ (m/s)	$\bar{w}$ (m/s)	u_{rms} (m/s)	v_{rms} (m/s)	w_{rms} (m/s)	$\overline{u'v'}$ (m^2/s^2)	$\overline{u'w'}$ (m^2/s^2)	$\overline{v'w'}$ (m^2/s^2)
0.1495	0.5421	-1.38e-2	1.93e-2	0.5426	4.31e-4	3.48e-4	8.16e-2	4.45e-2	6.26e-2	-1.15e-3	-3.56e-4	1.20e-4
0.1394	0.5166	-1.00e-2	1.97e-2	0.5171	-9.82e-3	1.62e-3	8.70e-2	4.94e-2	6.29e-2	-1.95e-3	-3.42e-4	1.38e-4
0.1199	0.4845	-8.79e-3	1.59e-2	0.4848	-3.36e-4	-9.90e-4	9.44e-2	5.16e-2	6.44e-2	-2.49e-3	-9.95e-5	-1.23e-4
0.1108	0.4685	-1.06e-2	1.57e-2	0.4689	-4.24e-4	-6.69e-4	9.21e-2	4.91e-2	6.28e-2	-2.35e-3	1.30e-4	-8.14e-5
0.1002	0.4486	-1.16e-2	1.04e-2	0.4488	1.69e-4	-5.24e-3	9.35e-2	5.07e-2	6.43e-2	-2.63e-3	3.52e-4	-1.23e-4
0.0805	0.3808	-5.72e-3	5.73e-3	0.3808	-7.36e-4	-7.57e-3	8.79e-2	4.84e-2	6.16e-2	-2.54e-3	1.60e-4	-1.58e-4
0.0654	0.3377	-7.88e-3	8.63e-3	0.3379	-5.08e-4	-3.16e-3	7.95e-2	4.53e-2	5.46e-2	-2.09e-3	-1.33e-4	-9.26e-5
0.0500	0.3015	-3.37e-3	1.31e-2	0.3018	5.81e-4	2.58e-3	6.11e-2	3.94e-2	5.17e-2	-1.06e-3	1.26e-5	-2.24e-4
0.0298	0.2576	-1.91e-3	1.08e-2	0.2578	3.37e-4	1.79e-3	5.24e-2	2.67e-2	5.65e-2	-2.20e-4	-4.57e-4	-4.51e-5
0.0094	0.2575	3.55e-3	1.29e-2	0.2578	1.76e-4	3.95e-3	4.04e-2	2.01e-2	4.25e-2	-1.50e-4	-1.77e-4	-1.83e-5

Experiment 3 Laboratory Measurements

H = 0.164 m S = 0.0036 Q = 46 L/s a = 1.09 m^{-1} T = 25.5 °C h_p = 0.1175 m

Profile 1

	Raw Velocities			Corrected Velocities			RMS Velocity Fluctuations			Reynolds Stresses		
y (m)	$\bar{u}$ (m/s)	$\bar{v}$ (m/s)	$\bar{w}$ (m/s)	$\bar{u}$ (m/s)	$\bar{v}$ (m/s)	$\bar{w}$ (m/s)	u_{rms} (m/s)	v_{rms} (m/s)	w_{rms} (m/s)	$\overline{u'v'}$ (m^2/s^2)	$\overline{u'w'}$ (m^2/s^2)	$\overline{v'w'}$ (m^2/s^2)
0.0949	0.3265	-4.04e-3	2.51e-2	0.3275	2.31e-4	-5.49e-4	4.43e-2	2.40e-2	3.10e-2	-4.19e-4	-8.67e-5	9.25e-5
0.0877	0.3087	-7.74e-3	2.24e-2	0.3096	3.46e-4	-1.85e-3	4.62e-2	2.34e-2	3.99e-2	-3.56e-4	-5.92e-5	6.32e-5
0.0797	0.2932	-1.04e-2	1.56e-2	0.2937	-1.33e-4	-7.43e-3	4.66e-2	2.14e-2	4.17e-2	-2.49e-4	2.41e-5	9.72e-5
0.0698	0.2823	-1.35e-2	9.03e-3	0.2825	3.15e-5	-1.31e-2	4.28e-2	2.16e-2	3.39e-2	-3.32e-4	1.24e-4	1.17e-4
0.0599	0.2641	-1.37e-2	1.03e-2	0.2645	1.34e-4	-1.05e-2	3.93e-2	2.05e-2	2.88e-2	-3.34e-4	5.73e-5	4.87e-5
0.0500	0.2384	-8.23e-3	9.87e-3	0.2386	9.55e-5	-8.87e-3	3.16e-2	1.93e-2	2.51e-2	-2.20e-4	-2.89e-5	1.93e-5
0.0423	0.2299	-5.07e-3	9.16e-3	0.2299	-5.75e-5	-8.90e-3	2.71e-2	1.71e-2	2.17e-2	-1.33e-4	-2.66e-5	1.74e-5
0.0328	0.2143	-5.70e-3	1.06e-2	0.2146	-8.33e-5	-6.29e-3	3.68e-2	1.59e-2	3.82e-2	-6.31e-5	-1.59e-4	2.88e-5
0.0172	0.2145	2.33e-3	9.35e-3	0.2146	4.62e-4	-7.51e-3	2.35e-2	1.28e-2	2.13e-2	-5.60e-5	2.80e-5	-8.45e-6
0.0063	0.2022	2.21e-3	9.24e-3	0.2023	-4.33e-4	-6.65e-3	2.46e-2	1.18e-2	3.47e-2	-1.18e-4	-4.40e-4	1.64e-4

Profile 2

	Raw Velocities			Corrected Velocities			RMS Velocity Fluctuations			Reynolds Stresses		
y (m)	$\bar{u}$ (m/s)	$\bar{v}$ (m/s)	$\bar{w}$ (m/s)	$\bar{u}$ (m/s)	$\bar{v}$ (m/s)	$\bar{w}$ (m/s)	u_{rms} (m/s)	v_{rms} (m/s)	w_{rms} (m/s)	$\overline{u'v'}$ (m^2/s^2)	$\overline{u'w'}$ (m^2/s^2)	$\overline{v'w'}$ (m^2/s^2)
0.0943	0.1899	-2.31e-2	5.70e-3	0.1914	1.79e-4	7.30e-4	5.06e-2	3.08e-2	5.24e-2	-1.65e-6	-5.63e-4	-5.80e-4
0.0874	0.1599	-2.24e-2	1.46e-2	0.1618	1.05e-4	1.04e-2	6.38e-2	3.41e-2	6.48e-2	5.19e-4	-8.50e-4	-7.10e-4
0.0798	0.1559	-1.51e-2	-1.94e-3	0.1566	-9.90e-5	-6.02e-3	6.26e-2	3.14e-2	6.49e-2	5.61e-4	-8.34e-4	-3.12e-4
0.0699	0.1678	-4.72e-3	-9.01e-3	0.1676	-3.23e-4	-1.34e-2	4.67e-2	2.45e-2	5.96e-2	9.85e-5	-6.05e-4	4.26e-5
0.0597	0.1634	-4.18e-3	-8.67e-3	0.1632	9.78e-5	-1.29e-2	4.46e-2	2.29e-2	5.79e-2	9.20e-6	-5.04e-4	2.26e-5
0.0500	0.1532	-4.00e-3	-9.49e-3	0.1530	1.23e-5	-1.35e-2	4.49e-2	2.35e-2	5.98e-2	4.16e-5	-5.94e-4	-9.30e-6
0.0423	0.1463	-3.73e-3	-7.78e-3	0.1462	1.03e-4	-1.16e-2	4.38e-2	2.25e-2	6.02e-2	1.04e-4	-4.43e-4	-4.59e-5
0.0328	0.1394	-4.83e-3	-1.20e-2	0.1392	4.25e-5	-1.57e-2	5.88e-2	2.38e-2	7.17e-2	1.26e-4	-6.08e-4	-1.73e-5
0.0171	0.1569	1.31e-3	-1.61e-2	0.1563	-5.41e-5	-2.02e-2	4.99e-2	2.38e-2	6.62e-2	-1.58e-4	-4.28e-4	9.51e-5
0.0069	0.1502	4.40e-3	-2.43e-2	0.1496	-1.89e-4	-2.83e-2	4.90e-2	2.37e-2	6.08e-2	-8.94e-5	-5.95e-4	1.40e-4

Profile 3

	Raw Velocities			Corrected Velocities			RMS Velocity Fluctuations			Reynolds Stresses		
y (m)	$\bar{u}$ (m/s)	$\bar{v}$ (m/s)	$\bar{w}$ (m/s)	$\bar{u}$ (m/s)	$\bar{v}$ (m/s)	$\bar{w}$ (m/s)	u_{rms} (m/s)	v_{rms} (m/s)	w_{rms} (m/s)	$\overline{u'v'}$ (m^2/s^2)	$\overline{u'w'}$ (m^2/s^2)	$\overline{v'w'}$ (m^2/s^2)
0.0929	0.2811	6.31e-3	9.95e-3	0.2813	1.77e-4	1.35e-4	4.83e-2	2.38e-2	3.19e-2	-2.30e-4	-6.49e-4	-1.42e-5
0.0876	0.2703	1.64e-3	7.52e-3	0.2704	4.59e-4	-1.92e-3	5.14e-2	2.35e-2	3.88e-2	-2.41e-4	-7.94e-4	-1.73e-5
0.0795	0.2628	8.93e-4	3.72e-3	0.2627	-2.53e-4	-5.45e-3	5.00e-2	2.28e-2	3.80e-2	-3.37e-4	-7.39e-4	3.72e-5
0.0696	0.2599	2.61e-3	5.83e-4	0.2598	3.41e-4	-8.49e-3	4.06e-2	2.15e-2	2.98e-2	-3.20e-4	-4.37e-4	8.92e-5
0.0595	0.2480	2.85e-3	-8.23e-4	0.2479	-4.00e-4	-9.48e-3	3.42e-2	1.95e-2	2.58e-2	-2.36e-4	-2.33e-4	6.44e-5
0.0500	0.2383	4.69e-3	-1.23e-3	0.2381	-5.11e-4	-9.55e-3	2.70e-2	1.68e-2	2.28e-2	-1.04e-4	-9.44e-5	4.91e-5
0.0424	0.2347	2.80e-3	-2.89e-3	0.2344	-2.68e-4	-1.11e-2	2.53e-2	1.55e-2	2.24e-2	-6.80e-5	-8.32e-5	4.66e-5
0.0324	0.2219	-9.35e-4	-3.33e-3	0.2217	3.36e-5	-1.11e-2	4.08e-2	1.54e-2	4.13e-2	-6.80e-5	-2.23e-4	4.27e-5
0.0175	0.2278	4.05e-3	-4.63e-3	0.2276	7.27e-5	-1.26e-2	2.64e-2	1.33e-2	2.45e-2	-2.59e-5	-1.03e-4	3.96e-5
0.0077	0.2236	5.49e-3	-7.44e-3	0.2233	-3.61e-4	-1.52e-2	2.00e-2	1.17e-2	1.95e-2	-2.85e-5	-1.98e-5	-1.61e-6

Profile 4

	Raw Velocities			Corrected Velocities			RMS Velocity Fluctuations			Reynolds Stresses		
y (m)	$\bar{u}$ (m/s)	$\bar{v}$ (m/s)	$\bar{w}$ (m/s)	$\bar{u}$ (m/s)	$\bar{v}$ (m/s)	$\bar{w}$ (m/s)	u_{rms} (m/s)	v_{rms} (m/s)	w_{rms} (m/s)	$\overline{u'v'}$ (m^2/s^2)	$\overline{u'w'}$ (m^2/s^2)	$\overline{v'w'}$ (m^2/s^2)
0.0907	0.2955	-2.06e-3	9.58e-3	0.2957	5.22e-4	-7.41e-4	4.11e-2	2.16e-2	2.94e-2	-2.93e-4	3.58e-4	3.12e-5
0.0874	0.2842	-3.66e-3	8.52e-3	0.2843	6.50e-5	-1.40e-3	3.86e-2	2.00e-2	2.78e-2	-2.84e-4	2.68e-4	4.74e-6
0.0796	0.2658	-8.73e-3	1.12e-2	0.2662	5.52e-4	1.88e-3	4.18e-2	1.90e-2	3.43e-2	-2.30e-4	1.30e-4	1.07e-5
0.0693	0.2452	-4.70e-3	1.11e-2	0.2455	-4.15e-4	2.56e-3	3.45e-2	2.09e-2	2.54e-2	-2.34e-4	1.11e-4	-1.62e-5
0.0596	0.2231	1.62e-3	1.12e-2	0.2234	-3.26e-4	3.38e-3	2.66e-2	1.86e-2	2.39e-2	-7.90e-5	1.80e-6	4.52e-6
0.0497	0.2189	4.61e-3	1.18e-2	0.2193	-1.66e-4	4.19e-3	2.61e-2	1.71e-2	2.30e-2	-1.37e-5	-1.58e-5	-9.32e-6
0.0418	0.2159	5.61e-3	9.52e-3	0.2161	-4.30e-5	1.98e-3	2.48e-2	1.48e-2	2.33e-2	-1.84e-5	-1.35e-6	-7.16e-7
0.0332	0.2053	2.95e-3	9.39e-3	0.2056	2.66e-4	2.22e-3	4.86e-2	1.77e-2	5.23e-2	-1.22e-4	-2.94e-4	6.60e-5
0.0174	0.2065	8.85e-3	9.02e-3	0.2069	-1.69e-4	1.80e-3	2.93e-2	1.41e-2	2.65e-2	-1.35e-5	-2.02e-5	3.23e-6
0.0074	0.2043	9.85e-3	9.81e-3	0.2047	3.44e-5	2.67e-3	2.21e-2	1.21e-2	2.17e-2	-1.47e-5	-3.85e-5	2.37e-5

Experiment 4 Laboratory Measurements

H = 0.276 m S = 0.0076 Q = 178 L/s a = 1.09 m^{-1} T = 27.2 °C h_p = 0.1175 m

Profile 1

	Raw Velocities			Corrected Velocities			RMS Velocity Fluctuations			Reynolds Stresses		
y (m)	$\bar{u}$ (m/s)	$\bar{v}$ (m/s)	$\bar{w}$ (m/s)	$\bar{u}$ (m/s)	$\bar{v}$ (m/s)	$\bar{w}$ (m/s)	u_{rms} (m/s)	v_{rms} (m/s)	w_{rms} (m/s)	$\overline{u'v'}$ (m^2/s^2)	$\overline{u'w'}$ (m^2/s^2)	$\overline{v'w'}$ (m^2/s^2)
0.1947	0.7453	-1.38e-2	7.58e-3	0.7454	-7.94e-4	1.08e-3	0.1394	7.58e-2	0.1221	-4.06e-3	-3.08e-3	2.78e-4
0.1798	0.7427	-1.93e-2	5.73e-3	0.7429	9.74e-5	-7.56e-4	0.1384	7.87e-2	0.1045	-4.32e-3	-6.60e-5	4.42e-5
0.1650	0.7154	-1.97e-2	5.27e-3	0.7157	-9.37e-4	-9.75e-4	0.1402	8.22e-2	0.1026	-5.38e-3	-3.55e-4	1.20e-4
0.1396	0.6557	-9.69e-3	-1.76e-3	0.6557	-1.10e-3	-7.48e-3	0.1583	8.57e-2	0.1049	-7.27e-3	-2.13e-4	1.76e-4
0.1204	0.5888	-7.85e-3	5.43e-3	0.5888	-1.46e-4	2.90e-4	0.1484	8.41e-2	0.1066	-6.59e-3	1.94e-4	-2.38e-4
0.0995	0.5429	-1.66e-2	1.15e-3	0.5422	-4.05e-5	-3.58e-3	0.1402	7.87e-2	0.1026	-6.44e-3	5.63e-4	-5.61e-4
0.0806	0.4630	-1.55e-2	7.23e-3	0.4633	6.28e-4	3.19e-3	0.1235	7.11e-2	9.75e-2	-4.80e-3	9.24e-4	-6.27e-4
0.0593	0.4170	-1.81e-2	4.81e-3	0.4174	5.72e-5	1.17e-3	0.1060	6.41e-2	8.95e-2	-3.28e-3	6.40e-4	-7.34e-4
0.0381	0.3597	-1.11e-2	2.55e-3	0.3598	-1.56e-4	-5.92e-4	8.78e-2	4.79e-2	7.73e-2	-1.56e-3	-1.11e-4	-2.28e-4
0.0100	0.3258	-1.27e-4	-3.94e-3	0.3258	-1.27e-4	-6.78e-3	6.28e-2	2.98e-2	5.96e-2	-5.49e-4	-3.28e-4	-7.25e-5

Profile 2

	Raw Velocities			Corrected Velocities			RMS Velocity Fluctuations			Reynolds Stresses		
y (m)	$\bar{u}$ (m/s)	$\bar{v}$ (m/s)	$\bar{w}$ (m/s)	$\bar{u}$ (m/s)	$\bar{v}$ (m/s)	$\bar{w}$ (m/s)	u_{rms} (m/s)	v_{rms} (m/s)	w_{rms} (m/s)	$\overline{u'v'}$ (m^2/s^2)	$\overline{u'w'}$ (m^2/s^2)	$\overline{v'w'}$ (m^2/s^2)
0.1937	0.7403	-7.98e-3	1.85e-2	0.7406	-1.52e-3	-8.64e-4	0.1401	7.62e-2	0.1139	-4.30e-3	-9.91e-4	4.46e-4
0.1802	0.7380	-9.68e-3	7.16e-3	0.7380	-2.43e-5	-1.22e-2	0.1324	8.01e-2	0.1065	-4.51e-3	4.87e-4	-5.33e-4
0.1648	0.7114	-7.13e-3	4.79e-3	0.7114	-9.21e-4	-1.38e-2	0.1488	8.31e-2	0.1030	-6.07e-3	2.62e-5	1.77e-4
0.1402	0.6606	-6.66e-3	9.68e-3	0.6607	-8.94e-4	-7.62e-3	0.1524	8.31e-2	0.1039	-6.99e-3	5.13e-4	-5.86e-5
0.1199	0.6103	6.56e-3	1.51e-2	0.6105	-1.24e-3	-8.62e-4	0.1562	8.32e-2	0.1028	-7.27e-3	2.68e-4	1.88e-5
0.9980	0.5423	-1.42e-2	1.71e-2	0.5428	-3.50e-5	2.86e-3	0.1566	7.47e-2	9.88e-2	-7.12e-3	9.88e-4	-1.03e-4
0.0796	0.4597	-2.26e-2	8.83e-3	0.4603	-5.57e-4	-3.21e-3	0.1396	7.61e-2	9.54e-2	-6.10e-3	-3.67e-4	1.59e-4
0.0598	0.3828	-8.38e-3	5.18e-3	0.3829	-2.54e-5	-4.84e-3	9.71e-2	6.12e-2	8.82e-2	-2.20e-3	-2.28e-4	4.20e-5
0.0375	0.3460	3.51e-4	-1.41e-5	0.3459	3.51e-4	-9.07e-3	8.06e-2	4.58e-2	7.75e-2	-1.16e-3	-3.44e-4	2.14e-4
0.0094	0.3276	1.35e-2	-4.27e-3	0.3277	6.34e-4	-1.28e-2	5.77e-2	3.12e-2	5.76e-2	-4.00e-4	-3.60e-4	2.41e-4

Profile 3

	Raw Velocities			Corrected Velocities			RMS Velocity Fluctuations			Reynolds Stresses		
y (m)	$\bar{u}$ (m/s)	$\bar{v}$ (m/s)	$\bar{w}$ (m/s)	$\bar{u}$ (m/s)	$\bar{v}$ (m/s)	$\bar{w}$ (m/s)	u_{rms} (m/s)	v_{rms} (m/s)	w_{rms} (m/s)	$\overline{u'v'}$ (m^2/s^2)	$\overline{u'w'}$ (m^2/s^2)	$\overline{v'w'}$ (m^2/s^2)
0.1935	0.7327	1.92e-3	4.31e-4	0.7327	-1.27e-3	4.31e-4	0.1373	7.51e-2	0.1221	-4.11e-3	-2.89e-3	3.55e-4
0.1801	0.7229	-2.42e-3	-2.08e-3	0.7229	7.35e-4	-2.08e-3	0.1347	7.68e-2	9.59e-2	-4.50e-3	-9.83e-4	4.47e-4
0.1652	0.6980	-1.38e-3	-6.09e-4	0.6980	-1.38e-3	-6.09e-4	0.1438	7.96e-2	0.1021	-5.87e-3	-1.06e-3	4.09e-4
0.1403	0.6425	-6.47e-3	-9.92e-3	0.6426	-8.64e-4	-9.92e-3	0.1540	7.77e-2	0.1025	-6.62e-3	-1.91e-3	7.08e-4
0.1199	0.5668	-4.68e-3	-7.64e-3	0.5669	2.70e-4	-7.64e-3	0.1521	8.26e-2	0.1001	-7.63e-3	-1.37e-3	1.16e-5
0.0997	0.4949	-1.61e-3	-9.61e-3	0.4949	5.48e-4	-9.61e-3	0.1371	7.99e-2	9.50e-2	-6.32e-3	-1.96e-3	-8.83e-5
0.0804	0.4376	3.82e-3	-8.07e-3	0.4376	-2.98e-6	-8.07e-3	0.1061	6.64e-2	8.84e-2	-3.01e-3	-1.38e-3	-1.79e-4
0.0595	0.4035	1.71e-3	-5.62e-3	0.4036	-5.26e-5	-5.62e-3	9.63e-2	5.30e-2	8.34e-2	-2.15e-3	-1.17e-3	1.03e-4
0.0380	0.367	2.18e-3	-5.80e-3	0.3667	5.76e-4	-5.80e-3	7.86e-2	4.30e-2	7.59e-2	-1.20e-3	-8.91e-4	1.25e-4
0.0103	0.3351	5.63e-3	-3.69e-3	0.3351	-2.15e-4	-3.69e-3	5.53e-2	2.78e-2	5.83e-2	-3.76e-4	-2.73e-4	4.61e-5

Profile 4

	Raw Velocities			Corrected Velocities			RMS Velocity Fluctuations			Reynolds Stresses		
y (m)	$\bar{u}$ (m/s)	$\bar{v}$ (m/s)	$\bar{w}$ (m/s)	$\bar{u}$ (m/s)	$\bar{v}$ (m/s)	$\bar{w}$ (m/s)	u_{rms} (m/s)	v_{rms} (m/s)	w_{rms} (m/s)	$\overline{u'v'}$ (m^2/s^2)	$\overline{u'w'}$ (m^2/s^2)	$\overline{v'w'}$ (m^2/s^2)
0.1844	0.7415	-1.07e-2	5.05e-3	0.7415	-1.02e-3	-1.42e-3	0.1369	7.69e-2	0.1049	-4.10e-3	-7.57e-4	1.54e-4
0.1804	0.7423	-1.34e-2	1.17e-2	0.7425	-4.72e-4	5.17e-3	0.1391	7.75e-2	0.1111	-4.46e-3	-1.76e-3	4.12e-4
0.1652	0.7323	-1.64e-2	7.91e-3	0.7325	-4.63e-4	1.52e-3	0.1412	8.13e-2	0.1071	-5.10e-3	-1.40e-3	2.13e-5
0.1399	0.6759	-1.65e-2	5.52e-3	0.676	1.18e-3	-7.90e-5	0.1605	8.10e-2	0.1058	-6.73e-3	-7.51e-4	2.72e-4
0.1199	0.5901	-1.52e-2	-1.83e-3	0.5902	2.22e-4	-6.98e-3	0.1673	8.16e-2	0.1039	-7.96e-3	-6.28e-4	7.16e-4
0.0999	0.4997	-1.16e-2	-5.93e-3	0.4998	-7.06e-4	-1.03e-2	0.1438	8.18e-2	9.63e-2	-6.48e-3	1.28e-3	5.13e-4
0.0797	0.4270	1.13e-2	-1.18e-2	0.4271	1.14e-4	-1.55e-2	0.1105	7.03e-2	8.52e-2	-3.16e-3	-1.19e-4	1.09e-4
0.0602	0.3961	6.67e-3	4.90e-3	0.3963	-5.47e-4	1.44e-3	9.70e-2	5.38e-2	7.96e-2	-1.88e-3	-2.60e-5	-4.99e-4
0.0369	0.3673	8.85e-4	-9.38e-4	0.3673	-7.18e-4	-4.14e-3	8.54e-2	4.30e-2	6.98e-2	-1.17e-3	-1.75e-4	-3.07e-4
0.0104	0.3354	4.99e-3	-3.50e-3	0.3354	5.97e-4	-6.43e-3	6.79e-2	3.11e-2	6.34e-2	-5.82e-4	-5.29e-4	-1.15e-4

Experiment 5 Laboratory Measurements

H = 0.203 m S = 0.0076 Q = 98 L/s $a = 1.09\ m^{-1}$ T = 27.6 °C $h_p = 0.1175$ m

Profile 1

	Raw Velocities			Corrected Velocities			RMS Velocity Fluctuations			Reynolds Stresses		
y (m)	$\bar{u}$ (m/s)	$\bar{v}$ (m/s)	$\bar{w}$ (m/s)	$\bar{u}$ (m/s)	$\bar{v}$ (m/s)	$\bar{w}$ (m/s)	u_{rms} (m/s)	v_{rms} (m/s)	w_{rms} (m/s)	$\overline{u'v'}$ (m^2/s^2)	$\overline{u'w'}$ (m^2/s^2)	$\overline{v'w'}$ (m^2/s^2)
0.1298	0.6282	-1.30e-2	1.30e-2	0.6285	7.31e-4	2.05e-3	0.1142	5.74e-2	7.47e-2	-3.26e-3	-6.35e-4	6.87e-4
0.1196	0.5922	-1.54e-2	1.12e-2	0.5925	7.24e-5	8.92e-4	0.1199	5.80e-2	7.51e-2	-3.91e-3	-2.88e-4	2.79e-4
0.1099	0.5536	-2.15e-2	7.23e-3	0.5540	2.26e-4	-2.43e-3	0.1152	5.68e-2	7.77e-2	-3.58e-3	-3.73e-5	1.87e-4
0.1003	0.5047	-2.03e-2	1.65e-3	0.5051	-5.09e-4	-7.16e-3	0.1086	5.71e-2	7.80e-2	-3.33e-3	-7.42e-4	-6.68e-5
0.0799	0.4362	-1.42e-2	7.16e-3	0.4364	-8.30e-4	-4.58e-4	8.99e-2	5.03e-2	7.16e-2	-1.48e-3	-1.36e-3	-2.93e-4
0.0656	0.4235	-1.64e-2	3.09e-3	0.4238	2.38e-4	-4.30e-3	8.40e-2	4.48e-2	6.14e-2	-1.17e-3	-1.11e-3	-6.84e-5
0.0503	0.3958	-1.62e-2	6.37e-3	0.3962	-6.99e-4	-5.34e-4	8.00e-2	4.22e-2	5.45e-2	-1.38e-3	-9.02e-4	-8.88e-6
0.0374	0.3757	-1.62e-2	6.83e-3	0.3761	1.80e-2	6.83e-3	7.03e-2	3.70e-2	5.02e-2	-8.41e-4	-7.55e-4	1.60e-5
0.0170	0.3502	-1.16e-2	5.95e-3	0.3505	6.20e-4	-1.63e-4	5.65e-2	2.90e-2	4.44e-2	-4.08e-4	-4.69e-4	4.48e-5
0.0076	0.3451	-1.09e-2	5.18e-3	0.3453	-3.68e-4	-8.44e-4	5.41e-2	2.62e-2	4.26e-2	-2.82e-4	-5.07e-4	1.13e-5

Profile 2

	Raw Velocities			Corrected Velocities			RMS Velocity Fluctuations			Reynolds Stresses		
y (m)	$\bar{u}$ (m/s)	$\bar{v}$ (m/s)	$\bar{w}$ (m/s)	$\bar{u}$ (m/s)	$\bar{v}$ (m/s)	$\bar{w}$ (m/s)	u_{rms} (m/s)	v_{rms} (m/s)	w_{rms} (m/s)	$\overline{u'v'}$ (m^2/s^2)	$\overline{u'w'}$ (m^2/s^2)	$\overline{v'w'}$ (m^2/s^2)
0.1276	0.5692	8.70e-3	5.17e-3	0.5693	-1.23e-3	1.98e-4	0.1210	5.87e-2	7.54e-2	-3.75e-3	8.59e-4	1.98e-4
0.1205	0.5522	4.57e-3	2.31e-3	0.5522	-2.49e-4	-2.50e-3	0.1225	6.25e-2	7.52e-2	-4.42e-3	8.02e-4	1.00e-5
0.1096	0.5159	5.59e-3	-2.04e-3	0.5159	1.09e-3	-6.54e-3	0.1138	6.10e-2	7.67e-2	-3.80e-3	1.76e-3	-2.75e-4
0.0998	0.4839	4.97e-3	4.34e-4	0.4839	7.45e-4	-3.79e-3	0.1082	5.94e-2	7.40e-2	-3.51e-3	1.38e-3	-9.86e-5
0.0802	0.4175	5.59e-3	3.93e-3	0.4176	1.24e-4	2.85e-4	9.21e-2	5.62e-2	6.52e-2	-2.69e-3	1.17e-3	-4.79e-4
0.0654	0.3715	6.28e-3	7.97e-3	0.3716	-2.05e-4	4.73e-3	7.19e-2	4.70e-2	5.84e-2	-1.32e-3	6.25e-4	-4.22e-4
0.0503	0.3450	6.89e-3	6.70e-3	0.3451	-6.40e-4	3.69e-3	5.62e-2	3.65e-2	4.84e-2	-5.17e-4	-2.41e-5	-2.04e-4
0.0377	0.3299	8.59e-3	6.87e-3	0.3301	-5.16e-5	3.99e-3	4.78e-2	3.07e-2	4.46e-2	-2.97e-4	1.20e-5	-1.26e-4
0.0173	0.3112	1.13e-2	5.34e-3	0.3114	4.59e-4	2.62e-3	4.01e-2	2.33e-2	3.91e-2	-1.38e-4	-7.78e-5	-3.02e-5
0.0079	0.3069	1.39e-2	7.81e-3	0.3073	5.14e-4	5.13e-3	3.83e-2	2.13e-2	3.81e-2	-1.62e-4	-1.20e-4	3.57e-5

Profile 3

	Raw Velocities			Corrected Velocities			RMS Velocity Fluctuations			Reynolds Stresses		
y (m)	$\bar{u}$ (m/s)	$\bar{v}$ (m/s)	$\bar{w}$ (m/s)	$\bar{u}$ (m/s)	$\bar{v}$ (m/s)	$\bar{w}$ (m/s)	u_{rms} (m/s)	v_{rms} (m/s)	w_{rms} (m/s)	$\overline{u'v'}$ (m^2/s^2)	$\overline{u'w'}$ (m^2/s^2)	$\overline{v'w'}$ (m^2/s^2)
0.1267	0.5909	-8.84e-3	7.18e-5	0.5910	-1.11e-3	7.18e-5	0.1199	5.87e-2	8.97e-2	-3.90e-3	-4.79e-4	-3.79e-4
0.1195	0.5703	-1.39e-2	-9.93e-3	0.5705	1.01e-3	-9.93e-3	0.1237	5.95e-2	7.32e-2	-3.59e-3	-6.21e-4	-7.77e-4
0.1103	0.4765	-5.39e-3	-5.81e-3	0.4766	8.52e-4	-5.81e-3	0.1387	6.50e-2	9.10e-2	-3.12e-3	-3.52e-3	-9.71e-4
0.0996	0.4310	-6.23e-4	1.25e-3	0.4310	-6.23e-4	1.25e-3	0.1340	5.80e-2	9.61e-2	-1.63e-3	-3.48e-3	-2.76e-4
0.0798	0.3942	-9.65e-4	-2.72e-3	0.3943	7.56e-4	-2.72e-3	9.79e-2	4.90e-2	8.19e-2	-1.40e-3	-1.64e-3	-5.41e-5
0.0657	0.3855	-1.87e-3	-4.32e-3	0.3855	-1.84e-4	-4.32e-3	8.48e-2	4.42e-2	7.36e-2	-1.04e-3	-1.37e-3	1.27e-4
0.0498	0.3621	-1.97e-3	-3.70e-3	0.3621	-3.90e-4	-3.70e-3	7.56e-2	4.00e-2	6.46e-2	-9.00e-4	-1.11e-3	1.41e-4
0.0376	0.3453	9.51e-4	-6.50e-3	0.3453	-6.50e-3	6.78e-2	6.78e-2	3.66e-2	6.39e-2	-7.62e-4	-9.75e-4	1.79e-4
0.0176	0.3102	-3.94e-3	-5.79e-3	0.3102	1.23e-4	-5.79e-3	6.24e-2	3.19e-2	6.49e-2	-3.86e-4	-8.85e-4	7.18e-5
0.0076	0.2955	-3.21e-3	-4.95e-3	0.2955	-6.33e-4	-4.95e-3	5.77e-2	2.95e-2	6.46e-2	-2.84e-4	-8.91e-4	1.57e-4

Profile 4

	Raw Velocities			Corrected Velocities			RMS Velocity Fluctuations			Reynolds Stresses		
y (m)	$\bar{u}$ (m/s)	$\bar{v}$ (m/s)	$\bar{w}$ (m/s)	$\bar{u}$ (m/s)	$\bar{v}$ (m/s)	$\bar{w}$ (m/s)	u_{rms} (m/s)	v_{rms} (m/s)	w_{rms} (m/s)	$\overline{u'v'}$ (m^2/s^2)	$\overline{u'w'}$ (m^2/s^2)	$\overline{v'w'}$ (m^2/s^2)
0.1224	0.6027	-4.36e-3	1.20e-2	0.6028	8.96e-4	1.53e-3	0.1243	5.91e-2	8.13e-2	-4.03e-3	-5.75e-4	7.10e-4
0.1202	0.5975	-4.34e-3	1.01e-2	0.5976	8.81e-4	-3.45e-4	0.1277	5.92e-2	7.75e-2	-4.20e-3	-9.24e-4	7.86e-4
0.1097	0.5615	-9.54e-3	6.65e-3	0.5616	2.56e-4	-3.15e-3	0.1249	6.21e-2	8.32e-2	-4.45e-3	-1.28e-4	1.02e-3
0.0995	0.4971	-7.37e-3	7.89e-3	0.4972	-8.62e-4	-7.82e-4	0.1098	6.23e-2	8.55e-2	-3.35e-3	1.56e-4	6.90e-4
0.0803	0.4395	-4.47e-3	5.21e-3	0.4395	-6.34e-4	-2.46e-3	9.03e-2	5.18e-2	6.81e-2	-1.81e-3	1.04e-3	-6.43e-5
0.0651	0.4134	-4.34e-3	1.65e-3	0.4134	-7.28e-4	-5.57e-3	7.89e-2	4.48e-2	6.23e-2	-1.53e-3	9.15e-4	-1.44e-4
0.0504	0.3808	-4.65e-3	1.39e-3	0.3808	3.35e-4	-5.26e-3	6.82e-2	3.85e-2	5.46e-2	-8.94e-4	6.22e-4	-7.45e-5
0.0371	0.3445	-6.23e-3	1.45e-3	0.34445	-2.22e-4	-4.56e-3	5.88e-2	3.20e-2	5.30e-2	-4.32e-4	2.88e-4	3.86e-5
0.0174	0.3339	-4.98e-4	8.79e-4	0.3338	-4.98e-4	-4.95e-3	4.81e-2	2.76e-2	4.33e-2	-2.12e-4	4.12e-4	-2.70e-6
0.0069	0.3277	-5.32e-4	1.52e-3	0.3276	-5.32e-4	-4.20e-3	4.45e-2	2.39e-2	4.35e-2	-1.10e-4	3.91e-4	-2.25e-5

Experiment 6 Laboratory Measurements

H = 0.267 m S = 0.0036 Q = 178 L/s $a = 0.273\ m^{-1}$ T = 26.3 °C $h_p = 0.1175$ m

Profile 1

	Raw Velocities			Corrected Velocities			RMS Velocity Fluctuations			Reynolds Stresses		
y (m)	$\bar{u}$ (m/s)	$\bar{v}$ (m/s)	$\bar{w}$ (m/s)	$\bar{u}$ (m/s)	$\bar{v}$ (m/s)	$\bar{w}$ (m/s)	u_{rms} (m/s)	v_{rms} (m/s)	w_{rms} (m/s)	$\overline{u'v'}$ (m^2/s^2)	$\overline{u'w'}$ (m^2/s^2)	$\overline{v'w'}$ (m^2/s^2)
0.1799	0.7430	1.82e-2	1.43e-2	0.7434	-1.29e-3	1.31e-3	0.1087	6.09e-2	7.97e-2	-2.43e-2	-8.00e-4	1.37e-5
0.1594	0.6840	2.29e-2	8.33e-3	0.6844	-9.64e-4	-3.61e-3	0.1064	6.15e-2	6.97e-2	-2.70e-3	3.13e-5	-2.36e-4
0.1396	0.6658	2.17e-2	4.06e-3	0.6661	1.36e-3	-7.56e-3	0.1081	6.12e-2	7.11e-2	-3.13e-3	-4.81e-4	-3.81e-4
0.1204	0.6116	2.69e-2	4.88e-3	0.6121	2.24e-4	-5.80e-3	0.1015	5.68e-2	6.69e-2	-2.47e-3	-1.61e-3	-7.44e-5
0.1047	0.5936	1.71e-2	7.05e-3	0.5939	-1.08e-3	-3.31e-3	0.1038	5.23e-2	6.88e-2	-2.20e-3	-1.48e-3	-5.97e-5
0.0897	0.5588	1.08e-2	2.84e-3	0.5588	1.07e-3	-6.91e-3	9.92e-2	5.07e-2	6.56e-2	-2.38e-3	-1.03e-3	2.14e-5
0.0697	0.5271	7.08e-3	-3.03e-3	0.5270	1.84e-4	-1.22e-2	8.76e-2	4.86e-2	6.08e-2	-1.88e-3	-4.21e-4	-8.48e-5
0.0497	0.4849	9.91e-3	-3.95e-3	0.4849	7.45e-4	-1.24e-2	7.35e-2	4.06e-2	5.31e-2	-9.99e-4	-5.79e-5	-5.67e-5
0.0097	0.4256	6.07e-4	-6.38e-3	0.4254	6.07e-4	-1.38e-2	6.48e-2	2.57e-2	4.44e-2	-4.72e-4	-6.45e-5	-7.63e-5

Profile 2

	Raw Velocities			Corrected Velocities			RMS Velocity Fluctuations			Reynolds Stresses		
y (m)	$\bar{u}$ (m/s)	$\bar{v}$ (m/s)	$\bar{w}$ (m/s)	$\bar{u}$ (m/s)	$\bar{v}$ (m/s)	$\bar{w}$ (m/s)	u_{rms} (m/s)	v_{rms} (m/s)	w_{rms} (m/s)	$\overline{u'v'}$ (m^2/s^2)	$\overline{u'w'}$ (m^2/s^2)	$\overline{v'w'}$ (m^2/s^2)
0.1786	0.7081	1.07e-2	-5.76e-3	0.7082	1.41e-3	4.15e-4	0.1090	5.78e-2	8.44e-2	-2.55e-3	-1.07e-3	3.39e-4
0.1599	0.6918	1.43e-2	-1.03e-3	0.6920	-7.70e-4	5.00e-3	0.1075	6.06e-2	6.97e-2	-2.90e-3	-3.12e-4	6.65e-5
0.1402	0.6212	2.03e-2	-4.54e-3	0.6215	1.34e-3	8.81e-4	0.1095	5.87e-2	6.40e-2	-3.14e-3	1.21e-4	1.50e-4
0.1196	0.5730	2.35e-2	-5.14e-3	0.5735	1.00e-3	-1.43e-4	0.1019	5.55e-2	6.35e-2	-2.82e-3	5.11e-4	-2.19e-4
0.1045	0.5498	2.25e-2	-4.26e-3	0.5503	9.39e-4	5.34e-4	9.63e-2	5.53e-2	6.09e-2-	-2.94e-3	3.76e-4	-2.47e-4
0.0903	0.5144	2.08e-2	6.99e-5	0.5148	5.41e-4	4.56e-3	8.36e-2	5.06e-2	5.67e-2	-2.07e-3	2.91e-4	-2.50e-4
0.0713	0.4833	2.15e-2	6.42e-3	0.4837	3.79e-4	1.06e-2	6.87e-2	4.36e-2	5.33e-2	-1.08e-3	-1.68e-4	-2.91e-4
0.0503	0.4637	1.90e-2	4.21e-3	0.4640	7.32e-4	8.26e-3	6.02e-2	3.70e-2	4.88e-2	-5.88e-4	-3.60e-4	-1.43e-4
0.0098	0.4318	8.05e-3	1.07e-2	0.4317	5.11e-4	1.45e-2	5.59e-2	2.22e-2	4.46e-2	-3.77e-4	-2.23e-4	1.18e-4

Profile 3

	Raw Velocities			Corrected Velocities			RMS Velocity Fluctuations			Reynolds Stresses		
y (m)	$\bar{u}$ (m/s)	$\bar{v}$ (m/s)	$\bar{w}$ (m/s)	$\bar{u}$ (m/s)	$\bar{v}$ (m/s)	$\bar{w}$ (m/s)	u_{rms} (m/s)	v_{rms} (m/s)	w_{rms} (m/s)	$\overline{u'v'}$ (m^2/s^2)	$\overline{u'w'}$ (m^2/s^2)	$\overline{v'w'}$ (m^2/s^2)
0.1780	0.7004	1.81e-2	-2.49e-3	0.7007	-2.24e-4	-2.49e-3	9.91e-2	5.89e-2	6.47e-2	-2.26e-3	4.21e-4	-8.87e-5
0.1597	0.6650	1.59e-2	-5.17e-3	0.6652	1.35e-3	-5.17e-3	0.1113	5.78e-2	6.47e-2	-3.16e-3	7.02e-5	-1.16e-4
0.1400	0.6202	1.58e-2	-6.13e-3	0.6205	-4.73e-4	-6.13e-3	0.1075	5.71e-2	6.61e-2	-3.29e-3	1.86e-4	-2.24e-4
0.1197	0.5491	1.82e-2	-9.68e-4	0.5494	-9.71e-4	-9.68e-4	0.1093	5.69e-2	6.49e-2	-3.24e-3	-4.17e-4	-2.62e-4
0.1050	0.5140	2.06e-2	-1.21e-3	0.5144	3.86e-4	-1.21e-3	9.26e-2	5.75e-2	6.27e-2	-2.46e-3	-1.03e-3	-1.40e-4
0.0899	0.4938	2.57e-2	-1.71e-4	0.4944	-1.64e-4	-1.71e-4	7.99e-2	5.03e-2	5.97e-2	-1.17e-3	-9.35e-4	9.56e-5
0.0696	0.4895	2.27e-2	-2.69e-3	0.4900	-7.83e-4	-2.69e-3	7.74e-2	4.62e-2	5.18e-2	-1.29e-3	-8.08e-4	2.26e-4
0.0505	0.4702	2.18e-2	-3.26e-3	0.4707	-7.46e-4	-3.26e-3	6.69e-2	3.88e-2	4.66e-2	-9.10e-4	-7.11e-4	2.09e-4
0.0094	0.4342	9.99e-3	-1.01e-2	0.4343	5.16e-4	-1.01e-2	5.65e-2	2.68e-2	4.50e-2	-5.39e-4	-3.77e-4	2.61e-4

Profile 4

	Raw Velocities			Corrected Velocities			RMS Velocity Fluctuations			Reynolds Stresses		
y (m)	$\bar{u}$ (m/s)	$\bar{v}$ (m/s)	$\bar{w}$ (m/s)	$\bar{u}$ (m/s)	$\bar{v}$ (m/s)	$\bar{w}$ (m/s)	u_{rms} (m/s)	v_{rms} (m/s)	w_{rms} (m/s)	$\overline{u'v'}$ (m^2/s^2)	$\overline{u'w'}$ (m^2/s^2)	$\overline{v'w'}$ (m^2/s^2)
0.1773	0.7473	4.86e-3	1.50e-2	0.7475	1.60e-3	1.99e-3	9.39e-2	5.64e-2	6.54e-2	-1.64e-3	-9.32e-4	-3.33e-4
0.1594	0.7508	3.69e-3	1.90e-2	0.7510	4.11e-4	5.93e-3	0.1028	5.92e-2	6.79e-2	-2.15e-3	-8.37e-4	-3.82e-4
0.1401	0.7057	7.83e-3	1.52e-2	0.7059	-1.41e-3	2.93e-3	0.1000	5.61e-2	6.91e-2	-2.06e-3	-1.00e-3	-6.29e-4
0.1205	0.6901	4.02e-3	1.11e-2	0.6902	1.01e-3	-9.26e-4	0.1049	5.79e-2	6.88e-2	-2.59e-3	-9.43e-4	-5.78e-4
0.1047	0.6527	4.10e-3	1.01e-2	0.6528	1.25e-3	-1.28e-3	0.1085	5.58e-2	6.64e-2	-2.75e-3	-1.45e-3	-3.57e-4
0.0904	0.6235	1.64e-2	1.56e-2	0.6239	5.60e-5	4.68e-3	9.72e-2	5.50e-2	5.98e-2	-2.42e-3	-8.24e-4	-3.40e-4
0.0701	0.5765	1.20e-2	-3.03e-3	0.5762	-5.90e-4	-1.31e-2	8.94e-2	4.96e-2	6.07e-2	-1.88e-3	5.77e-5	-2.80e-4
0.0494	0.5510	2.03e-5	-1.86e-2	0.5505	2.03e-5	-2.82e-2	8.34e-2	4.00e-2	5.91e-2	-1.22e-3	2.64e-3	6.12e-5
0.0096	0.4975	-7.26e-3	-7.33e-3	0.4973	-7.44e-4	-1.60e-2	7.20e-2	2.72e-2	4.76e-2	-6.47e-4	2.23e-4	4.74e-5

Experiment 7 Laboratory Measurements

H = 0.183 m S = 0.0036 Q = 95 L/s a = 0.273 m^{-1} T = 26.6 °C h_p = 0.1175 m

Profile 1

	Raw Velocities			Corrected Velocities			RMS Velocity Fluctuations			Reynolds Stresses		
y (m)	$\bar{u}$ (m/s)	$\bar{v}$ (m/s)	$\bar{w}$ (m/s)	$\bar{u}$ (m/s)	$\bar{v}$ (m/s)	$\bar{w}$ (m/s)	u_{rms} (m/s)	v_{rms} (m/s)	w_{rms} (m/s)	$\overline{u'v'}$ (m^2/s^2)	$\overline{u'w'}$ (m^2/s^2)	$\overline{v'w'}$ (m^2/s^2)
0.1169	0.6080	-6.06e-3	2.55e-2	0.6086	-7.50e-4	-1.03e-3	8.10e-2	3.62e-2	4.74e-2	-1.57e-3	-2.98e-4	1.28e-4
0.1046	0.5785	-1.03e-2	3.00e-2	0.5794	-1.83e-4	4.78e-3	7.41e-2	3.63e-2	4.78e-2	-1.38e-3	-5.13e-4	1.40e-4
0.0949	0.5749	-1.66e-2	3.96e-2	0.5763	9.41e-4	1.44e-2	7.42e-2	3.59e-2	5.03e-2	-1.39e-3	-5.55e-4	3.61e-4
0.0846	0.5442	-2.33e-2	3.87e-2	0.5459	4.79e-4	1.49e-2	8.23e-2	4.01e-2	5.54e-2	-1.52e-3	-3.05e-4	6.75e-4
0.0702	0.4785	-1.91e-2	1.33e-2	0.4791	-3.11e-4	-7.59e-3	8.85e-2	4.53e-2	6.30e-2	-8.60e-4	1.14e-3	8.52e-4
0.0599	0.4480	1.13e-2	1.13e-2	0.4482	2.61e-4	-8.20e-3	7.46e-2	3.86e-2	5.73e-2	-2.05e-4	1.11e-3	3.47e-4
0.0494	0.4475	-4.56e-3	1.48e-2	0.4477	-6.53e-4	-4.76e-3	6.88e-2	3.42e-2	5.16e-2	-4.84e-4	9.49e-4	7.81e-5
0.0377	0.4457	-6.41e-3	2.02e-2	0.4462	-5.79e-4	7.17e-4	6.33e-2	3.18e-2	4.73e-2	-6.18e-4	7.74e-4	-2.88e-5
0.1780	0.4201	-7.30e-3	2.43e-2	0.4208	3.12e-5	5.94e-3	6.17e-2	2.87e-2	4.34e-2	-5.45e-4	6.13e-4	-1.28e-4
0.0077	0.4048	-5.51e-3	2.56e-2	0.4056	-2.11e-4	7.94e-3	5.58e-2	2.60e-2	3.95e-2	-5.56e-4	5.66e-4	-1.61e-4

Profile 2

	Raw Velocities			Corrected Velocities			RMS Velocity Fluctuations			Reynolds Stresses		
y (m)	$\bar{u}$ (m/s)	$\bar{v}$ (m/s)	$\bar{w}$ (m/s)	$\bar{u}$ (m/s)	$\bar{v}$ (m/s)	$\bar{w}$ (m/s)	u_{rms} (m/s)	v_{rms} (m/s)	w_{rms} (m/s)	$\overline{u'v'}$ (m^2/s^2)	$\overline{u'w'}$ (m^2/s^2)	$\overline{v'w'}$ (m^2/s^2)
0.1145	0.5597	-9.08e-3	2.21e-2	0.5602	6.86e-4	-2.31e-3	9.39e-2	4.33e-2	5.94e-2	-2.14e-3	4.67e-4	3.74e-4
0.1049	0.5172	-6.92e-3	1.75e-2	0.5175	-1.54e-4	-5.03e-3	8.89e-2	4.72e-2	5.35e-2	-2.10e-3	8.33e-4	1.96e-4
0.0948	0.4979	1.63e-4	1.53e-2	0.4981	1.63e-4	-6.44e-3	7.89e-2	4.81e-2	5.36e-2	-1.50e-3	1.06e-3	1.07e-4
0.0847	0.4819	9.50e-3	1.94e-2	0.4824	-1.01e-3	-1.62e-3	6.83e-2	4.04e-2	4.90e-2	-5.31e-4	1.09e-3	1.84e-5
0.0705	0.4829	1.51e-2	2.45e-2	0.4837	3.40e-4	3.45e-3	6.39e-2	3.55e-2	4.56e-2	-6.14e-4	9.64e-4	-1.49e-4
0.0605	0.4771	1.35e-2	2.62e-2	0.4779	1.01e-3	5.34e-3	5.77e-2	3.27e-2	4.39e-2	-5.64e-4	7.55e-4	-1.94e-4
0.0509	0.4645	1.41e-2	2.51e-2	0.4654	-1.20e-4	4.82e-3	5.66e-2	3.09e-2	4.24e-2	-6.76e-4	6.82e-4	-1.71e-4
0.0377	0.4540	1.26e-2	2.40e-2	0.4548	7.08e-4	4.16e-3	5.47e-2	2.91e-2	3.97e-2	-6.68e-4	5.55e-4	-1.85e-4
0.0177	0.4317	1.16e-2	2.34e-2	0.4325	3.45e-4	4.52e-3	5.37e-2	2.70e-2	4.00e-2	-6.02e-4	5.04e-4	-1.82e-4
0.0071	0.4131	1.37e-2	2.49e-2	0.4140	-7.41e-4	6.88e-3	4.86e-2	2.30e-2	3.51e-2	-4.42e-4	3.98e-4	-1.40e-4

Profile 3

	Raw Velocities			Corrected Velocities			RMS Velocity Fluctuations			Reynolds Stresses		
y (m)	$\bar{u}$ (m/s)	$\bar{v}$ (m/s)	$\bar{w}$ (m/s)	$\bar{u}$ (m/s)	$\bar{v}$ (m/s)	$\bar{w}$ (m/s)	u_{rms} (m/s)	v_{rms} (m/s)	w_{rms} (m/s)	$\overline{u'v'}$ (m^2/s^2)	$\overline{u'w'}$ (m^2/s^2)	$\overline{v'w'}$ (m^2/s^2)
0.1140	0.5719	-5.43e-3	1.38e-2	0.5721	-4.37e-4	-1.14e-3	8.34e-2	4.08e-2	5.61e-2	-1.91e-3	-2.85e-5	-8.46e-5
0.1048	0.5432	-6.12e-3	1.36e-2	0.5434	9.90e-4	-6.54e-4	7.68e-2	4.28e-2	5.15e-2	-1.69e-3	1.92e-4	-1.83e-4
0.0947	0.5217	-6.01e-3	1.76e-2	0.5220	8.15e-4	3.96e-3	6.69e-2	4.19e-2	5.03e-2	-1.27e-3	-2.25e-6	-5.40e-5
0.0853	0.5030	2.72e-3	1.59e-2	0.5033	5.23e-4	2.74e-3	5.77e-2	3.88e-2	4.94e-2	-6.62e-4	5.72e-6	-4.56e-5
0.0701	0.4966	2.62e-3	1.27e-2	0.4967	4.58e-4	-3.14e-4	5.46e-2	3.34e-2	4.23e-2	-5.19e-4	-2.71e-4	7.17e-5
0.0600	0.4915	3.45e-3	1.23e-2	0.4916	-8.42e-4	-5.67e-4	5.13e-2	3.01e-2	4.01e-2	-4.56e-4	-2.16e-4	5.75e-5
0.0494	0.4838	4.62e-3	9.37e-3	0.4839	3.97e-4	-3.30e-3	5.15e-2	2.82e-2	3.86e-2	-4.81e-4	-2.35e-4	1.15e-4
0.0369	0.4667	5.22e-3	7.36e-3	0.4668	-8.91e-4	-4.86e-3	4.81e-2	2.61e-2	3.60e-2	-4.11e-4	-2.00e-4	8.85e-5
0.0172	0.4373	2.61e-3	5.01e-3	0.4373	7.01e-4	-6.44e-3	4.86e-2	2.21e-2	3.76e-2	-3.26e-4	-1.30e-4	9.42e-5
0.0078	0.4268	2.89e-3	3.46e-3	0.4268	-8.31e-4	-7.72e-3	4.73e-2	2.04e-2	3.27e-2	-3.45e-4	-2.96e-4	1.39e-4

Profile 4

	Raw Velocities			Corrected Velocities			RMS Velocity Fluctuations			Reynolds Stresses		
y (m)	$\bar{u}$ (m/s)	$\bar{v}$ (m/s)	$\bar{w}$ (m/s)	$\bar{u}$ (m/s)	$\bar{v}$ (m/s)	$\bar{w}$ (m/s)	u_{rms} (m/s)	v_{rms} (m/s)	w_{rms} (m/s)	$\overline{u'v'}$ (m^2/s^2)	$\overline{u'w'}$ (m^2/s^2)	$\overline{v'w'}$ (m^2/s^2)
0.1134	0.6058	-8.71e-3	3.14e-2	0.6067	-7.80e-4	-3.93e-4	7.71e-2	3.69e-2	5.43e-2	-1.38e-3	-9.31e-4	1.26e-4
0.1053	0.5840	-1.06e-2	2.92e-2	0.5848	-3.59e-4	-1.41e-3	7.17e-2	3.64e-2	4.83e-2	-1.26e-3	-6.35e-4	4.42e-5
0.0948	0.5721	-1.09e-2	2.72e-2	0.5729	-9.18e-4	-2.76e-3	7.04e-2	3.76e-2	4.75e-2	-1.31e-3	-5.92e-4	1.07e-4
0.0850	0.5535	-9.83e-3	2.66e-2	0.5542	-1.66e-4	-2.42e-3	6.79e-2	3.62e-2	4.74e-2	-1.09e-3	-5.86e-4	8.34e-5
0.0702	0.5290	-5.34e-3	2.20e-2	0.5294	-7.26e-4	-5.74e-3	5.94e-2	3.29e-2	4.35e-2	-6.78e-4	-5.57e-4	1.30e-5
0.0604	0.5166	4.24e-3	1.77e-2	0.5169	2.66e-4	-9.37e-3	5.65e-2	2.92e-2	4.12e-2	-5.44e-4	-4.79e-4	-3.63e-5
0.0497	0.5009	-4.83e-3	1.40e-2	0.5010	-4.57e-4	-1.22e-2	5.53e-2	2.70e-2	3.89e-2	-5.31e-4	-5.92e-4	5.53e-5
0.0376	0.4854	-4.58e-3	1.26e-2	0.4854	-3.47e-4	-1.29e-2	5.36e-2	2.55e-2	3.73e-2	-4.67e-4	-5.60e-4	5.45e-5
0.0177	0.4634	-3.15e-3	1.36e-2	0.4635	8.99e-4	-1.06e-2	5.07e-2	2.18e-2	3.52e-2	-3.72e-4	-5.03e-4	8.70e-5
0.0070	0.4528	-3.28e-3	1.24e-2	0.4529	6.72e-4	-1.13e-2	4.90e-2	1.91e-2	3.45e-2	-2.79e-4	-4.65e-4	4.81e-5

Experiment 8 Laboratory Measurements

H = 0.391 m S = 0.0036 Q = 180 L/s $a = 2.46\ m^{-1}$ T = 27.0 °C $h_p = 0.1175$ m

Profile 1

	Raw Velocities			Corrected Velocities			RMS Velocity Fluctuations			Reynolds Stresses		
y (m)	$\bar{u}$ (m/s)	$\bar{v}$ (m/s)	$\bar{w}$ (m/s)	$\bar{u}$ (m/s)	$\bar{v}$ (m/s)	$\bar{w}$ (m/s)	u_{rms} (m/s)	v_{rms} (m/s)	w_{rms} (m/s)	$\overline{u'v'}$ (m^2/s^2)	$\overline{u'w'}$ (m^2/s^2)	$\overline{v'w'}$ (m^2/s^2)
0.3199	0.7810	-2.35e-3	6.20e-2	0.7835	1.05e-3	5.47e-4	7.26e-2	4.39e-2	5.67e-2	-4.57e-4	-4.72e-4	-1.02e-4
0.2798	0.7680	-7.57e-3	5.56e-2	0.7701	-8.69e-4	-4.83e-3	8.30e-2	5.70e-2	6.56e-2	-1.06e-3	-7.92e-4	-3.60e-4
0.2399	0.7509	-7.50e-3	5.38e-2	0.7529	-9.51e-4	-5.28e-3	9.67e-2	6.50e-2	7.63e-2	-1.69e-3	-7.91e-4	-5.09e-4
0.1998	0.6854	-8.51e-3	4.20e-2	0.6867	4.65e-4	-1.19e-2	0.1248	7.57e-2	8.93e-2	-3.92e-3	-5.73e-4	-3.72e-4
0.1596	0.5959	-7.88e-3	3.31e-2	0.5968	-7.41e-5	-1.37e-2	0.1392	8.04e-2	0.1032	-5.02e-3	-1.27e-3	-3.29e-4
0.1197	0.4539	-1.13e-2	2.94e-2	0.4549	5.69e-4	-6.29e-3	0.1497	8.30e-2	0.1066	-7.25e-3	5.87e-4	6.47e-4
0.0898	0.3162	-6.62e-3	2.42e-2	0.3172	2.79e-4	-6.90e-4	0.1124	7.11e-2	8.87e-2	-3.68e-3	2.49e-3	-4.82e-4
0.0599	0.2382	-2.12e-3	1.89e-2	0.2389	-4.33e-5	2.03e-4	8.05e-2	5.48e-2	7.67e-2	-1.76e-3	1.36e-3	-2.25e-4
0.0352	0.2027	-9.40e-3	1.99e-2	0.2038	3.31e-4	3.89e-3	6.48e-2	3.76e-2	6.99e-2	-5.88e4	7.65e-4	-2.21e-4
0.0097	0.1734	-1.78e-3	1.11e-2	0.1737	-2.64e-4	-2.56e-3	5.24e-2	2.64r-2	5.36e-2	-2.17e-4	6.37e-4	-9.25e-5

Profile 2

	Raw Velocities			Corrected Velocities			RMS Velocity Fluctuations			Reynolds Stresses		
y (m)	$\bar{u}$ (m/s)	$\bar{v}$ (m/s)	$\bar{w}$ (m/s)	$\bar{u}$ (m/s)	$\bar{v}$ (m/s)	$\bar{w}$ (m/s)	u_{rms} (m/s)	v_{rms} (m/s)	w_{rms} (m/s)	$\overline{u'v'}$ (m^2/s^2)	$\overline{u'w'}$ (m^2/s^2)	$\overline{v'w'}$ (m^2/s^2)
0.3193	0.7059	4.60e-3	6.57e-2	0.7090	1.52e-3	-2.22e-3	8.75e-2	5.55e-2	6.88e-2	-6.51e-4	-1.37e-3	-4.89e-4
0.2800	0.6687	8.54e-3	6.07e-2	0.6715	-2.18e-4	-3.72e-3	0.1029	6.69e-2	7.91e-2	-1.72e-3	-1.78e-3	-6.37e-4
0.2394	0.6419	9.78e-3	4.72e-2	0.6435	1.38e-3	-1.45e-2	0.1151	7.41e-2	8.84e-2	-2.75e-3	-1.88e-3	-6.82e-4
0.1997	0.5983	7.87e-3	3.83e-2	0.5992	4.01e-5	-1.92e-2	0.1324	7.68e-2	9.23e-2	-3.82e-3	-1.56e-3	-5.60e-4
0.1599	0.5206	4.56e-3	3.10e-2	0.5211	1.24e-5	-1.91e-2	0.1308	8.34e-2	0.1012	-5.13e-3	-1.38e-3	-5.26e-4
0.1202	0.4209	-5.34e-3	9.52e-3	0.4199	1.74e-4	-3.09e-2	0.1460	8.65e-2	0.1025	-7.73e-3	1.69e-4	-6.06e-4
0.0898	0.3308	-7.90e-3	3.32e-3	0.3297	-6.86e-4	-2.84e-2	0.1221	7.89e-2	9.71e-2	-5.28e-3	1.08e-4	-4.46e-4
0.0605	0.2701	-8.96e-3	-8.03e-4	0.2689	4.67e-4	-2.67e-2	0.1005	6.34e-2	8.50e-2	-3.09e-3	8.32e-4	-4.00e-4
0.0359	0.2239	-1.14e-2	-4.57e-3	0.2227	3.74e-4	-2.60e-2	7.75e-2	4.79e-2	7.44e-2	-1.54e-3	4.00e-4	-3.30e-4
0.0106	0.1843	-2.68e-3	-8.21e-3	0.1827	-2.64e-4	-2.58e-2	6.00e-2	3.06e-2	6.28e-2	-5.60e-4	-1.92e-4	1.13e-4

Profile 3

	Raw Velocities			Corrected Velocities			RMS Velocity Fluctuations			Reynolds Stresses		
y (m)	$\bar{u}$ (m/s)	$\bar{v}$ (m/s)	$\bar{w}$ (m/s)	$\bar{u}$ (m/s)	$\bar{v}$ (m/s)	$\bar{w}$ (m/s)	u_{rms} (m/s)	v_{rms} (m/s)	w_{rms} (m/s)	$\overline{u'v'}$ (m^2/s^2)	$\overline{u'w'}$ (m^2/s^2)	$\overline{v'w'}$ (m^2/s^2)
0.3188	0.7999	-4.44e-3	5.40e-2	0.8018	-9.49e-4	-1.89e-3	7.66e-2	9.55e-2	5.05e-2	-3.93e-4	-5.08e-5	9.12e-5
0.2793	0.7884	-4.53e-3	5.25e-2	0.7902	-1.09e-3	-2.58e-3	9.31e-2	6.30e-2	7.13e-2	-1.52e-3	-2.05e-4	1.48e-4
0.2399	0.7414	-2.95e-3	4.78e-2	0.7429	2.80e-4	-4.06e-3	0.1179	7.19e-2	8.82e-2	-2.11e-3	-4.98e-4	-3.95e-5
0.2006	0.6945	-7.30e-3	4.48e-2	0.6960	-1.24e-3	-3.79e-3	0.1305	7.63e-2	9.81e-2	-3.46e-3	-2.88e-4	-2.97e-4
0.1601	0.6041	-4.81e-3	4.06e-2	0.6054	4.60e-4	-1.68e-3	0.1491	8.44e-2	0.1030	-6.07e-3	-6.75e-4	6.59e-5
0.4464	0.4464	-6.21e-3	2.95e-2	0.4474	-3.65e-4	-1.73e-3	0.1506	8.00e-2	0.1000	-6.98e-3	-2.19e-4	2.92e-4
0.0896	0.3141	-3.03e-2	1.46e-2	0.3158	-4.76e-5	-7.40e-3	0.1264	7.58e-2	0.1084	-5.44e-3	7.69e-4	2.84e-4
0.0599	0.2295	-6.72e-3	1.14e-2	0.2298	2.91e-4	-4.61e-3	7.88e-2	5.86e-2	8.42e-2	-1.37e-3	3.91e-5	3.64e-4
0.0354	0.2012	-7.32e-3	4.65e-3	0.2012	-2.98e-4	9.40e-3	6.62e-2	4.28e-2	7.11e-2	-6.62e-4	-6.21e-4	2.05e-4
0.0105	0.1767	4.95e-4	5.03e-3	0.1766	-2.76e-4	-7.30e-3	5.30e-2	2.65e-2	5.85e-2	-2.04e-4	-3.60e-4	1.55e-4

Profile 4

	Raw Velocities			Corrected Velocities			RMS Velocity Fluctuations			Reynolds Stresses		
y (m)	$\bar{u}$ (m/s)	$\bar{v}$ (m/s)	$\bar{w}$ (m/s)	$\bar{u}$ (m/s)	$\bar{v}$ (m/s)	$\bar{w}$ (m/s)	u_{rms} (m/s)	v_{rms} (m/s)	w_{rms} (m/s)	$\overline{u'v'}$ (m^2/s^2)	$\overline{u'w'}$ (m^2/s^2)	$\overline{v'w'}$ (m^2/s^2)
0.3173	0.7543	4.20e-3	6.02e-2	0.7567	9.08e-4	8.51e-4	10.00e-2	5.86e-2	7.16e-2	-1.02e-3	-1.26e-3	-3.39e-4
0.2802	0.7403	1.49e-3	6.04e-2	0.7427	1.49e-3	2.09e-3	0.1095	6.76e-2	7.66e-2	-1.98e-3	-1.73e-3	-4.13e-5
0.2396	0.6983	1.44e-3	5.23e-2	0.7002	1.44e-3	-2.63e-2	0.1265	7.34e-2	8.90e-2	-2.81e-3	-1.96e-3	-2.53e-4
0.2006	0.6724	-3.09e-3	4.65e-2	0.6740	-1.59e-4	-6.38e-3	0.1394	7.62e-2	9.74e-2	-3.60e-3	-1.32e-3	-5.59e-4
0.1593	0.5877	-9.53e-3	4.57e-2	0.5896	7.33e-4	-5.25e-4	0.1448	8.09e-2	0.1083	-5.09e-3	-1.09e-3	-7.61e-4
0.1203	0.4400	-5.97e-3	3.44e-2	0.4414	-2.05e-4	-2.40e-4	0.1539	7.97e-2	9.65e-2	-6.90e-3	-3.29e-4	-3.99e-4
0.0902	0.3354	-8.90e-3	2.81e-2	0.3367	-1.16e-4	1.73e-3	0.1215	7.22e-2	8.61e-2	-4.74e-3	7.49e-5	-1.95e-4
0.0596	0.2614	-5.26e-3	1.65e-2	0.2620	4.46e-4	-4.02e-3	9.61e-2	5.51e-2	7.41e-2	-2.37e-3	7.33e-4	4.79e-5
0.0353	0.2128	-8.53e-3	2.21e-2	0.2141	-1.72e-4	5.33e-3	7.80e-2	4.17e-2	6.43e-2	-1.13e-3	1.06e-3	-1.87e-4
0.0100	0.1791	-1.35e-3	1.31e-2	0.1796	2.14e-4	-9.92e-4	6.68e-2	2.83e-2	6.02e-2	-5.60e-4	1.44e-3	-1.20e-4

Experiment 9 Laboratory Measurements

H = 0.214 m S = 0.0036 Q = 58 L/s $a = 2.46\ m^{-1}$ T = 27.1 °C $h_p = 0.1175$ m

Profile 1

	Raw Velocities			Corrected Velocities			RMS Velocity Fluctuations			Reynolds Stresses		
y (m)	$\bar{u}$ (m/s)	$\bar{v}$ (m/s)	$\bar{w}$ (m/s)	$\bar{u}$ (m/s)	$\bar{v}$ (m/s)	$\bar{w}$ (m/s)	u_{rms} (m/s)	v_{rms} (m/s)	w_{rms} (m/s)	$\overline{u'v'}$ (m^2/s^2)	$\overline{u'w'}$ (m^2/s^2)	$\overline{v'w'}$ (m^2/s^2)
0.1450	0.3138	6.46e-3	7.71e-3	0.3140	-3.90e-4	-5.11e-4	7.57e-2	4.41e-2	5.33e-2	-1.80e-3	-1.02e-5	-2.13e-5
0.1301	0.2843	8.38e-3	1.20e-2	0.2846	-3.10e-4	4.55e-3	7.82e-2	4.34e-2	4.88e-2	-1.95e-3	-2.42e-4	1.38e-5
0.1195	0.2528	7.06e-3	1.67e-2	0.2533	4.36e-4	1.01e-2	7.03e-2	4.30e-2	5.19e-2	-1.77e-3	-4.49e-4	-2.19e-5
0.1052	0.2231	-9.61e-4	2.51e-2	0.2237	1.28e-5	1.93e-2	6.82e-2	4.19e-2	4.40e-2	-1.70e-3	-4.60e-4	9.88e-5
0.0895	0.1947	-4.71e-3	2.30e-2	0.1953	3.83e-4	1.79e-2	6.29e-2	3.78e-2	4.95e-2	-9.81e-4	-2.56e-4	1.41e-4
0.0702	0.1669	4.13e-3	1.99e-2	0.1674	-2.38e-4	1.55e-2	4.52e-2	2.89e-2	4.17e-2	-5.36e-4	3.22e-4	6.11e-5
0.0497	0.1546	1.15e-3	1.70e-2	0.1550	-2.02e-4	1.29e-2	3.28e-2	2.11e-2	2.85e-2	-2.19e-4	-4.04e-6	5.22e-5
0.0349	0.1437	-3.97e-3	1.63e-2	0.1442	-2.02e-4	1.26e-2	4.27e-2	1.88e-2	4.17e-2	-1.09e-4	-3.33e-4	8.02e-5
0.0175	0.1408	-8.18e-4	1.87e-2	0.1412	-2.03e-4	1.50e-2	2.58e-2	1.43e-2	2.45e-2	-7.16e-5	-5.32e-5	2.12e-5
0.0076	0.1382	-3.84e-4	1.67e-2	0.1386	2.19e-4	1.31e-2	2.37e-2	1.23e-2	2.36e-2	-4.20e-5	-3.75e-5	2.23e-5

Profile 2

	Raw Velocities			Corrected Velocities			RMS Velocity Fluctuations			Reynolds Stresses		
y (m)	$\bar{u}$ (m/s)	$\bar{v}$ (m/s)	$\bar{w}$ (m/s)	$\bar{u}$ (m/s)	$\bar{v}$ (m/s)	$\bar{w}$ (m/s)	u_{rms} (m/s)	v_{rms} (m/s)	w_{rms} (m/s)	$\overline{u'v'}$ (m^2/s^2)	$\overline{u'w'}$ (m^2/s^2)	$\overline{v'w'}$ (m^2/s^2)
0.1446	0.3556	-4.23e-3	7.61e-3	0.3557	4.31e-4	1.40e-3	7.38e-2	4.26e-2	5.40e-2	-1.50e-3	2.79e-4	1.06e-4
0.1299	0.3337	-5.31e-4	5.56e-3	0.3337	-5.31e-4	-2.60e-4	7.49e-2	4.30e-2	5.30e-2	-1.71e-3	3.31e-4	1.89e-4
0.1201	0.3259	-8.12e-3	6.80e-3	0.3261	4.16e-4	1.11e-3	8.28e-2	4.23e-2	5.23e-2	-1.81e-3	6.93e-4	4.67e-5
0.1050	0.2750	-2.66e-3	4.59e-3	0.2750	-2.61e-4	-2.05e-4	7.58e-2	4.06e-2	5.10e-2	-1.56e-3	8.97e-4	9.44e-5
0.0896	0.2434	-7.29e-3	5.47e-3	0.2436	1.47e-4	1.22e-3	8.01e-2	4.14e-2	5.24e-2	-1.69e-3	5.51e-4	1.27e-4
0.0699	0.2090	-7.33e-3	1.69e-3	0.2091	-3.01e-5	-1.96e-3	6.39e-2	3.43e-2	4.33e-2	-1.11e-3	7.20e-5	3.27e-5
0.0495	0.1706	-4.66e-3	2.61e-3	0.1706	-1.98e-4	-3.70e-4	4.44e-2	2.77e-2	3.26e-2	-5.50e-4	-1.75e-4	3.62e-5
0.0350	0.1525	-7.96e-3	3.72e-3	0.1527	3.17e-5	1.06e-3	4.65e-2	2.32e-2	4.06e-2	-1.35e-4	-2.06e-4	-2.89e-6
0.0176	0.1426	-4.74e-3	2.89e-3	0.1427	2.42e-4	3.96e-4	3.36e-2	1.75e-2	2.75e-2	-8.05e-5	-1.08e-4	-4.85e-5
0.0079	0.1322	-3.40e-3	3.95e-3	0.1323	6.58e-5	1.64e-3	3.18e-2	1.49e-2	2.76e-2	-5.49e-5	-1.71e-4	-8.14e-6

Profile 3

	Raw Velocities			Corrected Velocities			RMS Velocity Fluctuations			Reynolds Stresses		
y (m)	$\bar{u}$ (m/s)	$\bar{v}$ (m/s)	$\bar{w}$ (m/s)	$\bar{u}$ (m/s)	$\bar{v}$ (m/s)	$\bar{w}$ (m/s)	u_{rms} (m/s)	v_{rms} (m/s)	w_{rms} (m/s)	$\overline{u'v'}$ (m^2/s^2)	$\overline{u'w'}$ (m^2/s^2)	$\overline{v'w'}$ (m^2/s^2)
0.1451	0.3400	8.91e-3	4.54e-3	0.3401	5.05e-6	-1.39e-3	7.31e-2	4.10e-2	5.16e-2	-1.42e-3	3.66e-4	1.54e-4
0.1296	0.3199	2.54e-3	7.02e-3	0.3200	-2.55e-4	1.44e-3	7.54e-2	4.41e-2	5.08e-2	-1.71e-3	6.80e-4	1.94e-4
0.1201	0.3074	-1.98e-3	3.43e-3	0.3074	-6.35e-4	-1.94e-3	7.95e-2	4.23e-2	4.93e-2	-1.84e-3	5.96e-4	1.06e-4
0.1049	0.2532	-5.86e-3	-1.65e-3	0.2532	3.37e-4	-6.07e-3	7.38e-2	3.88e-2	5.00e-2	-1.69e-3	4.75e-4	-2.08e-4
0.0899	0.2104	-1.58e-2	2.07e-3	0.2110	-1.44e-4	-1.61e-3	7.45e-2	3.85e-2	5.77e-2	-1.42e-3	-5.22e-5	-3.70e-4
0.0695	0.1804	-6.30e-3	-1.31e-3	0.1804	2.53e-6	-4.46e-3	5.04e-2	3.25e-2	4.35e-2	-4.22e-4	-4.23e-4	2.27e-5
0.0495	0.1611	-6.31e-6	-1.84e-3	0.1610	-6.31e-6	-4.65e-3	4.03e-2	2.53e-2	3.61e-2	-3.10e-4	-2.34e-4	2.96e-5
0.0359	0.1488	2.79e-3	-2.01e-3	0.1487	1.96e-4	-4.61e-3	3.25e-2	1.98e-2	3.15e-2	-1.60e-4	-2.45e-4	6.49e-5
0.0172	0.1405	9.44e-4	-4.17e-3	0.1404	-2.82e-4	-6.62e-3	3.19e-2	1.67e-2	3.03e-2	-1.08e-4	-2.31e-4	2.59e-5
0.0070	0.1441	1.98e-3	-7.16e-3	0.1440	9.46e-5	-9.67e-3	2.66e-2	1.38e-2	2.67e-2	-4.97e-5	-1.47e-4	7.50e-5

Profile 4

	Raw Velocities			Corrected Velocities			RMS Velocity Fluctuations			Reynolds Stresses		
y (m)	$\bar{u}$ (m/s)	$\bar{v}$ (m/s)	$\bar{w}$ (m/s)	$\bar{u}$ (m/s)	$\bar{v}$ (m/s)	$\bar{w}$ (m/s)	u_{rms} (m/s)	v_{rms} (m/s)	w_{rms} (m/s)	$\overline{u'v'}$ (m^2/s^2)	$\overline{u'w'}$ (m^2/s^2)	$\overline{v'w'}$ (m^2/s^2)
0.1393	0.3508	-1.52e-3	8.32e-3	0.3509	1.54e-5	-8.66e-4	8.16e-2	4.23e-2	5.47e-2	-1.85e-3	1.32e-4	1.21e-4
0.0130	0.3138	-1.80e-3	1.95e-3	0.3138	-4.32e-4	-6.26e-3	8.44e-2	4.08e-2	5.29e-2	-2.10e-3	3.77e-4	-1.27e-4
0.1203	0.2793	-4.50e-3	-2.87e-3	0.2792	3.80e-4	-1.02e-2	8.80e-2	4.33e-2	5.36e-2	-2.40e-3	-1.81e-4	-1.31e-4
0.1062	0.2329	-2.51e-4	-1.18e-3	0.2327	-2.51e-4	-7.27e-3	6.62e-2	4.36e-2	5.12e-2	-1.42e-3	-4.69e-4	8.27e-5
0.0902	0.2105	4.70e-3	1.52e-3	0.2105	1.08e-4	-3.99e-3	5.51e-2	3.42e-2	4.68e-2	-7.29e-4	-4.86e-4	1.93e-4
0.0693	0.1958	-3.03e-3	5.79e-3	0.1959	3.88e-4	6.63e-4	4.68e-2	2.92e-2	4.26e-2	-5.00e-4	-3.42e-4	1.01e-4
0.0493	0.1709	-1.01e-3	4.06e-3	0.1710	-2.59e-4	-4.18e-4	3.64e-2	2.24e-2	3.69e-2	-2.13e-4	-2.46e-4	3.73e-5
0.0374	0.1646	-4.33e-3	-8.25e-4	0.1646	-2.15e-5	-5.13e-3	4.37e-2	2.09e-2	4.49e-2	-1.51e-4	-4.50e-4	3.78e-5
0.1740	0.1554	-2.70e-3	-1.75e-3	0.1554	8.46e-6	-5.81e-3	3.44e-2	1.80e-2	3.52e-2	-8.41e-5	-2.47e-4	3.62e-5
0.0069	0.1550	4.47e-4	1.81e-3	0.1550	-2.30e-4	-2.25e-3	2.89e-2	1.52e-2	3.26e-2	-6.53e-5	-2.10e-4	6.66e-5

Experiment 10 Laboratory Measurements

H = 0.265 m S = 0.0161 Q = 180 L/s $a = 2.46\ m^{-1}$ T = 27.2 °C $h_p = 0.1175$ m

Profile 1

	Raw Velocities			Corrected Velocities			RMS Velocity Fluctuations			Reynolds Stresses		
y (m)	$\bar{u}$ (m/s)	$\bar{v}$ (m/s)	$\bar{w}$ (m/s)	$\bar{u}$ (m/s)	$\bar{v}$ (m/s)	$\bar{w}$ (m/s)	u_{rms} (m/s)	v_{rms} (m/s)	w_{rms} (m/s)	$\overline{u'v'}$ (m^2/s^2)	$\overline{u'w'}$ (m^2/s^2)	$\overline{v'w'}$ (m^2/s^2)
0.1695	0.8245	2.89e-2	2.21e-2	0.8223	2.18e-4	5.56e-4	0.2343	0.1142	0.2063	-1.18e-2	-1.60e-3	1.73e-3
0.1506	0.8251	1.32e-2	3.89e-3	0.8250	-1.19e-3	-1.77e-2	0.2112	0.1111	0.1489	-1.20e-2	-1.01e-3	3.75e-4
0.1351	0.7227	8.17e-2	8.20e-3	0.7230	-3.44e-4	-1.07e-2	0.2193	0.1165	0.1468	-1.50e-2	-8.54e-4	3.55e-4
0.1195	0.6493	1.10e-2	6.07e-4	0.6491	-3.56e-4	-1.64e-2	0.2111	0.1087	0.1498	-1.31e-2	-1.74e-3	-1.26e-4
0.1049	0.5429	7.62e-4	-1.82e-2	0.5423	7.62e-4	-3.24e-2	0.2077	0.1151	0.1393	-1.30e-2	-8.28e-3	-1.20e-3
0.0901	0.4569	1.73e-2	-2.09e-2	0.4568	-6.36e-4	-3.29e-2	0.1627	0.1027	0.1259	-6.91e-3	-8.78e-3	1.63e-3
0.0703	0.3971	1.54e-2	-1.71e-2	0.3969	-2.15e-4	-2.75e-2	0.1330	8.56e-2	0.1088	-5.17e-3	-5.50e-3	2.12e-3
0.0552	0.3552	1.06e-2	-9.18e-3	0.3550	-2.24e-4	-1.85e-2	0.1083	6.75e-2	9.89e-2	-2.75e-3	-3.63e-3	1.08e-3
0.0380	0.3191	8.38e-3	-9.15e-3	0.3189	2.35e-5	-1.75e-2	9.40e-2	5.33e-2	9.01e-2	-1.56e-3	-2.42e-3	6.11e-4
0.0093	0.3081	6.68e-3	-1.49e-2	0.3077	-4.54e-5	-2.30e-2	6.72e-2	2.98e-2	6.21e-2	-4.40e-4	-1.12e-3	3.87e-4

Profile 2

	Raw Velocities			Corrected Velocities			RMS Velocity Fluctuations			Reynolds Stresses		
y (m)	$\bar{u}$ (m/s)	$\bar{v}$ (m/s)	$\bar{w}$ (m/s)	$\bar{u}$ (m/s)	$\bar{v}$ (m/s)	$\bar{w}$ (m/s)	u_{rms} (m/s)	v_{rms} (m/s)	w_{rms} (m/s)	$\overline{u'v'}$ (m^2/s^2)	$\overline{u'w'}$ (m^2/s^2)	$\overline{v'w'}$ (m^2/s^2)
0.1699	0.8234	1.37e-2	2.16e-2	0.8238	-7.14e-4	4.21e-5	0.2038	0.1078	0.1617	-9.72e-3	-9.98e-4	6.35e-4
0.1489	0.7795	5.14e-3	1.05e-2	0.7795	-1.66e-3	-9.93e-3	0.2071	0.1088	0.1397	-1.15e-2	1.43e-3	2.25e-4
0.1346	0.7098	9.52e-3	5.02e-3	0.7097	2.28e-4	-1.36e-2	0.2140	0.1115	0.1395	-1.37e-2	2.87e-3	6.01e-4
0.1199	0.6419	1.44e-2	3.87e-3	0.6419	4.13e-4	-1.29e-2	0.2084	0.1090	0.1370	-1.36e-2	3.07e-3	4.72e-4
0.1048	0.5719	9.03e-3	-3.51e-3	0.5717	-9.50e-4	-1.85e-2	0.1999	0.1079	0.1277	-1.30e-2	5.10e-3	-8.20e-4
0.0898	0.4839	6.47e-3	-6.78e-3	0.4836	1.35e-4	-1.94e-2	0.1738	0.1016	0.1219	-1.01e-2	4.08e-3	-5.48e-4
0.0705	0.4151	-7.76e-4	1.59e-3	0.4150	-7.76e-4	-9.28e-3	0.1426	8.74e-2	0.1141	-6.23e-3	3.18e-3	-6.53e-4
0.0548	0.3692	-3.85e-3	9.47e-3	0.3693	-6.31e-4	-2.00e-4	0.1190	7.33e-2	0.1020	-4.09e-3	2.89e-3	-1.16e-3
0.0371	0.3292	-1.94e-3	1.10e-2	0.3293	-5.02e-4	2.36e-3	9.75e-2	5.82e-2	8.59e-2	-2.43e-3	9.60e-4	-5.16e-4
0.0096	0.2945	5.66e-3	1.24e-2	0.2947	5.19e-4	4.68e-3	6.44e-2	3.38e-2	6.59e-2	-5.68e-4	5.12e-4	-2.97e-4

Profile 3

	Raw Velocities			Corrected Velocities			RMS Velocity Fluctuations			Reynolds Stresses		
y (m)	$\bar{u}$ (m/s)	$\bar{v}$ (m/s)	$\bar{w}$ (m/s)	$\bar{u}$ (m/s)	$\bar{v}$ (m/s)	$\bar{w}$ (m/s)	u_{rms} (m/s)	v_{rms} (m/s)	w_{rms} (m/s)	$\overline{u'v'}$ (m^2/s^2)	$\overline{u'w'}$ (m^2/s^2)	$\overline{v'w'}$ (m^2/s^2)
0.1696	0.8357	1.68e-2	2.19e-2	0.8361	-1.41e-3	6.01e-6	0.2208	0.1096	0.1954	-1.22e-2	-6.31e-4	1.93e-4
0.1506	0.7972	9.85e-3	1.10e-2	0.7973	-5.86e-4	-9.88e-2	0.2096	0.1090	0.1371	-1.25e-2	1.18e-4	1.07e-4
0.1353	0.7184	1.16e-2	1.38e-2	0.7186	-9.38e-4	-5.04e-3	0.2138	0.1083	0.1381	-1.37e-2	-4.74e-5	-2.39e-4
0.1207	0.6497	2.63e-4	2.48e-2	0.6501	2.63e-4	7.80e-3	0.2091	0.1077	0.1321	-1.38e-2	-1.42e-3	1.14e-4
0.1051	0.5530	-2.05e-3	2.68e-2	0.5535	3.63e-4	1.24e-2	0.1805	9.54e-2	0.1237	-1.00e-2	-6.46e-4	2.35e-5
0.0905	0.4498	-1.56e-2	2.34e-2	0.4505	7.03e-5	1.17e-2	0.1530	8.43e-2	0.1161	-7.51e-3	-1.44e-4	1.58e-4
0.0702	0.3573	-9.91e-3	2.15e-2	0.3580	-5.53e-4	1.21e-2	0.1095	7.82e-2	9.90e-2	-3.50e-3	-4.52e-4	3.35e-4
0.0549	0.3253	-1.55e-3	1.61e-2	0.3256	-1.34e-4	7.54e-3	9.12e-2	5.74e-2	9.10e-2	-1.19e-3	-6.42e-4	5.52e-4
0.0373	0.3012	-3.87e-3	1.76e-2	0.3016	6.98e-5	9.72e-3	7.94e-2	4.60e-2	8.35e-2	-7.13e-4	-2.06e-4	1.41e-4
0.0098	0.2798	3.50e-4	1.79e-2	0.2802	3.50e-4	1.05e-2	6.36e-2	3.27e-2	7.18e-2	-2.76e-4	6.61e-4	2.38e-4

Profile 4

	Raw Velocities			Corrected Velocities			RMS Velocity Fluctuations			Reynolds Stresses		
y (m)	$\bar{u}$ (m/s)	$\bar{v}$ (m/s)	$\bar{w}$ (m/s)	$\bar{u}$ (m/s)	$\bar{v}$ (m/s)	$\bar{w}$ (m/s)	u_{rms} (m/s)	v_{rms} (m/s)	w_{rms} (m/s)	$\overline{u'v'}$ (m^2/s^2)	$\overline{u'w'}$ (m^2/s^2)	$\overline{v'w'}$ (m^2/s^2)
0.1622	0.8292	6.23e-3	2.68e-2	0.8296	-1.01e-3	-2.19e-3	0.2103	0.1062	0.1920	-1.08e-2	1.49e-4	6.95e-4
0.1494	0.8068	1.02e-3	2.02e-2	0.8071	1.02e-3	-7.95e-3	0.2043	0.1031	0.1414	-1.10e-2	1.28e-4	6.37e-4
0.1350	0.7495	-1.76e-3	4.29e-2	0.7504	1.51e-3	1.67e-2	0.2176	0.1091	0.1325	-1.42e-2	7.36e-4	5.16e-4
0.1199	0.6267	9.28e-3	3.80e-2	0.6277	1.08e-3	1.61e-2	0.2020	9.86e-2	0.1216	-1.13e-2	1.94e-3	-2.61e-4
0.1048	0.5714	-6.10e-3	4.68e-2	0.5728	-1.11e-3	2.68e-2	0.1752	0.1016	0.1132	-9.73e-3	2.79e-4	-2.32e-4
0.0902	0.5102	-6.24e-3	3.72e-2	0.5113	4.38e-4	1.94e-2	0.1560	9.02e-2	0.1043	-7.33e-3	1.01e-3	-7.27e-4
0.0699	0.4523	-1.20e-2	2.69e-2	0.4531	-1.98e-4	1.11e-2	0.1410	7.73e-2	9.26e-2	-6.02e-3	-1.45e-4	-1.07e-4
0.0551	0.4038	-8.70e-3	2.51e-2	0.4045	1.08e-4	1.10e-2	0.1155	6.63e-2	8.82e-2	-3.58e-3	-4.29e-5	-7.99e-5
0.0375	0.3680	-1.00e-2	2.13e-2	0.3686	-3.66e-4	8.40e-3	9.36e-2	5.35e-2	7.95e-2	-1.73e-3	-2.12e-4	-1.77e-4
0.0104	0.3318	-3.56e-3	1.83e-2	0.3322	-6.68e-4	6.71e-3	6.62e-2	3.22e-2	6.01e-2	-4.32e-4	-7.93e-5	-6.79e-5

Experiment 11 Laboratory Measurements

H = 0.311 m S = 0.0036 Q = 177 L/s a = 0.615 m^{-1} T = 26.5 °C h_p = 0.1175 m

Profile 1

	Raw Velocities			Corrected Velocities			RMS Velocity Fluctuations			Reynolds Stresses		
y (m)	$\bar{u}$ (m/s)	$\bar{v}$ (m/s)	$\bar{w}$ (m/s)	$\bar{u}$ (m/s)	$\bar{v}$ (m/s)	$\bar{w}$ (m/s)	u_{rms} (m/s)	v_{rms} (m/s)	w_{rms} (m/s)	$\overline{u'v'}$ (m^2/s^2)	$\overline{u'w'}$ (m^2/s^2)	$\overline{v'w'}$ (m^2/s^2)
0.2348	0.7318	-8.19e-3	3.52e-2	0.7327	1.39e-3	-3.15e-3	0.1129	6.15e-2	8.38e-2	-2.01e-3	-1.17e-3	-1.48e-4
0.1998	0.6998	-1.29e-2	3.04e-2	0.7005	-6.49e-4	-6.30e-3	0.1078	6.73e-2	8.30e-2	-2.38e-3	-8.34e-4	-3.60e-4
0.1695	0.6561	-4.35e-3	2.51e-2	0.6565	1.38e-3	-9.30e-3	0.1243	6.98e-2	8.52e-2	-3.37e-3	-1.59e-3	-1.97e-4
0.1394	0.6033	-8.70e-3	1.96e-2	0.6036	-8.05e-4	-1.20e-2	0.1317	7.11e-2	8.65e-2	-4.36e-3	-6.46e-4	-2.02e-4
0.1192	0.5726	-6.63e-3	2.38e-2	0.5731	8.66e-4	-6.22e-3	0.1325	7.16e-2	8.44e-2	-5.15e-3	-9.16e-4	-3.46e-5
0.1005	0.4978	-1.31e-3	3.04e-2	0.4988	8.58e-4	4.34e-3	0.1259	6.73e-2	7.42e-2	-4.80e-3	-1.02e-3	2.51e-4
0.0809	0.4703	-1.30e-3	2.70e-2	0.4711	7.54e-4	2.32e-3	0.1204	6.60e-2	7.53e-2	-3.98e-3	2.00e-4	3.40e-4
0.0547	0.4060	1.08e-4	2.38e-2	0.4067	1.08e-4	2.48e-3	0.1043	4.97e-2	6.28e-2	-2.40e-3	4.08e-6	2.39e-4
0.0379	0.3814	-1.60e-4	2.53e-2	0.3822	-1.60e-4	5.31e-3	8.48e-2	4.42e-2	5.86e-2	-1.60e-3	-1.30e-4	1.25e-4
0.0010	0.3459	5.22e-4	3.27e-2	0.3471	5.22e-4	1.45e-2	7.77e-2	3.05e-2	5.14e-2	-8.49e-4	-2.52e-4	2.15e-4

Profile 2

	Raw Velocities			Corrected Velocities			RMS Velocity Fluctuations			Reynolds Stresses		
y (m)	$\bar{u}$ (m/s)	$\bar{v}$ (m/s)	$\bar{w}$ (m/s)	$\bar{u}$ (m/s)	$\bar{v}$ (m/s)	$\bar{w}$ (m/s)	u_{rms} (m/s)	v_{rms} (m/s)	w_{rms} (m/s)	$\overline{u'v'}$ (m^2/s^2)	$\overline{u'w'}$ (m^2/s^2)	$\overline{v'w'}$ (m^2/s^2)
0.2296	0.7473	-8.88e-3	2.34e-2	0.7477	9.03e-4	-2.67e-3	0.1061	6.09e-2	7.97e-2	-1.79e-3	7.77e-4	-1.28e-4
0.1999	0.7036	-1.42e-3	3.03e-2	0.7042	-1.42e-3	5.74e-3	0.1143	6.66e-2	8.35e-2	-3.16e-3	7.11e-4	-2.88e-4
0.1697	0.6711	-2.67e-3	2.78e-2	0.6717	2.62e-4	4.56e-3	0.1178	6.85e-2	8.53e-2	-3.73e-3	8.46e-4	-3.02e-4
0.1402	0.6213	-5.09e-4	1.84e-2	0.6216	-5.09e-4	-3.27e-3	0.1221	6.84e-2	8.15e-2	-3.93e-3	5.17e-4	-5.17e-4
0.1196	0.5648	4.99e-4	2.01e-2	0.5651	4.99e-4	3.33e-4	0.1286	6.74e-2	8.32e-2	-4.10e-3	-1.16e-3	-1.81e-4
0.0996	0.5377	-6.36e-3	2.63e-2	0.5383	6.80e-4	7.49e-3	0.1203	6.44e-2	8.07e-2	-4.01e-3	5.10e-4	-3.70e-4
0.0805	0.4940	-1.47e-2	1.75e-2	0.4945	4.12e-4	2.02e-4	0.1096	6.20e-2	7.53e-2	-3.44e-3	1.61e-4	-1.50e-4
0.0546	0.4403	-1.07e-2	1.00e-2	0.4405	8.49e-4	-5.38e-3	8.79e-2	5.38e-2	6.67e-2	-1.98e-3	2.47e-4	2.09e-4
0.0379	0.4147	-1.12e-2	6.97e-3	0.4148	-3.75e-4	-7.51e-3	7.69e-2	4.45e-2	6.08e-2	-1.28e-3	2.32e-4	3.25e-4
0.0098	0.3862	-1.37e-2	5.09e-3	0.3864	-2.26e-4	-8.39e-3	7.14e-2	2.77e-2	4.93e-2	-5.32e-4	1.98e-4	9.23e-5

Profile 3

	Raw Velocities			Corrected Velocities			RMS Velocity Fluctuations			Reynolds Stresses		
y (m)	$\bar{u}$ (m/s)	$\bar{v}$ (m/s)	$\bar{w}$ (m/s)	$\bar{u}$ (m/s)	$\bar{v}$ (m/s)	$\bar{w}$ (m/s)	u_{rms} (m/s)	v_{rms} (m/s)	w_{rms} (m/s)	$\overline{u'v'}$ (m^2/s^2)	$\overline{u'w'}$ (m^2/s^2)	$\overline{v'w'}$ (m^2/s^2)
0.2257	0.7415	-7.23e-3	2.39e-2	0.7419	-7.62e-4	-2.00e-3	0.1039	6.16e-2	7.59e-2	-1.72e-3	-3.36e-5	-5.87e-5
0.2002	0.7227	-9.48e-3	2.26e-2	0.7231	-2.25e-5	-2.61e-3	0.1094	6.31e-2	8.16e-2	-2.46e-3	1.48e-4	-8.37e-5
0.1707	0.6845	-9.19e-3	1.99e-2	0.6849	-2.26e-4	-4.01e-3	0.1209	6.75e-2	8.53e-2	-3.38e-3	2.67e-4	4.36e-5
0.1409	0.6427	-9.85e-3	4.05e-2	0.6438	1.36e-3	1.81e-2	0.1262	7.06e-2	8.02e-2	-4.51e-3	9.62e-4	1.40e-4
0.1205	0.6024	1.35e-2	3.09e-2	0.6033	3.91e-4	9.84e-3	0.1317	6.14e-2	7.69e-2	-4.17e-3	1.78e-3	-7.70e-4
0.1001	0.5453	-4.64e-3	2.43e-2	0.5458	1.20e-4	5.24e-3	0.1207	6.48e-2	7.00e-2	-4.36e-3	6.54e-4	5.53e-5
0.0793	0.5021	3.90e-4	3.16e-2	0.5029	3.90e-4	1.40e-2	0.1090	6.42e-2	6.63e-2	-3.79e-3	3.49e-4	-4.13e-5
0.0554	0.4558	8.19e-4	2.90e-2	0.4566	8.19e-4	1.31e-2	8.84e-2	4.90e-2	5.83e-2	-1.85e-3	1.39e-4	-1.96e-4
0.0381	0.4292	1.54e-3	2.67e-2	0.4298	-3.31e-4	1.17e-2	7.02e-2	3.94e-2	5.20e-2	-9.00e-4	1.86e-4	-1.98e-4
0.0104	0.3989	-1.17e-3	2.59e-2	0.3996	5.73e-4	1.19e-2	6.18e-2	2.46e-2	4.95e-2	-3.52e-4	2.30e-4	-3.53e-5

Profile 4

	Raw Velocities			Corrected Velocities			RMS Velocity Fluctuations			Reynolds Stresses		
y (m)	$\bar{u}$ (m/s)	$\bar{v}$ (m/s)	$\bar{w}$ (m/s)	$\bar{u}$ (m/s)	$\bar{v}$ (m/s)	$\bar{w}$ (m/s)	u_{rms} (m/s)	v_{rms} (m/s)	w_{rms} (m/s)	$\overline{u'v'}$ (m^2/s^2)	$\overline{u'w'}$ (m^2/s^2)	$\overline{v'w'}$ (m^2/s^2)
0.2239	0.7347	-8.16e-3	3.64e-2	0.7356	1.46e-3	-2.09e-3	0.1026	6.15e-2	9.26e-2	-1.78e-3	-2.03e-3	2.90e-4
0.2002	0.6972	-7.85e-3	2.98e-2	0.6978	1.28e-3	-6.72e-3	0.1110	6.24e-2	7.92e-2	-2.57e-3	1.37e-4	-3.42e-4
0.1696	0.6838	-1.09e-2	2.93e-2	0.6846	9.90e-4	-6.51e-3	0.1161	6.84e-2	8.25e-2	-3.58e-3	1.73e-4	-8.42e-5
0.1410	0.6044	-3.80e-3	5.24e-2	0.6051	-1.16e-3	-3.29e-3	0.1307	6.56e-2	8.38e-2	-4.52e-3	-2.78e-4	-3.71e-4
0.1205	0.5974	-1.28e-2	2.51e-2	0.5980	2.77e-4	-6.17e-3	0.1360	7.07e-2	8.29e-2	-5.11e-3	-1.15e-3	-4.79e-4
0.1007	0.5219	-5.86e-3	2.42e-2	0.5225	9.69e-4	-3.19e-3	0.1231	6.63e-2	8.16e-2	-3.63e-3	-2.32e-3	-1.64e-4
0.0799	0.4767	-3.26e-3	2.95e-2	0.4776	9.02e-4	4.47e-3	0.1143	5.95e-2	7.38e-2	-3.09e-3	-1.38e-3	-1.44e-4
0.0554	0.4089	7.57e-4	2.08e-2	0.4094	7.57e-4	-6.06e-4	9.08e-2	4.97e-2	6.07e-2	-2.07e-3	-9.43e-4	-6.21e-6
0.0375	0.3884	-1.57e-3	1.89e-2	0.3889	1.21e-4	-1.41e-3	8.59e-2	4.16e-2	5.58e-2	-1.55e-3	-9.73e-4	1.69e-4
0.0104	0.3595	1.45e-3	2.00e-2	0.3601	-1.24e-4	1.13e-3	6.97e-2	3.02e-2	5.33e-2	-5.91e-4	-6.54e-4	1.70e-4

Experiment 12 Laboratory Measurements

H = 0.233 m S = 0.0108 Q = 181 L/s $a = 0.615\ m^{-1}$ T = 26.5 °C $h_p = 0.1175$ m

Profile 1

	Raw Velocities			Corrected Velocities			RMS Velocity Fluctuations			Reynolds Stresses		
y (m)	$\bar{u}$ (m/s)	$\bar{v}$ (m/s)	$\bar{w}$ (m/s)	$\bar{u}$ (m/s)	$\bar{v}$ (m/s)	$\bar{w}$ (m/s)	u_{rms} (m/s)	v_{rms} (m/s)	w_{rms} (m/s)	$\overline{u'v'}$ (m^2/s^2)	$\overline{u'w'}$ (m^2/s^2)	$\overline{v'w'}$ (m^2/s^2)
0.1203	0.8426	-6.99e-3	4.20e-2	0.8437	3.65e-4	-2.13e-3	0.1672	8.03e-2	0.1038	-7.47e-3	2.98e-3	-8.16e-5
0.1058	0.7848	-6.19e-3	5.17e-2	0.7865	6.59e-4	1.06e-2	0.1567	8.41e-2	0.1025	-7.76e-3	1.99e-3	-1.41e-4
0.0956	0.7262	-2.21e-3	5.91e-2	0.7283	9.56e-4	2.11e-2	0.1420	8.11e-2	9.67e-2	-6.65e-3	4.57e-4	3.40e-4
0.0802	0.6600	9.24e-3	5.81e-2	0.6621	6.01e-4	2.35e-2	0.1214	7.42e-2	8.93e-2	-4.37e-3	5.38e-4	9.49e-5
0.0704	0.6139	1.13e-2	4.46e-2	0.6155	5.81e-4	1.24e-2	0.1079	6.17e-2	8.87e-2	-2.33e-3	8.56e-4	2.21e-4
0.0608	0.6102	3.95e-3	4.11e-2	0.6115	1.28e-3	9.10e-3	0.1053	5.67e-2	8.46e-2	-1.80e-3	2.92e-4	5.12e-4
0.0484	0.5745	8.58e-4	3.61e-2	0.5753	8.58e-4	5.98e-3	9.23e-2	4.94e-2	7.59e-2	-1.21e-3	2.81e-5	5.18e-4
0.0382	0.5635	-4.55e-3	3.66e-2	0.5647	3.71e-4	7.03e-3	9.12e-2	4.68e-2	7.49e-2	-1.14e-3	1.54e-4	5.54e-4
0.0181	0.5482	-9.66e-4	4.39e-2	0.5497	-9.66e-4	1.52e-2	8.11e-2	3.85e-2	5.64e-2	-8.07e-4	2.87e-4	2.88e-4
0.0075	0.5434	-4.04e-3	4.12e-2	0.5449	6.99e-4	1.27e-2	8.69e-2	3.28e-2	6.31e-2	-7.05e-4	7.47e-4	2.42e-4

Profile 2

	Raw Velocities			Corrected Velocities			RMS Velocity Fluctuations			Reynolds Stresses		
y (m)	$\bar{u}$ (m/s)	$\bar{v}$ (m/s)	$\bar{w}$ (m/s)	$\bar{u}$ (m/s)	$\bar{v}$ (m/s)	$\bar{w}$ (m/s)	u_{rms} (m/s)	v_{rms} (m/s)	w_{rms} (m/s)	$\overline{u'v'}$ (m^2/s^2)	$\overline{u'w'}$ (m^2/s^2)	$\overline{v'w'}$ (m^2/s^2)
0.1203	0.8732	-1.88e-2	1.38e-2	0.8735	2.49e-4	-1.44e-3	0.1513	7.60e-2	1.1063	-2.06e-3	-1.04e-3	5.96e-6
0.1049	0.8112	-1.98e-2	2.62e-3	0.8114	1.43e-3	-1.15e-2	0.1585	7.73e-2	0.1065	-6.34e-3	-3.36e-4	-7.87e-5
0.0941	0.7710	-1.90e-2	-4.81e-3	0.7710	1.16e-3	-1.83e-2	0.1586	7.89e-2	0.1048	-6.86e-3	-4.76e-4	-1.52e-4
0.0804	0.7027	-2.24e-2	-7.16e-3	0.7029	-9.04e-4	-1.94e-2	0.1551	7.47e-2	9.86e-2	-6.34e-3	-3.76e-4	9.20e-5
0.0705	0.6447	-1.32e-2	-3.55e-3	0.6446	8.83e-4	-1.48e-2	0.1380	7.18e-2	9.72e-2	-5.03e-3	-7.27e-4	9.32e-5
0.0595	0.6273	-1.93e-4	-2.00e-3	0.6274	-1.05e-4	-1.29e-2	0.1240	6.49e-2	9.39e-2	-3.71e-3	-1.07e-4	-1.55e-4
0.0474	0.5789	-1.40e-2	-2.38e-4	0.5790	1.16e-3	-1.03e-2	0.1126	6.04e-2	8.44e-2	-2.79e-3	-1.35e-5	-4.57e-4
0.0377	0.5749	-1.64e-2	9.11e-4	0.5750	1.17e-3	-9.12e-3	0.1088	5.38e-2	8.37e-2	-2.35e-3	1.03e-4	-5.18e-4
0.0183	0.5492	-9.25e-3	7.86e-3	0.5493	3.36e-4	-1.73e-3	9.17e-2	4.36e-2	6.25e-2	-1.47e-3	2.96e-4	-3.55e-4
0.0081	0.5534	-9.50e-4	1.27e-2	0.5536	-9.50e-4	3.06e-3	8.66e-2	3.52e-2	6.02e-2	-9.57e-4	9.85e-5	-1.55e-4

Profile 3

	Raw Velocities			Corrected Velocities			RMS Velocity Fluctuations			Reynolds Stresses		
y (m)	$\bar{u}$ (m/s)	$\bar{v}$ (m/s)	$\bar{w}$ (m/s)	$\bar{u}$ (m/s)	$\bar{v}$ (m/s)	$\bar{w}$ (m/s)	u_{rms} (m/s)	v_{rms} (m/s)	w_{rms} (m/s)	$\overline{u'v'}$ (m^2/s^2)	$\overline{u'w'}$ (m^2/s^2)	$\overline{v'w'}$ (m^2/s^2)
0.1200	0.8113	-6.06e-3	2.93e-2	0.8119	1.02e-3	9.76e-4	0.1615	8.01e-2	0.1038	-6.09e-3	3.23e-3	9.67e-4
0.1044	0.7203	1.73e-3	1.89e-2	0.7205	1.41e-3	-6.26e-3	0.1510	8.12e-2	9.98e-2	-5.40e-3	4.07e-3	7.28e-4
0.0951	0.6837	8.35e-3	2.35e-2	0.6842	-6.04e-4	-4.08e-4	0.1393	7.64e-2	9.63e-2	-4.35e-3	3.87e-3	4.66e-4
0.0801	0.6451	1.12e-2	2.44e-2	0.6456	-1.01e-4	1.91e-3	0.1241	7.06e-2	8.94e-2	-3.61e-3	2.81e-3	1.25e-5
0.0700	0.6250	1.48e-2	2.95e-2	0.6259	1.78e-3	7.71e-3	0.1207	6.37e-2	8.49e-2	-3.19e-3	2.56e-3	-2.32e-4
0.0604	0.6105	1.50e-2	2.84e-2	0.6113	-1.02e-3	7.07e-3	0.1134	5.87e-2	8.27e-2	-2.50e-3	2.29e-3	-5.17e-4
0.0468	0.5872	1.30e-2	2.67e-2	0.5879	1.61e-4	6.20e-3	0.1072	5.50e-2	7.76e-2	-2.39e-3	1.95e-3	-5.03e-4
0.0380	0.5736	1.30e-2	2.40e-2	0.5742	5.10e-4	3.99e-3	0.1027	5.09e-2	7.46e-2	-2.10e-3	1.51e-3	-3.18e-4
0.0173	0.5506	1.92e-2	1.65e-2	0.5511	-5.01e-5	-2.74e-3	8.60e-2	4.39e-2	6.37e-2	-1.40e-3	1.35e-3	-4.91e-4
0.0073	0.5709	2.38e-2	1.11e-2	0.5714	-1.08e-3	-8.80e-3	8.46e-2	4.10e-2	6.61e-2	-1.22e-3	1.08e-3	-6.26e-4

Profile 4

	Raw Velocities			Corrected Velocities			RMS Velocity Fluctuations			Reynolds Stresses		
y (m)	$\bar{u}$ (m/s)	$\bar{v}$ (m/s)	$\bar{w}$ (m/s)	$\bar{u}$ (m/s)	$\bar{v}$ (m/s)	$\bar{w}$ (m/s)	u_{rms} (m/s)	v_{rms} (m/s)	w_{rms} (m/s)	$\overline{u'v'}$ (m^2/s^2)	$\overline{u'w'}$ (m^2/s^2)	$\overline{v'w'}$ (m^2/s^2)
0.1205	0.8866	-8.56e-3	3.12e-2	0.8872	-8.22e-4	2.47e-4	0.1564	7.75e-2	0.1128	-6.31e-3	-1.63e-3	-2.20e-4
0.1053	0.8053	-6.31e-3	4.11e-2	0.8063	7.18e-4	1.30e-2	0.1484	7.81e-2	0.1031	-5.84e-3	-2.63e-3	-5.89e-4
0.0953	0.7930	-1.22e-2	4.73e-2	0.7942	1.62e-3	1.96e-2	0.1433	7.73e-2	0.1023	-4.71e-3	-2.46e-3	-8.69e-4
0.0808	0.7448	-1.18e-2	4.11e-2	0.7458	1.19e-3	1.51e-2	0.1327	7.05e-2	9.81e-2	-3.85e-3	-1.52e-3	-1.03e-3
0.0703	0.7270	-1.49e-2	3.04e-2	0.7278	9.74e-4	5.04e-3	0.1352	6.87e-2	9.43e-2	-4.40e-3	-7.67e-4	-7.02e-4
0.0606	0.6788	-1.34e-2	2.45e-2	0.6794	1.40e-3	7.85e-4	0.1253	6.33e-2	8.92e-2	-3.93e-3	-8.10e-4	-2.79e-4
0.0478	0.6412	-1.19e-2	1.96e-2	0.6416	-6.90e-4	-2.79e-3	0.1138	5.80e-2	8.54e-2	-2.94e-3	-7.58e-4	-1.39e-4
0.0377	0.6190	-1.29e-2	2.24e-2	0.6196	5.67e-4	8.01e-4	0.1084	5.35e-2	8.08e-2	-2.60e-3	-9.46e-4	6.23e-5
0.0177	0.5756	-5.65e-3	2.12e-2	0.5760	-6.26e-4	1.11e-3	8.65e-2	4.14e-2	6.21e-2	-1.31e-3	-8.14e-4	1.65e-4
0.0070	0.5833	-1.25e-3	2.29e-2	0.5837	-1.25e-3	2.52e-3	8.32e-2	3.59e-2	6.50e-2	-7.53e-4	-7.58e-4	3.49e-4

Experiment 13 Laboratory Measurements

H = 0.368 m S = 0.0036 Q = 179 L/s a = 1.09 m^{-1} T = 27.0 °C h_p = 0.152 m

Profile 1

	Raw Velocities			Corrected Velocities			RMS Velocity Fluctuations			Reynolds Stresses		
y (m)	$\bar{u}$ (m/s)	$\bar{v}$ (m/s)	$\bar{w}$ (m/s)	$\bar{u}$ (m/s)	$\bar{v}$ (m/s)	$\bar{w}$ (m/s)	u_{rms} (m/s)	v_{rms} (m/s)	w_{rms} (m/s)	$\overline{u'v'}$ (m^2/s^2)	$\overline{u'w'}$ (m^2/s^2)	$\overline{v'w'}$ (m^2/s^2)
0.2898	0.7213	-7.56e-3	2.78e-2	0.7219	-1.27e-3	2.59e-3	9.30e-2	5.66e-2	7.87e-2	-1.59e-3	-7.87e-4	-3.85e-4
0.2495	0.6823	-6.86e-3	2.09e-2	0.6827	-9.01e-4	-2.94e-3	0.1071	6.65e-2	8.47e-2	-2.68e-3	-5.74e-4	-3.54e-4
0.1997	0.6151	-7.86e-3	1.51e-2	0.6153	1.91e-4	-6.38e-3	0.1208	7.18e-2	9.89e-2	-3.74e-3	-2.02e-4	-1.88e-4
0.1596	0.5104	-8.87e-3	1.55e-2	0.5107	3.81e-5	-2.30e-3	0.1426	7.09e-2	9.59e-2	-5.26e-3	-8.46e-4	-1.52e-4
0.1398	0.4371	-1.00e-2	1.92e-2	0.4376	-4.57e-4	3.90e-3	0.1316	6.99e-2	9.65e-2	-4.37e-3	-9.86e-4	2.37e-5
0.1199	0.3744	-1.28e-3	1.07e-2	0.3745	3.50e-4	-2.36e-3	0.1137	7.00e-2	8.41e-2	-3.62e-3	-6.94e-4	5.29e-4
0.0905	0.3306	-3.85e-3	8.36e-3	0.3307	4.79e-4	-3.18e-3	9.03e-2	5.44e-2	7.72e-2	-1.77e-3	-7.20e-4	3.58e-4
0.0647	0.3057	-5.73e-3	6.67e-3	0.3058	-3.91e-4	-4.00e-3	7.52e-2	4.06e-2	6.81e-2	-7.36e-4	-2.85e-4	1.83e-4
0.0375	0.2791	-9.83e-3	8.54e-3	0.2794	-8.11e-5	-1.21e-3	6.48e-2	3.08e-2	5.72e-2	-3.92e-4	-1.87e-4	5.95e-6
0.0098	0.2646	-2.58e-3	1.30e-2	0.2649	-2.71e-4	3.76e-3	4.82e-2	2.16e-2	4.38e-2	-1.43e-4	9.84e-5	3.95e-5

Profile 2

	Raw Velocities			Corrected Velocities			RMS Velocity Fluctuations			Reynolds Stresses		
y (m)	$\bar{u}$ (m/s)	$\bar{v}$ (m/s)	$\bar{w}$ (m/s)	$\bar{u}$ (m/s)	$\bar{v}$ (m/s)	$\bar{w}$ (m/s)	u_{rms} (m/s)	v_{rms} (m/s)	w_{rms} (m/s)	$\overline{u'v'}$ (m^2/s^2)	$\overline{u'w'}$ (m^2/s^2)	$\overline{v'w'}$ (m^2/s^2)
0.2894	0.7280	-9.76e-5	2.44e-2	0.7284	-9.76e-5	-1.04e-3	0.1089	6.29e-2	8.00e-2	-1.71e-3	-4.88e-4	-6.65e-4
0.2505	0.6698	5.12e-4	2.46e-2	0.6703	5.12e-4	1.16e-3	0.1205	7.33e-2	9.13e-2	-2.96e-3	6.08e-5	-1.02e-3
0.2006	0.5967	4.01e-4	1.41e-2	0.5969	4.01e-4	-6.73e-3	0.1288	7.97e-2	9.98e-2	-4.94e-3	5.77e-5	-4.19e-4
0.1600	0.4927	4.07e-3	1.75e-2	0.4930	-2.31e-4	3.21e-4	0.1321	7.84e-2	9.66e-2	-5.48e-3	4.26e-4	-4.46e-4
0.1400	0.4325	-4.11e-5	1.64e-2	0.4328	-4.11e-5	1.34e-3	0.1333	7.47e-2	8.82e-2	-5.71e-3	5.51e-4	-2.28e-4
0.1197	0.3698	-8.69e-4	1.86e-2	0.3703	7.44e-4	5.72e-3	0.1193	7.37e-2	8.47e-2	-4.74e-3	9.22e-4	5.95e-4
0.0898	0.3186	4.89e-3	1.67e-2	0.3190	-6.67e-4	5.58e-3	8.59e-2	5.73e-2	7.25e-2	-1.77e-3	-3.50e-4	-2.63e-4
0.0648	0.2960	7.49e-3	9.59e-3	0.2963	-2.63e-4	-7.45e-4	6.42e-2	4.16e-2	5.71e-2	-6.97e-4	-5.61e-4	9.78e-5
0.0376	0.2774	6.08e-4	5.21e-3	0.2774	-6.02e-4	-4.48e-3	5.17e-2	3.15e-2	4.62e-2	-3.36e-4	-3.64e-4	2.56e-5
0.0099	0.2570	-9.35e-4	1.35e-2	0.2573	1.86e-4	4.56e-3	4.19e-2	1.88e-2	3.90e-2	-1.98e-4	-3.70e-4	1.27e-4

Profile 3

	Raw Velocities			Corrected Velocities			RMS Velocity Fluctuations			Reynolds Stresses		
y (m)	$\bar{u}$ (m/s)	$\bar{v}$ (m/s)	$\bar{w}$ (m/s)	$\bar{u}$ (m/s)	$\bar{v}$ (m/s)	$\bar{w}$ (m/s)	u_{rms} (m/s)	v_{rms} (m/s)	w_{rms} (m/s)	$\overline{u'v'}$ (m^2/s^2)	$\overline{u'w'}$ (m^2/s^2)	$\overline{v'w'}$ (m^2/s^2)
0.2828	0.6966	-9.38e-4	2.21e-2	0.6969	-9.38e-4	-2.24e-3	0.1077	6.68e-2	8.53e-2	-2.02e-3	-1.20e-3	-3.35e-4
0.2498	0.6539	6.92e-3	2.44e-2	0.6543	1.22e-3	1.52e-3	0.1135	7.28e-2	8.92e-2	-2.92e-3	-7.46e-4	-4.16e-4
0.2002	0.5820	1.00e-3	1.99e-2	0.5823	1.00e-3	-4.71e-4	0.1313	7.49e-2	9.39e-2	-4.57e-3	-3.83e-4	-6.25e-4
0.1595	0.4822	2.15e-3	1.38e-2	0.4824	4.47e-5	-3.08e-3	0.1365	7.59e-2	9.06e-2	-5.49e-3	2.24e-4	-6.30e-4
0.1394	0.3660	-4.79e-3	1.37e-2	0.3663	4.92e-6	9.38e-4	0.1689	7.83e-2	9.90e-2	-8.11e-3	5.55e-4	-2.01e-4
0.1206	0.2652	3.69e-2	1.00e-2	0.2679	-3.95e-4	7.60e-4	0.1357	7.95e-2	0.1241	-5.76e-3	3.12e-4	-1.67e-4
0.0902	0.2476	3.92e-2	1.01e-2	0.2509	-9.47e-6	1.47e-3	8.61e-2	5.96e-2	8.60e-2	-2.01e-3	-6.29e-5	8.37e-5
0.0648	0.2572	3.01e-2	1.57e-2	0.2593	-3.18e-4	6.66e-3	6.90e-2	4.44e-2	6.94e-2	-9.25e-4	9.44e-5	-1.08e-4
0.0381	0.2619	1.41e-2	1.69e-2	0.2627	3.74e-4	7.72e-3	4.82e-2	3.00e-2	5.26e-2	-2.89e-4	3.04e-5	-1.32e-4
0.0100	0.2536	4.90e-3	2.04e-2	0.2543	4.76e-4	1.16e-2	4.31e-2	2.08e-2	4.41e-2	-2.45e-4	2.73e-4	-1.43e-4

Profile 4

	Raw Velocities			Corrected Velocities			RMS Velocity Fluctuations			Reynolds Stresses		
y (m)	$\bar{u}$ (m/s)	$\bar{v}$ (m/s)	$\bar{w}$ (m/s)	$\bar{u}$ (m/s)	$\bar{v}$ (m/s)	$\bar{w}$ (m/s)	u_{rms} (m/s)	v_{rms} (m/s)	w_{rms} (m/s)	$\overline{u'v'}$ (m^2/s^2)	$\overline{u'w'}$ (m^2/s^2)	$\overline{v'w'}$ (m^2/s^2)
0.2831	0.7014	-8.42e-4	3.11e-2	0.7021	-8.42e-4	4.44e-4	0.1083	6.75e-2	8.90e-2	-2.15e-3	-5.15e-4	-4.15e-4
0.2499	0.6604	-2.00e-3	3.17e-2	0.6611	8.85e-4	2.89e-3	0.1191	7.07e-2	9.12e-2	-3.28e-3	-1.90e-4	-5.71e-4
0.2003	0.5829	1.66e-3	2.71e-2	0.5835	-8.84e-4	1.65e-3	0.1262	7.77e-2	9.97e-2	-4.58e-3	-5.05e-5	-6.18e-4
0.1593	0.4994	-2.63e-4	2.55e-2	0.5001	-2.63e-4	3.67e-3	0.1297	7.43e-2	9.72e-2	-4.85e-3	8.47e-5	-1.85e-4
0.1399	0.4387	-5.23e-3	2.29e-2	0.4393	5.17e-4	3.69e-3	0.1286	7.38e-2	9.13e-2	-5.02e-3	1.55e-4	4.05e-5
0.1203	0.3829	-5.05e-3	1.72e-2	0.3833	-3.99e-5	5.02e-4	0.1022	6.38e-2	8.26e-2	-2.63e-3	8.73e-5	7.13e-5
0.0896	0.3353	-7.37e-3	1.33e-2	0.3356	-5.71e-5	-1.35e-3	7.96e-2	5.41e-2	6.31e-2	-1.56e-3	-5.39e-5	3.46e-4
0.0652	0.3128	-7.41e-3	1.76e-2	0.3134	-5.81e-4	3.98e-3	7.12e-2	4.57e-2	5.87e-2	-1.41e-3	1.71e-4	1.59e-4
0.0380	0.2707	-5.88e-3	2.21e-2	0.2714	2.35e-5	1.02e-2	4.98e-2	3.43e-2	4.51e-2	-4.98e-4	2.03e-4	8.02e-5
0.0099	0.2398	-3.70e-3	3.70e-2	0.2412	4.89e-4	2.65e-2	3.89e-2	1.83e-2	3.84e-2	-1.14e-4	3.11e-5	-7.61e-5

Experiment 14 Laboratory Measurements

H = 0.232 m S = 0.0101 Q = 180 L/s a = 1.09 m^{-1} T = 27.4 °C h_p = 0.115 m

Profile 1

	Raw Velocities			Corrected Velocities			RMS Velocity Fluctuations			Reynolds Stresses		
y (m)	$\bar{u}$ (m/s)	$\bar{v}$ (m/s)	$\bar{w}$ (m/s)	$\bar{u}$ (m/s)	$\bar{v}$ (m/s)	$\bar{w}$ (m/s)	u_{rms} (m/s)	v_{rms} (m/s)	w_{rms} (m/s)	$\overline{u'v'}$ (m^2/s^2)	$\overline{u'w'}$ (m^2/s^2)	$\overline{v'w'}$ (m^2/s^2)
0.1199	0.9597	-5.86e-2	1.06e-2	0.9616	1.10e-4	2.20e-3	0.1220	6.31e-2	9.14e-2	-2.24e-3	-1.92e-3	-9.45e-4
0.1100	0.9514	-6.29e-2	6.97e-3	0.9535	-5.69e-4	-1.33e-3	0.1287	6.20e-2	9.15e-2	-2.74e-3	-1.73e-3	-8.72e-4
0.0945	0.8870	-6.00e-2	6.25e-3	0.8890	-1.86e-3	-1.49e-3	0.1324	6.13e-2	9.25e-2	-3.26e-3	-9.72e-4	-9.38e-4
0.0796	0.8307	-5.38e-2	4.62e-3	0.8345	6.64e-4	-2.63e-3	0.1324	5.96e-2	8.81e-2	-3.59e-3	-3.75e-4	-9.86e-4
0.0644	0.7395	-4.97e-2	2.68e-2	0.7413	-1.25e-3	2.03e-2	0.1273	5.73e-2	9.08e-2	-2.82e-3	-1.53e-3	-4.90e-4
0.0491	0.6772	-5.24e-2	1.34e-2	0.6793	9.25e-4	7.51e-3	0.1107	6.42e-2	7.40e-2	-2.92e-3	-2.19e-4	-6.10e-4
0.0381	0.6198	-2.67e-2	-3.95e-4	0.6203	3.66e-4	-5.80e-3	0.1078	6.01e-2	6.89e-2	-3.23e-3	-4.48e-4	-2.69e-4
0.0174	0.5113	2.96e-3	-4.26e-3	0.5112	7.32e-4	-8.72e-3	8.23e-2	3.98e-2	5.08e-2	-1.55e-3	-9.47e-4	1.81e-4
0.0077	0.4774	4.19e-3	2.73e-3	0.4774	2.35e-5	-1.44e-3	7.83e-2	3.02e-2	5.55e-2	-1.02e-3	-1.19e-3	3.46e-4

Profile 2

	Raw Velocities			Corrected Velocities			RMS Velocity Fluctuations			Reynolds Stresses		
y (m)	$\bar{u}$ (m/s)	$\bar{v}$ (m/s)	$\bar{w}$ (m/s)	$\bar{u}$ (m/s)	$\bar{v}$ (m/s)	$\bar{w}$ (m/s)	u_{rms} (m/s)	v_{rms} (m/s)	w_{rms} (m/s)	$\overline{u'v'}$ (m^2/s^2)	$\overline{u'w'}$ (m^2/s^2)	$\overline{v'w'}$ (m^2/s^2)
0.1202	1.0198	-4.18e-2	2.34e-2	1.0209	-1.77e-3	-3.31e-3	0.1245	5.97e-2	8.62e-2	-2.79e-3	1.33e-3	-1.04e-4
0.1100	0.9605	-3.30e-2	1.94e-2	0.9612	5.10e-4	-5.73e-3	0.1345	6.50e-2	9.07e-2	-4.08e-3	2.28e-3	-2.85e-4
0.0948	0.9029	-1.19e-2	3.61e-2	0.9036	-1.09e-4	1.24e-2	0.1184	6.81e-2	9.70e-2	-3.56e-3	1.76e-3	-5.66e-4
0.0798	0.8051	-5.52e-3	4.84e-2	0.8061	1.50e-3	2.73e-2	0.1353	5.76e-2	8.83e-2	-3.29e-3	1.44e-3	-8.02e-4
0.0648	0.8123	-6.37e-3	-6.58e-3	0.8118	7.20e-4	-2.78e-2	0.1180	6.91e-2	9.79e-2	-1.55e-3	4.02e-4	2.36e-4
0.0497	0.7640	-2.42e-3	2.17e-2	0.7643	9.13e-4	1.70e-3	0.1095	4.77e-2	9.85e-2	-1.66e-3	1.33e-3	1.76e-4
0.0376	0.6833	-1.07e-2	2.71e-2	0.6839	1.22e-3	9.16e-3	0.1051	4.30e-2	8.83e-2	-1.67e-3	1.18e-3	-1.26e-4
0.0179	0.5705	-1.43e-2	1.15e-2	0.5708	6.04e-4	-3.43e-3	8.39e-2	3.73e-2	6.87e-2	-1.09e-3	-1.86e-4	1.29e-6
0.0072	0.5359	-6.68e-3	1.33e-2	0.5361	3.33e-4	-7.40e-4	7.63e-2	3.36e-2	6.54e-2	-6.25e-4	-4.23e-4	-3.96e-6

Profile 3

	Raw Velocities			Corrected Velocities			RMS Velocity Fluctuations			Reynolds Stresses		
y (m)	$\bar{u}$ (m/s)	$\bar{v}$ (m/s)	$\bar{w}$ (m/s)	$\bar{u}$ (m/s)	$\bar{v}$ (m/s)	$\bar{w}$ (m/s)	u_{rms} (m/s)	v_{rms} (m/s)	w_{rms} (m/s)	$\overline{u'v'}$ (m^2/s^2)	$\overline{u'w'}$ (m^2/s^2)	$\overline{v'w'}$ (m^2/s^2)
0.1199	1.0398	-3.81e-2	4.53e-2	1.0415	-1.79e-3	-1.17e-4	0.1156	5.96e-2	8.95e-2	-1.95e-3	1.10e-3	5.45e-4
0.1102	1.0255	-3.48e-2	5.41e-2	1.0274	9.61e-4	9.31e-3	0.1124	5.85e-2	9.24e-2	-2.03e-3	6.71e-4	7.55e-4
0.0952	0.9800	-4.45e-2	5.35e-2	0.9824	-1.67e-3	1.07e-2	0.1244	5.81e-2	9.41e-2	-2.63e-3	6.62e-4	4.06e-4
0.0796	0.9188	-4.61e-2	3.01e-2	0.9304	2.01e-3	-9.98e-3	0.1179	6.27e-2	8.40e-2	-3.10e-3	4.85e-4	2.86e-4
0.0654	0.8652	-3.56e-2	2.75e-2	0.8663	-1.63e-3	-1.02e-2	0.1147	5.64e-2	8.14e-2	-2.79e-3	-4.17e-4	5.60e-4
0.0504	0.7913	-3.97e-2	2.34e-2	0.7926	-1.70e-3	-1.11e-2	0.1118	4.85e-2	7.93e-2	-2.40e-3	-7.78e-4	4.43e-4
0.0373	0.7091	-3.23e-2	2.68e-2	0.7103	-1.29e-3	-4.19e-3	0.1125	4.50e-2	7.26e-2	-2.49e-3	-1.43e-3	4.64e-4
0.0174	0.5984	-1.63e-2	2.82e-2	0.5993	-6.06e-4	2.07e-3	8.98e-2	3.74e-2	5.98e-2	-1.54e-3	-1.31e-3	4.17e-4
0.0074	0.5687	-2.85e-2	3.15e-2	0.5702	-1.19e-3	6.71e-3	8.43e-2	3.15e-2	5.91e-2	-9.73e-4	-9.45e-4	4.13e-4

Profile 4

	Raw Velocities			Corrected Velocities			RMS Velocity Fluctuations			Reynolds Stresses		
y (m)	$\bar{u}$ (m/s)	$\bar{v}$ (m/s)	$\bar{w}$ (m/s)	$\bar{u}$ (m/s)	$\bar{v}$ (m/s)	$\bar{w}$ (m/s)	u_{rms} (m/s)	v_{rms} (m/s)	w_{rms} (m/s)	$\overline{u'v'}$ (m^2/s^2)	$\overline{u'w'}$ (m^2/s^2)	$\overline{v'w'}$ (m^2/s^2)
0.1149	1.0377	1.48e-2	8.88e-2	1.0416	1.24e-3	-1.98e-3	0.1315	6.56e-2	0.1656	-3.84e-3	-1.09e-2	2.83e-3
0.1098	1.0483	1.15e-2	5.41e-2	1.0491	-2.22e-3	-3.74e-2	0.1120	6.12e-2	0.1097	-2.57e-3	-4.00e-3	2.44e-4
0.0948	0.9596	6.70e-3	4.10e-2	0.9595	-1.68e-3	-4.28e-2	0.1292	6.85e-2	9.22e-2	-4.37e-3	7.94e-4	-1.18e-3
0.0803	0.9274	-6.45e-3	8.36e-2	0.9312	1.64e-3	2.48e-3	0.1141	6.81e-2	8.56e-2	-3.46e-3	4.86e-4	-1.64e-3
0.0654	0.8974	-3.53e-2	5.05e-2	0.8991	-8.71e-5	-2.79e-2	0.1061	6.34e-2	8.80e-2	-2.94e-3	1.61e-3	-1.97e-3
0.0497	0.8196	-1.46e-2	2.80e-2	0.8190	-2.58e-4	-4.36e-2	0.1130	5.19e-2	7.98e-2	-2.80e-3	1.21e-3	-6.31e-4
0.0374	0.7154	-1.60e-2	3.20e-2	0.7157	-3.71e-4	-3.04e-2	0.1095	4.82e-2	7.50e-2	-2.65e-3	-2.59e-4	-2.00e-4
0.0178	0.5856	-1.17e-2	3.19e-2	0.5863	1.05e-3	-1.92e-2	9.25e-2	4.28e-2	6.15e-2	-1.85e-3	-2.81e-4	-8.99e-5
0.0079	0.5400	-7.49e-3	3.61e-2	0.5412	-4.17e-4	-1.11e-2	8.80e-2	3.73e-2	6.46e-2	-1.22e-3	-2.84e-4	1.22e-4

Experiment 15 Laboratory Measurements

H = 0.257 m S = 0.0036 Q = 93 L/s a = 1.09 m^{-1} T = 27.7 °C h_p = 0.132 m

Profile 1

	Raw Velocities			Corrected Velocities			RMS Velocity Fluctuations			Reynolds Stresses		
y (m)	$\bar{u}$ (m/s)	$\bar{v}$ (m/s)	$\bar{w}$ (m/s)	$\bar{u}$ (m/s)	$\bar{v}$ (m/s)	$\bar{w}$ (m/s)	u_{rms} (m/s)	v_{rms} (m/s)	w_{rms} (m/s)	$\overline{u'v'}$ (m^2/s^2)	$\overline{u'w'}$ (m^2/s^2)	$\overline{v'w'}$ (m^2/s^2)
0.1852	0.4775	-1.28e-3	2.44e-2	0.4781	8.03e-4	-6.25e-4	8.48e-2	5.06e-2	6.72e-2	-2.00e-3	5.16e-5	1.00e-4
0.1650	0.4446	2.41e-3	3.30e-2	0.4457	4.70e-4	9.67e-3	9.01e-2	5.40e-2	6.47e-2	-2.62e-3	2.50e-4	-1.97e-5
0.1498	0.4013	1.01e-2	4.38e-2	0.4032	-3.76e-4	2.27e-2	9.26e-2	5.23e-2	6.12e-2	-2.67e-3	-4.26e-4	1.94e-4
0.1298	0.3627	-1.53e-2	3.72e-2	0.3645	5.58e-4	1.82e-2	8.49e-2	4.87e-2	6.30e-2	-1.86e-3	4.48e-4	-9.34e-5
0.1101	0.3110	-1.32e-2	8.76e-3	0.3113	3.95e-4	-7.53e-3	8.41e-2	5.04e-2	5.52e-2	-1.85e-3	5.03e-4	1.82e-4
0.0901	0.2546	-7.02e-3	4.13e-3	0.2545	-3.50e-4	-9.20e-3	6.40e-2	4.02e-2	4.68e-2	-5.32e-4	2.86e-4	8.83e-5
0.0719	0.2619	4.74e-3	4.87e-3	0.2618	1.69e-4	-8.84e-3	5.03e-2	3.13e-2	4.27e-2	-2.32e-4	4.53e-4	-1.80e-4
0.0556	0.2721	4.17e-3	7.20e-3	0.2721	-5.84e-4	-7.05e-3	4.09e-2	2.90e-2	3.92e-2	-2.64e-4	2.59e-4	-2.32e-4
0.0356	0.2643	-1.09e-4	1.78e-2	0.2648	-1.09e-4	3.94e-3	4.23e-2	2.43e-2	4.04e-2	-2.23e-4	-9.61e-5	-1.75e-4
0.0101	0.2654	-2.96e-3	1.86e-2	0.2660	5.09e-4	4.67e-3	3.15e-2	1.66e-2	2.77e-2	-9.96e-5	4.20e-5	-8.95e-5

Profile 2

	Raw Velocities			Corrected Velocities			RMS Velocity Fluctuations			Reynolds Stresses		
y (m)	$\bar{u}$ (m/s)	$\bar{v}$ (m/s)	$\bar{w}$ (m/s)	$\bar{u}$ (m/s)	$\bar{v}$ (m/s)	$\bar{w}$ (m/s)	u_{rms} (m/s)	v_{rms} (m/s)	w_{rms} (m/s)	$\overline{u'v'}$ (m^2/s^2)	$\overline{u'w'}$ (m^2/s^2)	$\overline{v'w'}$ (m^2/s^2)
0.1853	0.4805	-6.17e-3	1.36e-2	0.4807	1.20e-4	1.06e-3	8.38e-2	4.78e-2	6.10e-2	-1.66e-3	-1.61e-4	-1.30e-4
0.1648	0.4340	-5.45e-3	1.09e-2	0.4342	2.35e-4	-4.42e-4	8.28e-2	5.11e-2	6.15e-2	-2.07e-3	5.11e-5	-3.13e-4
0.1500	0.4111	-4.56e-3	1.12e-2	0.4112	8.25e-4	3.92e-4	8.55e-2	5.02e-2	6.04e-2	-2.28e-3	1.50e-4	-2.55e-4
0.0129	0.3545	-5.61e-3	1.47e-2	0.3548	5.75e-4	5.37e-3	8.95e-2	4.57e-2	5.89e-2	-2.17e-3	-9.45e-4	-2.77e-4
0.1101	0.2680	-1.73e-3	1.17e-2	0.2682	-5.58e-4	4.69e-3	8.12e-2	4.64e-2	5.20e-2	-1.57e-3	-7.08e-4	8.36e-6
0.0903	0.2295	-5.02e-4	7.84e-3	0.2296	-5.02e-4	1.83e-3	6.42e-2	4.01e-2	4.85e-2	-7.66e-4	-7.49e-4	1.20e-4
0.0721	0.2408	5.50e-3	1.15e-2	0.2411	2.42e-4	5.20e-3	5.13e-2	3.54e-2	4.29e-2	-4.54e-4	-2.79e-4	1.82e-4
0.0545	0.2323	1.10e-2	1.20e-2	0.2328	-1.80e-4	5.88e-3	4.15e-2	2.92e-2	3.78e-2	-2.12e-4	-2.21e-4	1.46e-4
0.0351	0.2228	1.14e-2	1.11e-2	0.2233	-2.52e-4	5.24e-3	4.64e-2	2.61e-2	4.17e-2	-2.54e-4	-3.53e-4	1.94e-4
0.0102	0.2200	1.50e-2	2.28e-2	0.2210	-3.74e-4	1.71e-2	2.88e-2	1.70e-2	2.90e-2	-1.33e-4	-1.17e-4	9.06e-5

Profile 3

	Raw Velocities			Corrected Velocities			RMS Velocity Fluctuations			Reynolds Stresses		
y (m)	$\bar{u}$ (m/s)	$\bar{v}$ (m/s)	$\bar{w}$ (m/s)	$\bar{u}$ (m/s)	$\bar{v}$ (m/s)	$\bar{w}$ (m/s)	u_{rms} (m/s)	v_{rms} (m/s)	w_{rms} (m/s)	$\overline{u'v'}$ (m^2/s^2)	$\overline{u'w'}$ (m^2/s^2)	$\overline{v'w'}$ (m^2/s^2)
0.1854	0.4594	5.17e-3	1.57e-2	0.4597	-8.47e-4	-3.34e-4	8.24e-2	4.79e-2	6.08e-2	-1.80e-3	7.56e-4	-1.79e-4
0.1649	0.4206	9.62e-3	1.59e-2	0.4210	4.37e-4	1.23e-3	8.08e-2	4.90e-2	5.82e-2	-1.99e-3	1.07e-3	-1.54e-4
0.1500	0.3912	1.93e-2	4.87e-3	0.3916	4.78e-4	-8.78e-3	8.38e-2	4.88e-2	5.74e-2	-2.20e-3	1.23e-3	-2.54e-4
0.1296	0.2822	4.06e-3	9.80e-3	0.2824	3.68e-4	-5.23e-5	0.1233	4.90e-2	7.68e-2	-3.12e-3	2.54e-4	-2.18e-4
0.1100	0.2830	7.85e-3	3.08e-2	0.2840	4.38e-4	2.09e-2	7.09e-2	5.03e-2	5.68e-2	-1.74e-3	1.08e-3	-6.09e-4
0.0900	0.2680	3.59e-4	3.17e-2	0.2689	3.59e-4	2.23e-2	5.17e-2	3.39e-2	4.40e-2	-4.26e-4	-9.79e-6	-1.78e-4
0.0724	0.2691	1.79e-3	3.02e-2	0.2700	-5.56e-4	2.08e-2	4.11e-2	2.66e-2	3.52e2	-1.82e-4	-7.75e-6	-5.91e-5
0.0558	0.2671	-2.54e-3	3.80e-2	0.2683	-2.06e-4	2.86e-2	3.16e-2	2.11e-2	2.93e-2	-9.27e-5	-1.55e-5	-5.75e-5
0.0368	0.2630	-1.56e-2	6.62e-2	0.2646	5.17e-4	2.70e-2	3.58e-2	1.84e-2	3.30e-2	-5.25e-5	-1.68e-4	2.23e-5
0.0099	0.2465	-1.24e-2	-1.36e-2	0.2461	5.27e-4	-2.22e-2	2.89e-2	1.47e-2	2.78e-2	-6.17e-5	1.76e-4	-3.71e-5

Profile 4

	Raw Velocities			Corrected Velocities			RMS Velocity Fluctuations			Reynolds Stresses		
y (m)	$\bar{u}$ (m/s)	$\bar{v}$ (m/s)	$\bar{w}$ (m/s)	$\bar{u}$ (m/s)	$\bar{v}$ (m/s)	$\bar{w}$ (m/s)	u_{rms} (m/s)	v_{rms} (m/s)	w_{rms} (m/s)	$\overline{u'v'}$ (m^2/s^2)	$\overline{u'w'}$ (m^2/s^2)	$\overline{v'w'}$ (m^2/s^2)
0.1822	0.4450	-1.63e-3	2.80e-2	0.4459	3.16e-4	8.17e-4	8.09e-2	4.58e-2	5.82e-2	-1.72e-3	-3.13e-4	1.97e-4
0.1646	0.4045	-3.25e-3	2.63e-2	0.4054	2.76e-4	1.57e-3	8.73e-2	4.65e-2	5.79e-2	-2.14e-3	-2.25e-5	1.46e-4
0.1501	0.3552	-2.80e-3	2.29e-2	0.3560	3.02e-4	1.21e-3	8.98e-2	4.73e-2	5.70e-2	-2.36e-3	-2.21e-4	3.38e-4
0.1295	0.2698	-1.74e-3	2.44e-2	0.2708	-5.66e-4	7.88e-3	8.75e-2	4.69e-2	5.35e-2	-2.06e-3	-2.69e-4	9.89e-5
0.1099	0.2031	7.61e-3	2.01e-2	0.2041	-3.74e-4	7.67e-3	6.10e-2	4.09e-2	4.65e-2	-5.04e-4	-4.75e-4	-3.14e-5
0.0901	0.1997	5.50e-3	1.54e-2	0.2003	2.74e-4	3.17e-3	5.31e-2	2.88e-2	4.69e-2	-2.93e-5	-6.73e-4	1.00e-5
0.0726	0.2290	1.01e-2	1.45e-2	0.2297	6.58e-5	5.23e-4	3.88e-2	2.52e-2	3.73e-2	3.26e-5	-2.11e-4	8.44e-5
0.0554	0.2405	9.15e-3	1.14e-2	0.2409	-3.00e-4	-3.27e-3	3.09e-2	2.01e-2	3.17e-2	2.35e-5	-7.97e-5	1.30e-4
0.0362	0.2346	3.28e-3	9.46e-3	0.2348	2.07e-4	-4.88e-3	3.62e-2	1.68e-2	3.71e-2	-2.23e-5	-2.16e-4	8.71e-5
0.0104	0.2358	9.35e-4	4.15e-3	0.2356	9.40e-5	-1.03e-2	2.27e-2	1.22e-2	2.33e-2	4.43e-6	2.42e-5	4.53e-5

Experiment 16 Laboratory Measurements

H = 0.230 m S = 0.0036 Q = 179 L/s a = 0.273 m^{-1} T = 26.9 °C h_p = 0.097 m

Profile 1

	Raw Velocities			Corrected Velocities			RMS Velocity Fluctuations			Reynolds Stresses		
y	$\bar{u}$	$\bar{v}$	$\bar{w}$	$\bar{u}$	$\bar{v}$	$\bar{w}$	u_{rms}	v_{rms}	w_{rms}	$\overline{u'v'}$	$\overline{u'w'}$	$\overline{v'w'}$
(m)	(m/s)	(m/s)	(m/s)	(m/s)	(m/s)	(m/s)	(m/s)	(m/s)	(m/s)	(m^2/s^2)	(m^2/s^2)	(m^2/s^2)
0.1206	0.8921	-2.13e-2	6.92e-2	0.8950	-1.81e-3	-9.59e-4	9.09e-2	4.38e-2	7.56e-2	-1.51e-3	-7.61e-4	2.07e-4
0.1100	0.8752	-2.42e-2	5.62e-2	0.8772	-1.30e-3	-1.26e-2	9.06e-2	4.16e-2	6.59e-2	-1.47e-3	-1.60e-4	-6.83e-5
0.0996	0.8443	-2.13e-2	5.53e-2	0.8463	8.10e-4	-1.11e-2	9.41e-2	4.10e-2	6.60e-2	-1.69e-3	-2.37e-4	-1.38e-5
0.0852	0.8063	-2.16e-2	5.17e-2	0.8081	-4.58e-4	-1.17e-2	9.61e-2	3.91e-2	6.22e-2	-1.59e-3	-4.01e-4	-6.34e-5
0.0699	0.7637	-1.70e-2	4.29e-2	0.7649	-3.17e-4	-1.72e-2	9.85e-2	4.18e-2	6.10e-2	-2.05e-3	-2.70e-4	-2.30e-5
0.0597	0.7232	-1.11e-2	3.84e-2	0.7241	1.56e-3	-1.85e-2	8.86e-2	3.92e-2	6.14e-2	-1.47e-3	-2.84e-4	-9.12e-5
0.0501	0.6858	-4.17e-3	3.50e-2	0.6864	-1.18e-3	-1.89e-2	8.43e-2	3.78e-2	6.05e-2	-1.29e-3	-2.81e-4	-1.49e-4
0.0380	0.6547	-1.63e-3	3.70e-2	0.6556	1.22e-3	-1.45e-2	7.85e-2	3.39e-2	5.98e-2	-8.92e-4	-1.93e-4	-8.70e-5
0.0180	0.6108	-1.09e-3	3.45e-2	0.6117	-1.09e-3	-1.35e-2	7.58e-2	3.12e-2	4.62e-2	-9.76e-4	3.00e-4	-2.09e-4
0.0075	0.5947	1.27e-3	3.73e-2	0.5958	1.27e-3	-9.52e-3	8.12e-2	2.85e-2	4.86e-2	-8.34e-4	1.63e-4	-1.25e-4

Profile 2

	Raw Velocities			Corrected Velocities			RMS Velocity Fluctuations			Reynolds Stresses		
y	$\bar{u}$	$\bar{v}$	$\bar{w}$	$\bar{u}$	$\bar{v}$	$\bar{w}$	u_{rms}	v_{rms}	w_{rms}	$\overline{u'v'}$	$\overline{u'w'}$	$\overline{v'w'}$
(m)	(m/s)	(m/s)	(m/s)	(m/s)	(m/s)	(m/s)	(m/s)	(m/s)	(m/s)	(m^2/s^2)	(m^2/s^2)	(m^2/s^2)
0.1201	0.8535	-1.98e-2	4.28e-2	0.8548	-1.16e-3	-1.89e-3	8.62e-2	4.20e-2	6.83e-2	-1.35e-3	-3.65e-4	1.11e-5
0.1096	0.8530	-1.89e-2	3.88e-2	0.8540	-3.02e-4	-5.94e-3	8.73e-2	4.14e-2	6.86e-2	-1.42e-3	-2.82e-4	-1.32e-5
0.1000	0.8375	-2.40e-2	4.10e-2	0.8389	1.54e-3	-2.93e-3	8.97e-2	3.97e-2	6.96e-2	-1.23e-3	-1.16e-4	-1.09e5
0.0853	0.8160	-2.92e-2	3.45e-2	0.8172	-7.44e-4	-8.25e-3	8.42e-2	3.86e-2	6.67e-2	-1.20e-3	1.25e-4	-1.31e-4
0.0701	0.7901	-3.26e-2	3.10e-2	0.7914	-1.56e-3	-1.04e-2	8.78e-2	3.83e-2	6.63e-2	-1.10e-3	-1.98e-4	-7.52e-5
0.0599	0.7719	-3.39e-2	3.03e-2	0.7731	-2.45e-4	-1.01e-2	8.46e-2	3.53e-2	6.34e-2	-9.91e-4	-3.00e-5	-9.67e-5
0.0503	0.7518	-3.62e-2	2.74e-2	0.7531	-6.03e-5	-1.19e-2	8.22e-2	3.33e-2	6.08e-2	-9.07e-4	-1.45e-4	-4.48e-5
0.0375	0.7106	-3.46e-2	2.65e-2	0.7119	-4.81e-4	-1.07e-2	8.18e-2	3.23e-2	6.09e-2	-9.29e-4	-3.98e-4	-3.18e-5
0.0176	0.6751	-3.07e-2	2.90e-2	0.6764	-1.26e-3	-6.35e-3	7.58e-2	2.86e-2	4.62e-2	-7.81e-4	-3.16e-4	-6.15e-5
0.0071	0.6464	-2.38e-2	2.82e-2	0.6475	-1.19e-3	-5.70e-3	7.98e-2	2.57e-2	4.69e-2	-6.91e-4	-1.74e-4	-2.44e-5

Profile 3

	Raw Velocities			Corrected Velocities			RMS Velocity Fluctuations			Reynolds Stresses		
y	$\bar{u}$	$\bar{v}$	$\bar{w}$	$\bar{u}$	$\bar{v}$	$\bar{w}$	u_{rms}	v_{rms}	w_{rms}	$\overline{u'v'}$	$\overline{u'w'}$	$\overline{v'w'}$
(m)	(m/s)	(m/s)	(m/s)	(m/s)	(m/s)	(m/s)	(m/s)	(m/s)	(m/s)	(m^2/s^2)	(m^2/s^2)	(m^2/s^2)
0.1204	0.9072	1.51e-2	4.86e-2	0.9086	-7.58e-4	1.02e-3	8.41e-2	4.40e-2	6.79e-2	-1.21e-3	-4.08e-4	-9.11e-5
0.1100	0.8980	8.87e-3	4.27e-2	0.8991	1.04e-3	-4.35e-3	9.24e-2	4.32e-2	6.82e-2	-1.35e-3	-7.46e-4	-1.44e-5
0.1000	0.8786	8.91e-3	4.06e-2	0.8796	1.24e-3	-5.45e-3	9.01e-2	4.22e-2	6.82e-2	-1.31e-3	-6.81e-4	-3.05e-5
0.0851	0.8520	1.21e-3	2.95e-2	0.8523	1.21e-3	-1.51e-2	8.88e-2	4.34e-2	6.82e-2	-1.51e-3	-4.26e-4	-2.91e-5
0.0697	0.8225	-1.18e-3	2.09e-2	0.8225	-1.18e-3	-2.22e-2	9.02e-2	4.20e-2	6.53e-2	-1.63e-3	-1.69e-4	8.77e-5
0.0603	0.7942	-2.43e-3	1.24e-2	0.7937	1.03e-3	-2.92e-2	8.89e-2	4.01e-2	6.43e-2	-1.53e-3	-2.78e-4	4.83e-5
0.0499	0.7678	-3.37e-3	7.28e-3	0.7672	-1.84e-5	-3.29e-2	8.84e-2	3.97e-2	6.22e-2	-1.52e-3	-1.41e-4	4.62e-5
0.0376	0.7280	-6.57e-3	1.96e-3	0.7272	-2.12e-4	-3.61e-2	8.47e-2	3.71e-2	5.90e-2	-1.36e-3	-5.22e-4	-2.49e-5
0.0171	0.7077	-1.05e-2	-2.25e-3	0.7067	-1.28e-3	-3.93e-2	7.86e-2	3.21e-2	4.86e-2	-1.03e-3	-5.58e-4	7.33e-6
0.0072	0.6927	-6.43e-3	-1.55e-3	0.6947	-3.88e-4	-3.78e-2	7.95e-2	2.60e-2	4.73e-2	-7.90e-4	-2.82e-4	1.82e-5

Profile 4

	Raw Velocities			Corrected Velocities			RMS Velocity Fluctuations			Reynolds Stresses		
y	$\bar{u}$	$\bar{v}$	$\bar{w}$	$\bar{u}$	$\bar{v}$	$\bar{w}$	u_{rms}	v_{rms}	w_{rms}	$\overline{u'v'}$	$\overline{u'w'}$	$\overline{v'w'}$
(m)	(m/s)	(m/s)	(m/s)	(m/s)	(m/s)	(m/s)	(m/s)	(m/s)	(m/s)	(m^2/s^2)	(m^2/s^2)	(m^2/s^2)
0.1134	0.9027	-2.78e-2	2.79e-2	0.9036	-2.98e-4	-3.66e-3	9.34e-2	4.10e-2	6.54e-2	-1.49e-3	-4.48e-4	-2.07e-4
0.1097	0.9007	-2.66e-2	2.81e-2	0.9016	9.37e-4	-3.30e-3	9.17e-2	4.16e-2	6.55e-2	-1.45e-3	-4.15e-4	-2.62e-4
0.1004	0.8803	-2.63e-2	2.06e-2	0.8809	6.06e-4	-1.01e-2	9.61e-2	4.23e-2	6.60e-2	-1.68e-3	-7.05e-4	-2.39e-4
0.0850	0.8396	-2.88e-2	1.63e-2	0.8402	4.75e-4	-1.30e-2	8.88e-2	3.91e-2	6.63e-2	-1.29e-3	-1.55e-4	-1.83e-4
0.0070	0.8160	-3.66e-2	2.70e-2	0.8172	-9.69e-4	-1.52e-3	8.98e-2	4.18e-2	6.28e-2	-1.37e-3	-4.26e-4	-3.22e-4
0.0603	0.7898	-3.06e-2	2.73e-2	0.7909	4.71e-4	-2.80e-4	8.56e-2	4.05e-2	6.03e-2	-1.33e-3	-1.10e-4	-3.58e-4
0.0500	0.7647	-2.73e-2	2.17e-2	0.7655	-5.46e-4	-5.03e-3	8.87e-2	3.78e-2	5.99e-2	-1.42e-3	-2.21e-4	-2.92e-4
0.0377	0.7114	-2.17e-2	1.55e-2	0.7118	7.87e-5	-9.37e-3	9.16e-2	3.74e-2	5.75e-2	-1.62e-3	3.75e-4	-2.14e-4
0.0173	0.6543	-1.22e-2	6.68e-3	0.6542	-7.98e-4	-1.62e-2	8.58e-2	3.42e-2	4.81e-2	-1.26e-3	8.85e-4	-3.49e-4
0.0078	0.6402	-3.64e-3	7.07e-3	0.6401	-8.50e-4	-1.53e-2	8.29e-2	2.99e-2	4.78e-2	-9.54e-4	6.51e-4	-2.70e-4

Experiment 17 Laboratory Measurements

H = 0.279 m S = 0.0036 Q = 78 L/s $a = 2.46\ m^{-1}$ T = 26.7 °C $h_p = 0.161$ m

Profile 1

	Raw Velocities			Corrected Velocities			RMS Velocity Fluctuations			Reynolds Stresses		
y (m)	$\bar{u}$ (m/s)	$\bar{v}$ (m/s)	$\bar{w}$ (m/s)	$\bar{u}$ (m/s)	$\bar{v}$ (m/s)	$\bar{w}$ (m/s)	u_{rms} (m/s)	v_{rms} (m/s)	w_{rms} (m/s)	$\overline{u'v'}$ (m^2/s^2)	$\overline{u'w'}$ (m^2/s^2)	$\overline{v'w'}$ (m^2/s^2)
0.2048	0.4234	-5.73e-3	1.94e-2	0.4239	-1.90e-4	8.87e-4	8.64e-2	5.39e-2	6.74e-2	-2.18e-3	6.14e-4	2.12e-4
0.1799	0.3429	4.02e-3	1.57e-2	0.3432	-4.71e-4	7.12e-4	8.90e-2	5.39e-2	6.48e-2	-2.29e-3	8.19e-4	6.86e-5
0.1654	0.3019	-1.73e-4	3.22e-3	0.3017	-1.73e-4	-9.95e-3	9.70e-2	5.13e-2	6.39e-2	-2.64e-3	1.30e-3	-5.43e-6
0.1547	0.2743	-5.02e-3	3.46e-3	0.2742	-2.36e-4	-8.51e-3	9.20e-2	5.14e-2	5.83e-2	-2.46e-3	9.22e-4	1.59e-4
0.1404	0.2414	-5.58e-3	1.40e-2	0.2419	-3.12e-4	3.42e-3	7.68e-2	4.99e-2	5.25e-2	-1.81e-3	6.71e-4	1.17e-4
0.1148	0.1913	-4.63e-3	2.42e-2	0.1922	3.77e-4	1.58e-2	5.17e-2	3.70e-2	4.18e-2	-8.14e-4	3.74e-4	-1.46e-4
0.0902	0.1733	-4.77e-3	2.33e-2	0.1742	-2.34e-4	1.58e-2	3.42e-2	2.51e-2	3.19e-2	-1.91e-4	1.33e-4	-1.28e-4
0.0650	0.1656	-1.59e-3	1.97e-2	0.1663	-1.50e-4	1.24e-2	2.72e-2	1.77e-2	2.75e-2	-3.63e-5	3.47e-5	-5.10e-5
0.0394	0.1633	-9.14e-4	1.57e-2	0.1639	-2.02e-4	8.56e-3	2.35e-2	1.35e-2	2.47e-2	-2.03e-5	4.38e-7	-1.42e-5
0.0107	0.1538	-4.34e-5	9.07e-3	0.1540	-4.34e-5	2.36e-3	2.68e-2	1.23e-2	2.68e-2	-1.13e-5	7.72e-5	-3.42e-5

Profile 2

	Raw Velocities			Corrected Velocities			RMS Velocity Fluctuations			Reynolds Stresses		
y (m)	$\bar{u}$ (m/s)	$\bar{v}$ (m/s)	$\bar{w}$ (m/s)	$\bar{u}$ (m/s)	$\bar{v}$ (m/s)	$\bar{w}$ (m/s)	u_{rms} (m/s)	v_{rms} (m/s)	w_{rms} (m/s)	$\overline{u'v'}$ (m^2/s^2)	$\overline{u'w'}$ (m^2/s^2)	$\overline{v'w'}$ (m^2/s^2)
0.2049	0.3918	1.66e-3	1.22e-2	0.3920	-4.58e-5	-1.46e-3	8.70e-2	5.36e-2	6.68e-2	-2.24e-3	4.28e-5	-1.69e-4
0.1800	0.3395	-2.16e-3	1.50e-2	0.3398	-6.77e-4	3.17e-3	9.54e-2	5.62e-2	7.05e-2	-3.03e-3	-4.83e-4	-3.33e-4
0.1645	0.2823	-2.76e-4	9.00e-3	0.2824	-2.76e-4	-8.57e-4	9.04e-2	5.37e-2	6.34e-2	-2.53e-3	-1.30e-3	-9.79e-5
0.1556	0.2659	-3.09e-3	9.23e-3	0.2661	3.87e-4	-5.10e-5	8.63e-2	5.23e-2	6.34e-2	-1.88e-3	-1.74e-3	3.19e-5
0.1394	0.2407	-8.53e-3	7.89e-3	0.2410	-1.21e-4	-5.12e-4	8.33e-2	4.87e-2	5.79e-2	-1.94e-3	-1.54e-3	4.48e-4
0.1146	0.1810	-7.17e-3	4.24e-3	0.1811	-6.06e-5	-2.08e-3	5.88e-2	3.71e-2	4.92e-2	-7.66e-4	8.09e-5	3.08e-4
0.0905	0.1580	-6.02e-3	7.61e-3	0.1583	1.86e-4	2.09e-3	3.95e-2	3.02e-2	3.58e-2	-3.42e-4	1.77e-4	1.13e-4
0.0650	0.1470	-3.98e-3	8.95e-3	0.1473	-1.35e-4	3.81e-3	3.28e-2	1.98e-2	3.27e-2	-7.83e-5	2.41e-4	8.89e-6
0.0404	0.1409	-3.95e-3	1.00e-2	0.1412	-2.64e-4	5.07e-3	2.81e-2	1.53e-2	2.70e-2	5.58e-6	1.78e-4	3.29e-5
0.0099	0.1417	-4.11e-3	1.23e-2	0.1421	2.16e-4	7.30e-3	3.16e-2	1.32e-2	3.35e-2	-5.32e-5	1.29e-4	-1.24e-5

Profile 3

	Raw Velocities			Corrected Velocities			RMS Velocity Fluctuations			Reynolds Stresses		
y (m)	$\bar{u}$ (m/s)	$\bar{v}$ (m/s)	$\bar{w}$ (m/s)	$\bar{u}$ (m/s)	$\bar{v}$ (m/s)	$\bar{w}$ (m/s)	u_{rms} (m/s)	v_{rms} (m/s)	w_{rms} (m/s)	$\overline{u'v'}$ (m^2/s^2)	$\overline{u'w'}$ (m^2/s^2)	$\overline{v'w'}$ (m^2/s^2)
0.2045	0.4123	-1.17e-3	2.09e-2	0.4128	6.32e-4	-7.40e-4	9.01e-2	5.12e-2	6.51e-2	-2.00e-3	6.95e-4	-2.67e-6
0.1807	0.3621	5.48e-4	2.23e-2	0.3627	5.48e-4	3.33e-3	9.63e-2	5.45e-2	6.70e-2	-2.81e-3	1.35e-3	-1.02e-4
0.1648	0.3061	3.59e-3	2.00e-2	0.3068	-4.21e-4	3.96e-3	9.04e-2	5.30e-2	5.99e-2	-2.78e-3	1.13e-3	-5.33e-5
0.1553	0.2944	2.66e-3	2.25e-2	0.2951	8.91e-5	7.11e-3	8.35e-2	5.15e-2	6.15e-2	-2.18e-3	1.49e-3	-1.59e-4
0.1400	0.2673	-5.16e-3	2.89e-2	0.2684	-4.97e-4	1.18e-2	7.69e-2	4.66e-2	5.67e-2	-1.75e-3	1.19e-3	-8.01e-5
0.1149	0.1554	7.53e-3	1.56e-2	0.1562	6.44e-5	7.41e-3	5.17e-2	4.08e-2	5.41e-2	-5.43e-4	-1.96e-4	8.77e-5
0.0900	0.1511	1.42e-2	1.27e-2	0.1522	2.75e-4	4.82e-3	3.84e-2	2.71e-2	4.44e-2	-1.86e-4	-2.48e-4	1.36e-4
0.0648	0.1551	1.12e-2	1.16e-2	0.1559	-3.06e-4	3.42e-3	3.23e-2	2.04e-2	3.68e-2	-8.37e-5	-1.34e-4	7.44e-5
0.0399	0.1552	1.13e-2	1.32e-2	0.1561	-2.66e-4	5.04e-3	2.70e-2	1.69e-2	2.95e-2	-7.56e-5	-1.02e-4	6.98e-5
0.0095	0.1626	6.25e-3	1.03e-2	0.1630	-1.42e-4	1.76e-3	2.63e-2	1.29e-2	2.94e-2	-4.66e-5	-1.15e-4	8.56e-5

Profile 4

	Raw Velocities			Corrected Velocities			RMS Velocity Fluctuations			Reynolds Stresses		
y (m)	$\bar{u}$ (m/s)	$\bar{v}$ (m/s)	$\bar{w}$ (m/s)	$\bar{u}$ (m/s)	$\bar{v}$ (m/s)	$\bar{w}$ (m/s)	u_{rms} (m/s)	v_{rms} (m/s)	w_{rms} (m/s)	$\overline{u'v'}$ (m^2/s^2)	$\overline{u'w'}$ (m^2/s^2)	$\overline{v'w'}$ (m^2/s^2)
0.2039	0.4104	-1.57e-3	1.77e-2	0.4108	2.23e-4	-2.08e-4	8.34e-2	4.93e-2	6.65e-2	-1.63e-2	3.16e-4	-1.10e-5
0.1798	0.3512	-5.14e-3	1.73e-2	0.3516	-5.38e-4	1.99e-3	9.25e-2	5.32e-2	6.71e-2	-2.80e-3	9.75e-5	-5.34e-5
0.1648	0.3020	-5.48e-3	1.77e-2	0.3026	-2.07e-4	4.47e-3	8.72e-2	5.15e-2	6.52e-2	-2.40e-3	4.73e-4	8.96e-5
0.1544	0.2715	-1.14e-2	1.13e-2	0.2720	4.74e-4	-5.93e-4	7.96e-2	4.68e-2	6.57e-2	-1.79e-3	3.30e-4	1.20e-4
0.1410	0.2243	-2.21e-2	9.41e-4	0.2253	4.40e-4	-8.85e-3	7.86e-2	4.34e-2	6.65e-2	-1.40e-3	6.70e-6	-4.11e-4
0.1152	0.1545	-1.01e-2	1.27e-3	0.1547	6.15e-5	-5.47e-3	5.92e-2	3.72e-2	5.60e-2	-3.66e-4	-8.67e-4	-2.95e-5
0.0899	0.1548	-9.37e-3	4.52e-4	0.1549	1.01e-4	-6.30e-3	4.22e-2	2.84e-2	3.87e-2	-2.07e-4	-3.32e-4	2.99e-5
0.0645	0.1526	-4.65e-3	-2.57e-3	0.1525	1.27e-5	-9.22e-3	3.35e-2	2.08e-2	3.37e-2	-1.48e-5	-7.63e-5	-1.40e-5
0.0405	0.1588	-1.86e-3	4.56e-5	0.1586	2.17e-4	-6.88e-3	2.87e-2	1.64e-2	2.75e-2	2.51e-5	-1.16e-5	-8.83e-6
0.0102	0.1663	1.06e-2	-5.98e-3	0.1662	-3.29e-4	-1.32e-2	3.16e-2	1.46e-2	2.97e-2	-6.16e-5	2.37e-6	-7.83e-5

Experiment 18 Laboratory Measurements

H = 0.284 m S = 0.0101 Q = 179 L/s $a = 2.46\ m^{-1}$ T = 27.3 °C $h_p = 0.121$ m

Profile 1

	Raw Velocities			Corrected Velocities			RMS Velocity Fluctuations			Reynolds Stresses		
y (m)	$\bar{u}$ (m/s)	$\bar{v}$ (m/s)	$\bar{w}$ (m/s)	$\bar{u}$ (m/s)	$\bar{v}$ (m/s)	$\bar{w}$ (m/s)	u_{rms} (m/s)	v_{rms} (m/s)	w_{rms} (m/s)	$\overline{u'v'}$ (m^2/s^2)	$\overline{u'w'}$ (m^2/s^2)	$\overline{v'w'}$ (m^2/s^2)
0.1757	0.9008	-1.35e-2	3.86e-2	0.9017	-1.73e-3	-7.22e-4	0.1487	8.80e-2	0.1243	-4.83e-3	7.09e-5	-3.79e-4
0.1601	0.8655	-1.76e-2	3.60e-2	0.8664	1.26e-3	-1.78e-3	0.1593	8.65e-2	0.1212	-5.22e-3	-4.76e-5	-4.83e-4
0.1454	0.8066	-1.23e-2	3.20e-2	0.8073	1.76e-3	-3.23e-3	0.1691	8.82e-2	0.1223	-6.98e-3	5.02e-4	-3.54e-4
0.1353	0.7827	-1.84e-2	2.56e-2	0.7833	-1.31e-3	-8.58e-3	0.1694	8.88e-2	0.1224	-7.65e-3	6.26e-4	-6.57e-4
0.1203	0.6865	-1.67e-2	2.62e-2	0.6872	1.25e-3	-3.75e-3	0.1755	8.79e-2	0.1206	-7.92e-3	1.41e-3	-1.02e-4
0.1001	0.5908	-1.15e-2	4.64e-2	0.5924	-1.15e-3	2.06e-2	0.1507	8.37e-2	0.1109	-6.33e-3	8.47e-4	-2.61e-4
0.0801	0.5121	-3.96e-2	5.82e-2	0.5157	6.73e-4	3.58e-2	0.1266	6.97e-2	0.1032	-3.15e-3	8.85e-4	-1.30e-3
0.0572	0.4568	-3.06e-2	3.33e-2	0.4588	-6.66e-4	1.33e-2	0.1009	5.56e-2	7.36e-2	-1.91e-3	-5.51e-4	1.98e-4
0.0375	0.3719	-1.86e-2	5.21e-2	0.3743	-7.14e-4	3.59e-2	8.71e-2	4.25e-2	7.23e-2	-1.19e-3	-9.72e-4	1.61e-4
0.0103	0.3241	-1.46e-2	5.39e-2	0.3265	-3.99e-4	3.97e-2	6.35e-2	2.89e-2	4.53e-2	-4.33e-4	-4.24e-4	1.88e-5

Profile 2

	Raw Velocities			Corrected Velocities			RMS Velocity Fluctuations			Reynolds Stresses		
y (m)	$\bar{u}$ (m/s)	$\bar{v}$ (m/s)	$\bar{w}$ (m/s)	$\bar{u}$ (m/s)	$\bar{v}$ (m/s)	$\bar{w}$ (m/s)	u_{rms} (m/s)	v_{rms} (m/s)	w_{rms} (m/s)	$\overline{u'v'}$ (m^2/s^2)	$\overline{u'w'}$ (m^2/s^2)	$\overline{v'w'}$ (m^2/s^2)
0.1748	0.9195	-2.67e-2	5.07e-2	0.9212	1.36e-3	2.47e-3	0.1488	8.34e-2	0.1137	-4.56e-3	1.03e-3	4.06e-4
0.1600	0.8794	-2.76e-2	4.79e-2	0.8811	-7.10e-4	1.77e-3	0.1556	8.54e-2	0.1176	-5.23e-3	1.76e-3	4.78e-4
0.1448	0.8170	-2.65e-2	5.23e-2	0.8190	-1.54e-3	9.47e-3	0.1643	8.81e-2	0.1194	-6.67e-3	4.08e-4	7.12e-4
0.1351	0.7873	-3.13e-2	5.46e-2	0.7897	-3.63e-4	1.33e-2	0.1724	8.31e-2	0.1178	-6.74e-3	-3.71e-4	4.60e-4
0.1201	0.7116	-3.26e-2	4.54e-2	0.7137	-1.52e-3	8.05e-3	0.1754	8.20e-2	0.1127	-7.31e-3	-9.83e-4	4.50e-4
0.1000	0.5755	-3.11e-2	4.01e-2	0.5776	-9.72e-4	9.90e-3	0.1784	8.23e-2	0.1119	-7.75e-3	-3.36e-3	2.21e-4
0.0798	0.4700	-2.58e-2	5.04e-3	0.4703	8.57e-4	-1.96e-2	0.1400	8.22e-2	9.14e-2	-5.68e-3	-1.45e-3	2.14e-4
0.0570	0.3800	-2.78e-2	5.10e-3	0.3807	4.76e-4	-1.48e-2	0.1188	6.76e-2	8.88e-2	-2.73e-3	-1.81e-3	6.10e-4
0.0377	0.3216	6.92e-3	5.52e-2	0.3241	-1.01e-4	3.83e-2	8.16e-2	4.88e-2	6.99e-2	-1.55e-3	2.05e-5	-3.33e-4
0.0096	0.3030	8.83e-3	3.40e-3	0.3029	-4.27e-4	-1.25e-2	5.04e-2	2.74e-2	4.80e-2	-2.72e-4	2.45e-4	-3.25e-4

Profile 3

	Raw Velocities			Corrected Velocities			RMS Velocity Fluctuations			Reynolds Stresses		
y (m)	$\bar{u}$ (m/s)	$\bar{v}$ (m/s)	$\bar{w}$ (m/s)	$\bar{u}$ (m/s)	$\bar{v}$ (m/s)	$\bar{w}$ (m/s)	u_{rms} (m/s)	v_{rms} (m/s)	w_{rms} (m/s)	$\overline{u'v'}$ (m^2/s^2)	$\overline{u'w'}$ (m^2/s^2)	$\overline{v'w'}$ (m^2/s^2)
0.1756	0.8888	-2.31e-2	2.48e-2	0.8894	2.12e-4	1.57e-3	0.1375	8.20e-2	0.1114	-3.02e-3	-2.67e-3	-1.62e-3
0.1609	0.8510	-2.14e-2	1.86e-2	0.8515	8.89e-4	-3.67e-3	0.1427	8.44e-2	0.1124	-3.99e-3	-2.26e-3	-1.58e-3
0.1449	0.8285	-1.95e-2	6.44e-3	0.8286	-1.45e-3	-1.53e-2	0.1545	8.44e-2	0.1114	-4.90e-3	-1.30e-2	-1.59e-3
0.1347	0.8058	-2.20e-2	-3.52e-3	0.8057	-8.61e-4	-2.46e-2	0.1565	8.62e-2	0.1104	-5.78e-3	-5.04e-4	-1.40e-3
0.1199	0.6921	-9.48e-3	-8.06e-3	0.6917	-4.16e-4	-2.62e-2	0.2097	8.30e-2	0.1071	-8.05e-3	5.11e-5	-9.82e-4
0.0998	0.5300	2.32e-2	2.57e-2	0.5310	9.53e-5	1.18e-2	0.1765	0.1133	0.1509	-1.10e-2	-1.08e-3	-2.63e-3
0.0796	0.4378	2.81e-2	4.03e-2	0.4396	-6.12e-4	2.88e-2	0.1273	8.02e-2	0.1273	-4.43e-3	6.30e-4	-2.85e-3
0.0573	0.3889	-1.07e-2	4.04e-3	0.3890	-5.04e-4	-6.14e-3	9.25e-2	5.59e-2	8.58e-2	-1.26e-3	5.50e-4	-1.27e-3
0.0369	0.3724	-3.21e-2	2.53e-2	0.3743	4.72e-4	1.56e-2	7.93e-2	4.43e-2	6.09e-2	-1.10e-3	-2.45e-4	2.66e-5
0.0103	0.2696	2.79e-3	4.13e-2	0.2706	4.35e-4	3.43e-2	5.90e-2	2.64e-2	4.82e-2	-4.11e-4	-1.17e-4	1.76e-6

Profile 4

	Raw Velocities			Corrected Velocities			RMS Velocity Fluctuations			Reynolds Stresses		
y (m)	$\bar{u}$ (m/s)	$\bar{v}$ (m/s)	$\bar{w}$ (m/s)	$\bar{u}$ (m/s)	$\bar{v}$ (m/s)	$\bar{w}$ (m/s)	u_{rms} (m/s)	v_{rms} (m/s)	w_{rms} (m/s)	$\overline{u'v'}$ (m^2/s^2)	$\overline{u'w'}$ (m^2/s^2)	$\overline{v'w'}$ (m^2/s^2)
0.1746	0.9467	-1.37e-2	5.72e-2	0.9486	-1.33e-3	-6.80e-4	0.1384	7.86e-2	0.1311	-4.04e-3	-3.03e-3	2.41e-4
0.1600	0.9161	-1.59e-2	4.40e-2	0.9172	1.14e-4	-1.20e-2	0.1391	8.05e-2	0.1063	-4.31e-3	-2.97e-4	-8.97e-4
0.1450	0.8641	-9.90e-3	4.93e-2	0.8655	1.41e-3	-3.52e-3	0.1507	8.05e-2	0.1083	-5.47e-3	2.28e-4	-2.32e-4
0.1349	0.8160	-6.76e-3	4.90e-2	0.8175	3.60e-4	-8.74e-4	0.1584	7.95e-2	0.1129	-6.08e-3	4.42e-4	-3.53e-4
0.1199	0.6805	-1.61e-3	4.87e-2	0.6822	1.36e-3	7.10e-3	0.1765	8.69e-2	0.1204	-8.67e-3	-1.89e-3	-5.70e-5
0.0994	0.5739	1.53e-2	1.51e-2	0.5739	2.59e-4	-2.00e-2	0.1361	8.21e-2	0.1215	-5.25e-3	-2.00e-3	1.30e-3
0.0800	0.4932	7.48e-3	3.56e-3	0.4926	1.02e-3	-2.66e-2	0.1128	6.55e-2	0.1022	-2.55e-3	-1.11e-3	7.98e-4
0.0578	0.4322	-5.97e-2	-5.93e-2	0.4319	-8.63e-4	-8.56e-2	0.1142	5.02e-2	8.97e-2	-7.24e-4	1.32e-3	8.46e-4
0.0374	0.3887	-2.90e-2	-2.44e-3	0.3889	-1.09e-4	-2.62e-2	8.59e-2	4.28e-2	7.09e-2	-1.10e-3	-1.28e-3	4.38e-4
0.0093	0.2860	-9.36e-3	2.62e-2	0.2872	-6.19e-4	8.74e-3	6.84e-2	3.01e-2	6.13e-2	-4.01e-4	-1.31e-3	2.64e-5

APPENDIX C: Horizontally Averaged Data

This appendix contains the horizontally averaged profile data for the distance to the bed, streamwise velocity, Reynolds stress, and local drag coefficient for each experiment.

Experiment 1

y (m)	$\bar{u}_h$ (m/s)	$-\overline{u'v'}_h$ (m^2/s^2)	C_D'
0.2390	0.7394	2.12e-3	-
0.2003	0.6805	3.81e-3	-
0.1704	0.6459	4.40e-3	-
0.1504	0.6144	5.49e-3	-
0.1207	0.5353	6.29e-3	0.55
0.1001	0.4632	5.24e-3	0.82
0.0806	0.4032	3.91e-3	1.10
0.0552	0.3560	2.38e-3	1.31
0.0306	0.3159	1.35e-3	1.32
0.0107	0.2932	7.50e-4	1.03

Experiment 2

y (m)	$\bar{u}_h$ (m/s)	$-\overline{u'v'}_h$ (m^2/s^2)	C_D'
0.1562	0.5296	1.18e-3	-
0.1397	0.5098	1.82e-3	-
0.1203	0.4649	2.55e-3	-
0.1102	0.4317	2.74e-3	0.75
0.1000	0.3914	2.24e-3	0.87
0.0803	0.3476	1.53e-3	1.00
0.0651	0.3259	1.33e-3	1.06
0.0500	0.3008	8.60e-4	1.15
0.0302	0.2673	3.65e-4	1.33
0.0102	0.2577	2.08e-4	1.32

Experiment 3

y (m)	$\bar{u}_h$ (m/s)	$-\overline{u'v'}_h$ (m^2/s^2)	C_D'
0.0928	0.3015	3.14e-4	0.68
0.0876	0.2881	2.94e-4	0.79
0.0796	0.2742	2.72e-4	0.93
0.0696	0.2626	2.95e-4	1.07
0.0597	0.2453	2.16e-4	1.26
0.0499	0.2320	1.13e-4	1.41
0.0422	0.2268	7.32e-5	1.45
0.0328	0.2139	8.43e-5	1.57
0.0174	0.2163	3.18e-5	1.35
0.0071	0.2101	5.39e-5	1.25

Experiment 4

y (m)	$\bar{u}_h$ (m/s)	$-\overline{u'v'}_h$ (m^2/s^2)	C_D'
0.1916	0.7401	4.14e-3	-
0.1801	0.7366	4.44e-3	-
0.1651	0.7144	5.61e-3	-
0.1400	0.6588	6.90e-3	-
0.1200	0.5891	7.36e-3	0.61
0.0997	0.5199	6.59e-3	1.04
0.0801	0.4471	4.27e-3	1.55
0.0597	0.4000	2.38e-3	1.86
0.0376	0.3599	1.27e-3	1.81
0.0100	0.3310	4.77e-4	0.78

Experiment 5

y (m)	$\bar{u}_h$ (m/s)	$-\overline{u'v'}_h$ (m^2/s^2)	C_D'
0.1266	0.5979	3.73e-3	-
0.1200	0.5782	4.03e-3	0.77
0.1099	0.5270	3.74e-3	0.89
0.0998	0.4793	2.96e-3	1.04
0.0800	0.4220	1.85e-3	1.23
0.0654	0.3986	1.27e-3	1.29
0.0502	0.3710	9.23e-4	1.37
0.0375	0.3490	5.83e-4	1.43
0.0173	0.3265	2.86e-4	1.40
0.0075	0.3189	2.10e-4	1.35

Experiment 6

y (m)	$\bar{u}_h$ (m/s)	$-\overline{u'v'}_h$ (m^2/s^2)	C_D'
0.1785	0.7249	2.22e-3	-
0.1596	0.6982	2.73e-3	-
0.1400	0.6535	2.90e-3	-
0.1201	0.6063	2.78e-3	1.00
0.1047	0.5779	2.59e-3	1.31
0.0901	0.5480	2.01e-3	1.58
0.0702	0.5192	1.53e-3	1.79
0.0500	0.4925	9.29e-4	1.81
0.0096	0.4472	5.09e-4	0.99

Experiment 7

y (m)	$\bar{u}_h$ (m/s)	$-\overline{u'v'}_h$ (m^2/s^2)	C_D'
0.1147	0.5869	1.75e-3	1.53
0.1049	0.5563	1.61e-3	1.58
0.0948	0.5423	1.37e-3	1.53
0.0849	0.5214	9.50e-4	1.53
0.0702	0.4972	6.68e-4	1.49
0.0602	0.4837	4.42e-4	1.45
0.0499	0.4745	5.43e-4	1.39
0.0375	0.4633	5.41e-4	1.32
0.0176	0.4385	4.61e-4	1.28
0.0074	0.4248	3.98e-4	1.29

Experiment 8

y (m)	$\bar{u}_h$ (m/s)	$-\overline{u'v'}_h$ (m^2/s^2)	C_D'
0.3188	0.7627	6.29e-4	-
0.2798	0.7436	1.57e-3	-
0.2397	0.7099	2.34e-3	-
0.2002	0.6640	3.70e-3	-
0.1597	0.5782	5.33e-3	-
0.1200	0.4409	7.22e-3	0.47
0.0898	0.3249	4.79e-3	0.94
0.0600	0.2499	2.15e-3	1.39
0.0355	0.2104	9.81e-4	1.40
0.0102	0.1781	3.85e-4	0.72

Experiment 9

y (m)	$\bar{u}_h$ (m/s)	$-\overline{u'v'}_h$ (m^2/s^2)	C_D'
0.1435	0.3402	1.64e-3	-
0.1299	0.3130	1.87e-3	-
0.1200	0.2915	1.96e-3	0.59
0.1053	0.2462	1.59e-3	0.83
0.0898	0.2151	1.20e-3	1.07
0.0697	0.1882	6.41e-4	1.31
0.0495	0.1644	3.23e-4	1.52
0.0358	0.1525	1.39e-4	1.57
0.0174	0.1449	8.60e-5	1.37
0.0074	0.1425	5.30e-5	1.17

Experiment 10

y (m)	$\bar{u}_h$ (m/s)	$-\overline{u'v'}_h$ (m^2/s^2)	C_D'
0.1678	0.8280	1.11e-2	-
0.1499	0.8022	1.17e-2	-
0.1350	0.7255	1.42e-2	-
0.1200	0.6422	1.30e-2	0.60
0.1049	0.5601	1.14e-2	0.82
0.0901	0.4755	7.97e-3	1.15
0.0702	0.4057	5.23e-3	1.50
0.0550	0.3636	2.90e-3	1.71
0.0375	0.3296	1.61e-3	1.75
0.0098	0.3037	4.29e-4	1.14

Experiment 11

y (m)	$\bar{u}_h$ (m/s)	$-\overline{u'v'}_h$ (m^2/s^2)	C_D'
0.2285	0.7395	1.83e-3	-
0.2000	0.7064	2.64e-3	-
0.1699	0.6744	3.52e-3	-
0.1404	0.6185	4.33e-3	-
0.1200	0.5849	4.63e-3	0.33
0.1002	0.5263	4.20e-3	0.78
0.0801	0.4865	3.57e-3	1.16
0.0550	0.4283	2.07e-3	1.56
0.0379	0.4039	1.33e-3	1.55
0.0102	0.3733	5.81e-4	0.96

Experiment 12

y (m)	$\bar{u}_h$ (m/s)	$-\overline{u'v'}_h$ (m^2/s^2)	C_D'
0.1203	0.8541	6.23e-3	-
0.1051	0.7812	6.34e-3	-
0.0950	0.7444	5.64e-3	1.02
0.0804	0.6891	4.54e-3	1.10
0.0703	0.6534	3.76e-3	1.23
0.0603	0.6324	2.99e-3	1.33
0.0476	0.5959	2.33e-3	1.37
0.0379	0.5834	2.05e-3	1.46
0.0179	0.5565	1.25e-3	1.43
0.0075	0.5634	1.00e-3	1.30

Experiment 13

y (m)	$\bar{u}_h$ (m/s)	$-\overline{u'v'}_h$ (m^2/s^2)	C_D'
0.2874	0.7174	1.82e-3	-
0.2500	0.6714	2.98e-3	-
0.2002	0.5986	4.42e-3	-
0.1596	0.5013	5.20e-3	-
0.1399	0.4366	5.04e-3	1.18
0.1200	0.3760	3.67e-3	1.36
0.0900	0.3284	1.70e-3	1.37
0.0649	0.3052	9.49e-4	1.25
0.0377	0.2761	4.09e-4	1.17
0.0099	0.2545	1.52e-4	1.05

Experiment 14

y (m)	$\bar{u}_h$ (m/s)	$-\overline{u'v'}_h$ (m^2/s^2)	C_D'
0.1187	1.0164	2.71e-3	-
0.1100	0.9978	2.85e-3	0.14
0.0948	0.9336	3.45e-3	0.18
0.0798	0.8725	3.36e-3	0.26
0.0649	0.8297	2.53e-3	0.32
0.0497	0.7638	2.44e-3	0.40
0.0376	0.6825	2.51e-3	0.53
0.0176	0.5669	1.51e-3	0.79
0.0076	0.5312	9.61e-4	0.90

Experiment 15

y (m)	$\bar{u}_h$ (m/s)	$-\overline{u'v'}_h$ (m^2/s^2)	C_D'
0.1845	0.4661	1.79e-3	-
0.1648	0.4266	2.21e-3	-
0.1500	0.3905	2.38e-3	-
0.1296	0.3181	2.30e-3	1.90
0.1100	0.2669	1.42e-3	2.06
0.0901	0.2383	4.38e-4	1.95
0.0723	0.2507	2.09e-4	1.38
0.0553	0.2535	1.36e-4	1.12
0.0359	0.2469	1.38e-4	1.05
0.0102	0.2422	7.25e-5	1.17

Experiment 16

y (m)	$\bar{u}_h$ (m/s)	$-\overline{u'v'}_h$ (m^2/s^2)	C_D'
0.1186	0.8905	1.39e-3	-
0.1098	0.8830	1.42e-3	-
1.1000	0.8614	1.48e-3	0.34
0.0852	0.8295	1.40e-3	0.39
0.0699	0.7990	1.54e-3	0.45
0.0601	0.7705	1.33e-3	0.50
0.0501	0.7430	1.29e-3	0.57
0.0377	0.7016	1.20e-3	0.67
0.0175	0.6622	1.01e-3	0.81
0.0074	0.6438	8.17e-4	0.89

Experiment 17

y (m)	$\bar{u}_h$ (m/s)	$-\overline{u'v'}_h$ (m^2/s^2)	C_D'
0.2045	0.4099	2.01e-3	-
0.1801	0.3494	2.81e-3	-
0.1649	0.2984	2.59e-3	0.80
0.1550	0.2769	2.08e-3	0.86
0.1402	0.2441	1.73e-3	0.99
0.1149	0.1711	6.22e-4	1.66
0.0901	0.1599	2.32e-4	1.57
0.0648	0.1555	5.33e-5	1.37
0.0401	0.1550	1.63e-5	1.18
0.0101	0.1563	4.32e-5	1.00

Experiment 18

y (m)	$\bar{u}_h$ (m/s)	$-\overline{u'v'}_h$ (m^2/s^2)	C_D'
0.1752	0.9152	4.11e-3	-
0.1603	0.8791	4.69e-3	-
0.1450	0.8301	6.01e-3	-
0.1350	0.7990	6.56e-3	-
0.1201	0.6937	7.98e-3	0.26
0.0998	0.5687	7.59e-3	0.49
0.0799	0.4795	3.95e-3	0.76
0.0573	0.4151	1.66e-3	0.92
0.0374	0.3654	1.23e-3	0.92
0.0099	0.2968	3.79e-4	0.38